Design and Development of Proof-of-Concept Biosensors Based on Engineered Surfaces and Nanomaterials

DOCTOR OF PHILOSOPHY

by

KULDEEP MAHATO

JUNE 2019

Department of Biosciences and Bioengineering
Indian Institute of Technology Guwahati
Guwahati- 781039, INDIA

Design and Development of Proof-of-Concept Biosensors Based on Engineered Surfaces and Nanomaterials

A Thesis submitted in partial fulfillment of the requirements for the award of the degree of

DOCTOR OF PHILOSOPHY

by

KULDEEP MAHATO

JUNE 2019

Department of Biosciences and Bioengineering

Indian Institute of Technology Guwahati

Guwahati- 781039, INDIA

Dedicated to my Parents

Kuldeep Mahato
Registration No. 156106049
Department of Biosciences and Bioengineering
Indian Institute of Technology Guwahati
Guwahati-781039, Assam, INDIA

Statement

I hereby declare that the matter embodied in this thesis is the result of investigations carried out by me at the Department of Biosciences and Bioengineering, Indian Institute of Technology Guwahati, Guwahati, India, under the supervision of **Dr. Pranjal Chandra.** This thesis has not been submitted to any university, institute or elsewhere for the award of the any degree, diploma or associate-ship.

Date: ………………. **Kuldeep Mahato**

Department of Biosciences and Bioengineering
Indian Institute of Technology Guwahati
Guwahati-781039, Assam, INDIA

Certificate

It is to certify that the work described in this thesis entitled "Design and development of proof-of-concept biosensors based on engineered surfaces and nanomaterials" done by Mr. Kuldeep Mahato (Roll No - 156106049) for the award of degree of doctor of philosophy is an authentic record of the results obtained from the research work carried out under my supervision in the Department of Biosciences and Bioengineering, Indian Institute of Technology, Guwahati-India.

The results embodied in this thesis have not been submitted to any other university or institute for the award of any degree.

June 2019 **Dr. Pranjal Chandra**

(Supervisor)

ACKNOWLEDGEMENTS

Finally, at the end of a seemingly endless journey towards producing this thesis, I would like to thank everyone, whose critics, comments, questions, support and encouragement, personal as well as academic, have left a mark on this thesis work.

First and foremost, I would like to thank my research supervisor, Dr. Pranjal Chandra, for his constant support, precious advice, guidance, and supervision of the research helped to complete the PhD thesis. He gave me intellectual freedom in my work and endless hours discussed to improve the quality work in all my endeavors. I am fortunate enough that I had the opportunity to work as a student under his supervision.

I am also grateful to my doctoral committee members, Dr. Lalit Mohan Pandey, Dr. Narayanasamy Selvaraju, and Dr. Shrikrishna N. Joshi for their timely and invaluable suggestions, which helped me to improve the work pertaining to PhD thesis. I owe my sincere gratitude to Dr. Ananya Srivastava from National Institute of Pharmaceutical Education and Research Guwahati for her valuable suggestions and motivation, which helped me to improve the research work.

I owe my thanks to present and former Head of Department of Biosciences and Bioengineering, and Head of the Central Instrumentation Facility, Indian Institute of Technology Guwahati for providing me the necessary facilities to fulfill my PhD thesis objectives. I owe my thanks National Institute of Pharmaceutical Education and Research Guwahati for the animal facilities required for fulfilling my PhD thesis objectives.

I would like to thank Ministry of Human Resource Development, India and Indian Institute of Technology Guwahati for providing financial assistance during my Ph.D. tenure.

It was pleasure to work with my lab members Dr. Sharmili, Ashutosh, Budhhadev, Anupriya, Monalisha. Thanks to them for their suggestions, time, and help in experiments throughout my PhD tenure. I am deeply indebted to all my friends at IIT Guwahati; Abhishek, Krishna, Nirmal, Ramesh Babu, Sunil, Awadh, Ritesh and others for providing a soothing environment and helping in the critical situations during my PhD, whenever I needed. I must acknowledge all my school, university friends and PhD batch mates for their love, encouragement and support.

My special thanks and appreciation goes to my parents as well as my family for their blessings, love, patience, support and understanding throughout my studies and most of all to the Almighty Nature who governs everything.

Date: ………………

Kuldeep Mahato
Member at

MAKE IN INDIA
Chandra's
Laboratory of Bio/physio Sensors
and Nanobioengineering

Abstract

Biosensors have found great interest due to their advantages over the conventional lab-based, time-consuming, sophisticated analytical systems. For the fabrication of the biosensor, surface engineering at sensing zone and incorporation of nanomaterials play an important role in achieving the higher sensitivity. The surface engineering strategies facilitates stable immobilization of the recognition molecules; whereas the incorporation of the nanomaterials offers enhanced electronic properties and larger area, which eventually helps to deliver the sensitive determination of target analyte. In this work, we have developed the sensor systems, which not just provide sensitive analyses, but it actually detects the analytes of industrial/clinical importance in significant levels. In addition, this thesis work is inclined to resolve the few contemporary griming issues, such as food safety and silent clinical diseases *viz.* hypovitaminosis, liver and bone diseases, and carcinoid syndromes.

We have designed the study in four different sections, where in the first part; we have developed a colorimetric biosensor using an engineered paper surface, where the antibody has been covalently immobilized for the selective determination of the alkaline phosphatase in milk to assure the milk pasteurization process. The dynamic range for this biosensor was found to be of 10-1000 U/mL with the detection limit of 0.87 (±0.07) U/ml (RSD < 4.2%), which falls in the range of alkaline phosphatase level present in the raw milk. The sensor shows the stability for 8 weeks and successfully recovered alkaline phosphatase between 91-100% when spiked in pasteurized milk. In addition, we have fabricated a miniaturized disposable device for onsite determination based on the developed biosensor.

In the next section, we have attempted to enhance the analytical capabilities of the alkaline phosphatase biosensor. For that, we have designed an electrochemical biosensing system using nanomaterials assisted engineered sensor surface. Here, we have used electrochemically synthesized Au-nano-dendroid over the screen-printed carbon paste electrode surface and conjugated with the graphene oxide sheets for anchoring the bio-recognition elements. This biosensor probe was used for the determination of alkaline phosphatase, where we obtained the dynamic range and LOD of 100-1000 U/L and 9.32 (± 0.12) U/L (RSD < 3.4 %), respectively. The biosensor was employed for determining "serum alkaline phosphatase" since, it serves as biomarkers for various pathophysiological conditions associated with cancer relapse, bone, and liver diseases. This shows remarkable selectivity toward alkaline phosphatase even in the complex serum sample. The obtained level of the alkaline phosphatase is comparable with clinically accepted techniques.

The sensitivity in the electrochemical sensor systems depends on the charge transfer phenomenon, where the surface area plays an important role. Thus, we have employed porous nanomaterials for engineering the sensor surface as these materials are reported of having relatively larger surface contributed by its morphological features. Here, we have incorporated porous graphene-1,8-diaminonepthelene nanocomposite to fabricate the electrochemical sensor probe at Au nanoparticles deposited glassy carbon electrode surface. Since the charge transfer is a function of the electrochemical behavior of analyte, we have chosen vitamin C as a model molecule, as it shows the direct electrochemical activity at its oxidation potential. This sensor shows excellent analytical performance, where the dynamic range is found in between 1×10^{-14} M and 1×10^{-3} M with the DL of $4.4 (\pm 0.02) \times 10^{-17}$ M (RSD < 3.9%). This sensor probe has been used in clinical urine and fruit juice for determining vitamin C. In addition, the fabricated biosensor is used for determining vitamin C level in the contrasting physiological conditions of neurodegenerative mice model has been utilized.

In the complex matrices *viz.* urine, blood, serum, *in vitro*, *ex vivo*, and *in vivo* samples, interference and fouling of electrodes are the major concerns. In view of this, we have studied the impact of nanomaterial assisted engineered surface for electrochemical biosensing systems in the next part of the study. In this section, we have developed a biosensor using the Au-nanorattle-reduced graphene oxide engineered sensor surface. This sensor probe was used for the determination of small monoamine neurotransmitter serotonin, as it serves as indicator molecules in carcinoid tumors and in serotonin syndrome at its elevated level. The analytical performance was obtained with the dynamic range of $1x10^{-3}$ M - $3x10^{-6}$ M and the detection limit of 3.87 (±0.02) $x10^{-7}$ M, (RSD < 4.2%) which falls in the ranges of normal and pathophysiological conditions including carcinoid tumor and pre-eclampsia.

Thus, this work explores the role of surface engineering and incorporation of nanomaterials in the design and development of sensitive as well as selective optical/electrochemical biosensing approaches. In the future, these proof-of-concepts models may lead to the commercially acclaimed prototypes for onsite detection in various matrices.

Contents

Chapter IV

Chapter V

Chapter VI Summary and future work 181-184

Annexures 185-202

List of figures

List of tables

Chapter- I

General introduction

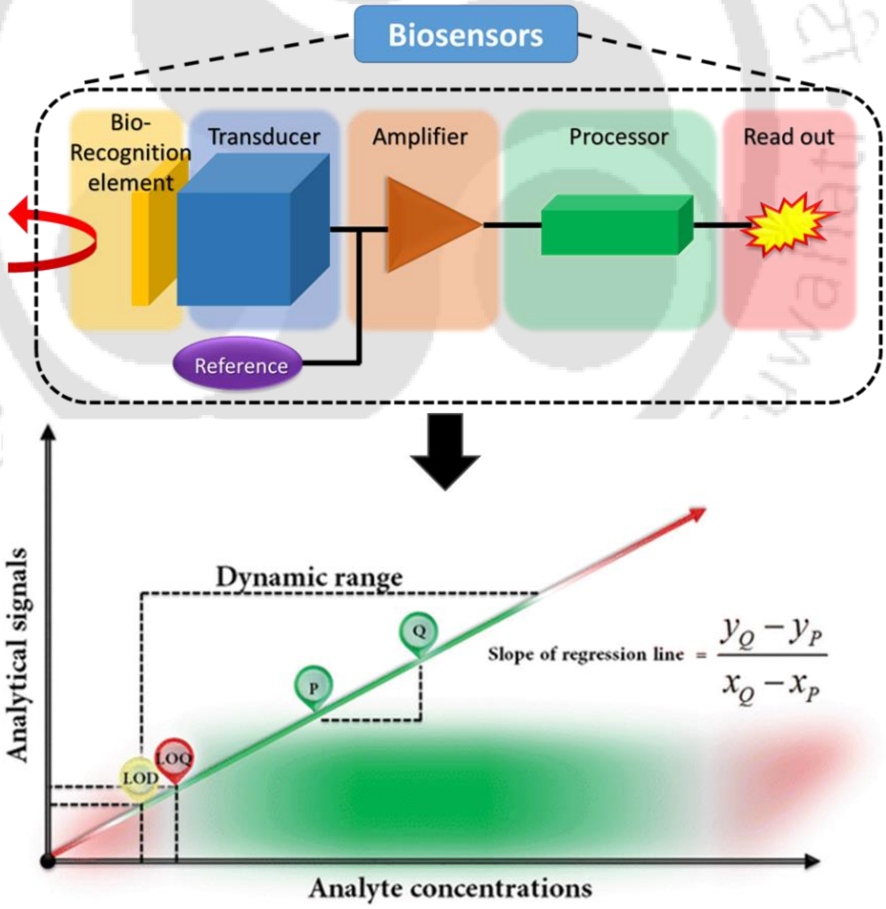

1. The need of miniaturized diagnostics:

Among various global challenges, food safety and health-related concerns are the major threats to humankind and it has tremendous importance. The exponential boom of population across the world have not only increased the demand for food exponentially but also affected the healthcare system greatly (McNally,2013; Speidel,2000). To meet this demands, various technological advancements have been observed recently, where the introduction of high yielding crops, food processing, and its preservation have majorly been employed to overcome the deficit (Godfray et al.,2010). Nevertheless, the nutritional values, as well as the quality of these processed /preserved food items, became a major concern (Amit et al.,2017). For ensuring the nutritional values, a number of regulatory bodies have been established in public as well as private sectors. These regulatory bodies not only ensures the quality output of the processed food but also checks the unauthorized productions (Kotsanopoulos and Arvanitoyannis,2017; Sharma et al.,2010). The major spoilage of food items is due to the post-packaging microbial attack, improper transportations, and poor preservation practices at retailing points, which eventually causes quality degradation. In addition to this, public healthcare systems have been disrupted because of improper sanitation, hygiene, and exposure to the various kind of infectious bio-chemicals. Not only these, the shift in dietary habits and sedentary lifestyles are causing serious non-communicable diseases, which serves as the major factors for unhealthy life (Stamatakis et al.,2019). According to the World Health Organization (WHO), a mega mass of several million are being infected per year due to food adulterates, various disease causing chemicals, and unhygienic lifestyles (Organization,2015).

In current scenarios, such issues related to food inspection and clinical diagnoses are done after the appearance of physical indicators, where the conventional detection/diagnostic systems are adopted (Mahato et al.,2018c). At the conventional quality controls and clinical-setups, various standard techniques are employed for the checkup, where instruments-based bio-molecular analyzers *viz.* spectrophotometers, fluorimeters, and chromatographic instruments are used to get the accurate determination of the causative agents. In addition, various techniques such as colorimetric, titrimetric, blotting, ELISA, radioimmunoassay, *etc.* are also used for precise estimations for various biomolecules (Chandra,2016). Although, these techniques are very powerful, however, they require well-equipped infrastructure, dedicated laboratory space, trained personnel, and large amount of sample, which not only restrict for delivering cheaper detection but also limits them for onsite determination (Mahato et al.,2018c). Therefore, it is very important to develop efficient miniaturized diagnostic devices that can perform bio-molecular analyses in remote areas, with low sample volumes, and having the ability to be operated by untrained personnel even in emergency conditions (Rateni et al.,2017). The recent paradigm of such analyses has been shifted towards the estimation of causative agents at a particular stage, where the bio-molecular indicators/ biomarkers begin to appear in minute level or at low concentrations(Mahato et al.,2018a). To achieve such ultrasensitive analyses, miniaturized point-of-care diagnostic devices have been developed which has been proven as an outstanding alternative for detection of numerous target molecules. For instance, detection of such indicators in food quality at this point could be able to check the contact-based mass spoilages; whereas, estimations of any biomarker in the clinics may provide the information regarding potential severity of infections and disorders. Therefore, biomarker based miniaturized bioanalytical systems have found great attention in food quality controls and clinics due to their capability of predicting the food spoilage as well as diseases diagnoses, respectively.

2. Introduction to biomarkers: importance in diagnostics:

Bio-molecular indicators or biomarkers for food quality estimations are the chemical or bio-chemical moieties that are found in the raw/processed food items that serve as an indicator of spoilage conditions (Pinu,2016). These biomarkers usually consist of adulterated chemicals, any pathogenic microbe or their metabolites, and other indicator molecules present in the food items (Garcia-Aloy et al.,2019). Similarly, clinical biomarkers are the moieties of chemical or biochemical origin, which are usually found in body tissues/fluids in various clinical conditions exhibiting a genuine real time indicator of diseases or its progression (Mahato et al.,2018a). The commencement of such clinical biomarkers in any diseased case are of either cellular, subcellular, or supramolecular origins which includes specific products / by-products of intracellular physiological processes (Henry and Hayes,2012; Mahato et al.,2018a). Depending of the biomedical usage, biomarkers are classified under predisposition, diagnostic, prognostic, and predictive biomarkers (Barh et al.,2014). Any molecule associated with the genetic setup of an individual is known as the predisposition biomarker and has the existence since birth (Meyer,2012). Diagnostic biomarkers are exclusively found after the onset/progress of disease/disorder either in form of altered levels or appearance of new biomarkers (Ziegler et al.,2012). Prognostic biomarkers uncover the likelihood of reappearances of the diseases after their treatment, whereas the predictive biomarkers are the set of biomarkers used for envisaging the best suitable therapeutic route for personalized medicine (Nalejska et al.,2014). The diagnoses based on biomarkers offers identification of associated mechanisms of diseases / disorder for minimizing the risk factors in various clinical cases (Laskowitz et al.,2009). Therefore, the biomarkers based determinations have found great attention not only in clinical diagnoses, but also in the quality control unit of various industries. Among numerous strategies of bio-molecular analyses, biosensor based analytical system has been found a great attention due to its tremendous miniaturization capability, robustness, selectivity, sensitivity, and point-of-care determinations even at trace levels.

3. Introduction to biosensors:

According to International Union of Pure and Applied Chemistry biosensors are defined as “A device that uses specific biochemical reactions mediated by isolated enzymes, immunosystems, tissues, organelles or whole cells to detect chemical compounds usually by electrical, thermal or optical signals” (McNaught and McNaught,1997). Historically, Clark and Lyon have reported the first biosensor in 1962, which was based on oxidase enzyme electrode for the detection of glucose. A decade later, yellow spring instruments under the trade name “Model 23A YSI analyzer” commercialized its variant in 1975. Since then a number of milestones have been observed in the biosensor development targeting various applications including food safety, clinical diagnoses of diseases *etc*. (Chandra,2016; Newman and Turner,1992; Palchetti and Mascini,2010)

Fundamentally, the biosensors are bio-analytical devices that detect the molecules of chemical or biochemical origin by electrical, thermal or optical signals using the specific reactions mediated by enzymes, immuno-systems or whole cells (Chandra,2016). It consists of bio-recognition element, transducer, amplifier, and readout components (figure 1.1) (Mahato et al.,2018b; Mahato et al.,2018c). The bio-recognition element plays a pivotal role in perceiving the changes (chemical or physical) occurred in its proximity, which is then used for the sensing of target analyte. A stimulus generated after the interaction between target

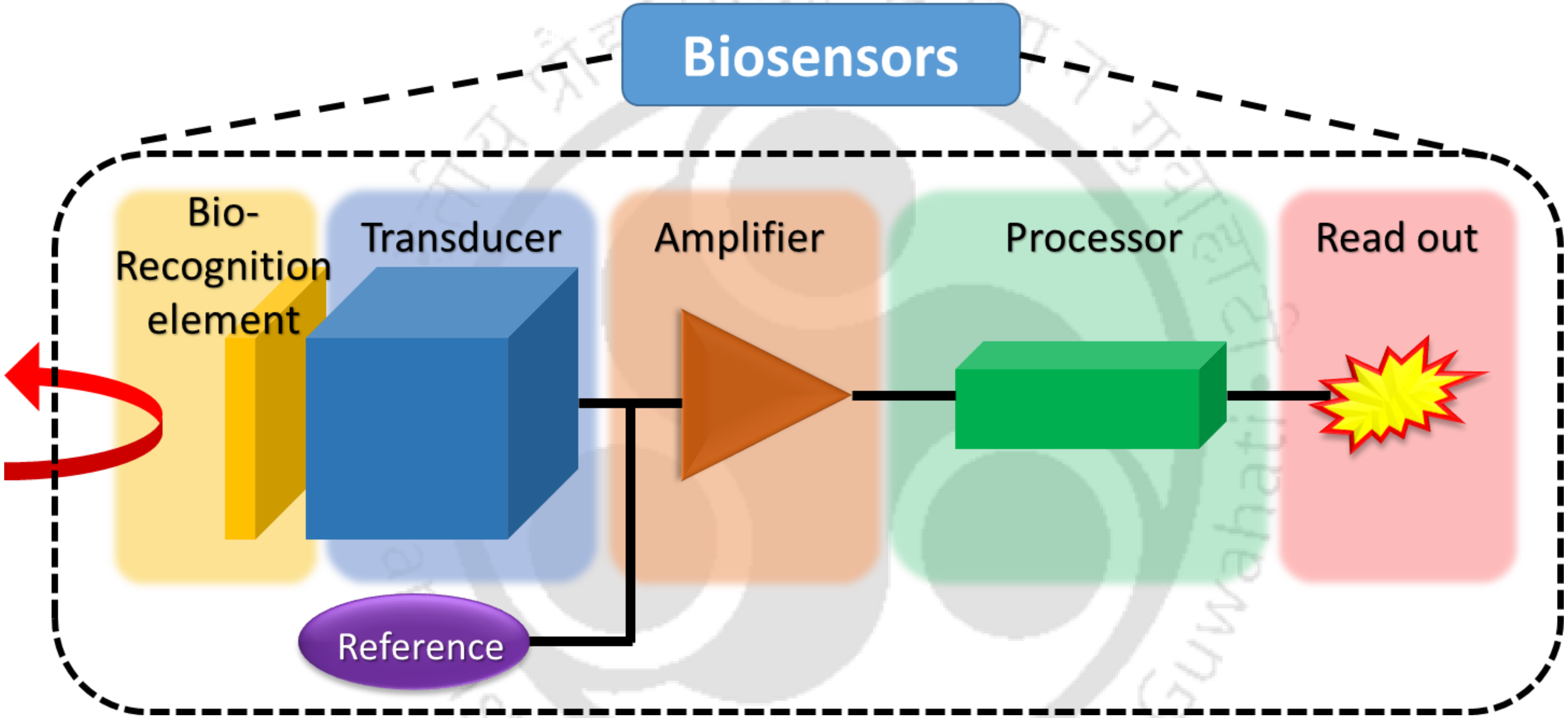

Figure 1.1: *Detailed schematic representation of the various components of biosensor (reprinted with the permission of Mahato et.al., Springer Inc.)*

analyte and bio-recognition element is then converted into quantifiable signal by the transducer coupled with the bio-recognition element. The amplifier strengthen weak signals passed by transducer, which are conventionally employed by incorporating external electrical circuit-based amplifiers in biosensor modules. In recent, advancements, the signal amplification has also been employed using mediators to the sensing mechanism or incorporating various nanomaterials and their composites. Mediators are the molecules that assist the flow of signals from bio-recognition point to transducer surface during the sensing process.

3.1. Classification of biosensors based on transducers:

The biosensors have been categorized under mainly three major types depending on the transducer used *viz.* optical, mechanical, and electrochemical biosensors, which are described in the following sections below. The detailed classification of biosensors based on various transducers has been shown in the figure 1.2.

3.1.1. Optical biosensor:

These biosensors are based on the change in optical properties *viz.* absorption, fluorescence, surface plasmon, luminescence *etc.*, where the signal generation occurs in terms of altered phase, polarization, or frequency of input light in response to physical or chemical changes at the biosensor surface (Damborský et al.,2016). In absorption biosensing a particular energy level of the electromagnetic spectrum of light is used as analytical signal. In the presence of target analyte and successful complexation of it with the probe, this absorption shifts towards high or low energy levels, producing an output signal. The amplitude of these shifts can be correlated with the concentration of analytes for quantification (Ligler and Taitt,2011).

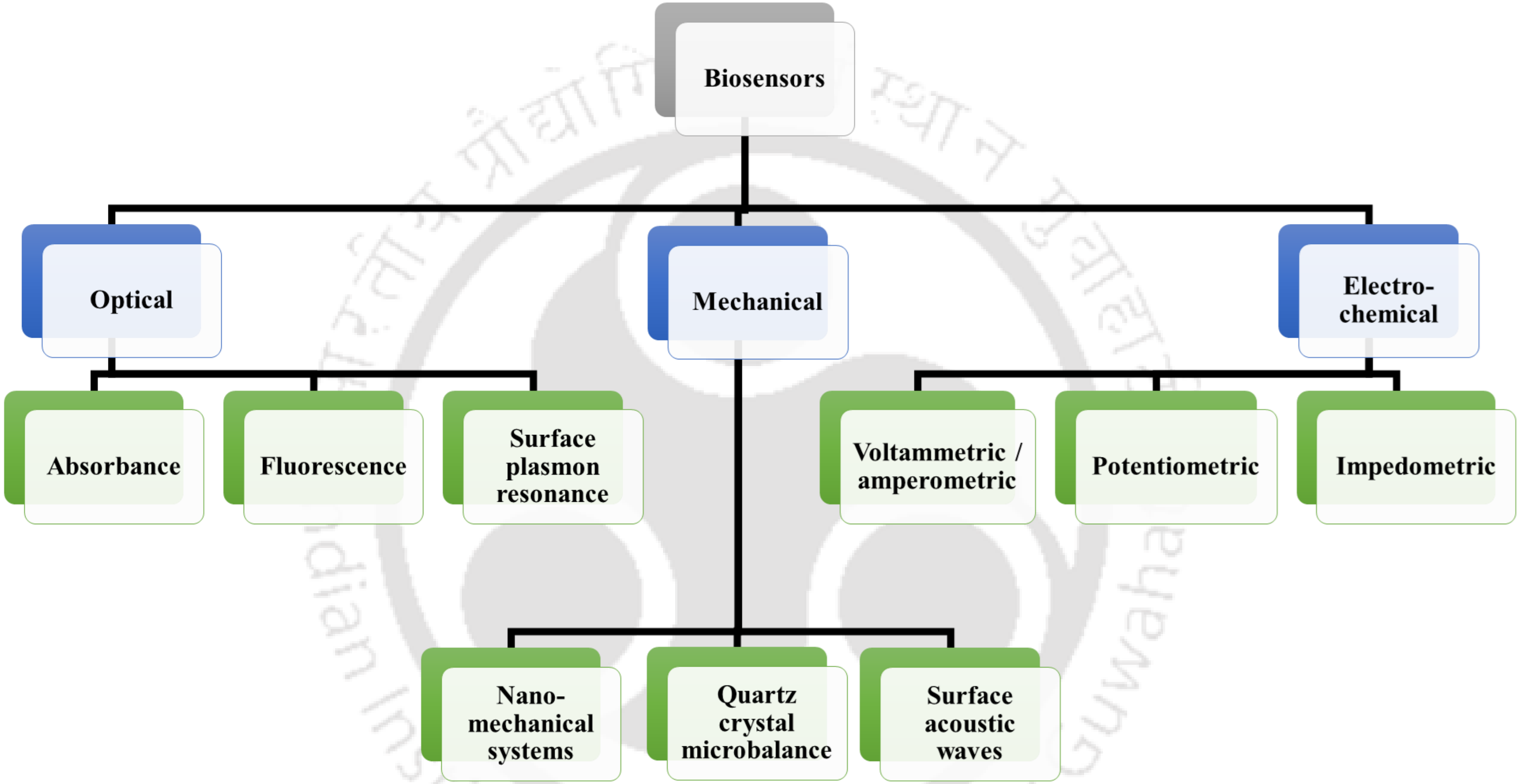

Figure 1.2. *Classification of biosensor based on transducer surface.*

The absorptive phenomena shown by analyte in response to the interacting electromagnetic radiations, when induces the absorption shift in visible frequency range, the sensor shows a color change in the presence of analyte. The absorptive phenomena shown by analyte in response to the interacting electromagnetic radiations, when induces the absorption shift in visible frequency range, the sensor shows a color change in presence of analyte is called as colorimetric biosensor are very promising due to the simplistic fabrication and naked eye detection (Aldewachi et al.,2018). Another approach in optical biosensing is based on fluorescence phenomenon, where the fluorescent properties of analytes have been exploited, where these are commonly based on the fluorescence based analytical approaches, *viz*. imaging, fluorescence resonance energy transfer, Fluorescence recovery after photobleaching *etc*. based techniques offers the molecular level selectivity (Strianese et al.,2012)

3.1.2. Mechanical biosensor:

Another major class is reported as mechanical biosensors, where mechano-physical properties of the probe materials are used to detect the analytes of chemical or biological origin (Hwang et al.,2009). Commonly, three types of mechanical biosensors have been reported so far, *viz*. surface acoustic wave, quartz microbalance, and nano-mechanical systems (Dagdeviren et al.,2016). Among all formats of mechanical biosensors, nano-mechanical system is widely accepted due to its high sensitivity and miniaturizability. The operational part of these systems consists of cantilever probe and mechanical transducer where the probe surface is modified to obtain better analytical performance. The signal is then transferred to amplifier and processor for the quantification. The analytical performance of the system is majorly dependent on the material properties as well as the dimension of cantilever probe (Tamayo et al.,2013). The fundamental processes involved in mechanical biosensors are the change in mass, surface stress, young’s modulus, and viscoelasticity after bio-molecular adsorption or coupling to the immobilized bioreceptor. These nano-mechanical based biosensors are mainly operated in the two modes *viz.* static and dynamic modes (Tamayo et al.,2013).

3.1.3. Electrochemical biosensor:

Electrochemical (EC) biosensors are another class of biosensors, which employ various electrochemical techniques (Prasad et al.,2016). Transducers in this format change chemical stimuli to the readable electrical signals. These biosensors have been widely explored due to their numerous advantages over other modes, which include better analytical performance, robustness, quick analysis, selectivity, and quantification of analytes in highly miniaturized experimental settings (Mahato et al.,2016). Fundamentally, these biosensors work on the principle of electron flow due to the chemical changes (particularly the redox processes), which directly generates the electrical signal (Chandra,2016). These are preferred over the optical- and mechanical-based techniques because of its remarkable detectability, experimental simplicity, and low-cost fabrication. Not only this, EC biosensors deliver better performances in terms of the detection limits and ranges, where the detection limits have reported up to the sub-attomolar or even lower levels with wider dynamic linear ranges. Other benefits associated with the miniaturization and integration capabilities of EC prototypes with smartphones and printed circuit boards have provided a unique ability for high-performance commercial products (Mahato et al.,2018a). EC biosensors are further classified under voltammetry (Bhatnagar et al.,2018), amperometry (Chandra et al.,2011), potentiometry (Ashmawy et al.,2019), and impedometry (Kashish et al.,2017) based biosensors.

3.2. Classification of biosensors based on bio-recognition elements:

Depending on the bio-recognition elements used in the biosensors, these are classified under bio-catalytic (*e.g.* enzymatic, bio-mimicked, nano-catalyst, direct electro-transfer *etc.*) and bio-affinity (*e.g.* immuno-sensor, geno-sensor, cyto-sensor, apta-sensor *etc.*) based biosensors, where the generation of signals depends on the interaction between bio-recognition elements and target molecules (Eggins,2013). The bio-catalytic receptor operates by cleaving the target analyte in order to obtain the signal during sensing process. In one such example, a cholesterol biosensor reported by Cevik and co-workers, where the cholesterol oxidase enzyme was immobilized on to the conducting 4-(4H-dithienol[3,2-b : 2′,3′-d]pyrrole-4)aniline polymer, (DTP(aryl)aniline) polymers at the sensor surface. Here, cholesterol oxidase catalyzes cholesterol to provide the analytical signals (Cevik et al.,2018). In bio-affinity based sensors, the sensor signal is obtained by the affinity-based interactions *viz.* antibody-antigen immuno-complexation, avidin-biotin streptavidin interaction, aptamers-ligand coupling *etc.* For instance, the breast cancer detection reported by Jayanthi et al. using immuno-sensing approach, where immobilized antibody and the target analyte (ubiquitin-conjugating enzymes 2C) gets immuno-complexed and thereby generates the analytical signals (Jayanthi et al.,2019). The detailed classification of biosensors based on the bio-recognition elements is shown in figure 1.3.

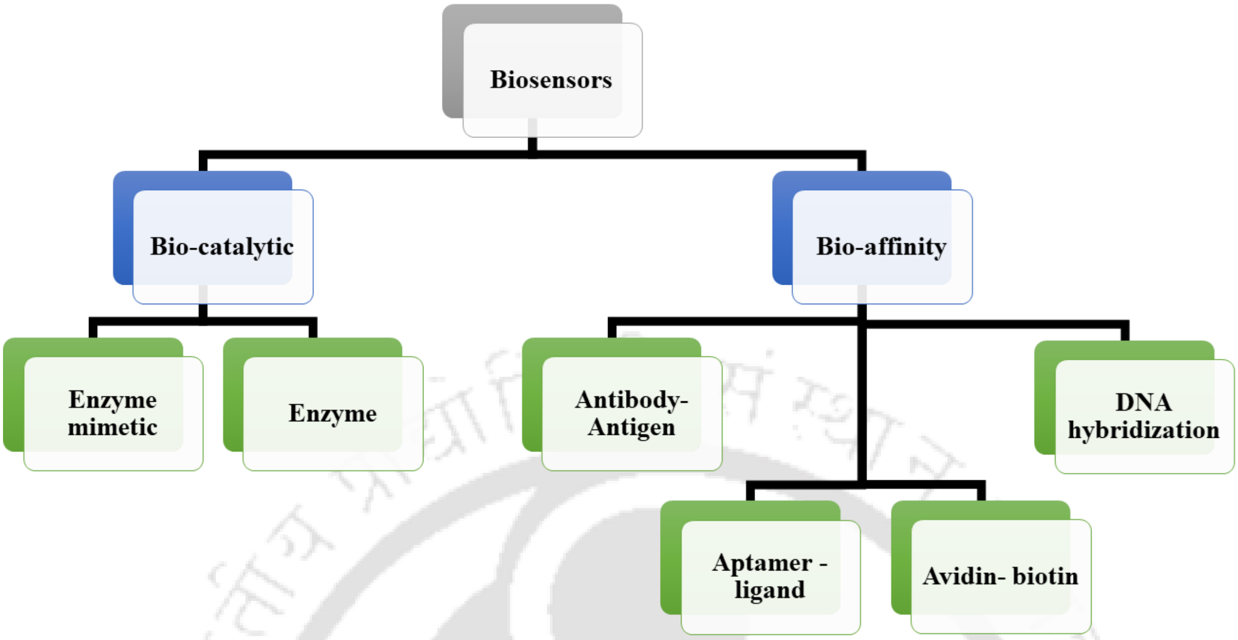

Figure 1.3: *Types of biosensors based on various bio-recognition elements.*

3.3. Label and label-free biosensing strategies:

Depending on the involvement of external labels (agents that facilitate the analytical process) in the determination of analytes, the biosensing methods have been categorized under two major categories, which includes label-assisted and label-free modes.

3.3.1. Label assisted biosensing methods:

In this type, the detection of target analyte uses an additional moieties for signal generation. For instance, in an amperometric nanobiosensor reported by Pallela and coworkers, where the developed sensor surface was used for capturing the target metastatic cell following sandwich ELISA format. Here, the signal generation was obtained after treatment of hydrogen peroxide, which was catalyzed by labeled hydrazine linked with the reporter antibody (Pallela et al.,2016). In another example, a colorimetric determination system has been reported for the of hydrogen peroxide detection, where target analyte was analyzed in terms of the blue color formation assisted by a chromogenic compound

3,3',5,5'-Tetramethylbenzidine (Üzer et al.,2017). In both cases, quantifiable signals were obtained only due to the presence / mediation of redox and chromogenic labels. Such type of the determinations is termed as label-assisted detection methods or processes.

3.3.2. Label-free biosensing methods:

When the target analyte itself is capable of providing the analytical signals, then it is termed as label-free biosensor (Sang et al.,2016). In these type of detections, the target analytes are either redox active molecules or the sensor has capability to catalyze / interact the analyte molecule to generate sensing signal. Conventionally, the most common mode for label-free analyses is based on impedometric and potentiometric sensing. Not only this, the optical signatures in terms of effective optical performance in porous silicon nano-chips are also considered to be a label-free format for sensing of various targets including bacteria, DNA, proteins *etc.* Many researchers traditionally and even in current scenario have detected various small molecules (*viz.* drugs, heavy metal ions, metabolites *etc.*) based on direct electron transfer reaction, which is also considered as label-free biosensing and a method of choice. In a label-free impedometric sensing cancer cells were detected and differentiated from normal cells utilizing their surface chemistry using aptamer immobilized on a nano-conducting surface (Chandra et al.,2013a). In another study, a label-free sensor was developed for the electrochemical detection of dopamine using the self-assembled peptide layers, where it electro-catalyzed at the sensor surface to give measurable signals (Matos and Alves,2011). In another example, a sensor for detection of glucose has been fabricated using self-assembled immobilization of glucose-oxidase at the reduced graphene oxide-magnetic nanoparticles (Pakapongpan and Poo-arporn,2017). In these cases, the targets; cancer cells, dopamine, and glucose itself contributes towards the signal generation at the sensor surface.

4. Biosensor probe development and characterization:

In all biosensing systems, the detection probe plays an important role, which significantly contributes to the analytical performance of the biosensor. The transducer materials are coupled with highly selective bio-recognition elements. For example, in electrochemical biosensors working electrode is functionalized for the selective detection of analytes, where the electrode surfaces are attached with antibodies, aptamers, enzymes, *etc* (Chandra et al.,2017). The selection of these bio-recognition elements is dependent on the nature of the target molecules. For instance, if the target molecule is protein biomarker, antibodies are preferred as recognition element (Shan and Ma,2017). However, to introduce the temperature stability to the probe, aptamers have been greatly applied in the sensing matrix in recent years (Jarczewska et al. 2016). Similarly, enzymes are applied in the matrix which generally produces electroactive species. The classical example is immobilization of glucose oxidase for glucose detection, where hydrogen peroxide is generated and detected at the electrode surface (Kausaite-Minkstimiene et al.,2017; Shen et al.,2017). These bio-recognition elements immobilized onto the sensor surface, where various strategies are employed for the modification including adsorption and covalent attachments. In adsorption based technique, the bio-recognition moieties are adsorbed onto the electrode surface by means of physical forces (Banica,2012). Moreover, sometimes these are entrapped within the immobilization matrix, but such processes are not always preferred due to their tendency of leaching out during operation. To overcome such limitations, covalent modifications are adopted using various bio-conjugate techniques. The fundamental process of these techniques is the activation of bio-recognition elements and / or modified electrode surface (Chandra,2016; Chandra et al.,2017). In the second step, covalent coupling process is employed for constructing the probe, offering highly stable sensor surface compared to physically adsorbed or entrapment-based methods. So far, various such techniques are employed based on coupling reaction using carbodiimides, carbonyldiimide, *etc.*(Arya et al.,2011; Wan et al.,2010). In addition to these, silane, biotin–avidin, streptavidin–biotin cross-linkers are extensively used for immobilizing the bio-recognition elements covalently over the modified electrode surface (Fu et al.,2011; Kim et al.,2017; Shuai et al.,2017).

For the detailed characterization of various components of biosensors *viz.* nanomaterials, nanocomposites, engineered surfaces *etc.*, various techniques have been employed. UV–visible spectroscopy (UV–Vis) enables preliminary determination of the particles or nanomaterial formation (Verma et al.,2014). The appearance of characteristics absorption confirms the preparation of the nanomaterial; however, in some cases, the poor dispersion of nanomaterials in solution restricts this technique for the characterization, such as graphene-based nanomaterials. Excellently dispersible nanomaterials show a characteristics absorption maxima depending upon the constituents and size of the grain or particle (Plascencia-Villa et al.,2016). Furthermore, the correlational size dependencies can also be obtained using the UV–Vis characterization (Plascencia-Villa et al.,2016). However, the exact sizes and morphologies of nanomaterial and surface topology of the modified electrodes are investigated by the scanning electron microscopy, atomic force microscopy or transmission electron microscopy (Kumar and Kumbhat,2016). The size distribution of dispersible engineered nanomaterials can be characterized by dynamic light scattering (DLS), which categorizes the particles on the basis of their hydrodynamic sizes, where hydrodynamic size is the equivalent size of the dispersed nanomaterial with the layer of other constituents along with water above it (Pecora,2000). This size depends on the physical properties of colloidal solution including the viscosity, temperature, and diffusion coefficient. The surface charge on nanostructured materials is another important property, which is determined by measuring the zeta potential (Berne and Pecora,2000).

During the course of probe fabrication, these nanomaterials play an important role for covalent immobilization of the bio-recognition elements (Baranwal et al.,2016). For instance, gold nanoparticle-based probe fabrication requires a strong adsorption forces to adhere the electrode in order to prevent the leaching out effects (Chandra et al.,2013b). Alternatively, this has also been achieved by entrapping the particle inside various immobilizing matrices. The confirmation of presence and adherence of nanomaterial on to the probe surface can be confirmed by various surface characterization techniques, including Fourier transformed infrared spectroscopy, Raman spectroscopy, energy dispersive X-ray spectroscopy, elemental mapping, and X-ray photoelectron spectroscopy (XPS), where elemental and functional group details are obtained (Chung et al.,2018). Fundamentally, such techniques are based on identification of either chemical bond or elemental composition by exploiting various physical properties of the materials, which also help in characterizing the essential probe modification stages. Furthermore, electrical, and optical properties of materials are dependent on the crystal structures which has been defined as the crystallinity and is obtained by X-ray diffraction (XRD), as well as the selective area electron diffraction (SAED) (Tang and Ouyang,2007).

Apart from these techniques, electrochemical characterization of the probe has also been employed, where the probes were assessed after each level of modifications, using amperometric, voltammetric, impedance based techniques. In all cases, the significant change in signal confirms the successful probe modification (Bollella et al.,2017; Quan et al.,2006; Zhu et al.,2012b). In recent years, a number of nanomaterial assisted bio-sensing mechanisms are reported (Choudhary et al.,2016; Lan et al.,2017; Li et al.,2015; Lu et al.,2017; Zhu et al.,2012a). In context to this, a number of nanomaterials including nanoparticles and nanocomposites have been used (Lan et al.,2017; Li et al.,2015; Lu et al.,2017). For instance, gold, silver and platinum nanoparticles with/without surface modification have widely been explored to design biosensor for different clinically and industrially important analytes (Kashish et al.,2017; Li et al.,2010).

5. Analytical performance of biosensor:

The analytical performance of any biosensor is assessed by various parameters, including dynamic range, limit of detection, limit of quantification, selectivity, stability, reproducibility, self- life, and the capability of target detection in complex real sample matrices (Eggins,2008). The mathematical modeling for these studies is usually done with regression plot. In this model, regression line is drawn for the different intensities of signals with varying concentrations of the analyte (shown in Figure 1.4).

5.1. Linear dynamic range:

It is a range in the calibration plot, where signal is directly proportional to the concentrations of analyte. The wider the dynamic range, the greater will be the clinical significance, as more number of concentrations can be extrapolated by these values for quantitative detection.

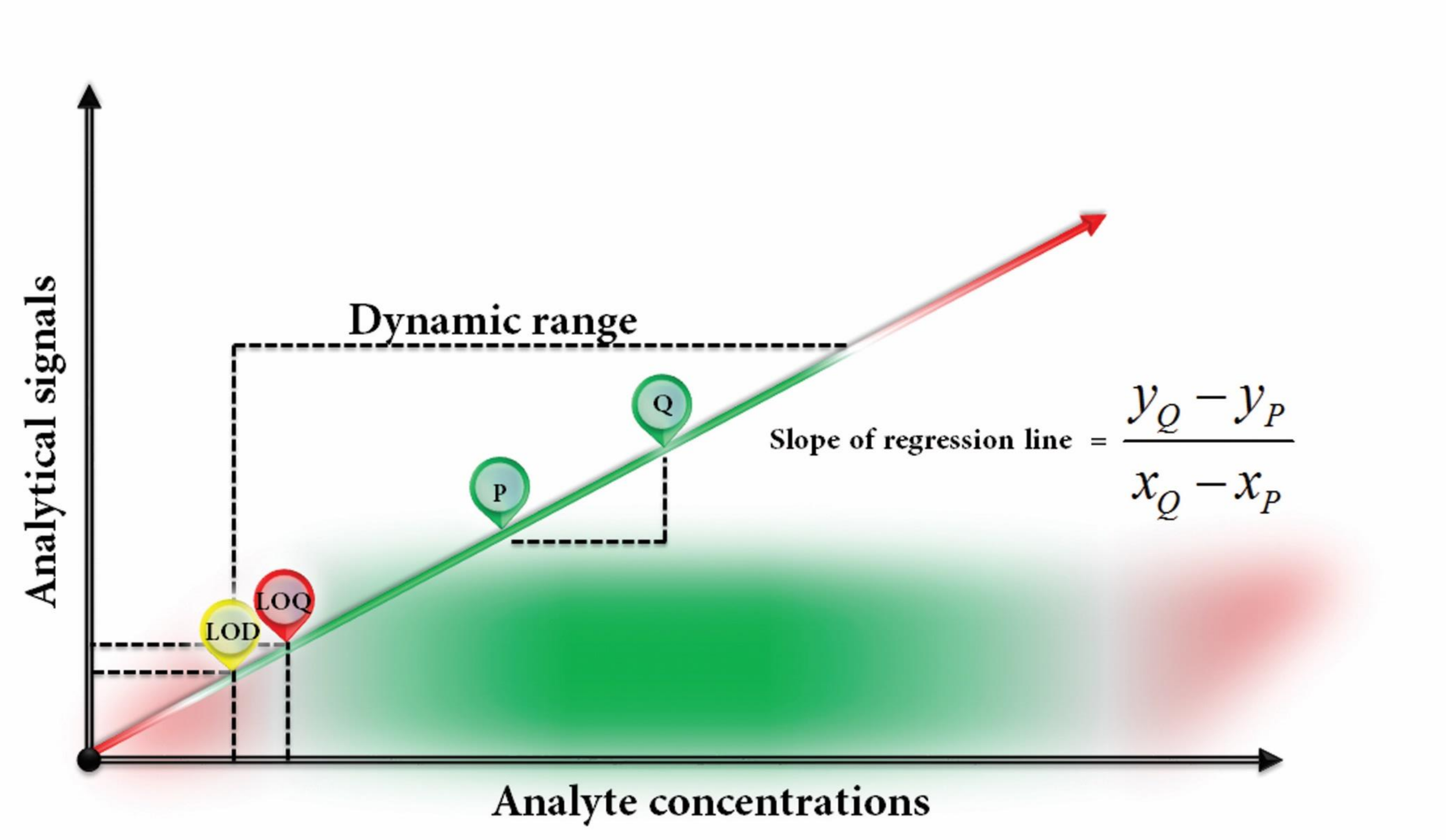

Figure 1.4: *Standard calibration plot used for calculating LOD, LOQ, Sensitivity and the dynamic range (reprinted with the permission of Mahato et.al., Springer Inc.).*

5.2. Limit of quantification (LOQ):

LOQ suggests that amount of analyte, which is detectable by the biosensors.

$$LOQ = \frac{10SD_{Blank}}{Slope} \text{ -- Equation 1.1}$$

Where LOQ is the limit of quantification; SD_{Blank} *is the standard deviation of blank and the slope signifies the sensitivity of probe for a particular analyte.*

5.3. Limit of detection (LOD):

The minimum amount of analyte that can be detected due to the biochemical reaction happening at the sensor surface. This is generally calculated by using the equation 1.2

$$LOD = \frac{3SD_{Blank}}{Slope} \text{ -- Equation 1.2}$$

Where LOD is the limit of detection, SD_{Blank} *is the standard deviation of blank and the slope signifies the sensitivity of probe for a particular analyte.*

5.4. Selectivity:

It is the most important criterion for the biosensor evaluation. It is the ability of biosensor for discriminating out the non-specific targets from the sample of analysis.

5.5. Shelf-life:

The working lifetime is related to the stability of biosensor, which usually depends on the retainment of activity of bio-recognition elements and life-time of the coupled transducers.

5.6. Sensitivity:

This is the property of a biosensor by virtue of which its responses to the fluctuation of analyte concentrations. It is defined by the slope of the regression line, where steeper slope signifies the relatively better sensitivity. This tells that the biosensor is capable of differentiating a small change due to the presence of target molecules very efficiently. The mathematical expression can be written as follows (equation 1.3).

$$Sensitivity \ = \ Slope\ of\ \ the\ regression\ line = \frac{y_Q - y_P}{x_Q - x_P}$$ ---------------- Equation 1.3

x_P, x_Q , y_P, *and* y_Q *are the coordinates of two points in the calibration plot, related to analyte concentrations and their corresponding signals.*

These parameters describe the analytical performance of the developed biosensors and help to analyze their suitability for various kind of applications including, biomedical, food safety, environmental monitoring *etc*.

6. Concept of surface engineering and importance of nanomaterials in biosensors:

Surface engineering is a most important step in sensor designing and their application in diverse matrices (Tiwari et al.,2016; Yüce and Kurt,2017). It involves the development of a stable and sensitive electrode surface by involving numerous modification steps including; wet chemistry approaches, nano-engineering, bio-conjugation, and signal amplification strategies (Chandra,2016). One of the major advantage of surface engineering is its tunability and optimization capability for the design and development of wide range of biosensors. Therefore, sensor surface development plays a pivotal role towards the commercial viability and tremendous analytical performance of biosensors.

Owing to the unique optical and electronic properties, nanomaterials have been used in biosensing systems to enhance their sensitivity by achieving the signal amplification (Ju,2011). Other properties *viz.* minuscule size, high surface area have added additional advantages for the immobilization of various recognition elements in greater extent. The incorporation of nanomaterials in the sensing matrices facilitates fast electron transfer between electrode and target, electro-catalysis, pre-concentration of analytes, and antifouling effects towards various interfering molecules (Merkoçi,2009). These unique characteristics of nanomaterials have been greatly explored, not only for the detection of small molecules based on direct electrochemistry but they are also well investigated for the detection of nucleotides, proteins, cells *etc.* Another role of nanomaterials in biosensor fabrication is to provide stable immobilization of the bio-recognition element to obtain higher sensitivity and amplified signal. Other aspects of the fabrication of biosensor is for downscaling the sensor to obtain miniaturized detection kits, which also requires various types of nanostructured materials and their composites. The major types of nanomaterials utilized in the development of various biosensor are shown in figure 1.5 (Mahato et al.,2018c). The synthesis of these nanomaterials are important aspects for their compatibility in biosensing application. Briefly, these nanomaterials can be synthesized by various ways: physical, chemical, and bio-mediated processes. Broadly, these approaches are classified under the top–down and bottom–up approaches (Baranwal et al.,2016). In the top–down approach, bulk materials are transformed into the nano-sized structures by means of mechanical attrition whereas, the bottom–up techniques follows synthetic processes. These syntheses show the addition of atoms followed by nucleation and thereafter ripening of the structures (Mahato et al.,2019). The major limitations to top–

down approach are the generation of surface defects on the nanostructures, which significantly alters the surface chemistry thereby making the nanostructures unsuitable for biosensing mechanisms

In the bottom–up strategies, such limitations are not reported; however, the time of syntheses is of utmost concern. Although, there are various practical problems related to both the strategies, yet nanomaterial designed by these approaches have been greatly applied in development of various nanocomposites, nanoscafolds, and their direct coating on to the electrode surface / support matrix for the development of biosensors.

7. Support matrices for biosensors:

The type of support matrices are selected based on the biosensing applications and signal transduction systems. These support matrices offers the surface to develop sensor probe / biosensor / detection zone. For instance, electrochemical biosensor requires the conducting support matrices, which should have the potential to facilitate the electron transfer at the electrode. Thus, to provide conductive matrices in cheaper cost carbon based materials / electrodes have been extensively used. In addition, for colorimetric based determination, the colorless matrices are desirable so that the matrix effects can be minimized in order to obtain the sensitive colorimetric detection.

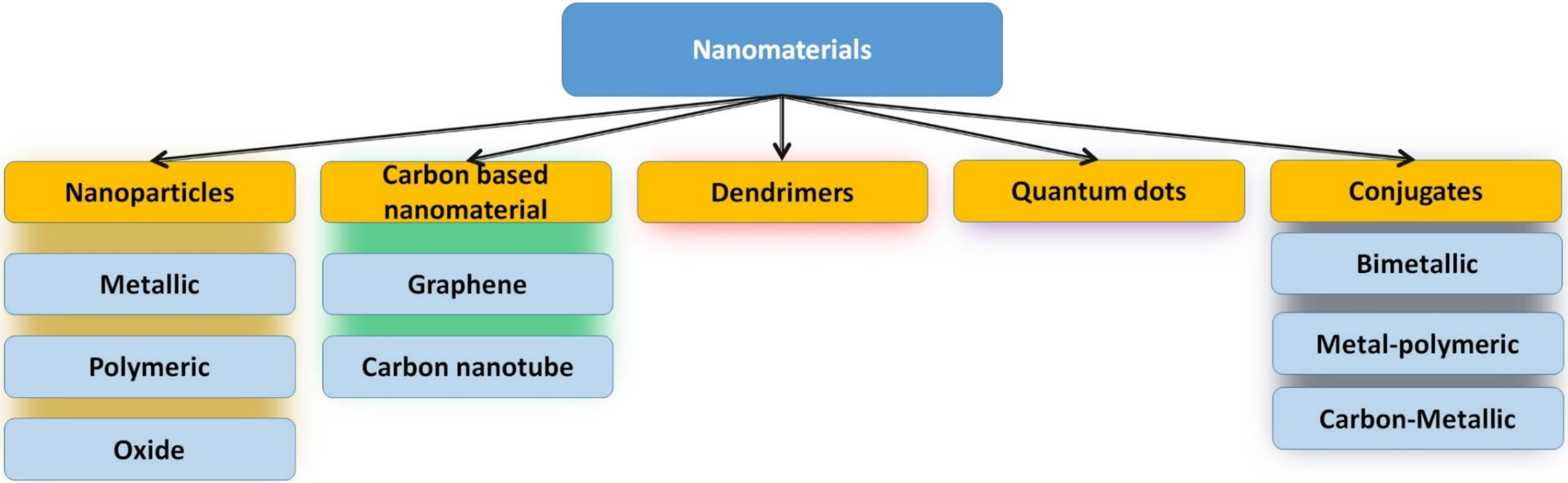

Figure 1.5: *Different types of nanomaterials used for biosensing application (reprinted with the permission of Mahato et.al., Springer Inc.).*

Moreover, the other factors including production dynamics and economics also plays an important role in the selection of matrix, where cheap and best suitable matrices are preferred. Therefore, various cheaper matrices are being used as the support materials for colorimetric and electrochemical based sensor probe fabrication *viz.* paper, thread, silk, carbon paste, glassy carbon *etc*. This section describes about the significance of various support matrices, which are cheaper and widely used for the low-cost biosensor developments.

7.1. Paper as support matrices:

Being an adequate and cheap matrix, it is widely used for delivering the low-cost disposable biosensors. Chemically, the composition of paper is cellulose a bio-polymer of glucose, and physically it is fibrous matrix, offering high porosity for the microfluidic wicking process. In context to the biosensor fabrication, this matrix can be used for the covalent or noncovalent immobilization of the bio-receptors. In the colorimetric format of biosensing, the white color background offers the naked eye detection (Mahato et al.,2017). Not only this, the paper matrices are also impregnated with various nanomaterials forming nano-paper electrode, which has been recently utilized for the electrochemical sensing of various molecules (Guo et al.,2018; Huang,2018).

7.2. Carbon paste as support matrix:

For the conducting matrices, carbon paste matrices / electrodes are of first choice due to their excellent reproducibility at probe fabrication and capability to offer higher sensitivity at relatively cheaper cost. Carbon paste based support materials consist of the graphite powder and pasting agent, which offers conductivity for electron flow, thus suitable for electrochemical determination. In order to improve the electron transfer they are often doped with metallic nanoparticles and conducting polymers (Noh et al.,2012). In addition, the final finished surfaces based on these support matrices are readily functionalized by depositing other nanomaterials coupled with bio-recognition element over its surface for selective analysis. Using the carbon paste, conventional and screen-printed electrodes are available for electrochemical biosensing applications.

7.3. Glassy carbon as support matrix:

Other most commonly used surfaces for biosensor design is the glassy carbon electrode, which is relatively more conducting, reproducible, and reusable compare to other electrodes (Zhang et al.,2016). The most important properties are high temperature resistance, hardness, low density, low electrical resistance, low friction, low thermal resistance, extreme resistance to chemical attack and impermeability to gases and liquids, which makes it widely acceptable for various electrochemical based sensing (McCreery,2008).

8. Techniques used for biosensors studies:

8.1. Techniques for sensor probe assessment:

The sensing probe is core component of any biosensor, which is responsible for the analytical performances. Thus, it is important to validate its fabrication for obtaining the optimum performances. These assessments of biosensors are also called as probe surface characterization, where the probes stability and determination capabilities are majorly analyzed. For example, if the biosensor is of electrochemical format, the electronic properties of the surface should be analyzed prior to the analysis of the target compound, whereas if the sensor probe is colorimetric, the color formation capabilities due to the biochemical reaction occurring at the sensor should be critically examined.

8.1.1. Colorimetric assessment:

The colorimetric biosensor relies on the color change at testing zone of the biosensor, which is usually facilitated by the catalytic capability of the sensor probe. Here, the catalysis of chromogenic substrate develops colorimetric signals at sensor surface. Using the colorimetric format, numbers of bioanalytical system have been reported by adopting the liquid based assays for quantification of target analytes. In addition, few attempts have also been given to build the sensing models with reagent-less yes / no systems by incorporating them in the dipstick and lateral flow formats. This section describes the major techniques used for the assessment of colorimetric biosensor.

8.1.1.1.Assessment based on spectrophotometer:

The UV-Visible range of electromagnetic spectrum has been used in such assessment to quantify the appearance / disappearance of the chromogenic substrate / product (Adiguzel,2017). In this technique, the functionality of testing probe is analyzed with the correlation of absorbance. For the assessment of proper probe fabrication, various controls are studied using UV-Vis spectra. For instance, Nirala et al. have reported a colorimetric biosensor based on molybdenum sulfide (MoS_2) nanocomposite coupled with the cholesterol oxidase as bio-recognition element where 3,3',5,5'-tetramethylbenzidine has been used as a chromogenic indicator molecule. Here, in the presence of cholesterol initiates the sensing reaction, where it was cleaved and produces hydrogen peroxide by the action of cholesterol oxidase, which was further decomposed in presence of MoS_2 to give the chromogenic reaction with 3,3',5,5'-tetramethylbenzidine. The sensing capability of probe was tested with gradual appearance of intense blue color which was then quantified using the absorbance at λ_{max} (652 nm) (Nirala et al.,2015).

8.1.1.2.Assessment based on digital image colorimetry:

This technique has been commonly employed to quantify the strip based colorimetric yes / no tests. Here, the color change at sensor surface is captured followed by the quantification of analytes using the correlation with change in color intensities. This analysis involves the acquisition of images of concentration dependent color changes and their analysis to obtain the correlation between colorimetric responses and concentrations of the target (Lin et al.,2018). The image analyses use grayscale, CMYK (cyan, magenta, yellow, and key/black), or RGB (red, green, and blue) based profiling systems, where RGB systems are widely accepted due to its simplicity (Soldat et al.,2009). Using the digital image colorimetry based techniques, a number of colorimetric biosensor systems have been reported. For instance, Lathwal and coworkers have reported malaria detection system using digital image colorimetry on paper strip following immuno-sensing (sandwich type) approach, where tagged HRP enzyme is employed for the colorimetric signal. The detection of target analyte (Plasmodium falciparum histidine-rich protein 2) was confirmed after its immuno-complexation with capture and reporter antibodies followed by the chromogenic signal development at the sensor surface. The colorimetric signal generation was obtained from HRP, hydrogen peroxide and 3,3',5,5'-tetramethylbenzidine system, which produces the blue color in presence of the target analyte (Lathwal and Sikes,2016). The color formation was then captured and digital image colorimetry based analysis using RGB system was performed to obtain quantifiable signals.

8.1.2. Electrochemical assessments of biosensor:

The electrochemical assessment of biosensors is done using classical three electrode system containing working, counter, and reference electrodes (Bard et al.,1980). For electrochemical biosensors, the electron transfer behavior and stability of the sensor probe plays an important role, which has been assessed by using various studies at the sensor surface. Rendles Sevcik and Brown Anson models are most widely accepted for the studying charge transfer behavior at electrode surface and interface(Eggins,2008). To study these models the voltammetric responses at every step of fabrication is recorded and the magnitude of anodic / cathodic peak currents (Ipa / Ipc) are utilized for further analysis to deduce the electron transfer properties at the modified surfaces. The stability of sensor and charge transfer dynamics at the surface are the other parameters, which are deduced by scan rate study. In addition, the electrochemical impedance spectroscopy has also been used for assessing the sensor probe, especially in case of deposition /functionalization of the sensing elements (Chandra,2016).

8.1.2.1. Electrochemical behavior assessment of sensor probe using voltammetry:

Voltammetric techniques are used for the assessment of electrochemical behavior of modified surfaces. This technique measures the electrochemical response of sensor surface when the voltage is applied (Compton and Banks,2011). In this case, the potential is varied to observe the oxidation / reduction of the electro-active molecules interacting at electrode surface. The commonly used mediator molecules are ruthenium hexacyanoferrate and Ferrocyanide / ferricyanide redox couples. In the voltammetric technique, potential is applied to the three electrode system and current responses are recorded, where the current responses come from the occurrence of redox activity at the interface. The strength of current responses in subsequent fabrication process tells about the behavior of the modified surface for its suitability in electrochemical determinations. For example, Zhang et al. have developed a sensor for simultaneous detection of dopamine, ascorbic acid and uric acid using poly(2-(N-morpholine)ethane sulfonic acid) / rGO modified electrode. Here, the increase in the current response was observed in subsequent fabrication process. This gradual increment tells about the increasing conductivity at the surface area on subsequent steps of probe fabrication, inferring that the sensing surface is capable of giving electrochemical signals (Zhang et al.,2018). These techniques are further categorized depending on the applied potential forms used *viz.* linear sweep voltammetry, cyclic voltammetry, differential pulse voltammetry *etc*.

8.1.2.2. Electrochemical behavior assessment of sensor probe using impedometry:

In above all methods, the electron flow or the developed charge at sensor surface is studied for obtaining the electrochemical responses (Orazem and Tribollet,2017). In impedometric technique, the insulating behavior of surface is used to assess the sensor probe fabrication and its analytical responses. Here, the varying alternating potential is employed to obtain the component of impedance *viz.* reactance, capacitance, and inductances (Bard et al.,1980; Eggins,2008). Using these obtained coordinates, the spectra are modeled, which consists of real and imaginary impedance values for studying the resistances in charge transfer at the electrode surface. The representation in this case is called Nyquist plot. Similarly, other plots have also been used including Bode plot, where the frequency dependent impedances are recorded for studying the insulating behavior of the sensor surface (Bard et al.,1980; Chandra,2016). For instance, a biosensor reported by Rushworth et al. for the specific detection of Alzheimer's amyloid-beta oligomers, where the sensing probe is analyzed by using impedometric method. Here, the increase in resistance to the surface charge transfer is observed on sequential addition of the probe components and the target molecule (Rushworth et al.,2014).

8.2. Techniques for real-sample analysis:

After the characterization of sensors and sensing capabilities assessments the analytical performances of the developed biosensors are analyzed. This is done by detecting the target molecules in various real sample matrices *viz.* beverages, blood serum, urine, saliva, tears *etc.* Sometimes, unavailability or complexity of clinical samples leads to inconsistencies in various levels in study. To overcome such issues, spike-recovery and standard addition methods have been employed over the years. These methods test the analytical performances in mimicked real samples, where these samples are prepared with the native interfering constituent molecules. The selection of the interfering analytes in mimicked samples is usually the coexisting molecules in the environment or similar structured molecules, which can potentially introduce interferences in detections.

8.2.1. Spike and recovery method:

In this method, the biosensor probe is analyzed for its interfering effects due to the presence of various unknown molecules present in real samples (Ravisankar et al.,2015). In this method, a known amount of the target analyte is taken and injected to the collected real samples and their recoveries were performed using fabricated biosensor.

The significantly lower level of recovered analyte levels infers a strong interference from the molecules present in the sample, which are limiting the performance of the sensor (Bhatnagar et al.,2018). If the recovery response is close to the spiked value, biosensing probe doesn't experience any hindrance from the matrices, whereas the significantly higher signals indicate the inherent presence of target analytes in the tested real sample. The mathematical calculation of % recovery and its interpretation is given below (equation 1.4)

$$\% \, Recovery = \frac{Observed - Neat}{Expected} \times 100$$ --------------------------------------- Equation 1.4

where "Observed" signifies the value of analyte concentration recorded after spiking of analyte; "Neat" signifies the value of analyte concentration present in sample before spiking. The "Expected" is exact concentration of analyte spiked into the sample.

8.2.2. Standard addition method:

In various real samples, the inherent presence of target analytes elevated the recovery percentages. In order to quantify the unknown levels of these inherently present concentrations, standard addition method is employed (Saxberg and Kowalski,1979). In this analysis, the sensor probe is used to obtain the unknown concentrations of the target present in the real sample matrices. By this assessment, the credibility of the biosensor is evaluated for its biomedical applications.

9. Objectives and goals of the study:

The objectives of this study are to achieve better sensitivity of biosensors by employing the surface engineering and nanomaterial assisted techniques. We have also tried to develop the sensor systems, which not just provide very wide dynamic ranges, but it actually detects the target molecule in industrially / clinically significant levels. At the same time, this thesis work is inclined to resolve the few griming issues, such as food safety and silent clinical diseases *viz.* hypo-vitaminosis, liver and bone diseases, and carcinoid syndromes. The work done in this thesis was aimed towards designing the miniaturized, deliverable, rapid and accurate biosensors for the ultrasensitive detection of clinical and food safety biomarkers utilizing novel engineered surfaces and nanomaterials.

The objectives are as follows:

Objective #1: Paper-based miniaturized immunosensor for naked eye ALP detection based on digital image colorimetry integrated with smartphone

Objective #2: Clinically comparable impedimetric determination of ALP based on electrochemically tuned Au-nanodendroids- graphene oxide nanocomposite in human serum

Objective #3: Development of miniaturized electrochemical nanobiosensor based on AuNPs-porous graphene-1,8-DAN for vitamin-C detection in juice, human urine, and neurodegenerative diseased mice brain

Objective #4: Novel electrochemical biosensor for serotonin detection based on gold nanorattles decorated reduced graphene oxide in biological fluids and *in vitro* model.

10. Thesis overview:

The overall study in the thesis is centered on the development of various biosensors by employing engineered surfaces and nanomaterials for obtaining the sensitive determination of analytes in bio-fluids. The entire study is sectioned into five chapters, where chapter I introduced the fundamental understanding of surface engineering, nanomaterials, and biosensors as discussed in the earlier sections. On the basis of the information in the literature we have designed four chapters (II - V) where various biosensors have been developed by utilizing novel surfaces and nano-biomaterials. In the chapter II, we have developed a colorimetric biosensor using an engineered paper surface, where the antibody has been covalently immobilized for the selective determination of the alkaline phosphatase in milk to assure the milk pasteurization process. In chapter III, we developed an electrochemical biosensor by incorporating nanomaterials for the sensitive determination of serum alkaline phosphatase in clinically relevant range. The chapter IV describes the development of biosensors based on porous nanomaterial and metal nanoparticles composite for ultrasensitive vitamin-C detection in various bio-fluids and mouse brain. In the chapter V, we have developed a biosensor by incorporating Au-nanorattles with reduced graphene oxide for the electrochemical determination of serotonin urine, blood serum, and *in vitro* model. A pictorial representation of the work carried out has been comprehensively described in figure 1.6

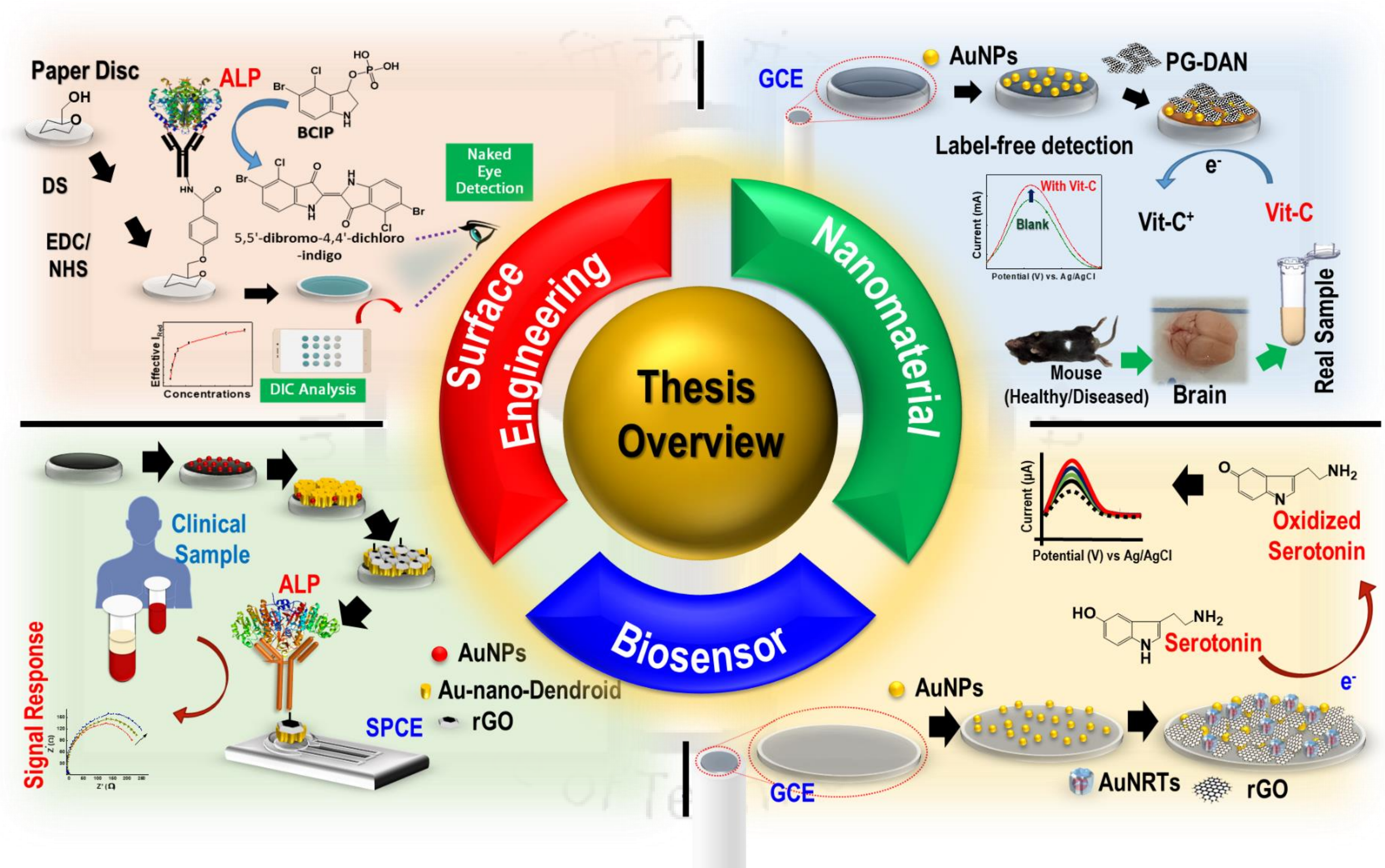

Figure 1.6: *Pictorial representation of the thesis work.*

11. References:

Adiguzel, Y., 2017. Biosensor with UV Spectrophotometric Detection. Multidisciplinary Digital Publishing Institute Proceedings, p. 113.

Aldewachi, H., Chalati, T., Woodroofe, M., Bricklebank, N., Sharrack, B., Gardiner, P., Gold nanoparticle-based colorimetric biosensors, ***2018***. *Nanoscale* 10(1), 18-33.

Amit, S.K., Uddin, M.M., Rahman, R., Islam, S.M.R., Khan, M.S., A review on mechanisms and commercial aspects of food preservation and processing, ***2017***. *Agriculture & Food Security* 6(1), 51.

Arya, S.K., Dey, A., Bhansali, S., Polyaniline protected gold nanoparticles based mediator and label free electrochemical cortisol biosensor, ***2011***. *Biosensors and Bioelectronics* 28(1), 166-173.

Ashmawy, N.H., Almehizia, A.A., Youssef, T.A., Amr, A.E.-G.E., Al-Omar, M.A., Kamel, A.H., Novel Carbon/PEDOT/PSS-Based Screen-Printed Biosensors for Acetylcholine Neurotransmitter and Acetylcholinesterase Detection in Human Serum, ***2019***. *Molecules* 24(8), 1539.

Banica, F.-G., 2012. Chemical sensors and biosensors: fundamentals and applications. John Wiley & Sons.

Baranwal, A., Mahato, K., Srivastava, A., Maurya, P.K., Chandra, P., Phytofabricated metallic nanoparticles and their clinical applications, ***2016***. *RSC Advances* 6(107), 105996-106010.

Bard, A.J., Faulkner, L.R., Leddy, J., Zoski, C.G., 1980. Electrochemical methods: fundamentals and applications. wiley New York.

Barh, D., Carpi, A., Verma, M., Gunduz, M., 2014. Cancer biomarkers: minimal and noninvasive early diagnosis and prognosis. CRC Press.

Berne, B.J., Pecora, R., 2000. Dynamic light scattering: with applications to chemistry, biology, and physics. Courier Corporation.

Bhatnagar, I., Mahato, K., Ealla, K.K.R., Asthana, A., Chandra, P., Chitosan stabilized gold nanoparticle mediated self-assembled gliP nanobiosensor for diagnosis of Invasive Aspergillosis, ***2018***. *International Journal of Biological Macromolecules* 110, 449-456.

Bollella, P., Schulz, C., Favero, G., Mazzei, F., Ludwig, R., Gorton, L., Antiochia, R., Green Synthesis and Characterization of Gold and Silver Nanoparticles and their Application for Development of a Third Generation Lactose Biosensor, ***2017***. *Electroanalysis* 29(1), 77-86.

Cevik, E., Cerit, A., Gazel, N., Yildiz, H.B., Construction of an Amperometric Cholesterol Biosensor Based on DTP(aryl)aniline Conducting Polymer Bound Cholesterol Oxidase, ***2018***. *Electroanalysis* 30(10), 2445-2453.

Chandra, P., 2016. Nanobiosensors for Personalized and Onsite Biomedical Diagnosis. IET.

Chandra, P., Noh, H.-B., Shim, Y.-B., Cancer cell detection based on the interaction between an anticancer drug and cell membrane components, ***2013a***. *Chemical Communications* 49(19), 1900-1902.

Chandra, P., Singh, J., Singh, A., Srivastava, A., Goyal, R.N., Shim, Y.B., Gold Nanoparticles and Nanocomposites in Clinical Diagnostics Using Electrochemical Methods, ***2013b***. *Journal of Nanoparticles* 2013, 12.

Chandra, P., Tan, Y.N., Singh, S.P., 2017. Next generation point-of-care biomedical sensors technologies for cancer diagnosis. Springer.

Chandra, P., Zaidi, S.A., Noh, H.-B., Shim, Y.-B., Separation and simultaneous detection of anticancer drugs in a microfluidic device with an amperometric biosensor, ***2011***. *Biosensors and Bioelectronics* 28(1), 326-332.

Choudhary, M., Yadav, P., Singh, A., Kaur, S., Ramirez-Vick, J., Chandra, P., Arora, K., Singh, S.P., CD 59 Targeted Ultrasensitive Electrochemical Immunosensor for Fast and Noninvasive Diagnosis of Oral Cancer, ***2016***. *Electroanalysis* 28(10), 2565-2574.

Chung, S., Chandra, P., Koo, J.P., Shim, Y.-B., Development of a bifunctional nanobiosensor for screening and detection of chemokine ligand in colorectal cancer cell line, ***2018***. *Biosensors and Bioelectronics* 100, 396-403.

Compton, R.G., Banks, C.E., 2011. Understanding voltammetry. World Scientific.

Dagdeviren, C., Joe, P., Tuzman, O.L., Park, K.-I., Lee, K.J., Shi, Y., Huang, Y., Rogers, J.A., Recent progress in flexible and stretchable piezoelectric devices for mechanical energy harvesting, sensing and actuation, ***2016***. *Extreme Mechanics Letters* 9, 269-281.

Damborský, P., Švitel, J., Katrlík, J., Optical biosensors, ***2016***. *Essays in biochemistry* 60(1), 91-100.

Eggins, B.R., 2008. Chemical sensors and biosensors. John Wiley & Sons.

Eggins, B.R., 2013. Biosensors: an introduction. Springer-Verlag.

Fu, G., Yue, X., Dai, Z., Glucose biosensor based on covalent immobilization of enzyme in sol–gel composite film combined with Prussian blue/carbon nanotubes hybrid, ***2011***. *Biosensors and Bioelectronics* 26(9), 3973-3976.

Garcia-Aloy, M., Hulshof, P.J., Estruel-Amades, S., Osté, M.C., Lankinen, M., Geleijnse, J.M., De Goede, J., Ulaszewska, M., Mattivi, F., Bakker, S.J., Biomarkers of food intake for nuts and vegetable oils: an extensive literature search, ***2019***. *Genes & nutrition* 14(1), 7.

Godfray, H.C.J., Beddington, J.R., Crute, I.R., Haddad, L., Lawrence, D., Muir, J.F., Pretty, J., Robinson, S., Thomas, S.M., Toulmin, C., Food Security: The Challenge of Feeding 9 Billion People, ***2010***. *Science* 327(5967), 812.

Guo, Y., Fang, Z., Du, M., Yang, L., Shao, L., Zhang, X., Li, L., Shi, J., Tao, J., Wang, J., Li, H., Fang, Y., Flexible and biocompatible nanopaper-based electrode arrays for neural activity recording, ***2018***. *Nano Research* 11(10), 5604-5614.

Henry, N.L., Hayes, D.F., Cancer biomarkers, ***2012***. *Molecular Oncology* 6(2), 140-146.

Huang, W., 2018. Graphene Oxide Nanopapers. Nanopapers, pp. 1-26. Elsevier.

Hwang, K.S., Lee, S.-M., Kim, S.K., Lee, J.H., Kim, T.S., Micro- and Nanocantilever Devices and Systems for Biomolecule Detection, ***2009***. *Annual Review of Analytical Chemistry* 2(1), 77-98.

Jayanthi, V.S.P.K.S.A., Das, A.B., Saxena, U., Fabrication of an immunosensor for quantitative detection of breast cancer biomarker UBE2C, ***2019***. *RSC Advances* 9(29), 16738-16745.

Ju, H., Sensitive biosensing strategy based on functional nanomaterials, ***2011***. *Science China Chemistry* 54(8), 1202.

Kashish, Bansal, S., Jyoti, A., Mahato, K., Chandra, P., Prakash, R., Highly Sensitive in vitro Biosensor for Enterotoxigenic Escherichia coli Detection Based on ssDNA Anchored on PtNPs-Chitosan Nanocomposite, ***2017***. *Electroanalysis* 29(11), 2665-2671.

Kausaite-Minkstimiene, A., Simanaityte, R., Ramanaviciene, A., Glumbokaite, L., Ramanavicius, A., Reagent-less amperometric glucose biosensor based on a graphite rod electrode layer-by-layer modified with 1,10-phenanthroline-5,6-dione and glucose oxidase, ***2017***. *Talanta* 171, 204-212.

Kim, S.H., Shin, K.-H., Moon, S.-H., Jang, J., Kim, H.S., Suh, J.-S., Yang, W.-I., Reassessment of alkaline phosphatase as serum tumor marker with high specificity in osteosarcoma, ***2017***. *Cancer medicine* 6(6), 1311-1322.

Kotsanopoulos, K.V., Arvanitoyannis, I.S., The role of auditing, food safety, and food quality standards in the food industry: A review, ***2017***. *Comprehensive reviews in food science and food safety* 16(5), 760-775.

Kumar, N., Kumbhat, S., 2016. Characterization Tools for Nanomaterials. Essentials in Nanoscience and Nanotechnology, pp. 77-148. John Wiley & Sons, Inc.

Lan, L., Yao, Y., Ping, J., Ying, Y., Recent advances in nanomaterial-based biosensors for antibiotics detection, ***2017***. *Biosensors and Bioelectronics* 91(Supplement C), 504-514.

Laskowitz, D.T., Kasner, S.E., Saver, J., Remmel, K.S., Jauch, E.C., Group, B.S., Clinical usefulness of a biomarker-based diagnostic test for acute stroke: the Biomarker Rapid Assessment in Ischemic Injury (BRAIN) study, ***2009***. *Stroke* 40(1), 77-85.

Lathwal, S., Sikes, H.D., Assessment of colorimetric amplification methods in a paper-based immunoassay for diagnosis of malaria, ***2016***. *Lab on a Chip* 16(8), 1374-1382.

Li, N., Su, X., Lu, Y., Nanomaterial-based biosensors using dual transducing elements for solution phase detection, ***2015***. *Analyst* 140(9), 2916-2943.

Li, Y., Schluesener, H.J., Xu, S., Gold nanoparticle-based biosensors, ***2010***. *Gold Bulletin* 43(1), 29-41.

Ligler, F.S., Taitt, C.R., 2011. Optical biosensors: today and tomorrow. Elsevier.

Lin, B., Yu, Y., Cao, Y., Guo, M., Zhu, D., Dai, J., Zheng, M., Point-of-care testing for streptomycin based on aptamer recognizing and digital image colorimetry by smartphone, ***2018***. *Biosensors and Bioelectronics* 100, 482-489.

Lu, S., Yu, T., Wang, Y., Liang, L., Chen, Y., Xu, F., Wang, S., Nanomaterial-based biosensors for measurement of lipids and lipoproteins towards point-of-care of cardiovascular disease, ***2017***. *Analyst* 142(18), 3309-3321.

Mahato, K., Baranwal, A., Srivastava, A., Maurya, P.K., Chandra, P., 2016. Smart materials for biosensing applications. Techno-Societal 2016, International Conference on Advanced Technologies for Societal Applications, pp. 421-431. Springer.

Mahato, K., Kumar, A., Maurya, P.K., Chandra, P., Shifting paradigm of cancer diagnoses in clinically relevant samples based on miniaturized electrochemical nanobiosensors and microfluidic devices, ***2018a***. *Biosensors and Bioelectronics* 100, 411-428.

Mahato, K., Kumar, S., Srivastava, A., Maurya, P.K., Singh, R., Chandra, P., 2018b. Electrochemical Immunosensors: Fundamentals and Applications in Clinical Diagnostics. Handbook of Immunoassay Technologies, pp. 359-414. Elsevier.

Mahato, K., Maurya, P.K., Chandra, P., Fundamentals and commercial aspects of nanobiosensors in point-of-care clinical diagnostics, ***2018c***. *3 Biotech* 8(3), 149.

Mahato, K., Nagpal, S., Shah, M.A., Srivastava, A., Maurya, P.K., Roy, S., Jaiswal, A., Singh, R., Chandra, P., Gold nanoparticle surface engineering strategies and their applications in biomedicine and diagnostics, ***2019***. *3 Biotech* 9(2), 57.

Mahato, K., Srivastava, A., Chandra, P., Paper based diagnostics for personalized health care: Emerging technologies and commercial aspects, ***2017***. *Biosensors and Bioelectronics* 96, 246-259.

Matos, I.d.O., Alves, W.A., Electrochemical Determination of Dopamine Based on Self-Assembled Peptide Nanostructure, ***2011***. *ACS Applied Materials & Interfaces* 3(11), 4437-4443.

McCreery, R.L., Advanced carbon electrode materials for molecular electrochemistry, ***2008***. *Chemical reviews* 108(7), 2646-2687.

McNally, S., Global population explosion: economic and health meltdown, ***2013***. *J R Soc Med* 106(2), 38-39.

McNaught, A.D., McNaught, A.D., 1997. Compendium of chemical terminology. Blackwell Science Oxford.

Merkoçi, A., 2009. Biosensing using nanomaterials. John Wiley & Sons.

Meyer, P.W., Biomarkers and genes predictive of disease predisposition and prognosis in rheumatoid arthritis, ***2012***. *Continuing Medical Education* 30(8), 286-290.

Nalejska, E., Mączyńska, E., Lewandowska, M.A., Prognostic and predictive biomarkers: tools in personalized oncology, ***2014***. *Molecular diagnosis & therapy* 18(3), 273-284.

Newman, J.D., Turner, A.P., Biosensors: principles and practice, ***1992***. *Essays in biochemistry* 27, 147-159.

Nirala, N.R., Pandey, S., Bansal, A., Singh, V.K., Mukherjee, B., Saxena, P.S., Srivastava, A., Different shades of cholesterol: Gold nanoparticles supported on MoS2 nanoribbons for enhanced colorimetric sensing of free cholesterol, ***2015***. *Biosensors and Bioelectronics* 74, 207-213.

Noh, H.-B., Chandra, P., Kim, Y.-J., Shim, Y.-B., A Simple Separation Method with a Microfluidic Channel Based on Alternating Current Potential Modulation, ***2012***. *Analytical Chemistry* 84(22), 9738-9744.

Orazem, M.E., Tribollet, B., 2017. Electrochemical impedance spectroscopy. John Wiley & Sons.

Organization, W.H., 2015. World health statistics 2015. World Health Organization.

Pakapongpan, S., Poo-arporn, R.P., Self-assembly of glucose oxidase on reduced graphene oxide-magnetic nanoparticles nanocomposite-based direct electrochemistry for reagentless glucose biosensor, ***2017***. *Materials Science and Engineering: C* 76, 398-405.

Palchetti, I., Mascini, M., 2010. Biosensor Technology: A Brief History. In: Malcovati, P., Baschirotto, A., d'Amico, A., Natale, C. (Eds.), Sensors and Microsystems, pp. 15-23. Springer Netherlands, Dordrecht.

Pallela, R., Chandra, P., Noh, H.-B., Shim, Y.-B., An amperometric nanobiosensor using a biocompatible conjugate for early detection of metastatic cancer cells in biological fluid, ***2016***. *Biosensors and Bioelectronics* 85, 883-890.

Pecora, R., Dynamic light scattering measurement of nanometer particles in liquids, ***2000***. *Journal of nanoparticle research* 2(2), 123-131.

Pinu, F.R., Early detection of food pathogens and food spoilage microorganisms: Application of metabolomics, ***2016***. *Trends in Food Science & Technology* 54, 213-215.

Plascencia-Villa, G., Demeler, B., Whetten, R.L., Griffith, W.P., Alvarez, M., Black, D.M., José-Yacamán, M., Analytical Characterization of Size-Dependent Properties of Larger Aqueous Gold Nanoclusters, ***2016***. *The Journal of Physical Chemistry C* 120(16), 8950-8958.

Prasad, A., Mahato, K., Chandra, P., Srivastava, A., Joshi, S.N., Maurya, P.K., Bioinspired Composite Materials: Applications in Diagnostics and Therapeutics, ***2016***. *Journal of Molecular and Engineering Materials* 04(01), 1640004.

Quan, D., Min, D.G., Cha, G.S., Nam, H., Electrochemical characterization of biosensor based on nitrite reductase and methyl viologen co-immobilized glassy carbon electrode, ***2006***. *Bioelectrochemistry* 69(2), 267-275.

Rateni, G., Dario, P., Cavallo, F., Smartphone-based food diagnostic technologies: a review, ***2017***. *Sensors* 17(6), 1453.

Ravisankar, P., Navya, C.N., Pravallika, D., Sri, D.N., A review on step-by-step analytical method validation, ***2015***. *International Organization of Scientific Research (IOSR) Journal of Pharmacy* 5(10).

Rushworth, J.V., Ahmed, A., Griffiths, H.H., Pollock, N.M., Hooper, N.M., Millner, P.A., A label-free electrical impedimetric biosensor for the specific detection of Alzheimer's amyloid-beta oligomers, ***2014***. *Biosensors and Bioelectronics* 56, 83-90.

Sang, S., Wang, Y., Feng, Q., Wei, Y., Ji, J., Zhang, W., Progress of new label-free techniques for biosensors: a review, ***2016***. *Critical reviews in biotechnology* 36(3), 465-481.

Saxberg, B.E.H., Kowalski, B.R., Generalized standard addition method, ***1979***. *Analytical Chemistry* 51(7), 1031-1038.

Shan, J., Ma, Z., A review on amperometric immunoassays for tumor markers based on the use of hybrid materials consisting of conducting polymers and noble metal nanomaterials, ***2017***. *Microchimica Acta* 184(4), 969-979.

Sharma, L.L., Teret, S.P., Brownell, K.D., The food industry and self-regulation: standards to promote success and to avoid public health failures, ***2010***. *American journal of public health* 100(2), 240-246.

Shen, X., Xia, X., Du, Y., Ye, W., Wang, C., Amperometric glucose biosensor based on aupd modified reduced graphene oxide/polyimide film with glucose oxidase, ***2017***. *Journal of The Electrochemical Society* 164(6), B285-B291.

Shuai, H.-L., Huang, K.-J., Chen, Y.-X., Fang, L.-X., Jia, M.-P., Au nanoparticles/hollow molybdenum disulfide microcubes based biosensor for microRNA-21 detection coupled with duplex-specific nuclease and enzyme signal amplification, ***2017***. *Biosensors and Bioelectronics* 89, 989-997.

Soldat, D.J., Barak, P., Lepore, B.J., Microscale Colorimetric Analysis Using a Desktop Scanner and Automated Digital Image Analysis, ***2009***. *Journal of Chemical Education* 86(5), 617.

Speidel, J.J., Environment and health: 1. Population, consumption and human health, ***2000***. *CMAJ* 163(5), 551-556.

Stamatakis, E., Ekelund, U., Ding, D., Hamer, M., Bauman, A.E., Lee, I.-M., Is the time right for quantitative public health guidelines on sitting? A narrative review of sedentary behaviour research paradigms and findings, ***2019***. *British Journal of Sports Medicine* 53(6), 377-382.

Strianese, M., Staiano, M., Ruggiero, G., Labella, T., Pellecchia, C., D'Auria, S., 2012. Fluorescence-Based Biosensors. In: Bujalowski, W.M. (Ed.), Spectroscopic Methods of Analysis: Methods and Protocols, pp. 193-216. Humana Press, Totowa, NJ.

Tamayo, J., Kosaka, P.M., Ruz, J.J., San Paulo, Á., Calleja, M., Biosensors based on nanomechanical systems, ***2013***. *Chemical Society Reviews* 42(3), 1287-1311.

Tang, Y., Ouyang, M., Tailoring properties and functionalities of metal nanoparticles through crystallinity engineering, ***2007***. *Nature Materials* 6, 754.

Tiwari, A., Wang, R., Wei, B., 2016. Advanced Surface Engineering Materials. John Wiley & Sons.

Üzer, A., Durmazel, S., Erçağ, E., Apak, R., Determination of hydrogen peroxide and triacetone triperoxide (TATP) with a silver nanoparticles—based turn-on colorimetric sensor, ***2017***. *Sensors and Actuators B: Chemical* 247, 98-107.

Verma, H.N., Praveen, S., Chavan, R., Gold nanoparticle: synthesis and characterization, ***2014***. *Veterinary world* 7(2), 72-77.

Wan, D., Yuan, S., Li, G.L., Neoh, K.G., Kang, E.T., Glucose Biosensor from Covalent Immobilization of Chitosan-Coupled Carbon Nanotubes on Polyaniline-Modified Gold Electrode, ***2010***. *ACS Applied Materials & Interfaces* 2(11), 3083-3091.

Yüce, M., Kurt, H., How to make nanobiosensors: surface modification and characterisation of nanomaterials for biosensing applications, ***2017***. *RSC Advances* 7(78), 49386-49403.

Zhang, K., Zhang, N., Zhang, L., Wang, H., Shi, H., Liu, Q., Simultaneous voltammetric detection of dopamine, ascorbic acid and uric acid using a poly(2-(N-morpholine)ethane sulfonic acid)/RGO modified electrode, ***2018***. *RSC Advances* 8(10), 5280-5285.

Zhang, W., Zhu, S., Luque, R., Han, S., Hu, L., Xu, G., Recent development of carbon electrode materials and their bioanalytical and environmental applications, ***2016***. *Chemical Society Reviews* 45(3), 715-752.

Zhu, Y., Chandra, P., Ban, C., Shim, Y.-B., Electrochemical Evaluation of Binding Affinity for Aptamer Selection Using the Microarray Chip, ***2012a***. *Electroanalysis* 24(5), 1057-1064.

Zhu, Y., Chandra, P., Shim, Y.-B., Ultrasensitive and selective electrochemical diagnosis of breast cancer based on a hydrazine–Au nanoparticle–aptamer bioconjugate, ***2012b***. *Analytical chemistry* 85(2), 1058-1064.

Ziegler, A., Koch, A., Krockenberger, K., Großhennig, A., Personalized medicine using DNA biomarkers: a review, ***2012***. *Human genetics* 131(10), 1627-1638.

Chapter- II

Paper-based miniaturized immuno-sensor for naked eye ALP detection based on digital image colorimetry integrated with smartphone

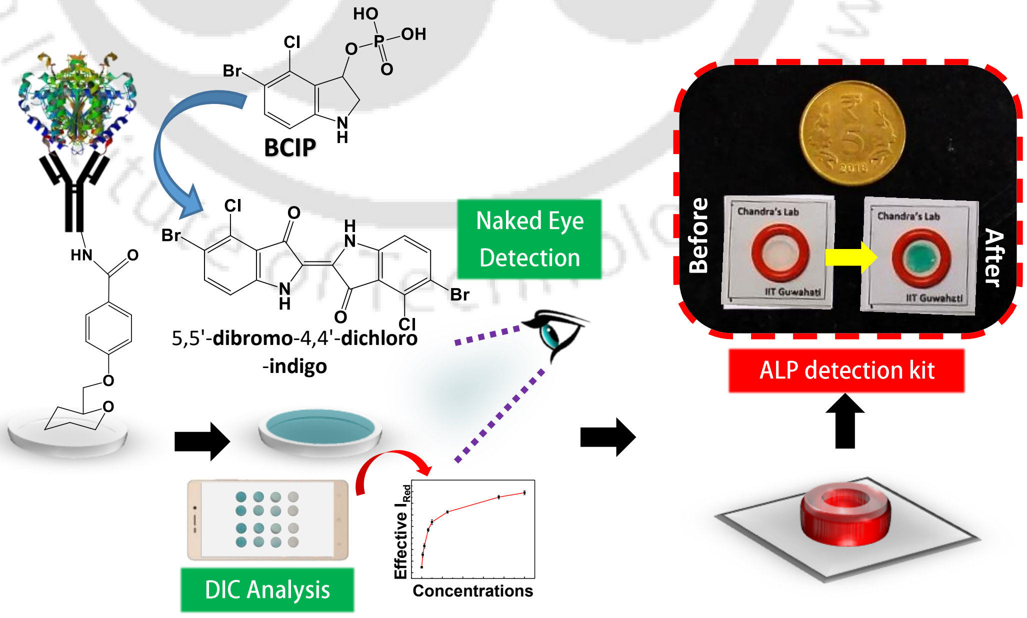

1. Introduction:

Here, our aim was to fabricate a biosensor based on engineered surface. For that, we have incorporated chemically modified surface for the immobilization of bio-recognition elements. During the study, the selection of the target analyte was done to address the problems of milk quality assessment, which is a griming socio-economic challenge, especially in the developing countries including India. As the milk is an adequate stable food ingredient enriched with high amount of proteins, carbohydrates, fats, vitamins, calcium, and phosphorus, it has been commercially accepted for revenue generation since long (Gaucheron,2011). The milk quality and its freshness have been a major concern, as the post-milking invasion of microbes causes sourness and are capable of harboring pathogenic bacteria, which not only downgrades the taste and quality of the milk, but also adds high chances of food borne diseases if consumed (Jay-Russell,2010; Klinger and Rosenthal,1997). In industries, raw milk is processed through pasteurization to kill the pathogenic microbes, which is an important step to maintain / extend the shelf-life of milk. To ensure the effective pasteurization, several methods, including methylene blue, phenol-based tests (Fasken and McClure,1940), and microbial culturing are commonly used in the quality control centers of various industries (Nayak,2018; Panigrahi et al.,2018; Yalcin and Atasever,2018). In methylene blue (MB) based tests, the dye is used as the redox indicator, which is injected into the milk samples followed by heat treatment and kept until the appearance of color change and therefore it takes 30 minutes to 480 minutes for the assessment depending on the milk samples (Barkworth and Hosking,1952). Due to its time-consuming process, it is not always preferred in the quality controls, especially where the number of samples are very large. Additionally, the commercial phenol-based tests utilizes the modified Scharer's colorimetric method, where liberated phenol is measured with the help of an indicator 2,6-dibromoquinonechloroimide (Payne and Wilbey,2009;

Scharer,1938) These tests requires sophisticated spectrophotometers and involves multistep procedure, which restricting them for onsite detection. Tests based on the microbial culture requires special laboratory facility and usually takes longer time for analysis. Limitations associated to these conventional testing procedures makes them non-robust and unsuitable for the assessment in miniaturized settings for determination at the point of collection, which is foremost need to ensure the quality of milk. Therefore, it is important and would be interesting to attempt a new biomarker-based method to differentiate the pasteurized and raw milk utilizing advanced bioengineering approaches.

Among various indicators of pasteurization and good quality milk, ALP, a metalloenzyme is widely targeted because of its heat resistant property, which has close destruction point to the killing temperature of pathogenic microbes (Rankin et al.,2010; Soares et al.,2013). Moreover, considerably high concentrations of ALP is found in raw milk, which denatures after the pasteurization process (Rankin et al.,2010), hence in an ideal situation the pasteurized milk should be devoid of ALP. Additionally, it has also been reported that in case of mastitis the ALP concentration in milk is tremendously high (Babaei et al.,2007; Kitchen,1981). Therefore, processing of such milk in industry requires special attention, and to do so, the detection of ALP in raw and pasteurized milk has tremendous commercial as well as health interest. In view of such importance of ALP in milk, several attempts have been taken to detect the ALP by various approaches; including spectroscopic (Al-Qadiri et al.,2008), fluorimetric (Kulmyrzaev et al.,2005; Rola and Sosnowski,2010), electrochemical (Ito et al.,2000; Serra et al.,2005), electro-chemi-luminescence (Park et al.,2011), and ELISA (Chen et al.,2006). Despite of their recognizable detection performance in native milk; multistep nature, requirement of sophisticated bulky analytical instruments as well as trained personnel, limits their usage in remote settings and in home kitchens. Therefore, development of a new user-friendly and economical method for ALP detection is of great interest. In order to develop such miniaturize devices, various research and development activities have been performed in recent past to introduce a portable testing kits (Chandan et al.,2015).

Among all types of testing kits, paper-based detection systems have found commercial interest because of their low-cost, adequate availability, and environment-friendly nature (Mahato et al.,2017). A paper-based approach has rarely been attempted for the detection of ALP in milk samples. In one such approach, ALP has been detected based on a colorimetric lateral flow assay (LFA) (Yu et al.,2015), which sometime suffers due to the irregularities in porosity causing interruption in flow of target molecule in the paper matrix due to the clogging of pores (Hosseini et al.,2017). This method based on LFA relies on the indirect ALP detection using adsorbed antibodies in the sensing matrix (Yu et al.,2015). The adsorbed antibodies in a sensing matrix are not homogeneously oriented compared to antibodies those are immobilized on to the surface using various conjugation methods (Tajima et al.,2011; Trilling et al.,2013). This may eventually compromise the analytical performance of biosensors. Therefore, it is extremely important to have stable and well oriented immobilization of antibodies onto the paper matrix and a dot-spot-based sensor chip. Stable immobilization of antibody retaining its biological activity can be achieved through conventional covalent immobilization processes (Akhtar et al.,2018; Chandra et al.,2012). Apart from this, the paper-based onsite colorimetric detections are mostly qualitative / semi-quantitative in nature (Yetisen et al.,2013), therefore several attempts have been given to quantify the "yes/no" signals, but the usage of additional analyzer confines the applicability of these in limited resources. Recent paradigm has been shifted toward the elimination of such dedicated analyzers and thus, smartphone being an omnipresent self-sufficient device has recently found the global attention for personalized analyses. A technique based on the image analysis also called DIC, that have gained attention for quantitative colorimetric estimations, which is one of the rapidly emerging robust technique (Rateni et al.,2017). Fundamentally, the DIC is based on image acquisition and its processing to obtain the quantifiable data-points, where former is performed by digital camera and latter is done with the help of analyzer software or smartphone-based application (Rateni et al.,2017). The digital images of color changing object are recorded and thereby the pixel values of these images are extracted for DIC analyses using 8-bit convention, which is universally accepted for the image analysis. According to this convention, colored image consists of three primary color channels, where 256 (0-255) unit pixel values are allocated of every primary color for the different shades *i.e.* red (R), green (G), and blue (B) (Choodum et al.,2017; Parkin,2016), which vary on the intensity and color change. Using these unit pixel values, one can obtain the calibration plot for almost every dose dependent colorimetric changes for biomolecular analysis (Lin et al.,2018; Peng et al.,2017).

In view of these, we have developed a very simple, onsite, quantitative detection of ALP using DIC-based paper sensor in milk. For that, an office punch crafted filter paper discs were used to fabricate sensing probe to obtain the naked eye ALP detection. The sensor-probe was fabricated by functionalizing paper discs for the covalent immobilization of Anti-ALP. The step-by-step characterization of the sensor-probe was evaluated by FTIR and DIC. The analytical signals were obtained based on the reaction between ALP bound sensor-probe and BCIP generating quantifiable blue-green precipitate, which were further processed using smartphone to obtain the quantitative results. Direct detection of ALP in commercial as well as raw milk obtained from the villages were performed using standard addition and spike-recovery methods. The selectivity and shelf-life of the developed biosensor was examined to evaluate its real market potential. Finally, a miniaturized prototype was developed for ALP detection to establish the direct in-kitchen household applicability of the designed biosensor.

2. Experimental:

2.1. Materials, apparatus, and reagent preparation:

ALP was procured from Roche, USA and anti-ALP, BCIP & p-nitrobenzoic acid ($C_7H_5NO_4$) were purchased from Sigma Aldrich, USA. Ascorbic acid ($C_6H_8O_6$), 1-(3 dimethylaminopropyl) 3-ethyl carbodiimide hydrochloride (EDC: $C_8H_{17}N_3.HCl$), sodium nitrite ($NaNO_2$), disodium hydrogen phosphate (Na_2HPO_4), potassium dihydrogen phosphate (KH_2PO_4), sodium chloride (NaCl), zinc chloride ($ZnCl_2$), calcium chloride ($CaCl_2$), casein hydrolysate, Magnesium chloride ($MgCl_2$), serum albumin (BSA), lactose, citric acid, potassium chloride (KCl) and n-hydroxysuccinimide (NHS: $C_4H_5NO_3$) were purchased from SRL India. The Whatman filter paper (grade 1) was procured from Whatman Inc., Merck-Millipore, USA. Vitamin A and vitamin B capsules were procured from Pfizer, USA. Tween-20 and tris-HCl were procured from Hi-media, USA. All the chemicals in the experiment have been used were of analytical grade.

All images of the paper discs have taken by the smartphone camera and its detailed specification has been indicated in table 2.1. Office paper punching machine (Kangaro ® 500; India) was used to obtain the paper discs of same size. The characterization of modified paper surfaces has been done with Fourier transformed infrared spectroscopy (FTIR) (Model: make: Perkin Elmer, USA) and Atomic force microscopy (AFM) (Model: Innova SPM Make: Bruker).

Features	Specification
Camera pixel	12 x 10^6
Make (model)	Xiaomi (Redmi 3s Prime)
F stop	f/2
Exposure time	1/50 sec
ISO speed	ISO-125
Color representation	RGB
Flash	No flash used
White balance	Auto
Camera and object distance (Image acquisition height)	32 centimeters

Table 2.1: *Details of smartphone camera and imaging conditions*

Phosphate buffered saline (PBS) (pH 7.4; 0.01M), PBS-Tween (pH 7.4; 0.01M, 1% tween) and tris-HCl (0.1M) buffers were prepared by following the standard protocols, where the salts were dissolved in deionized water. For PBS buffer preparation, the cold spring harbor method was followed, where 1.41 gram of Na_2HPO_4 (0.01M), 0.24g of KH_2PO_4 (0.0018M), 8.00g of NaCl (0.137M), and 0.20 g of KCl (0.0027M) salts were dissolved in one liter of deionized water and mixed it thoroughly (Sambrook,1989). PBS-Tween buffer was prepared using 500 ml of 0.01M PBS buffer with 5 ml of tween-20 (1% (v/v)). Zn enriched Tris-HCl (pH 7.4; 0.1M) buffer was prepared by mixing tris-HCl salt in deionized water with trace amount of $ZnCl_2$, which was used to prepare the dilutions of ALP. 4-carboxybenzenediazonium salt solution was prepared by sequential dissolution of 369 mg of p-nitrobenzoic acid, 260 mg of sodium nitrite, and 72 mg of ascorbic acid in 90 ml hydrochloric acid (1M).

2.2. Fabrication of P/DS/EDC-NHS/Anti-ALP biosensor:

At first stage, Whatman filter paper (P) grade 1 was chosen as the base material for sensor-probe fabrication. The paper discs were snipped using office paper punching machine and were carboxylated using 4-carboxybenzene diazonium (DS) solution for six hours followed by thorough washing with distilled water forming P/DS surface. Thereafter, the washed P/DS discs were treated with freshly prepared EDC/NHS (143 mM-100 mM) to activate the –COOH groups at P/DS surface. This was followed by immobilization of Anti-ALP (1.7µg/µL), which occurred due to the interaction between the $-NH_2$ groups of Anti-ALP and –COOH groups of functionalized P/DS surface. The final sensing probe after Anti-ALP immobilization was represented as P/DS/EDC-NHS/Anti-ALP probe. In order to minimize the nonspecific interaction of ALP and to avoid false positive signals, the P/DS/EDC-NHS/Anti-ALP probe was treated with 1% BSA for 30 mins. In order to remove the unabsorbed BSA, the sensor-probe was washed using sterile PBS-Tween (1.0%) for 1.0 min followed by gentle rinsing with PBS. The formation of each layers of the developed biosensor was examined by FTIR and DIC. The detailed schematic representation of probe fabrication process and principle involved in signal generation have been shown in scheme 2.1

2.3. Detection of ALP using the P/DS/EDC-NHS/Anti-ALP biosensor:

The detection of ALP relies on the immunocomplexation reaction between P/DS/EDC-NHS/Anti-ALP probe and ALP. For this purpose, varying concentrations of ALP was treated with the designed sensor-probe and allowed to react for 13.0 minutes. After this, the immunocomplexed assembly (P/DS/EDC-NHS/Anti-ALP/ALP) was gently washed with PBS and allowed to react with BCIP (10.0 mM), producing a blue-green colored complex catalyzed by ALP, which was bound to the P/DS/EDC-NHS/Anti-ALP probe surface. A detailed biochemical reaction involving the color generation has been shown in figure 2.1. The color change on paper discs were then recorded by smartphone camera in photographic conditions as mentioned in the table 2.1. This was followed by the image processing and colorimetric quantification, where the colored images of the paper surface were processed to obtain the corresponding RGB values. To eliminate the errors in pixel values in capturing condition and to avoid the false positive signals of the darker imprints left by the evaporated liquids at the edges of paper substrate, a uniform selective area was adapted for the image analysis. The selective area not only eliminates the dark rings and patches, but also provides the accurate changes in the pixel values by taking mean intensity values of the distributed uniform area. The effective RGB intensities of the colored paper discs were estimated by equation 2.1,

$$Effective\ I_{RGB} = \log_{10}\left(\frac{I_{\mathrm{RGB}\ (Blank)}}{I_{\mathrm{RGB}\ (Conc.)}}\right) \text{--- Equation 2.1}$$

where, I_{RGB} *is the mean pixel intensities of Red, Green, and Blue color channels obtained from selected area of BCIP treated P/DS/EDC-NHS/Anti-ALP/ALP discs.*

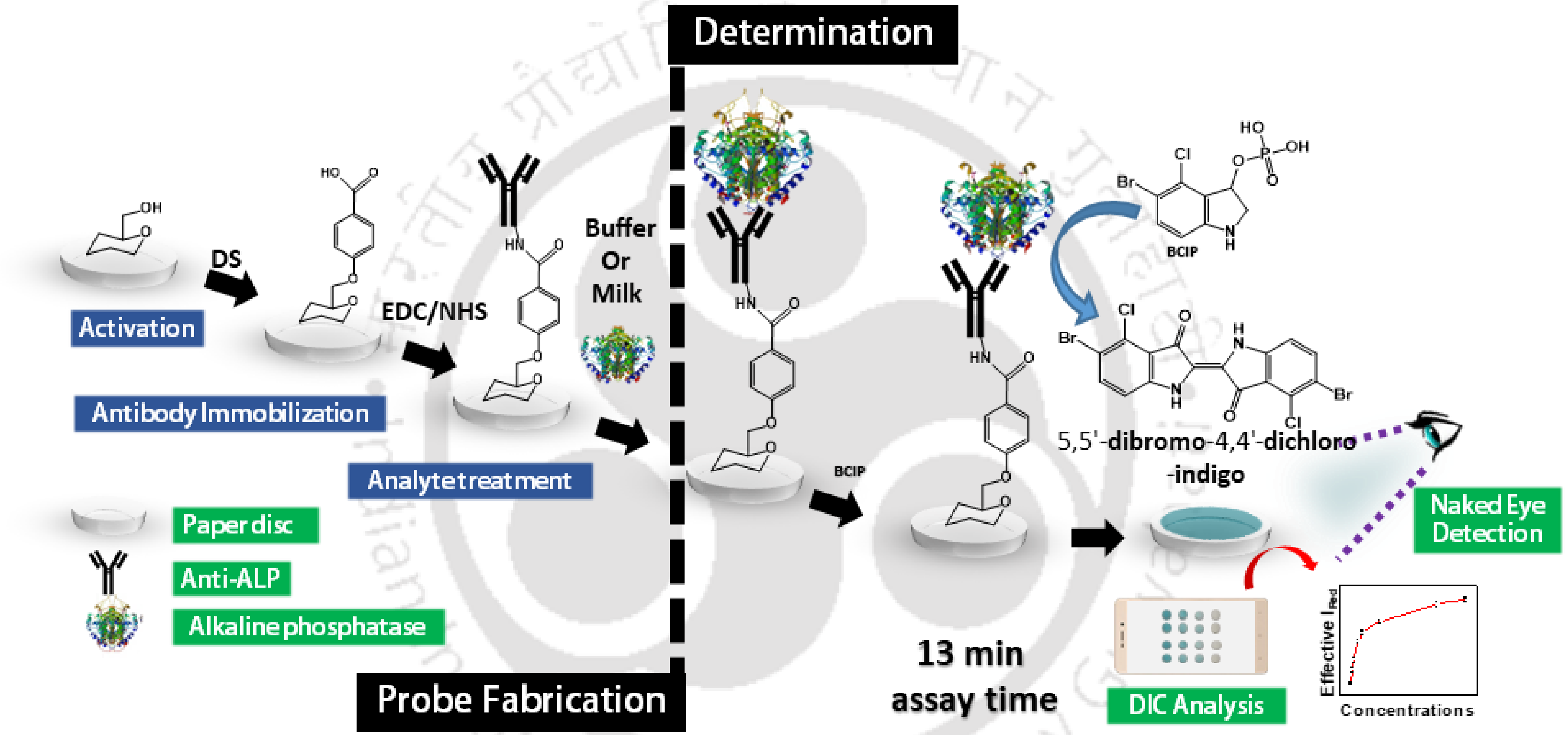

Scheme 2.1: *Schematic representation of the ALP biosensor fabrication and detection principle.*

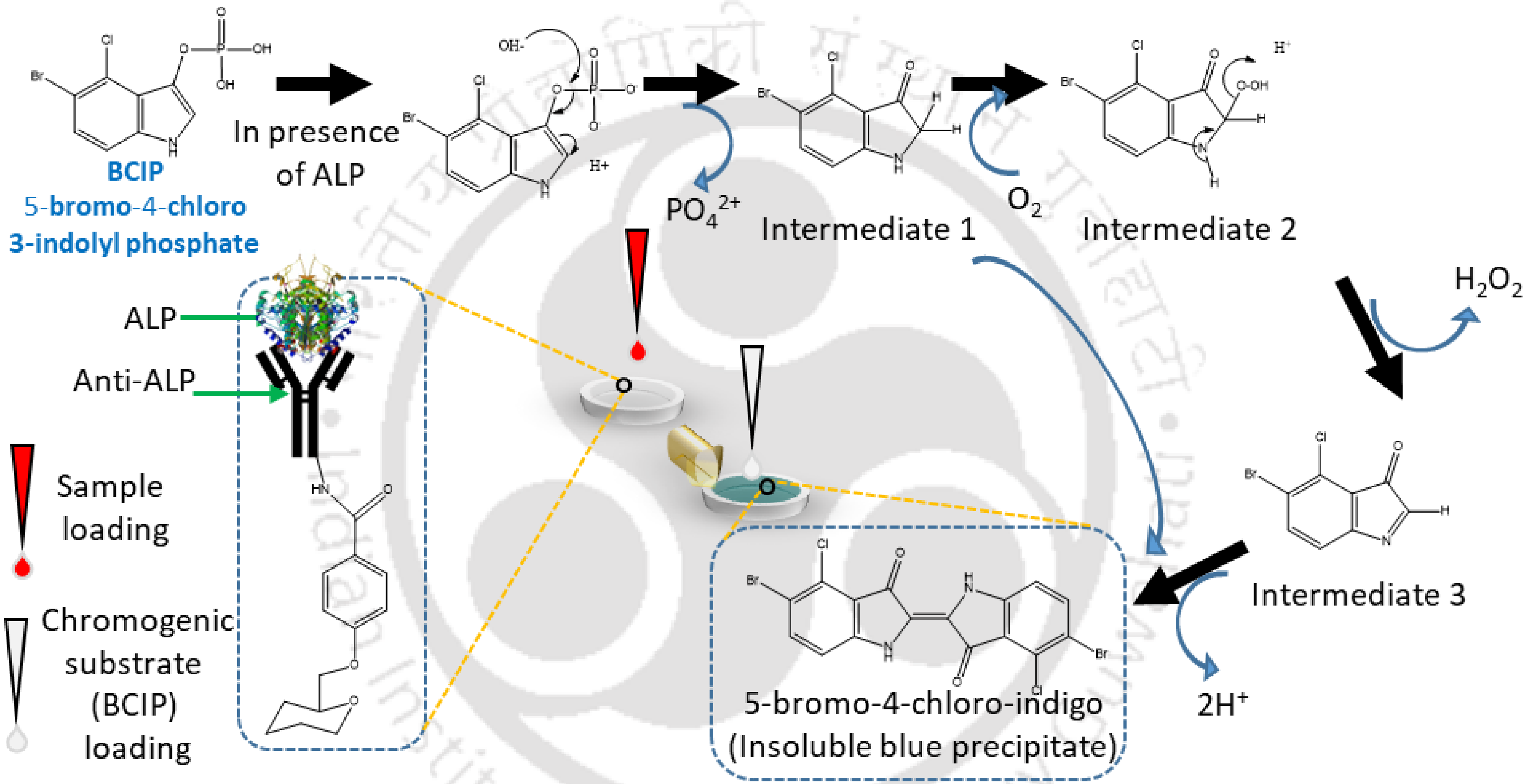

Figure 2.1: *Detailed reaction mechanism of the BCIP in presence of ALP.*

3. Results and discussion:

3.1. Selection of color channel for biosensing studies:

In order to evaluate the sensing capability of the biosensor, the RGB convention of image analysis is followed, where we first selected the most sensitive channels of these primary colors. In digital images, the I_{RGB} reflects pixel intensity of the true color (blue-green color in our case), which is composed of the intensities of three primary color channels, denoted as I_{Red}, I_{Green}, and I_{Blue}. In the colorimetric changes, gradual intensification of appeared color signifies the absorption of the complementary color (Firdaus et al.,2014). In order to find out the color channel that provides maximum sensitivity for the analytical applications of the designed biosensor, we individually tested and compared the R, G, and B color channels. Figure 2.2 (A-D) shows the time dependent appearance (blue-green color) of the biosensor surface and its corresponding histograms in RGB as well as R channels at 1.0 (A), 4.0 (B), 8.0 (C), 12.0 (D) minutes. Thereafter, we calculated the time dependent Effective I_{Red}, Effective I_{Green}, and Effective I_{Blue} from 1.0 to 12.0 minutes separately and plotted the time dependent plot (Figure 2.3). It was interesting to note that the maximum signal was obtained for Effective I_{Red} (0.0094 (± 0.0007) a.u./minutes), compared to the Effective I_{Green} (0.0019 (± 0.0005) a.u./minutes) and Effective I_{Blue} (0.0002 (± 0.0011) a.u./minutes), which was statistically significant ($p < 0.001; n = 3$). Therefore, in all subsequent biosensing experiments, Effective I_{Red} has been used as an analytical signal, which was calculated using equation 2.2.

$$Effective\ I_{\mathrm{Red}} = \log_{10}\left(\frac{I_{\mathrm{Red}\ (Blank)}}{I_{\mathrm{Red}\ (Conc.)}}\right) \text{-- Equation 2.2}$$

where, I_{Red} is the mean pixel intensity of red channel obtained from the selected area of BCIP treated P/DS/EDC-NHS/Anti-ALP/ALP discs.

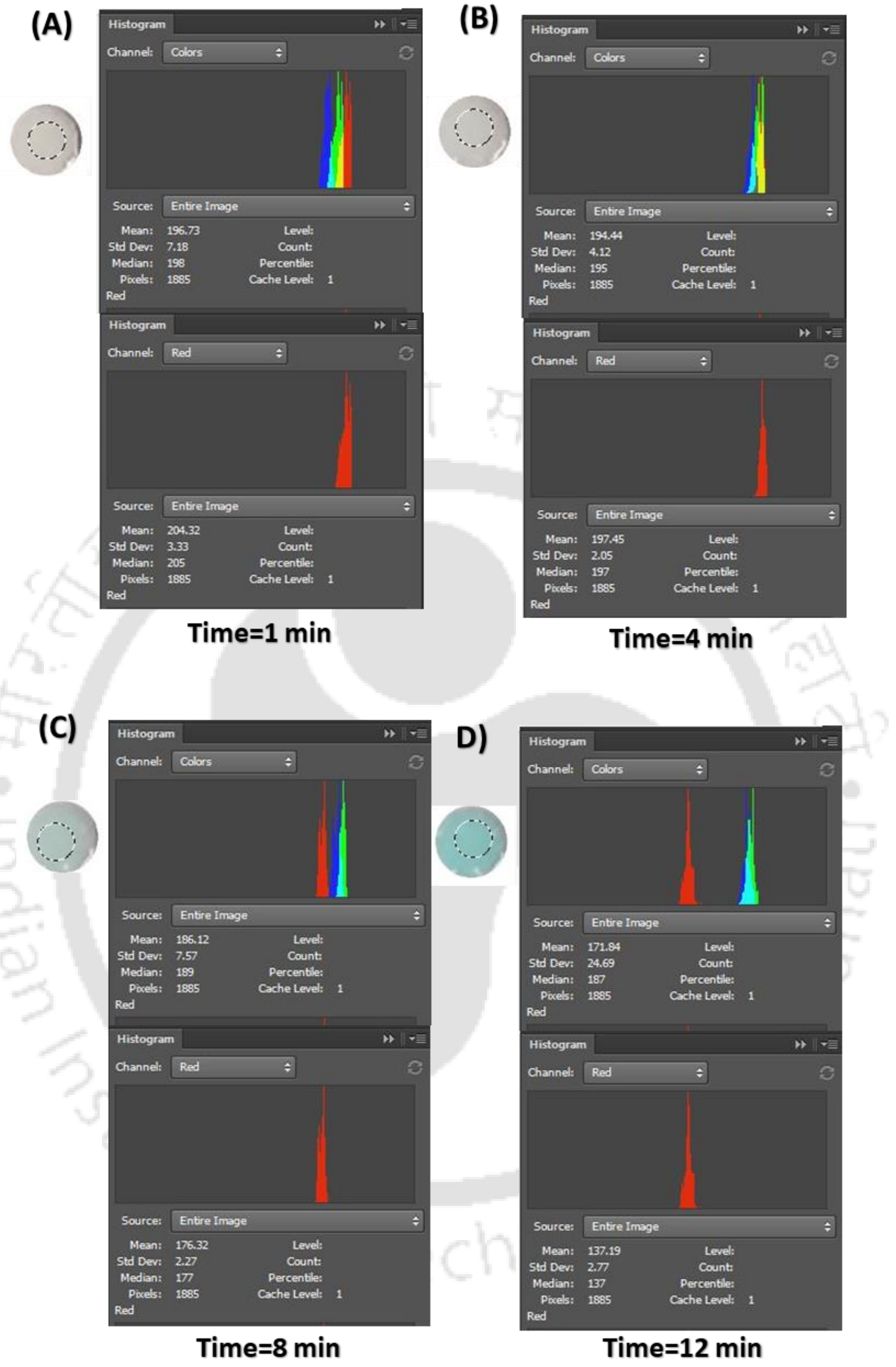

(A)

Histogram
Channel: Colors
Source: Entire Image
Mean: 196.73
Std Dev: 7.18
Median: 198
Pixels: 1885
Level:
Count:
Percentile:
Cache Level: 1
Red

Histogram
Channel: Red
Source: Entire Image
Mean: 204.32
Std Dev: 3.33
Median: 205
Pixels: 1885
Level:
Count:
Percentile:
Cache Level: 1
Red

Time=1 min

(B)

Histogram
Channel: Colors
Source: Entire Image
Mean: 194.44
Std Dev: 4.12
Median: 195
Pixels: 1885
Level:
Count:
Percentile:
Cache Level: 1
Red

Histogram
Channel: Red
Source: Entire Image
Mean: 197.45
Std Dev: 2.05
Median: 197
Pixels: 1885
Level:
Count:
Percentile:
Cache Level: 1
Red

Time=4 min

(C)

Histogram
Channel: Colors
Source: Entire Image
Mean: 186.12
Std Dev: 7.57
Median: 189
Pixels: 1885
Level:
Count:
Percentile:
Cache Level: 1
Red

Histogram
Channel: Red
Source: Entire Image
Mean: 176.32
Std Dev: 2.27
Median: 177
Pixels: 1885
Level:
Count:
Percentile:
Cache Level: 1
Red

Time=8 min

D)

Histogram
Channel: Colors
Source: Entire Image
Mean: 171.84
Std Dev: 24.69
Median: 187
Pixels: 1885
Level:
Count:
Percentile:
Cache Level: 1
Red

Histogram
Channel: Red
Source: Entire Image
Mean: 137.19
Std Dev: 2.77
Median: 137
Pixels: 1885
Level:
Count:
Percentile:
Cache Level: 1
Red

Time=12 min

Figure 2.2: *(A-D) Histogram showing gradual change of RGB and R intensities with time (from 1 minute to 12 minutes).*

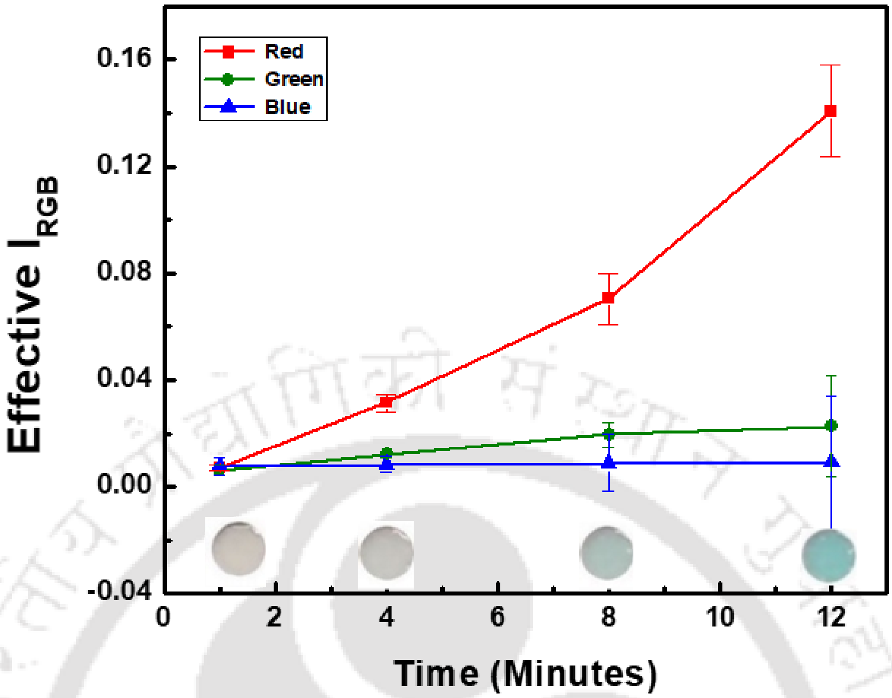

Figure 2.3: *Shows the plot obtained from the time dependent study of the Effective* I_{Red}*,* I_{Green}*, and* I_{Blue}*.*

3.2. Characterization of P/DS/EDC-NHS/Anti-ALP biosensing probe:

The characterization of the sensing probe was done by DIC and FTIR. At first phase, to confirm the step-wise construction of the biosensor, an immunocomplexation experiment was performed. For this purpose, ALP was allowed to react with the P/DS/EDC-NHS/Anti-ALP sensing probe followed by washing and treatment with BCIP, which forms the blue-green precipitation as shown in figure 2.4 (i). In order to confirm that the signal was merely due to the immunocomplexation followed by the catalytic reaction between ALP and BCIP, we characterized the sensing surface by performing series of control experiments. In the first experiment, ALP was allowed to react with the Anti-ALP unimmobilized paper surface followed by its interaction with BCIP (P/DS/ALP/BCIP) (ii). In the second experiment, no BCIP was treated after at the immunocomplexed sensor-probe (P/DS/EDC-NHS/Anti-ALP/ALP) (iii); whereas, in the third control experiment, no ALP was reacted with the sensing probe, but it was treated with BCIP in the final step (P/DS/EDC-NHS/Anti-ALP/BCIP) (iv). Interestingly, in all control experiments, no significant Effective I_{Red} was observed ($p < 0.001$; $n = 3$), compared to the Effective I_{Red} which was observed in the case of complete sensing probe i.e. P/DS/EDC-NHS/Anti-ALP/ALP in presence of BCIP. These results clearly indicate that the sensing probe has been correctly developed and is able to detect ALP.

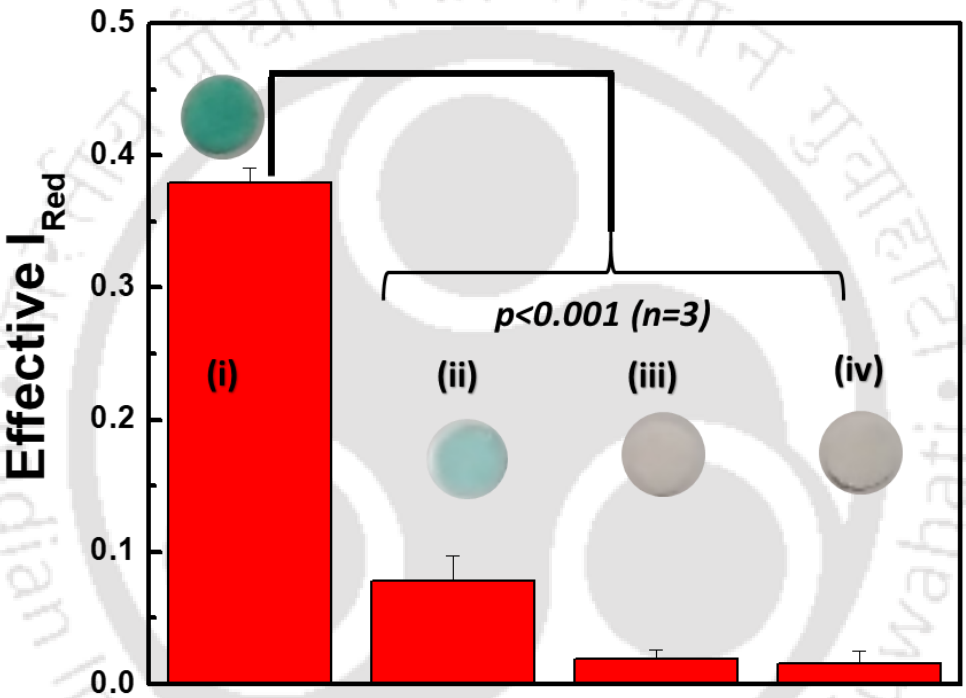

Figure 2.4: *Histograms showing the comparative Effective* I_{Red} *of the sensing probe (i) P/DS/EDC-NHS/Anti-ALP/ALP/BCIP; (ii), (iii), and (iv) represents controls; P/DS/ALP/BCIP, P/DS/EDC-NHS/Anti-ALP/ALP, and P/DS/EDC-NHS/Anti-ALP/BCIP, respectively. The respective visuals of paper discs shown above the histogram.*

In order to reconfirm the biosensor construction, each layer of the sensor-probe was characterized using FTIR. The representative FTIR spectra for bare paper (P) substrate, diazonium treated paper (P/DS), EDC-NHS activated paper (P/DS/EDC-NHS), and antibody immobilized paper surface (P/DS/EDC-NHS/Anti-ALP) have been shown in figure 2.5.

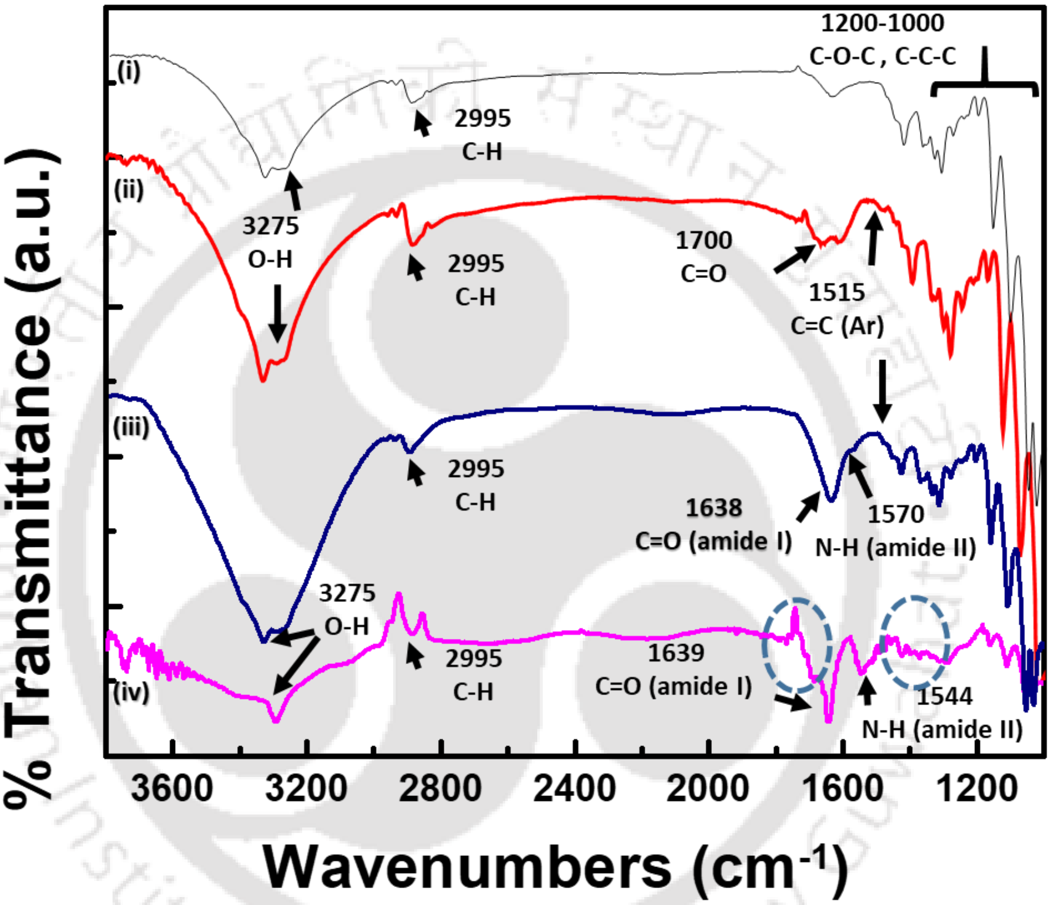

Figure 2.5: *FTIR spectra of different stages of the probe fabrication, where (i) P, (ii) P/DS, (iii) P/DS/EDC-NHS, and (iv) P/DS/EDC-NHS/Anti-ALP.*

For the P (i), peaks between 1000 -1200 cm^{-1}, 2995 cm^{-1}, and 3257 cm^{-1} were observed, which are due to the C-O-C and C-C-C vibrations, C-H stretching, and O-H stretching vibrations, respectively. After the treatment with diazonium solution, (ii) the appearance of peak at 1700 cm^{-1} and 1515 cm^{-1} correspond to the carboxyl group (C=O) and aryl (C=C), respectively; which are most likely due to the addition of caboxybenzyl flanking groups on to the cellulose fiber of the paper forming (P/DS). After the treatment of EDC/NHS at the P/DS surface, two representative peaks at 1638 cm^{-1} (amide I) and 1570 cm^{-1} (amide II) were observed in spectrum (iii), which was due to bending vibrations of amide bond formed after the coupling of NHS with carboxybenzyl flanking groups. Similar peaks in the FTIR spectra of EDC/NHS functionalized surface have also been observed previously (Massad-Ivanir et al.,2011). The Anti-ALP immobilized paper surface (P/DS/EDC-NHS/Anti-ALP) was characterized by the presence of two representative bands of protein IR spectrum (iv) i.e. amide I and amide II. Multiple peaks present between 1600-1700 cm^{-1} band were assigned to the C=O stretching vibrations of amide I. A new sharp peak at 1544 cm^{-1} was clearly observed in the band between 1510-1580 cm^{-1} due to the N-H bending vibrations and the C-N stretching vibrations of amide II present in the peptide moieties of Anti-ALP. These stretching vibrations are directly related to the protein (Anti-ALP) backbone conformation, which clearly indicates the immobilization of Anti-ALP onto the paper surface.

Further, in order to validate the sensor-probe fabrication, we have characterized the fabricated probe surface using AFM, where we recorded the surface morphologies after every steps of modification and *z-deflection* (Figure 2.6) was evaluated as reported earlier (Arun et al., 2016). Firstly, the surface morphology of untreated paper (P) was captured, where the appearance of fibrous topology with z-deflection of 67.38 nm was observed as shown in figure 2.6 (i). Thereafter, we examined the P/DS surface, where we observed granular surface with increased z-deflection (98.20 nm), which is due to the coupling of carboxybenzyl moieties on the paper surface after 4-carboxybenzenediazonium treatment (ii). In the next step, we observed the P/DS/EDC-NHS surface, where a clear change in the surface topology was observed with further increase in the z-deflection (102.90 nm) (iii).

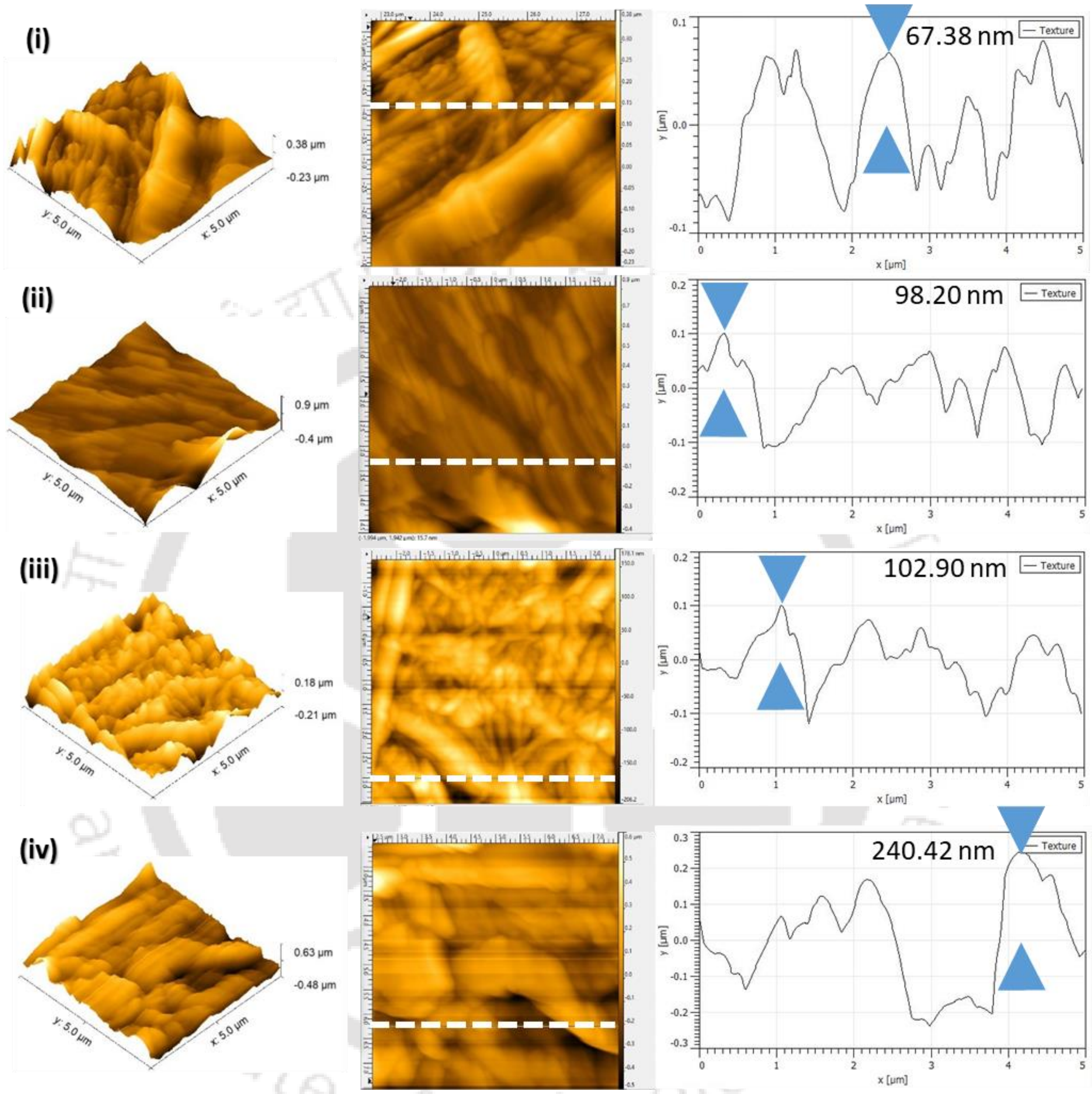

Figure 2.6: *AFM micrographs showing the 3D, 2D surface topologies, and z-deflection profiles of (i) P, (ii) P/DS, (iii) P/DS/EDC-NHS, and (iv) P/DS/EDC-NHS/Anti-ALP modified surface*

However, after the immobilization of anti-ALP, the z-deflection increased significantly over two folds (240.42 nm) and a significant change in the surface topology was observed (iv), which was due to the interaction of high molecular weight anti-ALP interacted with the sensor surface. The characterization results obtained from DIC, FTIR, and AFM complements each other, indicating the successful fabrication of biosensing probe.

3.3. Analytical performance of P/DS/EDC-NHS/Anti-ALP biosensor:

After the successful characterization of the sensor-probe, its analytical performance was evaluated by detecting the ALP in dose dependent manner. For this purpose, at first, the sensor-probe was treated with the buffer without ALP followed by BCIP, where no Effective I_{Red} was obtained. This is because of no colored product formation due to the absence of ALP in the sensing assembly. Thereafter, the P/DS/EDC-NHS/Anti-ALP probe was treated with the different concentrations of ALP followed by the treatment of BCIP and color change was recorded using the smartphone camera. Figure 2.7 displays the Effective I_{Red} responses of the developed biosensor in absence and presence of different concentrations of ALP between 10 - 1000 U/mL.

The change in the color of the paper surface clearly shows increase in Effective I_{Red} with increase in the ALP concentrations, indicating that the developed sensor can effectively detect ALP. Based on the Effective I_{Red} responses, two calibration plots were obtained. The linear regression equations for ALP are expressed for low and high concentrations calibration plots are as follow: Effective I_{red}(a.u.) = 0.06549(± 0.00797) + 0.0023(± 0.000183) [ALP] (U/mL) and Effective I_{red}(a.u.) = 0.2930(± 0.0146)+ 0.00030(± 0.000028)[ALP](U/mL), with a correlation coefficients of 0.996 and 0.949, respectively.

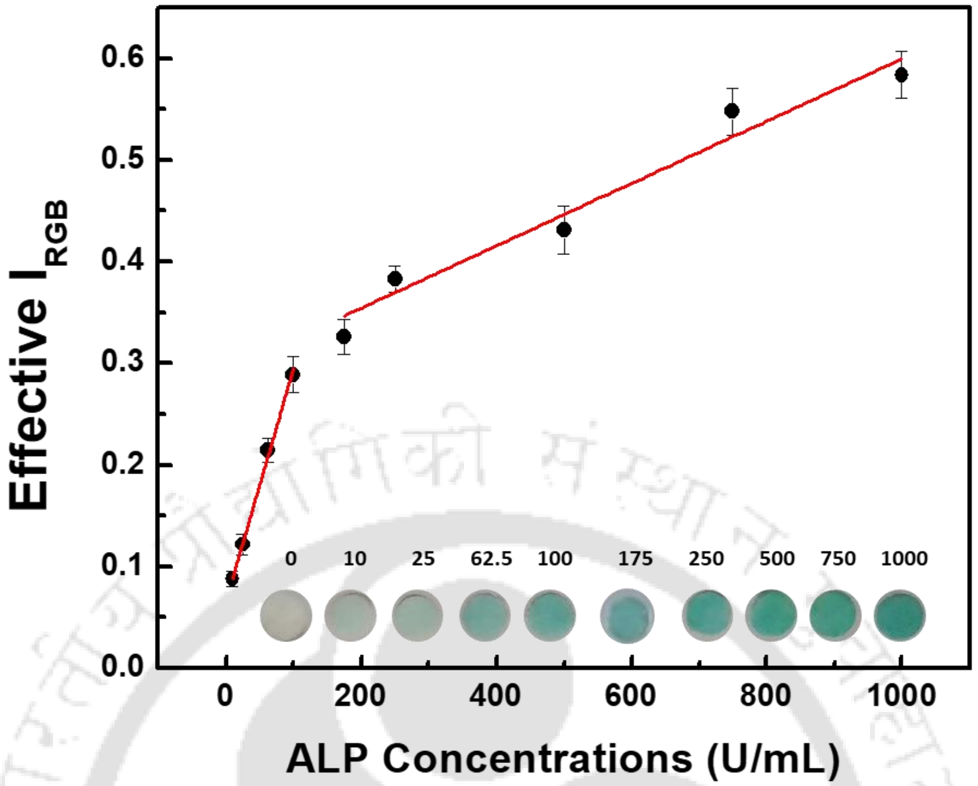

Figure 2.7 : *Calibration plots obtained from the responses of different ALP concentration ranging from 10 to 1000 U/mL using the P/DS/EDC-NHS/Anti-ALP probe. Dose dependent color changing of the paper discs (in bottom panel).*

The detection limit of ALP was determined to be 0.870(± 0.07) U/mL (RSD < 5.1%) based on the standard deviation of three repeated measurements of the blank (95.0 % confidence level, *n* = *3*). The detection ability of the designed biosensor falls well in the range of ALP concentrations present in the raw milk of healthy cow, which was reported to be ~ 191.0 U/mL (Kitchen,1981). It is worth mentioning that the overall detection time for ALP in this miniaturized, instrument-less, and commercially-viable method is merely 13.0 minutes, hence, it could be of tremendous use for onsite analysis.

3.4. Interference study:

Selectivity is one of the most critical parameter to evaluate the biomedical values of any biosensor (Chandra,2016; Mahato et al.,2018; Pallela et al.,2016). Thus, we performed selectivity assay using molecules present in milk *viz.* citric acid, bovine serum albumin (BSA), lactose, casein, vitamin A, vitamin B, and commonly present ions (Ca^{++}, Na^{+}, K^{+}, and Mg^{++}) separately, under the similar experimental conditions. Figure 2.8 shows a comparative Effective I_{red} for ALP and interfering molecules, where no signals were observed for any of the tested interfering molecules compared to ALP. This was due to the absence of ALP in the sensing matrix, which only generates blue-green precipitate meditated through BCIP. The selectivity of sensor-probe was mathematically analyzed by determining the selectivity coefficient (k_{sel}) using equation 2.3,

$$k_{sel} = \frac{(Signal)_{interferent}}{(Signal)_{ALP}} \quad \text{--- Equation 2.3}$$

where k_{sel} *is the coefficient of selectivity,* $(Signal)_{interferent}$ *is the signal strength shown by probe when treated with the interfering molecules, and* $(Signal)_{ALP}$ *is the signal strength corresponds to the presence of ALP, followed by the treatment of BCIP.*

The k_{sel} values for the interfering molecules were found to be extremely low ($k_{sel} << 1$), indicating that the fabricated biosensor is highly selective towards ALP. We also performed the T-test and calculated the *p*-values, which was found to be < 0.001 ($n = 3$) for the interfering molecules, indicating that the selectivity results are statistically significant.

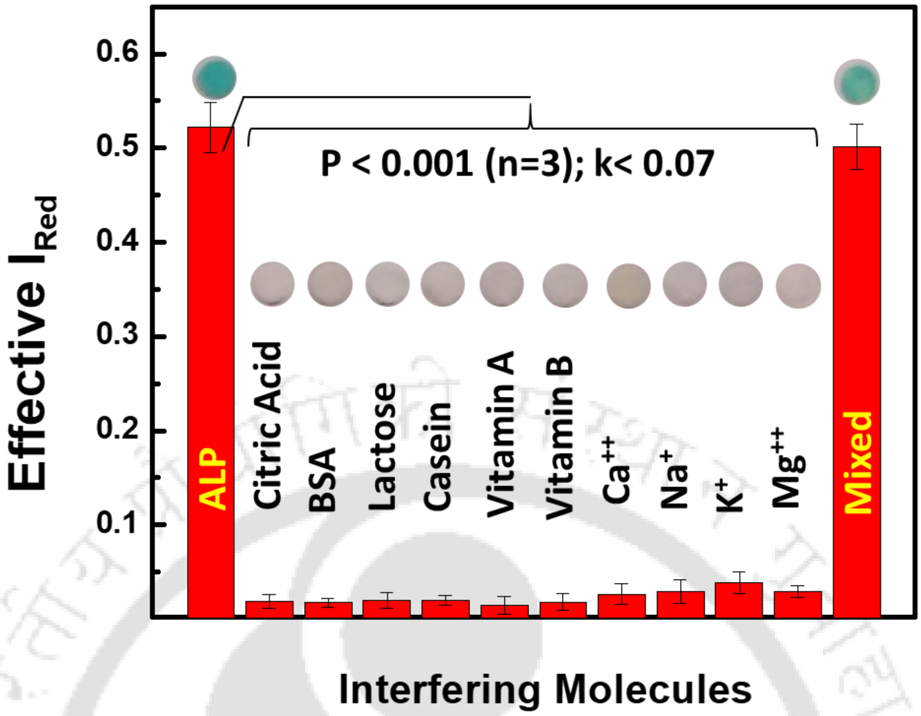

Figure 2.8: *Selectivity assay of P/DS/EDC-NHS/Anti-ALP sensor probe towards interfering molecules and mixed sample analysis.*

In real sense, ALP coexists with the interfering molecules in the milk sample, so to make the experimental design more factual, we have performed mixed sample analysis. For this purpose, the ALP was mixed in a solution containing all the interfering molecules in the same concentration found in the milk followed by ALP detection using the developed sensing probe. Interestingly, the sensitivity for ALP detection in this case was found to be 98.6 % (*n* = *3*) compared when ALP was detected alone, indicating the capability of designed sensor for selective detection of ALP even in a mixed sample solution.

3.5. Real sample analysis:

The practical implications of the sensor was evaluated by detecting ALP in milk samples. For this purpose, two different methods were adopted; (i) standard addition and (ii) spike-recovery methods. The intention of standard addition method was to evaluate the unknown concentration of ALP in raw milk samples obtained from villages. For this purpose, ALP was detected in raw milk samples (here no ALP was spiked), using the P/DS/EDC-NHS/Anti-ALP sensor-probe obtained from different locations. Interestingly, in this case, a clear Effective I_{Red} was observed (encircled point of standard addition plot), which increases with the increase in ALP concentrations when spiked from 25-100 U/mL. A standard addition plot was obtained which gives a linear regression equation for ALP detection as follows: Effective I_{Red} (a.u.) = 0.05726(± 0.00615) + 0.00153(± 1.59 x 10^{-4})[ALP](U/mL) with the correlation coefficient of 0.989. The representative standard addition plot is shown in figure 2.9, where the unknown concentration of the ALP in the raw milk was obtained to be 17.5 ± 1.32 U/mL based on the standard deviation of three repeated measurements (95.0 % confidence level, $n = 3$). Importantly, the ALP concentration observed in our study using the developed biosensor is comparable to the ALP level in raw milk of cow which has been reported in the literature (Kitchen,1981; Singh and Ganguli,1975). Next set of experiments were based on spike-recovery method, which was done to evaluate % recovery of ALP from pasteurized milk samples at various concentrations. In this case, known concentrations of ALP was spiked in the pasteurized milk samples and % recoveries of ALP were calculated using equation 2.4.

$$\% \text{ Recovery} = \frac{([A]_{ALP} - [B]_{ALP})}{[C]_{ALP}} \quad \text{---------------------------- Equation 2.4}$$

Where, $[A]_{ALP}$ *and* $[B]_{ALP}$ *are the analytical responses of ALP in the spiked and blank samples, respectively; and* $[C]_{ALP}$ *is the analytical response of ALP in the standard solutions.*

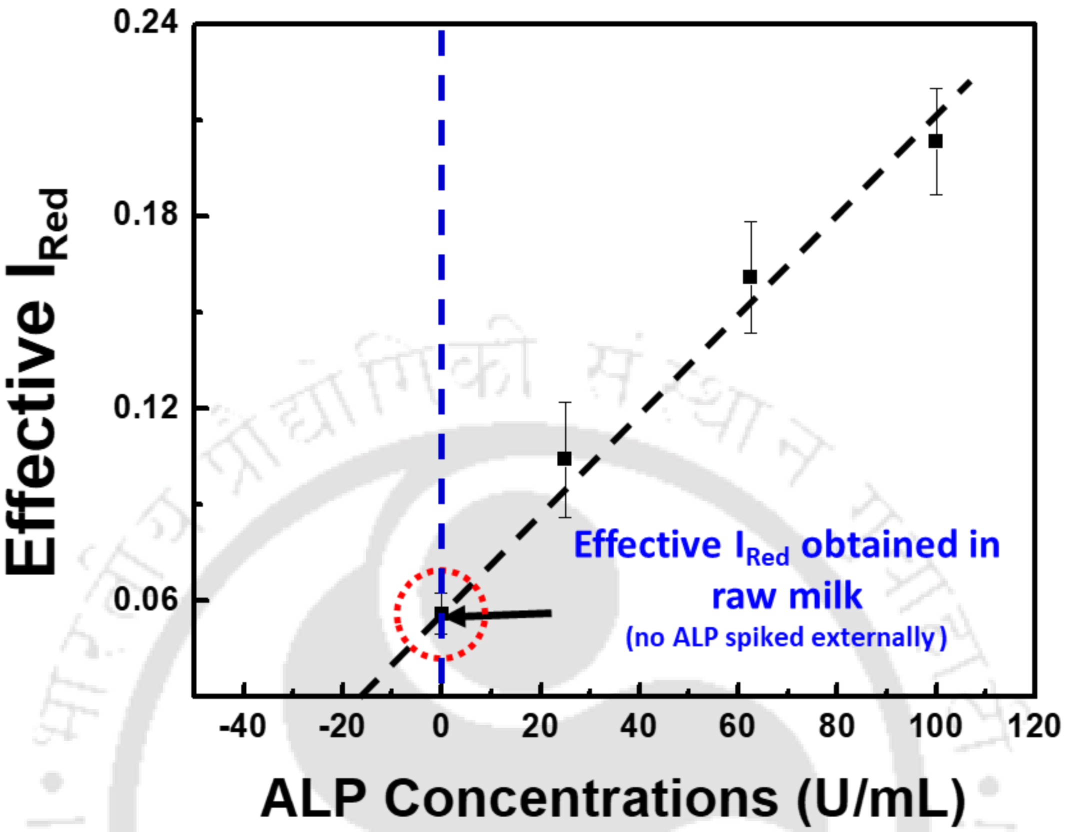

Figure 2.9: *Standard addition plot obtained for ALP detection in raw milk sample.*

Figure 2.10 shows a dose depended comparative response of ALP biosensor in milk samples, where increase in the Effective I_{Red} was observed with increase in ALP concentrations, however, no signal was observed when only pasteurized milk samples were analyzed (no ALP added). The sensitivity assay based on % recovery experiment was performed, which shows that the ALP biosensor is able to detect 91.0 % to 100.0 % of ALP from the milk samples. The analytical details for recovered ALP concentrations, RSD, and % recovery for all the tested concentrations are represented in Table 2.2. The detection limit of ALP in the milk sample was determined to be 1.51 ± 0.17 U/mL (RSD < 11.2 %) based on the standard deviation of three repeated measurements of the blank (95.0 % confidence level, $n = 3$). These results clearly indicate that the developed sensor-probe can effectively detect ALP in raw and pasteurized milk samples, hence it could be useful to differentiate pasteurized / boiled and raw milk effectively.

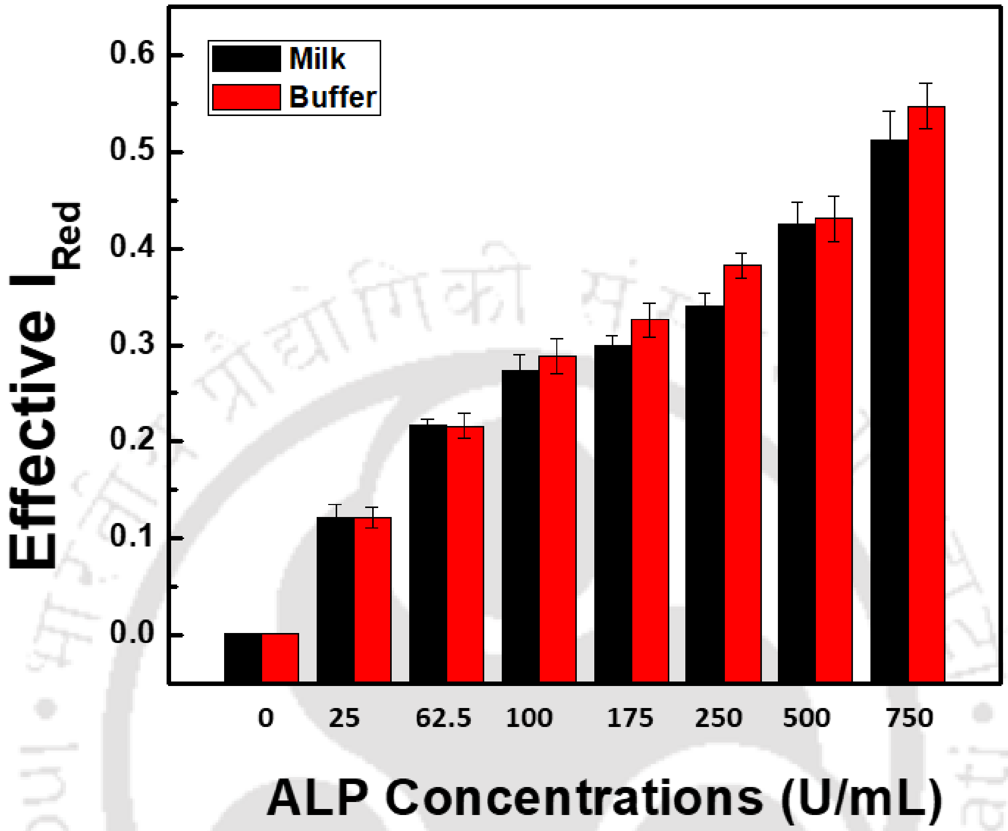

Figure 2.10: *Comparative dose dependent detection of ALP in pasteurized milk (black bars) and PBS (red bars) based on % recovery.*

3.6. Prototype design and ALP analysis in home kitchen:

After getting enthusiastic results in real samples, we extended our work towards the development of a biosensing prototype, which could help in safe, environmentally benign storage, and easy handling for in-kitchen analysis. The prototype has been fabricated using a cellulose acetate transparent film (CATF) of dimensions of 20.0 (*L*) mm x 20.0 mm (*W*) and 0.25 mm (*T*), which acts as a supporting layer for the developed paper

Samples	Spiked (U/mL)	Recovered (U/mL)	RSD (%)	% Recovery
1	25	24.99 ± 2.86	11.49	99.59
2	62.5	62.97 ± 1.33	2.14	100.76
3	100	94.51 ± 6.09	6.44	94.51
4	175	159.60 ± 7.10	4.45	91.20
5	250	227.78 ± 8.54	3.83	91.12
6	500	492.82 ± 27	5.47	98.56
7	750	703.72 ± 39.76	5.65	93.82

Table 2.2: *Recovery table of ALP from spiked milk samples*

sensor-probe (P/DS/EDC-NHS/Anti-ALP). The details of the prototype design has been shown in figure 2.11 (i). The modified paper surface (diameter = 5.0 mm) was pasted onto the CATF sheet using glue followed by placing the O-ring of outer diameter of 8.0 mm enclosing the paper disc. This not only provide reservoir for washing / solution exchange, but also provides mechanical strength to the fabricated sensor-probe (P/DS/EDC-NHS/Anti-ALP). In the next step, the upper lid of CATF with hole of 4.0 mm diameter was pasted covering the O-ring. The effective distance between sensor-probe and the upper CATF lid was 1.5 mm, which was sufficient enough for the sample processing. In order to show the applicability of developed prototype ALP detection on kitchen was performed. To do so, ALP containing milk sample was injected through the hole at sensing area of the chip followed by Effective I_{Red} analysis as discussed in earlier section. Interestingly, a blue-green precipitate was observed in the prototype and sensor was able to detect 91.0 % of ALP from the originally spiked concentration.

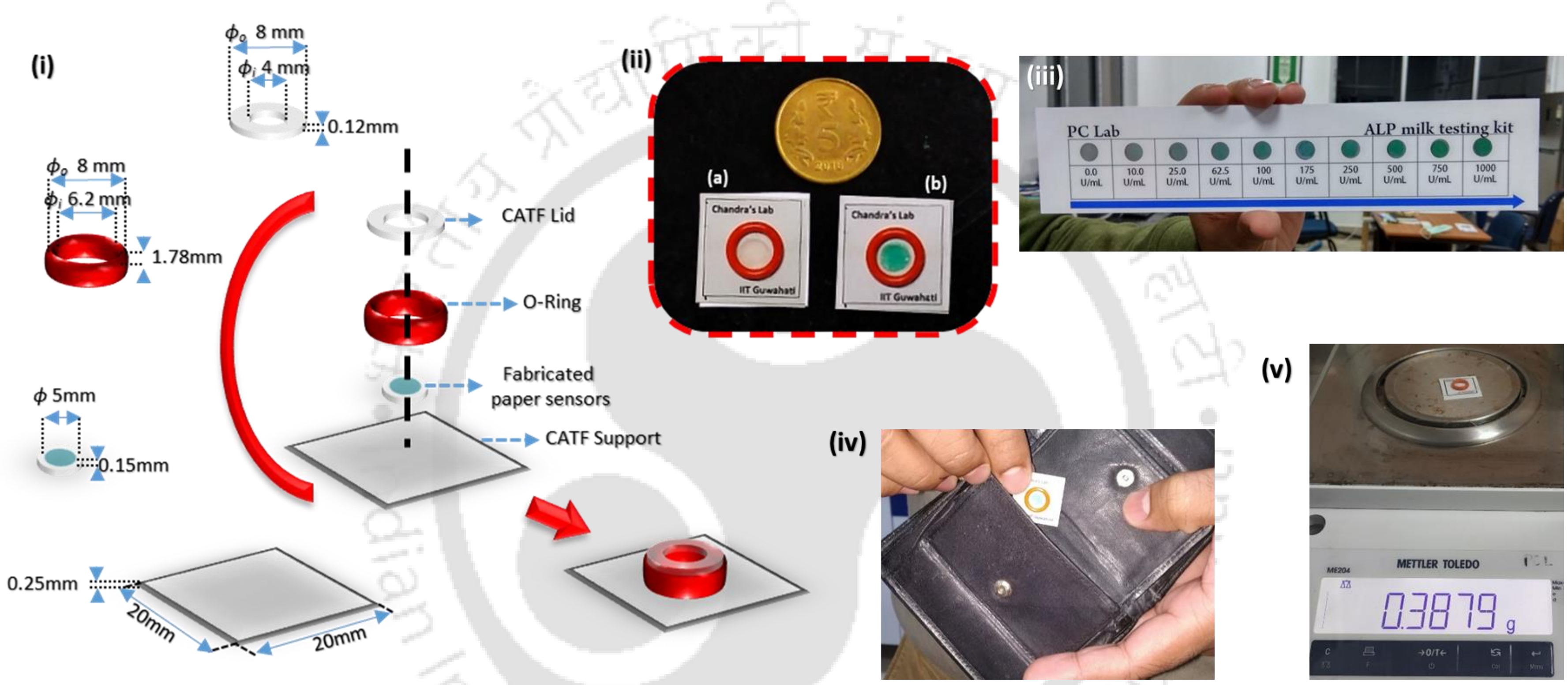

Figure 2.11: *(i) A detailed description of designed prototype with dimensions and (ii) the actual prototype showing the color change (a) before and (b) after interaction of ALP with the P/DS/EDC-NHS/Anti-ALP sensor probe. Images of (iii) dose dependent color chart, (iv) portable kit, and (v) light weight device.*

Thus, the designed miniaturized ALP sensing kit is extremely powerful for ALP detection and is very handy for the onsite analysis. The real prototype developed has been shown as figure 2.11 (ii), which shows before (a) and after (b) ALP analysis.

3.7. Storage conditions, stability test, and reproducibility assay:

The P/DS/EDC-NHS/Anti-ALP probe was stored at 4°C after the fabrication in moist condition and the Effective I_{Red} were recorded weekly. We have also studied the shelf-life of the probe, where we tested Effective I_{Red} of P/DS/EDC-NHS/Anti-ALP probe for every third day. The Effective I_{Red} response obtained by the probe shows that the sensor retained the sensitivity of 98.0 % up till 14th day, while decrement of the signal was recorded to 88.0 (± 2.15) % till 28th day. The considerably good shelf-life up to four weeks was most likely due to the stable immobilization of anti-ALP and retention of its biological activity on functionalized paper disc (figure 2.12).

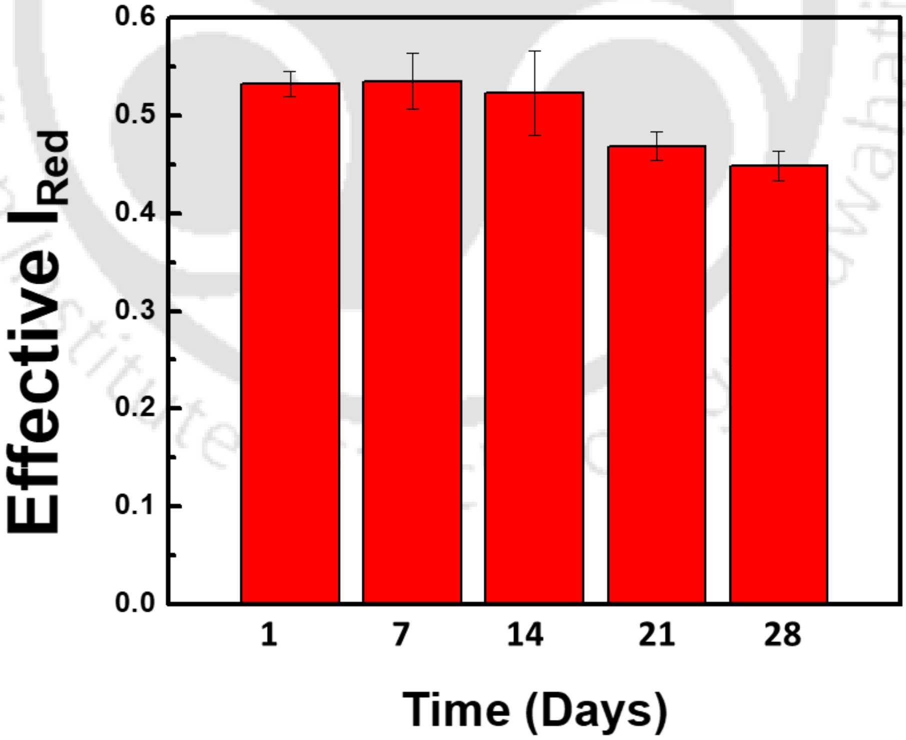

Figure 2.12: *The result on the shelf life study of the P/DS/EDC-NHS/Anti-ALP sensor probe tested after capturing 750 U/mL of ALP.*

It is also worth mentioning that the chemical modifications steps performed on the paper disc does not adversely affect the immobilized anti-ALP. After four weeks the signal was dropped up to 84.0 %, which was most likely due to the loss of biological activity of anti-ALP and /or the degradation of the chemical modification steps. The reproducibility of the biosensor was evaluated, which showed the RSD < 4.7% ($n = 3$) and disc to disc RSD was < 5.2% even when the same fabrication process was followed. This minor variation was most likely due to the negligible variation in the sensor fabrication process and handling errors.

4. Conclusions

The present study describes the first report of development of dot-spot, economical, paper-based biosensor for ALP detection in milk based on DIC integrated with smartphone. The fabrication of sensor-probe was characterized by DIC, FTIR, and AFM. The selection of color channel for colorimetric analyses was demonstrated for the first time in a paper matrix to the best of our knowledge, where the maximum sensitivity was observed for red channel. The limit of detection of proposed biosensor is 0.870 (± 0.07) U/mL, which is suitable for discriminating the raw milk (contains ~ 191.0 U/mL ALP) from the pasteurized/boiled milk at point of collection in merely 13.0 minutes without using any additional instrument. The biosensor was found to be highly selective ($k_{sel} << 1$; $p < 0.001$; $n = 3$) towards ALP and shows 91 -100 % recoveries of ALP from raw milk samples. Based on the sensing principle, a miniaturized kit has been developed and demonstrated for ALP detection in kitchens, indicating is real household and prospective industrial potential. In future, the sensing platform / principle described herein can be extended towards the detection of various molecules in different matrices.

Here in this present study, we have obtained a colorimetric system, which is capable of delivering the excellent determination of ALP in milk samples. However, it is limited in clinical serum samples, as the dynamic range of the fabricated system does not cover the normal and clinical range of ALP in serum. Thus, we have further extended the study to obtain the biosensing systems for ALP detection in clinical serum samples. For that, we have adopted electrochemical system, where the incorporation of the nanomaterials has been employed to obtain higher sensitivity. The detailed discussion is given in the next chapter.

5. References:

Akhtar, M.H., Hussain, K.K., Gurudatt, N.G., Chandra, P., Shim, Y.-B., Ultrasensitive dual probe immunosensor for the monitoring of nicotine induced-brain derived neurotrophic factor released from cancer cells, ***2018***. *Biosensors and Bioelectronics* 116, 108-115.

Al-Qadiri, H., Lin, M., Al-Holy, M., Cavinato, A., Rasco, B.A., Monitoring quality loss of pasteurized skim milk using visible and short wavelength near-infrared spectroscopy and multivariate analysis, ***2008***. *Journal of dairy science* 91(3), 950-958.

Babaei, H., Mansouri-Najand, L., Molaei, M.M., Kheradmand, A., Sharifan, M., Assessment of Lactate Dehydrogenase, Alkaline Phosphatase and Aspartate Aminotransferase Activities in Cow's Milk as an Indicator of Subclinical Mastitis, ***2007***. *Veterinary Research Communications* 31(4), 419-425.

Barkworth, H., Hosking, Z., Experiments with the methylene blue reduction test for milk, ***1952***. *Proceedings of the Society for Applied Bacteriology* 15(1), 116-125.

Chandan, R.C., Kilara, A., Shah, N.P., 2015. Dairy Processing and Quality Assurance, 2 ed. Wiley-Blackwell.

Chandra, P., 2016. Nanobiosensors for personalized and onsite biomedical diagnosis. The Institution of Engineering and Technology.

Chandra, P., Koh, W.C.A., Noh, H.-B., Shim, Y.-B., In vitro monitoring of i-NOS concentrations with an immunosensor: The inhibitory effect of endocrine disruptors on i-NOS release, ***2012***. *Biosensors and Bioelectronics* 32(1), 278-282.

Chen, C.-C., Tai, Y.-C., Shen, S.-C., Tu, Y.-Y., Wu, M.-C., Chang, H.-M., Detection of alkaline phosphatase by competitive indirect ELISA using immunoglobulin in yolk (IgY) specific against bovine milk alkaline phosphatase, ***2006***. *Food Chemistry* 95(2), 213-220.

Choodum, A., Keson, J., Kanatharana, P., Limsakul, W., Wongniramaikul, W., Selective pre and post blast trinitrotoluene detection with a novel ethylenediamine entrapped thin polymer film and digital image colorimetry, ***2017***. *Sensors and Actuators B: Chemical* 252, 463-469.

Fasken, J.E., McClure, A.D., Phosphatase Test in Pasteurization of Milk, ***1940***. *Canadian Journal of Comparative Medicine and Veterinary Science* 4(5), 128-137.

Firdaus, M.L., Alwi, W., Trinoveldi, F., Rahayu, I., Rahmidar, L., Warsito, K., Determination of chromium and iron using digital image-based colorimetry, ***2014***. *Procedia Environmental Sciences* 20, 298-304.

Gaucheron, F., Milk and Dairy Products: A Unique Micronutrient Combination, ***2011***. *Journal of the American College of Nutrition* 30(sup5), 400S-409S.

Hosseini, S., Vázquez-Villegas, P., Martínez-Chapa, S.O., Paper and Fiber-Based Bio-Diagnostic Platforms: Current Challenges and Future Needs, ***2017***. *Applied Sciences* 7(8), 863.

Ito, S., Yamazaki, S.-i., Kano, K., Ikeda, T., Highly sensitive electrochemical detection of alkaline phosphatase, ***2000***. *Analytica Chimica Acta* 424(1), 57-63.

Jay-Russell, M.T., Raw (Unpasteurized) Milk: Are Health-Conscious Consumers Making an Unhealthy Choice?, ***2010***. *Clinical Infectious Diseases* 51(12), 1418-1419.

Kitchen, B.J., Bovine mastitis: milk compositional changes and related diagnostic tests, ***1981***. *Journal of Dairy Research* 48(1), 167-188.

Klinger, I., Rosenthal, I., Public health and the safety of milk and milk products from sheep and goats, ***1997***. *Revue scientifique et technique-Office international des épizooties* 16, 482-488.

Kulmyrzaev, A.A., Levieux, D., Dufour, É., Front-Face Fluorescence Spectroscopy Allows the Characterization of Mild Heat Treatments Applied to Milk. Relations with the

Denaturation of Milk Proteins, ***2005***. *Journal of Agricultural and Food Chemistry* 53(3), 502-507.

Lin, B., Yu, Y., Cao, Y., Guo, M., Zhu, D., Dai, J., Zheng, M., Point-of-care testing for streptomycin based on aptamer recognizing and digital image colorimetry by smartphone, ***2018***. *Biosensors and Bioelectronics* 100, 482-489.

Mahato, K., Maurya, P.K., Chandra, P., Fundamentals and commercial aspects of nanobiosensors in point-of-care clinical diagnostics, ***2018***. *3 Biotech* 8(3), 149.

Mahato, K., Srivastava, A., Chandra, P., Paper based diagnostics for personalized health care: Emerging technologies and commercial aspects, ***2017***. *Biosensors and Bioelectronics* 96, 246-259.

Massad-Ivanir, N., Shtenberg, G., Tzur, A., Krepker, M.A., Segal, E., Engineering nanostructured porous SiO2 surfaces for bacteria detection via "direct cell capture", ***2011***. *Analytical chemistry* 83(9), 3282-3289.

Nayak, N., Detection of Different Adulterant in Different Milk Samples, ***2018***. *Research & Reviews: Journal of Dairy Science and Technology* 6(3), 17-29.

Pallela, R., Chandra, P., Noh, H.-B., Shim, Y.-B., An amperometric nanobiosensor using a biocompatible conjugate for early detection of metastatic cancer cells in biological fluid, ***2016***. *Biosensors and Bioelectronics* 85, 883-890.

Panigrahi, S., Devi, B., Swain, K., Priyadarshini, P., Microbiology of milk: Public health aspect, ***2018.*** The Pharma Innovation Journal; 7(1): 260-264.

Park, L., Bae, H., Kim, Y.-T., Lee, J.H., Rapid monitoring of alkaline phosphatase in raw milk using 1,1[prime or minute]-oxalyldiimidazole chemiluminescence detection, ***2011***. *Analytical Methods* 3(1), 156-160.

Parkin, A., 2016. Viewing 8-bit Image. Digital Imaging Primer, pp. 643-645. Springer.

Payne, C., Wilbey, R.A., Alkaline phosphatase activity in pasteurized milk: A quantitative comparison of Fluorophos and colourimetric procedures, ***2009***. *International journal of dairy technology* 62(3), 308-314.

Peng, B., Chen, G., Li, K., Zhou, M., Zhang, J., Zhao, S., Dispersive liquid-liquid microextraction coupled with digital image colorimetric analysis for detection of total iron in water and food samples, ***2017***. *Food Chemistry* 230, 667-672.

Rankin, S.A., Christiansen, A., Lee, W., Banavara, D.S., Lopez-Hernandez, A., The application of alkaline phosphatase assays for the validation of milk product pasteurization, ***2010***. *Journal of Dairy Science* 93(12), 5538-5551.

Rateni, G., Dario, P., Cavallo, F., Smartphone-based food diagnostic technologies: a review, ***2017***. *Sensors* 17(6), 1-22.

Rola, J.G., Sosnowski, M., Determination of alkaline phosphatase activity in milk and milk products by fluorimetric method, ***2010***. *Bull Vet Inst Pulawy* 54, 537-542.

Sambrook, F., and Maniatis, 1989. Molecular Cloning: A Laboratory Manual, 2nd ed. Cold Spring Harbor Laboratory Press.

Scharer, H., A Rapid Phosphomonoesterase Test for Control of Dairy Pasteurization, ***1938***. *Journal of Dairy Science* 21(1), 21-34.

Serra, B., Morales, M.D., Reviejo, A.J., Hall, E.H., Pingarrón, J.M., Rapid and highly sensitive electrochemical determination of alkaline phosphatase using a composite tyrosinase biosensor, ***2005***. *Analytical Biochemistry* 336(2), 289-294.

Singh, L.N., Ganguli, N.C., ***1975***. *Indian Journal of Dairy Science* 28, 67–68.

Soares, C., Fonseca, L., Leite, M., Oliveira, M., Application of Scharer's quantitative method for the determination of residual alkaline phosphatase activity in standard Minas, ***2013***. *Arquivo Brasileiro de Medicina Veterinária e Zootecnia* 65(4), 1223-1230.

Tajima, N., Takai, M., Ishihara, K., Significance of Antibody Orientation Unraveled: Well-Oriented Antibodies Recorded High Binding Affinity, ***2011***. *Analytical Chemistry* 83(6), 1969-1976.

Trilling, A.K., Beekwilder, J., Zuilhof, H., Antibody orientation on biosensor surfaces: a minireview, ***2013***. *Analyst* 138(6), 1619-1627.

Yalcin, B.K., Atasever, S., Relationships Between Dye Reduction Test Scores and Somatic Cell Count in Bovine Raw Milk, ***2018***. *Turkish Journal of Agriculture-Food Science and Technology* 6(5), 557-560.

Yetisen, A.K., Akram, M.S., Lowe, C.R., Paper-based microfluidic point-of-care diagnostic devices, ***2013***. *Lab on a Chip* 13(12), 2210-2251.

Yu, L., Shi, Z., Fang, C., Zhang, Y., Liu, Y., Li, C., Disposable lateral flow-through strip for smartphone-camera to quantitatively detect alkaline phosphatase activity in milk, ***2015***. *Biosensors and Bioelectronics* 69, 307-315.

Chapter- III

Clinically comparable impedimetric determination of ALP based on electrochemically tuned Au-nano-dendroid-graphene oxide nanocomposite in human serum

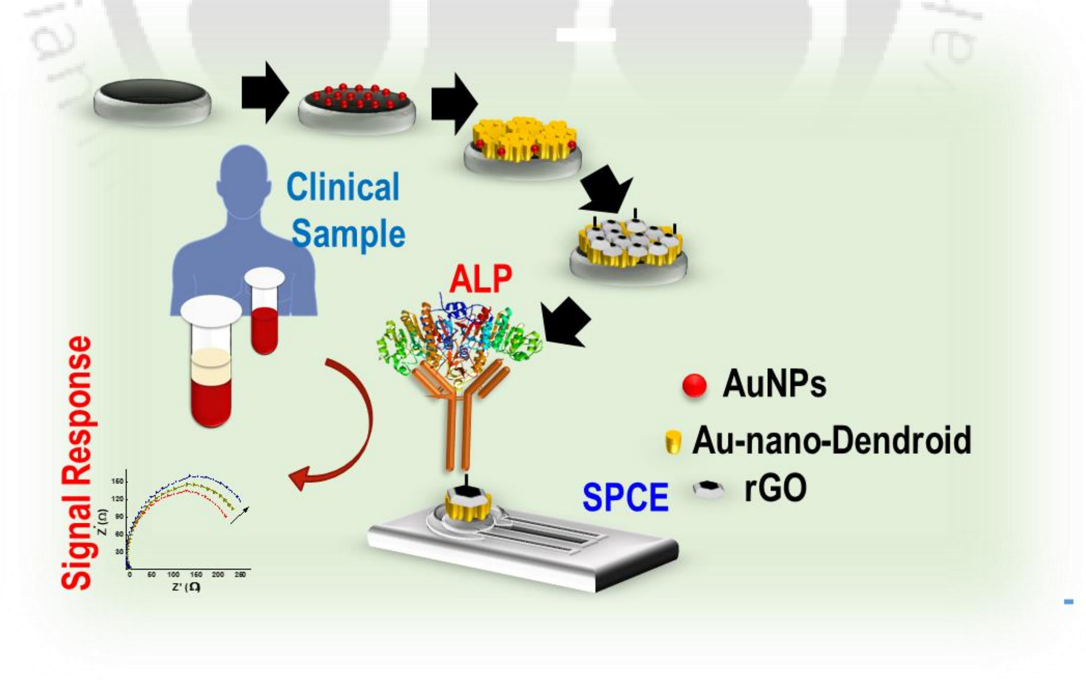

1. Introduction:

In this part of study, we have attempted to improvise the ALP determination system by adopting multilayered nanomaterials assisted electrochemical biosensing approach. The foremost reason for this adaption is to achieve the lower detection limit and attaining the clinically relevant dynamic range, which is reported as the 40-140 U/L in case of normal adult, which increased slightly higher in case of infants, kids and pregnant women. The clinical ranges above than 350 U/L were reported in the case of liver and bone associated disorders. Moreover, elevated serum ALP level is also found in various case of cancer relapse (Buonaguro et al.,2019) and at the onset of hepatitis C (Bodlaj et al.,2010; Keshaviah et al.,2007). In current clinical scenario, the serological determinations of ALP is performed using the method reported by the McComb and coworkers, where the detection signals were obtained from the formation of chromogenic product p-nitrophenol (McComb and Bowers,1972). This chromogenic product was obtained using the inherent transphosphorylation capability of ALP. Inspired by this spectrometric methods, various other methods have also been reported for the determination of ALP using a wide range of substrates, *viz.* 5-Bromo-4-chloro-3-indolyl phosphate (Xi et al.,2016), nitro blue tetrazolium (Takehana et al.,2019), 4-Aminophenylphosphate *etc* (Jiang et al.,2016). In addition to the colorimetric detection of ALP in blood serum, chemi-luminiscence, fluorescence, and surface-enhanced Raman spectroscopy based determination techniques have also been employed (Hallaway and O'Kane,2000; Kim et al.,2011; Ruan et al.,2006). Apart from these, electrochemical based techniques (*viz.* voltammetric, amperometric *etc.*) are employed for the determination of the ALP in recent past, where the product from ALP catalysis has been targeted for its quantification (Lee et al.,2018; Wang et al.,2009). These reported methods not only used the indirect format for the estimation process but also involves incorporation of the multiple enzymes in the sensor fabrications, which eventually introduced the higher complexity and non-robustness. Additionally, all such detection strategies are susceptible for the insensitive, false positive determination, especially in the real sample environments due to the possible coexistences of the other peroxidases and redox active molecules in the real samples (King and Delory,1948).

In recent past, the advances in nano-fabrication strategies have paved to obtain the robust biosensors for the direct determination of the bio-analytes (Chandra,2016; Chandra et al.,2017), where various metallic nanocomposite have been used by exploiting their excellent optoelectronic properties (Baranwal et al.,2016; Mahato et al.,2019). In recent days, branched like metallic structures based nano-composite have been employed in various applications, where energy storage and nano-catalysts were widely explored. In addition, these structures have also been attempted in various biosensing methods due to the capability of availing relatively larger surface area for the electron conduction at the sensor surface (Valera et al.,2019), that eventually contributes sensitive determination. However, most of the reported biosensor using metallic dendrites follow the direct electrochemical transfer method, where the target analyte participates in electro-catalysis at the sensor probe surface to generate the electrochemical signal. Few works have also been reported by immobilizing the recognition elements by physical adsorption on these nanostructures (Fu et al.,2017; Wang et al.,2018), which are considered to be unstable due to its susceptibility for leaching out. Therefore, these metallic branch-structured nanomaterials are limited when there is need of stable coupling of the bio- recognition element onto it due to the absence of flanking groups for covalent immobilization of the bio-receptors. Thus, branched structured based nanocomposite have been used for coupling the bio-recognition elements by incorporating additional materials comprising flanking functional groups for bioreceptor molecular immobilization. In one of these strategies the composite consisting of branched Au-metallic-structure and conducting polymers of poly-pyrrole has been used for the immobilization of the antibody (Valera et al.,2019), which may suffer for less sensitivity caused by loss of conductivity due to the disruption of molecular planarity in presence of added functional group upon the functionalization (Berezhetska et al.,2015; Jimison et al.,2012). In order to overcome such limitations, GO has been used for the sensor matrix fabrication due to the excellent availability of flanking groups for covalent immobilization. Interestingly, to the best of our knowledge this combination has never been utilized to immobilize bioreceptor for immunosensors. Therefore, it is interesting to use such kind of new materials for such fabrications to obtain sensitive determinations.

Here in this work, we demonstrate an immuno-sensor based on the Au-branched structures (Au-nano-dendroids) and GO nanocomposite using the electrochemical impedance spectroscopy (EIS). This sensor matrix was designed for the label-free direct determinations of serum ALP, where anti-ALP is used as a bioreceptor. The fabrication of sensor probe has been done in a stepwise manner at screen-printed carbon electrode (SPCE) surface, where the sequential depositions of AuNPs, Au-nano-dendroid, graphene oxide (GO) sheets were achieved followed by the immobilization of anti-ALP using EDC-NHS bio-conjugation technique. The sensor probe has been characterized systematically using Fourier Transformed Infrared Spectroscopy (FTIR), scanning electron microscopy (SEM), cyclic voltammetry (CV), electrochemical impedance spectroscopy (EIS), and digital image colorimetry (DIC). The analytical performance has been evaluated using EIS in the spectral range of 10^6 to 10 Hz. The interferences due to the coexisting molecules have also been evaluated which shows the sensor probe is extremely selective towards the ALP. The sensor probe has been tested in the blood serum sample to assess the analytical capability in the clinical samples, where spike-recovery and standard addition methods were adopted. The unknown concentration of ALP in the serum sample has also been evaluated using standard addition method, which was obtained to be 83.15 U/L and is comparable with clinically determined ALP level in serum. The shelf-life of the fabricated SPCE/AuNPs/Au-nano-dendroids /GO/Anti-ALP probe has also been evaluated and was found to be stable for 8 weeks.

2. Experimental:

2.1. Chemicals and instrumentation:

Chemicals used in the experiment have been used in analytical grade. Alkaline phosphatase (ALP), was procured from Roche scientific, USA. The antibody of ALP (anti-ALP), Graphite flakes (C), nafion ($C_7HF_{13}O_5S{\cdot}C_2F_4$) were procured from Sigma Aldrich, USA. Potassium chloride (KCl), Potassium permanganate ($KMnO_4$), Potassium ferrocynide ($K_4Fe(CN)_6.3H_2O$), Potassium ferricynide ($K_3Fe(CN)_6$), Sodium chloride (NaCl), Sodium phosphate monobasic (NaH_2PO_4), Sodium phosphate dibasic (Na_2HPO_4) were procured from SRL research laboratory, India. Serum albumin, immunoglobulin, glycine, alanine, glucose, glutamic acid, uric acid, cysteine, and citric acid were procured from hi-media chemicals. The acids solvents phosphoric acid (H_3PO_4), sulphuric acid (H_2SO_4), hydrochloric acid (HCl: 30%), ethanol (C_2H_5OH) and acetonitrile (C_2H_3N) were procured from Merck Millipore. All the chemicals used in experimentation were of AR grade and were used without any purification steps. Double distilled water (DW) (Milli-Q; 18.5 MΩ) was used throughout the experiment. Phosphate buffered saline (PBS: 5mM, pH-7.0) was prepared using a previously reported method. The phosphate-buffered saline (PBS; 5 mM; pH 7.0) has been prepared using the standard protocol. Briefly, sodium monobasic (5 mmoles) and sodium dibasic (5 mmoles) salts have been dissolved in ultra-pure double distilled water having the conductivity of 18.2 MΩ.cm (at 25 ˚C). The Zobell's solutions were prepared by dissolving the Potassium ferrocyanide (5 mM) and potassium ferricyanide (5 mM) salts into the phosphate-buffered saline.

FTIR (Cary 630: Agilent, USA) and scanning electron microscope (SEM: Sigma: Carl Zeiss Ltd, Germany) were used for characterizing the modified surfaces during the stepwise fabrication of the sensing probe, where the FTIR spectra were recorded in the range between 400 and 4000 cm^{-1} wavenumbers. The probe fabrication steps were also characterized using the electrochemical workstation (Autolab: Metrohm, Netherland), where screen-printed carbon electrode (SPCE) with working electrode is at the center, circumfused counter electrode along with the Ag/AgCl reference electrode. The electrochemical impedance spectroscopy (EIS) was performed using the frequency response analysis module of Autolab, where the spectra were recorded at open circuit potential (V) vs. Ag/AgCl with the modulation aptitude of 10mV in the variable frequency range of 10 Hz to 1000 KHz. The analysis of obtained spectra was done by obtaining the resistance to charge transfer (R_{ct}), which is parallel in the equivalent circuit of impedance spectra. Smartphone (Xiaomi; Redmi Note 5 pro) based camera has been used for capturing the color change followed by the digital image colorimetry for quantifying the change in color.

2.2. Synthesis of graphene oxide:

For the synthesis of GO modified Hummer's method is adopted. Briefly, 0.450 g of graphite flakes were treated with the 60 ml of the solution mixture prepared with concentrated H_2SO_4 and H_3PO_4 (9:1). Thereafter, $KMnO_4$ (2.64g) was added slowly and solution was allowed to stir for 6 hours. After that, H_2O_2 (30% v/v) was mixed and agitated for 10 minutes followed by HCl (30%) treatment. Thereafter, the product was extracted by spinning it ae 5000 rpm followed by overnight drying to obtain the GO.

2.3. Digital image colorimetry based control study:

For the DIC based study, 50 µL of 5 mM BCIP solution was employed on to the final probe after immuno-complexation at working electrode region. The captured ALP catalyzes BCIP to a blueish green colored compound 5,5'-dibromo-4,4'-dichloro-indigo. After 30 minutes, this solution over the working electrode was taken out to the hydrophobic cellulose acetate thin sheet with a white background and the appeared color was captured using the smartphone camera. Thereafter, the captured image was processed using the RGB (Red, Green, and Blue) profiler application at the droplet region and values were extracted to trace the color change. Further DIC analysis in the control studies was also performed using the procedure followed by the technique reported earlier (Mahato and Chandra,2019). Briefly, the effective normalized intensities corresponding to the color change were obtained using equation 3.1.

$$Effective\ I_{\mathrm{R}} = \log_{10}\left(\frac{I_{\mathrm{R}\ (Blank)}}{I_{\mathrm{R}\ (Conc.)}}\right) \text{ ---------------------- Equation 3.1}$$

Where I_R is the mean pixel intensity of red channel, which is obtained from selected area analyses.

2.4. SPCE/AuNPs/ Au-nano-dendroid /GO/Anti-ALP Sensor probe fabrication:

The sensor probe has been fabricated by sequential surface modifications on to the bare SPCE. In the first step, SPCE has been modified with the electrochemically deposited AuNPs. In this step, the AuNPs were deposited electrochemically on to the bare SPCE, where the acidic solution of $HAuCl_4$ (0.005% in 0.5M H_2SO_4) was taken as an electrolyte in three electrode system and allowed for consecutive five LSV scans under the potential window of 1.5 V to 0.4 V. The provided voltage and time for deposition of -0.6 V and 60 seconds, respectively. In the next step, Au-nano-dendroids were synthesized electrochemically on to the SPCE/AuNPs modified surface. The deposition of the Au-nano-dendroids was achieved by the electrochemical deposition process, where chrono-amperometric technique was employed, which has been performed at - 0.3 V for 600s using the three electrode system containing $HAuCl_4$ solution (5% in KCl 0.1M) as an electrolyte. In the further step, the synthesized GO has been coated onto the

SPCE/AuNPs/Au-nano-dendroid modified electrode surface. Briefly, the GO solution (1mg/mL) was prepared by dissolving the GO in the ethanol and coated 2 µL of the solution by spin coating method followed by 30 minutes of drying. The dried SPCE/AuNPs/ Au-nano-dendroid /GO electrode surface was then activated for the anti-ALP immobilization. For that, 50 microliters of the solution containing EDC-NHS (100 mM-100 mM) was treated and incubated for 30 minutes. After this incubation, the EDC-NHS was washed and 4 microliters of anti-ALP (pH 7.0) were treated and allowed to react with the SPCE/AuNPs/Au-nano-dendroid/GO modified surface for next 30 minutes. After the incubation, the probe surface was gently washed to remove the unreacted anti-ALP followed by the 0.1% BSA blocking to overcome the false positive results. The final modified sensor probe was termed as SPCE/AuNPs/Au-nano-dendroid/GO/anti-ALP. The step-by-step sensor probe fabrication and detection principle have been shown in the scheme 3.1.

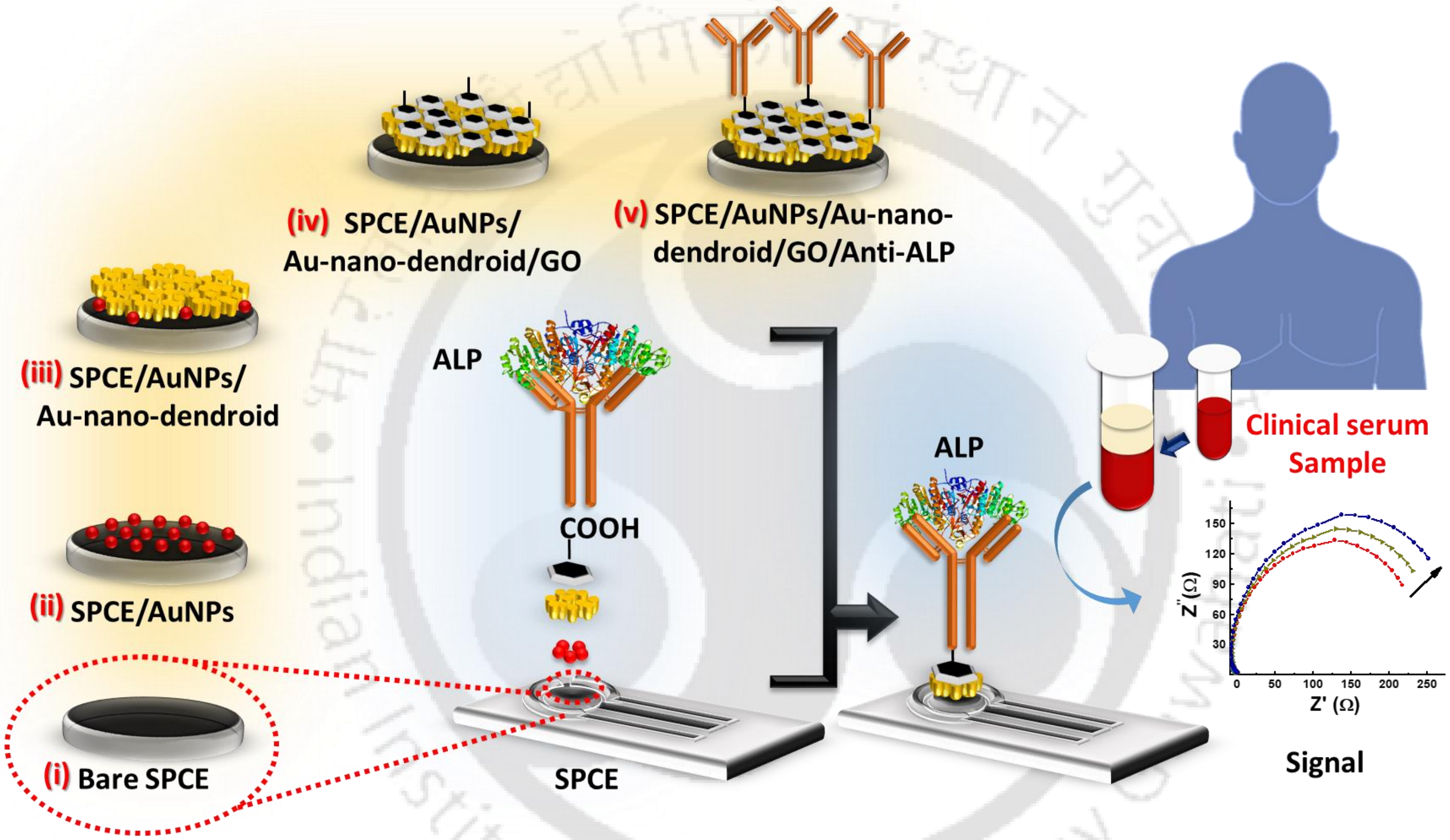

Scheme 3.1: *Schematic representation of the SPCE/AuNPs/ Au-nano-dendroid/GO/anti-ALP probe fabrication or ALP determination in clinical serum sample.*

3. Result and discussions:

3.1. Characterization of GO:

After the successful synthesis of GO using the modified hammers method, it has been systematically characterized using the TEM, EDX, SAED, and XRD technique. In the first step, the GO was exfoliated before the TEM imaging, where clear transparent sheet was observed, indicating the successful synthesis of the graphene sheets (figure 3.1A). In the following step, to know the elemental composition of the graphene sheets EDX have been recorded, where the clear elemental composition of C and O have been obtained, which indicates the sheets consisting the graphene oxides. Thereafter, the material properties of the GO have been studied using SAED and XRD, where the clear SAED ring pattern and the peak in X-ray diffrectograms show crystalline nature of the material.

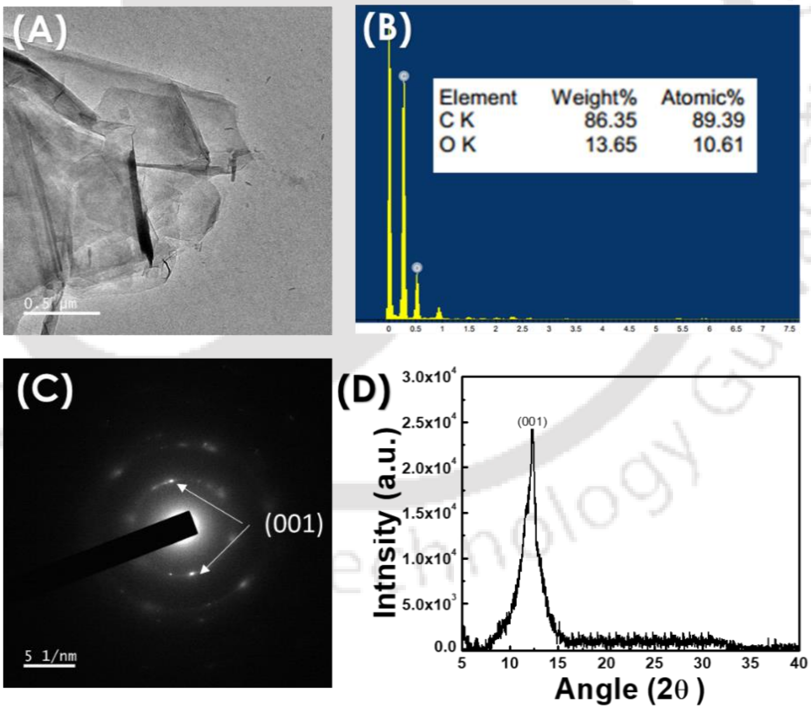

Element	Weight%	Atomic%
C K	86.35	89.39
O K	13.65	10.61

Figure 3.1: *Characterization of GO, showing (A) TEM micrograph, (B) EDX spectrum, (C) SAED pattern, (D) X-ray diffrectogram of GO.*

3.2. SPCE/AuNPs/ Au-nano-dendroid /GO/anti-ALP sensor probe characterization:

The fabrication of SPCE/AuNPs/Au-nano-dendroid/GO/anti-ALP sensor probe has been characterized using the physical as well as electrochemical techniques. For this purpose, FE-SEM, FTIR, CV, and EIS have been used. Firstly, the fabrication process has been assessed by FE-SEM, where the surface topological changes have been analyzed. For that, the FE-SEM micrographs of bare electrode surface, AuNPs deposited electrode surface, dendroid synthesized AuNPs deposited electrode surface, GO deposited on the dendroid grown electrode surface, and Anti-ALP immobilized at the GO modified electrode surface were captured (figure 3.2). From the figure, clear small bright uniform dot imprints have been observed at the AuNPs deposited electrode surface (ii), which was, however, not observed at the bare electrode surface (i). This indicates the successful deposition of AuNPs on to the electrode surface. In the next micrograph, a layer of irregular protruded features at the modified surface was observed at (iii), indicating the deposition of dendroid like Au-nanostructures. Thereafter, in the micrograph next to this (iv), the patches of small flakes were observed over the dendroids Au-nanostructures modified surface, indicating the successful deposition of GO over the previously modified surface. Thereafter, at the final step of modification, the EDC-NHS has been treated to immobilize the Anti-ALP. The FE-SEM micrograph recorded after the immobilization of anti-ALP (v), shows a clear change in surface topology with granular structure, indicating the successful anti-ALP immobilization. In order to confirm these modifications, corresponding FTIR spectra for bare SPCE, SPCE/AuNPs, SPCE/AuNPs/Au-nano-dendroid, SPCE/AuNPs/Au-nano-dendroid/GO, SPCE/AuNPs/Au-nano-dendroid/GO/EDC-NHS, and SPCE/AuNPs/Au-nano-dendroid/GO/EDC-NHS-anti-ALP were recorded and analyzed the changes during the modification process (figure 3.3).

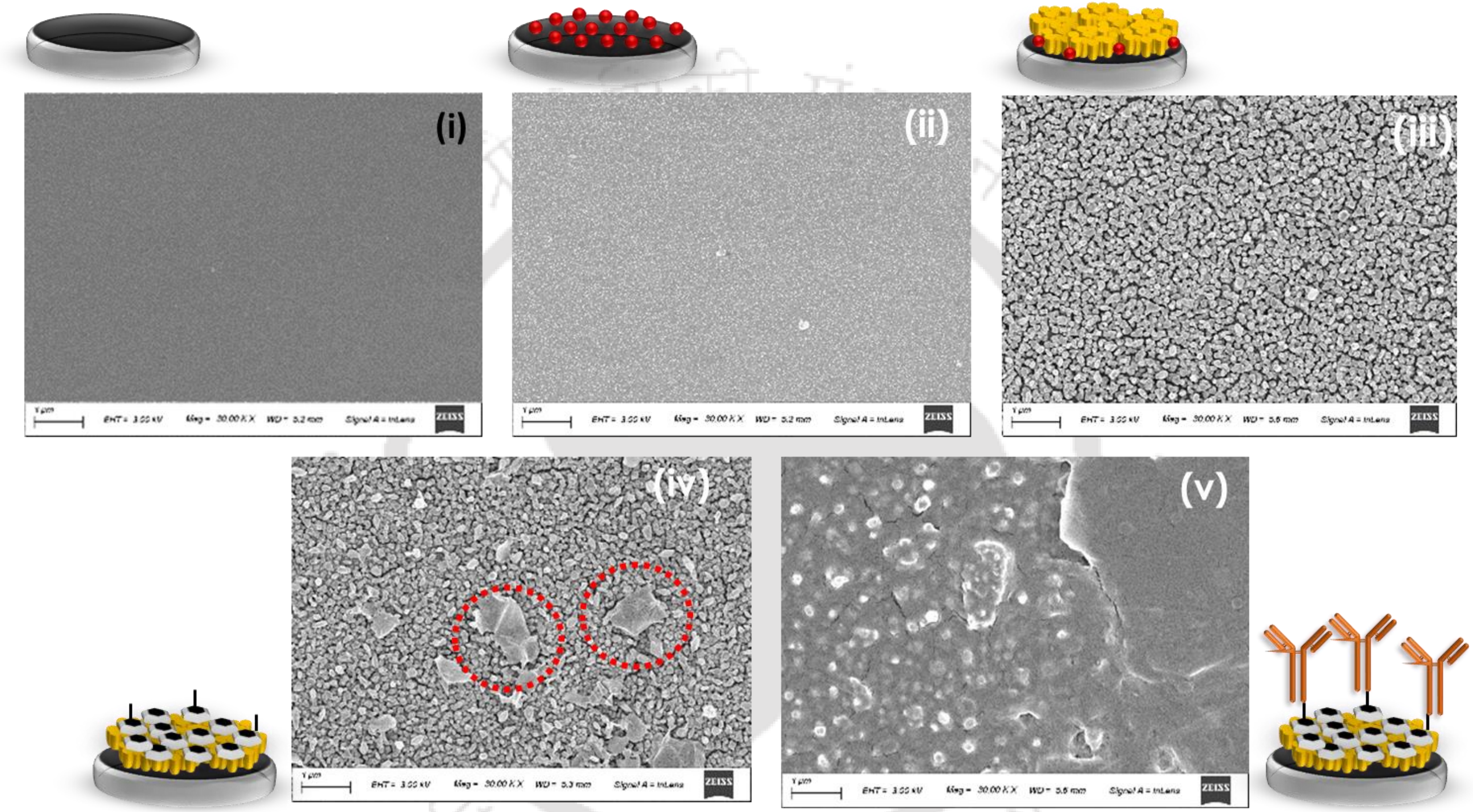

Figure 3.2: *FE-SEM micrographs of modified electrode surfaces (i) bare electrode* ***(ii)*** *AuNPs deposited electrode,* ***(iii)*** *Au dendroid structure synthesized electrode, (iv) subsequent GO deposited on the dendroid grown electrode surface,* ***(v)*** *Anti-ALP immobilized using EDC-NHS at the previously modified probe surface (GO deposited dendroid surface).*

In the FTIR spectrum corresponding to the bare SPCE, peaks at 3255 cm^{-1} and 1065 cm^{-1} were observed. These correspond to the -OH and C-C stretching vibrations, which are present in the carbon paste and used a binder. In the FTIR spectra taken after the SPCE/AuNPs, the peaks were observed much fainted, due to the deposition of AuNPs over the carbon paste material of SPCE. Not only in this step, the peaks completely disappeared in the next step of modification, where Au-nano-dendroid were grown which is due to the further metallic layering over the SPCE.

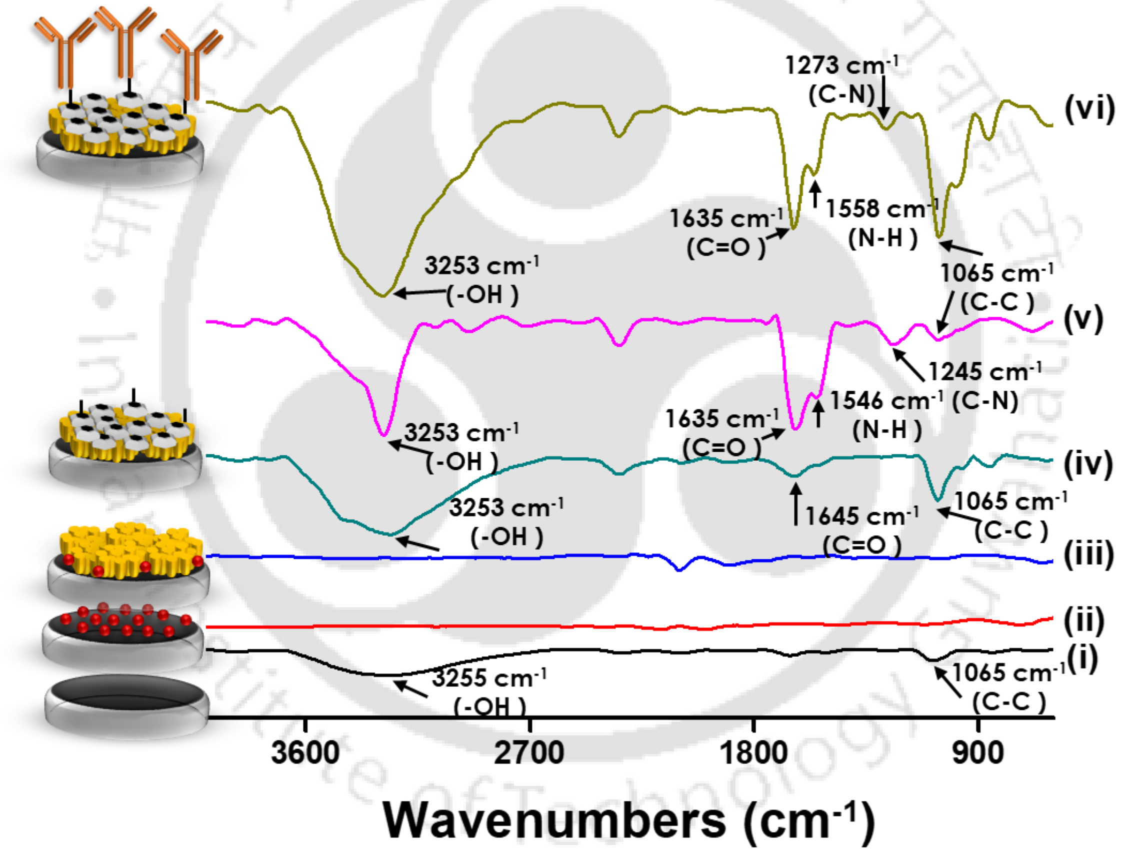

Figure 3.3. *FTIR spectra of the of the electrode surfaces including SPCE (i), SPCE/AuNPs(ii), SPCE/AuNPs/ Au-nano-dendroid (iii), SPCE/AuNPs/Au-nano-dendroid/GO (iv), SPCE/AuNPs/Au-nano-dendroid/GO/EDC-NHS (v), and SPCE/AuNPs/ Au-nano-dendroid /GO/EDC-NHS-anti-ALP (vi) surfaces.*

This layering of nano-dendroids was prominently visualized by the naked eye, where the color of SPCE surface changes from dark black to golden brown color. In the next spectrum, the appearance of peaks at 3253 cm^{-1}, 1645 cm^{-1}, 1420 cm^{-1}, and 1065 cm^{-1} were observed, which are due to the –OH, C=O, C-OH, and C-C vibrations of GO confirming the successful deposition of the GO at SPCE/AuNPs/ Au-nano-dendroid electrode surface. The appearance of new vibrational peaks along with the subtle shift has been observed in the next spectrum at EDC-NHS treated SPCE/AuNPs/Au-nano-dendroid/GO surface, where the broad peak at the 3253 cm^{-1} gets narrower and appearance of a new peak at 1546 cm^{-1} was observed. In addition to this, the slight shift of –C=O peak at 1635 cm^{-1} was found, indicating the successful formation of EDC-NHS mediated amide linkage at the present GO with the flanking sulpho-NHS. In the next spectrum, the persistence of peaks at different positions along with the amide signature peaks at 1558 cm^{-1}(amide I) and 1635 cm^{-1}(amide II) and the appearance of a new peak at 974 cm^{-1} (C-C-C) were observed, indicating the successful immobilization of the anti-ALP.

Thereafter, in order to characterize the charge transfer behavior of fabricated SPCE/AuNPs/ Au-nano-dendroid /GO/anti-ALP probe, we have assessed the fabrication process using electrochemical techniques. The deposition of AuNPs was characterized using the LSV technique where consecutive scans were performed. The clear reduction peak at 0.095 (V) vs. Ag/AgCl was observed. This reduction peak is most likely due to the reduction of Au^{3+} of the solution phase to Au^{0} at the electrode surface, which eventually forms AuNPs at SPCE electrode (figure 3.4 A). Interestingly, when the subsequent scans were performed, the increment on reduction peak was observed, indicating its gradual increment in charge transfer and enhanced conductivity of the modified surface. In the subsequent step, the nano-dendroid structures have been grown on to the SPCE/AuNPs modified electrode surface using chrono-amperometric technique. Figure 3.4 B shows the chorno-amperometric response due to nano-dendroid deposition, the gradual increment of the current in the beginning is due to the increased conductivity of the surface. After few seconds, the amperometric response attained its plateau, indicating the initiation of Au-nano-dendroid formation over the SPCE/AuNPs modified surface. On further continuation, the current response was observed constant at the plateau level, indicating the vertical growth of the Au-nano-dendroid (figure 3.4 B).

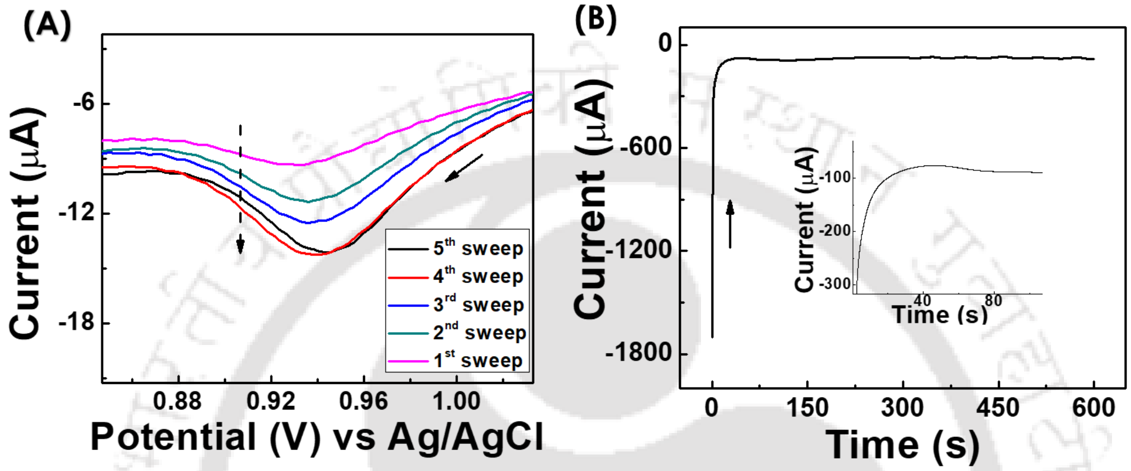

Figure 3.4: *(A) LSV responses for electrochemical deposition of gold on to the SPCE electrode; (B) chrono-amperometric response for the vertically grown gold nano-dendroid on to the SPCE/AuNPs surface at potential of 0.6V*

In the next step, modified electrode was assessed by recording LSV under the experimental conditions of the window -0.2 V to 0.6 V at a scan rate of 50 mV/s in 5mM Zobell's solution. Figure 3.5 shows the LSV responses for bare SPCE (black), SPCE/AuNPs (red), SPCE/AuNPs/ Au-nano-dendroid (blue), SPCE/AuNPs/Au-nano-dendroid /GO (grey), and SPCE/AuNPs/Au-nano-dendroid /GO/anti-ALP (pink). The representative peaks were observed at the 0.26 (Ipa) due to the electrochemical behavior of the mediator. It is interesting to note that the anodic peak current was found to be increased when SPCE/AuNPs was analyzed. This increment is due to the deposition of AuNPs over bare SPCE, making the surface conducting as well as increasing the effective surface area for charge transfer. Thereafter, Au-nano-dendroid were deposited over the SPCE/AuNPs surface, the LSV response has been observed with further increments in peak currents, indicating the SPCE/AuNPs/Au-nano-dendroid modified surface is capable of giving amplified signal. This amplification of the signal is due to the further increment of the surface area for charge transfer and its conducting behavior. In the next step, GO was deposited over the previously modified electrode surface and the LSV has been recorded at SPCE/AuNPs/ Au-nano-dendroid/GO surface and peak currents were analyzed. The effective current was decreased due to the less conducting behavior of GO.

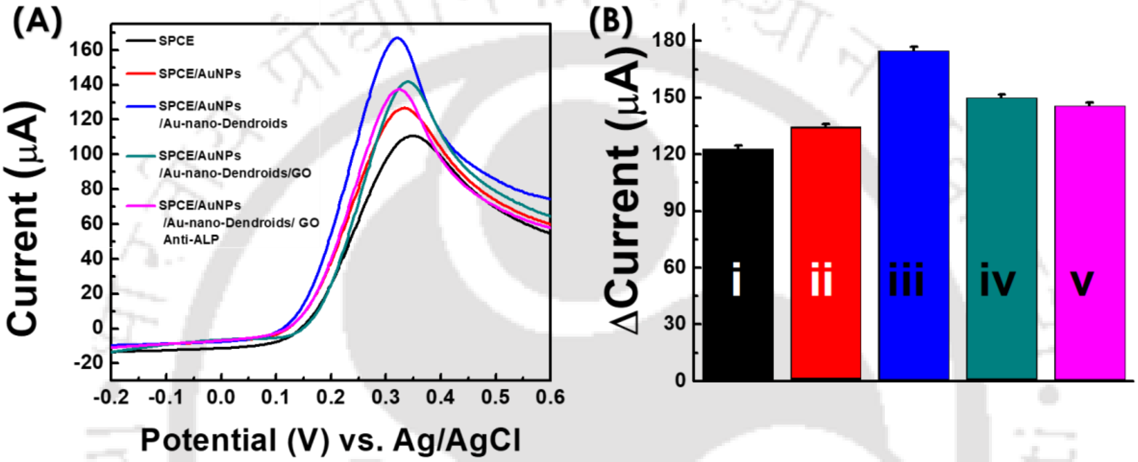

Figure 3.5: *CV responses of the modified surfaces (i) SPCE (black), (ii) SPCE/AuNPs (red), (iii) SPCE/AuNPs/ Au-nano-dendroid (blue), (iv) SPCE/AuNPs/ Au-nano-dendroid /GO (gray), (v) SPCE/AuNPs/ Au-nano-dendroid /GO/Anti-ALP (pink).*

Further, in the final step of probe fabrication, anti-ALP was conjugated using the EDC-NHS bio-conjugation technique over the SPCE/AuNPs/Au-nano-dendroid /GO modified surface and the LSV was recorded. The effective peak currents were found to be decreased in these modified electrodes, which is due to the insulating nature of anti-ALP. Finally, the fabricated sensing probe was termed as SPCE/AuNPs/Au-nano-dendroid/GO/anti-ALP. The electrochemical behavior of any fabricated surface depends on the charge transfer phenomena occurring at electrode/electrolyte interface, where the diffusion of charge carriers play an important role in electrochemical sensing. In order to assess the importance of modified surfaces for charge transfer capability in such phenomenon, we have deduced the diffusion coefficients of bare SPCE and every layer of the modified electrode using Randles-Sevick's model and found 1.5 fold greater transfer of charged species through SPCE/AuNPs/ Au-nano-dendroid /GO/anti-ALP modified electrode surface than the bare SPCE. The findings of Randles-Sevcik's model clearly suggests that the developed SPCE/AuNPs/Au-nano-dendroid/GO/anti-ALP sensing surface is relatively conducting and capable of transferring greater amount of charged species in order to provide better sensitivity. The results obtained by LSV were also validated using the EIS, where spectra in the Nyquist plot were recorded for bare SPCE (black), SPCE/AuNPs (red), SPCE/AuNPs/Au-nano-dendroid (blue), SPCE/AuNPs/Au-nano-dendroid/GO (grey), and SPCE/AuNPs/ Au-nano-dendroid /GO/ anti-ALP(pink) surfaces to obtain the resistance in charge transfer (Rct) (Figure 3.6 A).

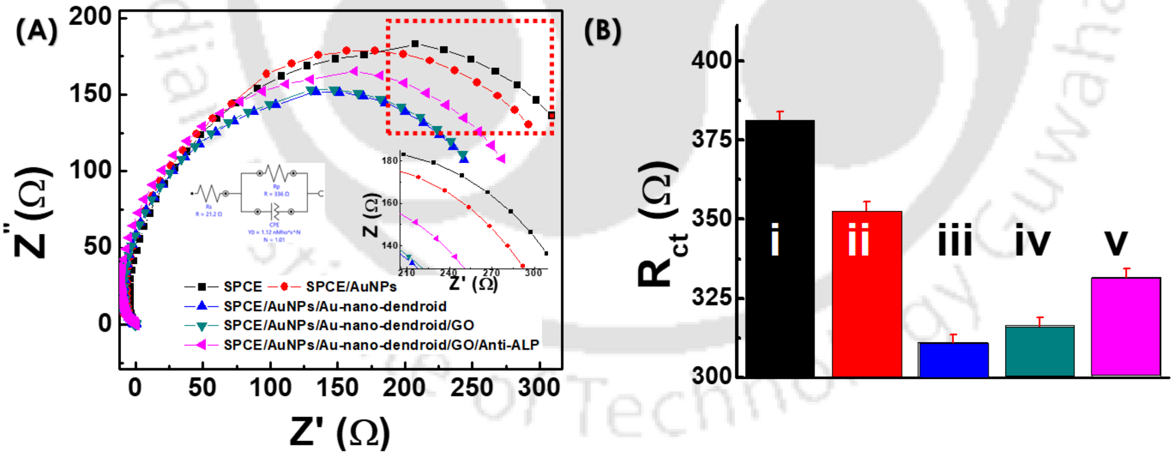

Figure 3.6: *(A) EIS responses of the modified surfaces (i) SPCE (black), (ii) SPCE/AuNPs (red), (iii)SPCE/AuNPs/ Au-nano-dendroid (blue), (iv) SPCE/AuNPs/ SPCE/AuNPs/ Au-nano-dendroid /GO/anti-ALP /GO (gray), (B) Histogram showing the corresponding Rct values.*

The Rct values obtained were 381.13 ±2.92, 352.71 ±2.72, 311.13 ± 2.42, 316.36 ±2.46, and 331.81 ± 2.58 for the bare SPCE (black), SPCE/AuNPs (red), SPCE/AuNPs/ Au-nano-dendroid (blue), SPCE/AuNPs/ Au-nano-dendroid /GO-Naf (grey), and SPCE/AuNPs/ Au-nano-dendroid /GO/anti-ALP(pink) surfaces, respectively (Figure 3.6 B). These results confirm that the developed SPCE/AuNPs/Au-nano-dendroid /GO/anti-ALP probe is capable of delivering the sensitive detection; hence, it is suitable for electrochemical analysis. In order to assess the process involved at the electrode / electrolyte interface, scan rate study has been performed, where the LSV at SPCE/AuNPs/Au-nano-dendroid/GO/anti-ALP sensor probe has been recorded with varying scan rates between 10-100 mV/s (shown in figure 3.7). Thereafter, the scan rate dependent plot is obtained, where peak currents were plotted against the square root of the scan rates.

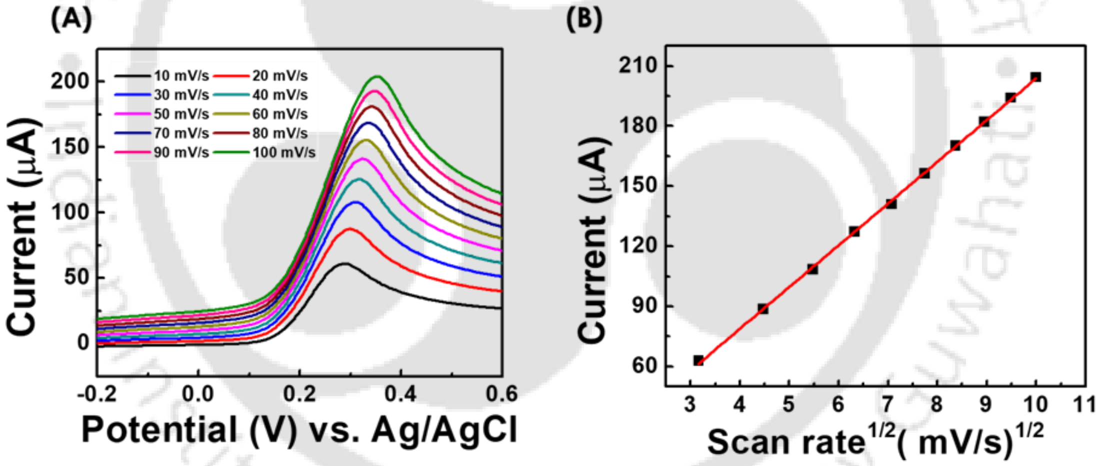

Figure 3.7: *(A) LSV responses of SPCE/AuNPs/Au-nano-dendroid/GO/Anti-ALP modified surface at different scan rates (10-100 mV/s) (B) scan rate dependent plot obtained from the LSV responses*

The linear relationship between current and square root of scan rate clearly suggests that the involvement of the diffusion controlled process at the electrode/electrolyte interface. The continuous increment of the peak currents with the scan rate also indicates the stable fabrication of the probe, which otherwise could be nonlinear increment with increasing scan rates.

3.3. Control studies for the SPCE/AuNPs/Au-nano-dendroid/GO/anti-ALP sensor probe:

Before assessing the analytical performance of the designed SPCE/AuNPs/Au-nano-dendroid/GO/anti-ALP sensor, its immuno-complexation ability with ALP was confirmed by performing the droplet assisted digital image colorimetry by exploiting the catalytic activity of the ALP. For that, we have incubated the sensor probe along with the modified control surfaces with the 50 µL of 10 mM BCIP solution, which is a substrate for the ALP and gives the blue-green colored complex (figure 3.8 A). Figure 3.8 B shows the effective intensities corresponds to the modified (i) SPCE/AuNPs/Au-nano-dendroid/GO, and EDC-NHS activated surfaces of (ii) SPCE/AuNPs/Au-nano-dendroid/GO/blocking agent/ALP, (iii) SPCE/AuNPs/Au-nano-dendroid/GO/anti-ALP/blocking agent, and (iv) SPCE/AuNPs/Au-nano-dendroid/GO/anti-ALP/blocking agent/ALP surfaces.

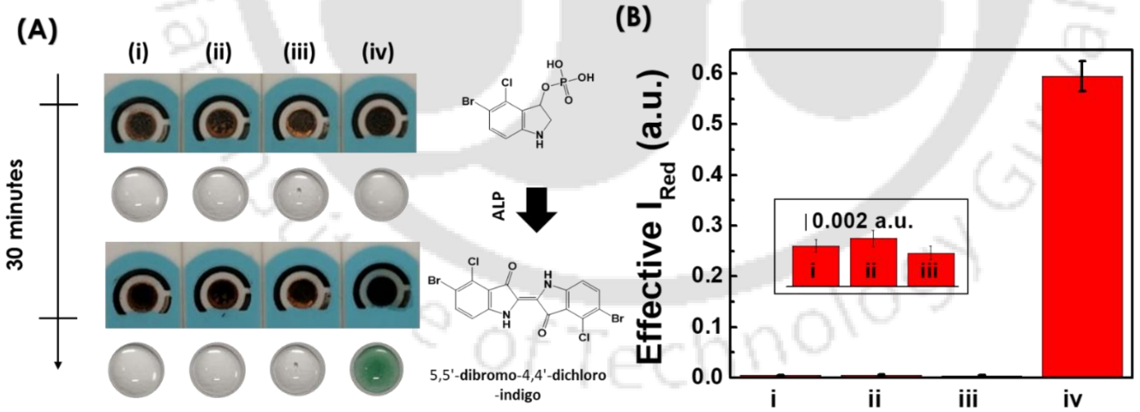

Figure 3.8: *(A) The colorimetric responses of controls (i-iii) and ALP immuno-complexed SPCE/AuNPs/Au-nano-dendroid/GO/anti-ALP sensor probe at the droplet extracted from the SPCE chip before and after (30 miniutes) the BCIP treatment. (B) Corresponding DIC responses.*

The effective intensity corresponds to SPCE/AuNPs/ Au-nano-dendroid/GO/anti-ALP/blocking agent/ALP surface was found to be 0.78 units, which is significantly ($p<0.01$, n=3) higher from the controls, suggesting the successful immuno-complexation of ALP with SPCE/AuNPs/Au-nano-dendroid/anti-ALP/blocking agent sensor probe and no adsorption of ALP in the fabrication process.

3.4. Analytical performance:

After the validation the ALP sensing by the fabricated SPCE/AuNPs/Au-nano-dendroid /GO/anti-ALP sensor probe, we have performed the dose dependent study for its analytical performance, where the dosage of different concentrations of ALP has been treated with the fabricated sensor. Briefly, the biosensor probe was incubated with the different concentrations of ALP for 30.0 minutes (optimized) followed by the gentle rinsing of the probe using sterile PBS buffer and the EIS measurement using Zobell’s solution (pH-7.0 mM, 5 mM). Figure 3.9 A shows the characteristics EIS responses of the SPCE/AuNPs/ Au-nano-dendroid /GO/anti-ALP before binding, which were found to be increased with the increasing concentration of ALP. This gradual increment of the Rct is contributed by ALP immuno-complexation, which eventually introduces the insulating layer to charge transfer, where the Rct values were increased in the Nyquist plot. A calibration plot was drown based on the Rct values obtained from EIS responses in a dose dependent study (figure 3.9 B). The linear dynamic range was found between 100-1000 U/L. The linear regression equation is expressed as follows: $Rct\ (\Omega) = 0.058\ (\pm\ 0.001)\ [ALP] - 4.072\ (\pm\ 1.117)$. The limit of detection has been calculated is 9.10 (± 0.12) U/L (RSD < 3.7 %,) based on the standard deviation of the three times consecutive analysis of the blank (95% confidence value, n=3). This clearly shows that the developed sensor has a great potential for the detection of the ALP. It is worth mentioning that the linear dynamic range of the biosensor falls within the ranges of various clinical conditions, which indicates the significance of the fabricated SPCE/AuNPs/ Au-nano-dendroid /GO/anti-ALP biosensor in potential clinical diagnostics.

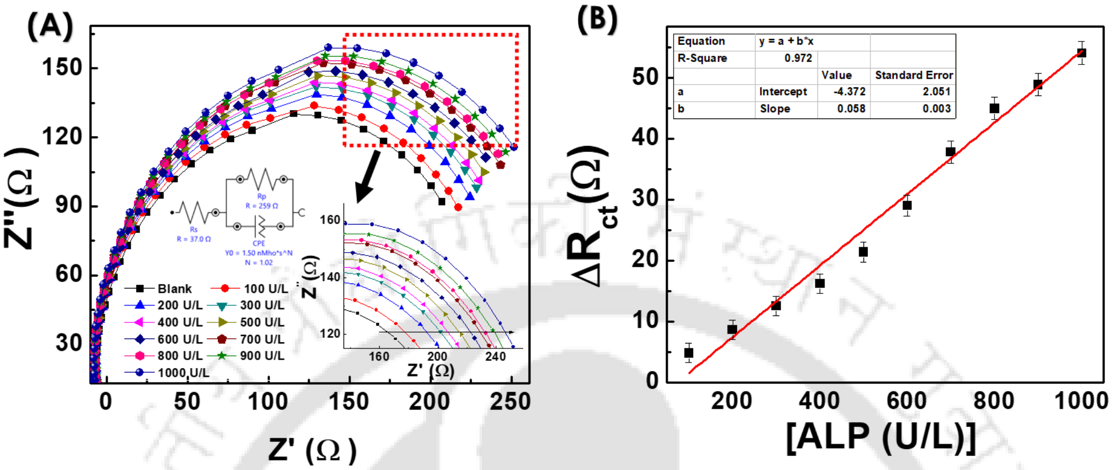

Figure 3.9: *(A) Dose dependent EIS responses of ALP (100-1000 U/L) at SPCE/AuNPs/ Au-nano-dendroid /GO/Anti-ALP modified sensor probe, (B) calibration plot obtained from the dose dependent spectrum.*

3.5. Selectivity assay:

In order to study the selectivity of the fabricated SPCE/AuNPs/ Au-nano-dendroid /GO/anti-ALP biosensor probe, the assessment of the sensor probe was obtained at potential interfering molecules found in biological fluids including, serum albumin, immunoglobulin, glycine, alanine, glucose, uric acid, cysteine, and citric acid. No interfering signals were observed from these under the tested experimental window. The selectivity of SPCE/AuNPs/ Au-nano-dendroid /GO/anti-ALP probe was mathematically deduced by determining the selectivity coefficient using the following equation 3.2

$$k_{sel} = \frac{(Signal)_{interferent}}{(Signal)_{ALP}} \qquad \text{------------ Equation 3.2}$$

Where k_{sel} *is the coefficient of selectivity,* $(Signal)_{interferent}$ *is the signal strength shown by probe when treated with the interfering molecules, and,* $(Signal)_{ALP}$ *is the signal strength corresponds to ALP.*

The calculated values for interfering molecules were extremely low (k_{sel} << 1), indicating that the fabricated sensor is highly selective towards ALP. The results were statistically analyzed by performing the T-test of the obtained Rct values, where p values were found to be << 0.001 (n = 3) for all the tested interfering molecules, indicating the selectivity results are of statistical relevance. Figure 3.10 shows the histogram shows the selectivity assay based on EIS analysis using the SPCE/AuNPs/ Au-nano-dendroid /GO/anti-ALP biosensing probe.

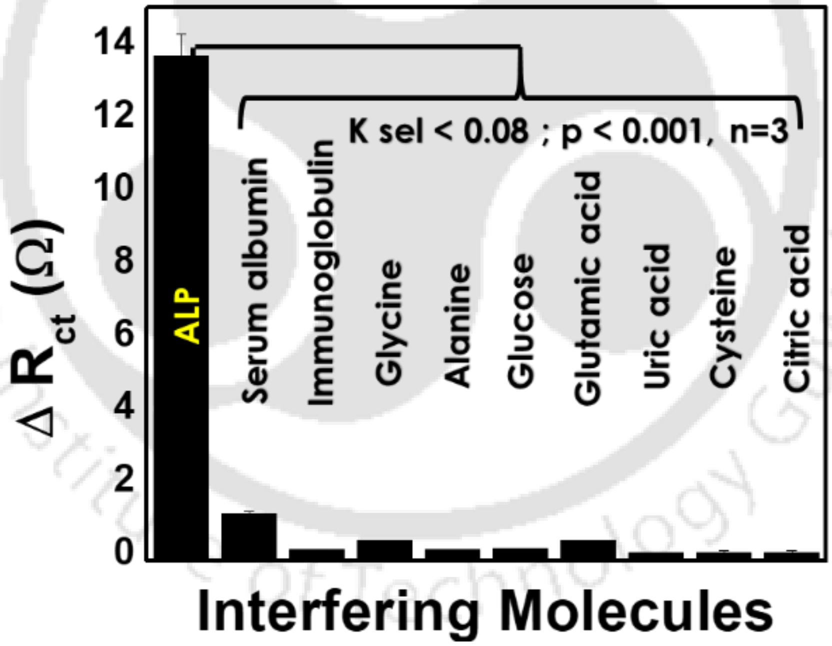

Figure 3.10: *Selectivity assay of SPCE/AuNPs/ Au-nano-dendroid /GO/anti-ALP sensor probe.*

3.6. Real sample studies:

For the commercial viability, the capability of the fabricated biosensor has been assessed using the real sample. Here we have used serum sample for the further assessment of the SPCE/AuNPs/ Au-nano-dendroid/GO/anti-ALP sensor probe. The whole study has been done systematically; where in the first step, spike and recovery model was used. In this method, a known concentrations of the ALP were spiked to the real sample and were recovered using fabricated sensor probe using equation 3.2

$$\% \text{ Recovery} = \frac{([A]_{ALP} - [B]_{ALP})}{[C]_{ALP}} \qquad \text{----------------------------------- Equation 3.2}$$

Where, $[A]_{ALP}$ *and* $[B]_{ALP}$ *are the analytical responses of ALP in the spiked and blank serum samples, respectively; and* $[C]_{ALP}$ *is the analytical response of* ALP *in the standard solutions.*

In this study, the dose dependent EIS responses from the serum samples containing no ALP/ ALP were recorded using the fabricated probe, where an increase in the Rct values was observed on increase in ALP concentrations. Figure 3.11 shows the histogram showing the Rct values obtained from the comparative dose dependent responses obtained from serum sample assessments using the sensor probe. The sensitivity using sensor probe was performed, where the % recovery obtained between 116% and 148% of ALP from the serum samples. The analytical details of recovered ALP, % recovery, and RSD has been shown in table 3.1. The detection limit was determined which was found to be 13.15 (± 0.17) U/L (RSD < 7.8%) based on the standard deviation of consecutive five times responses of the blank (95 % confidence level, n=5). The recovered concentrations obtained in this study were observed way greater than the spiked concentration, indicating the presence of residual ALP in the serum sample. Therefore, in the next phase, we have extended the study to find the residual (unknown) concentrations of the ALP in the serum sample. Here, the serum samples were collected from the volunteer and the collected sample was used for the ALP assessment using the fabricated SPCE/AuNPs/ Au-nano-dendroid/GO/anti-ALP sensor probe and by clinical method simultaneously. For the assessment using sensor probe, standard addition method has been adopted, where the probe is first tested using the five times diluted (in PBS) serum sample (no ALP spiked), and thereby subsequent spiking of the known concentration was done and the responses were recorded.

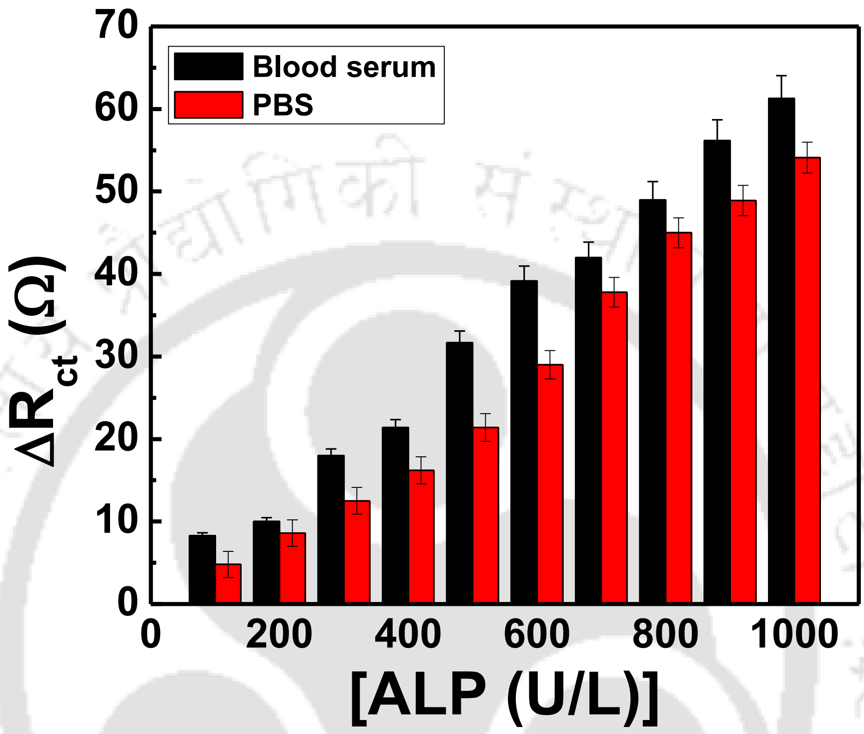

Figure 3.11: *Comparative dose dependent detection of ALP in blood serum and PBS based on % recovery.*

Sl. No.	Spiked ALP (U/L)	Recovered ALP (U/L)	% Recovery	RSD
1	100	130.83	130.83	0.059
2	200	232.79	116.39	0.043
3	300	431.52	143.84	0.045
4	400	527.9	131.97	0.046
5	500	740.18	148.03	0.044
6	600	810.62	135.1	0.042
7	700	777.4	111.05	0.041
8	800	870.75	108.84	0.043
9	900	1033.98	114.88	0.051
10	1000	1132.71	113.27	0.039

Table 3.1: *Details of the recovered ALP concentrations, % recovery and RSD.*

Thereafter, using the EIS responses from the biosensor probe, standard addition plot was obtained, the linear regression equation for ALP found to be Rct (Ω) = 0.058 (± 0.036) [ALP] +1.94 (± 0.677) with the correlation coefficient of 0.98. The representative standard addition plot has been shown in the figure 3.12, where the concentration of ALP in the serum sample was calculated as 83.15 (± 2.45) U/L (RSD < 2.9 %) (16.63 U/L x 5 dilution factor).

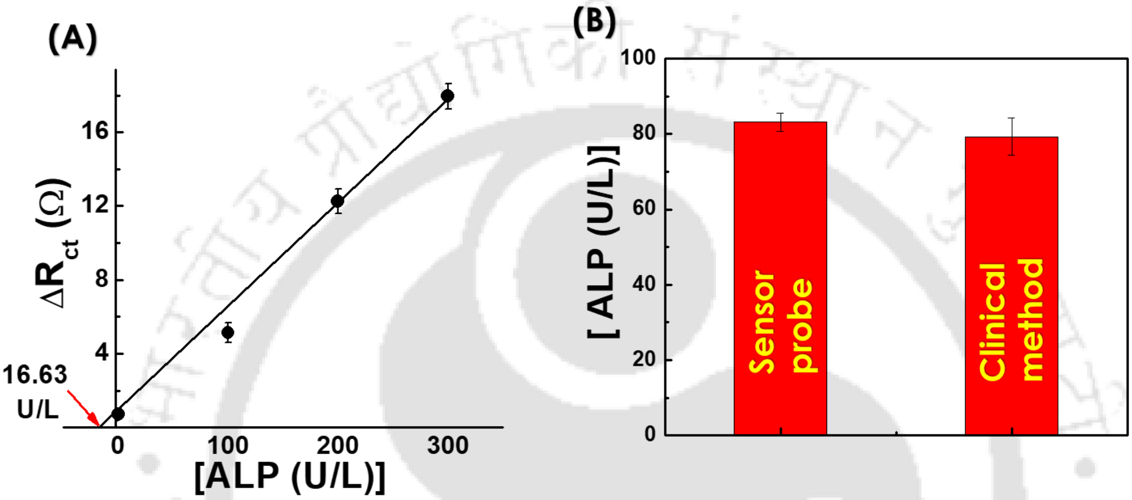

Figure 3.12: *Standard addition plot obtained for ALP detection in serum sample.*

The clinical validation of the fabricated sensor probe was done by determining the ALP level of the same serum sample, where the observed ALP level was found to be 79.31 (± 5.0) U/L. The concentration of ALP obtained by our sensor and the routine clinical assay were comparable, indicating the direct clinical application of the fabricated sensor in hospitals.

3.7. Storage conditions, stability, and reproducibility assessment:

The fabricated SPCE/AuNPs/Au-nano-dendroid/GO/anti-ALP biosensor probe was then stored at 4° C after its fabrication and the sensors were used for the determination of ALP after every week and the Rct values were recorded. The Rct responses obtained by the sensor probe shows that it retained the sensitivity of 98.03% until 8th week, while the significant decrement of the signal was observed afterwards, which is most likely due to the loss of biological activity of anti-ALP and/or the degradation of the chemical modification steps. The considerably good shelf life up to eight weeks was most likely due to the stable immobilization of anti-ALP and retention of its biological activity on SPCE sensor chip (figure 3.13).

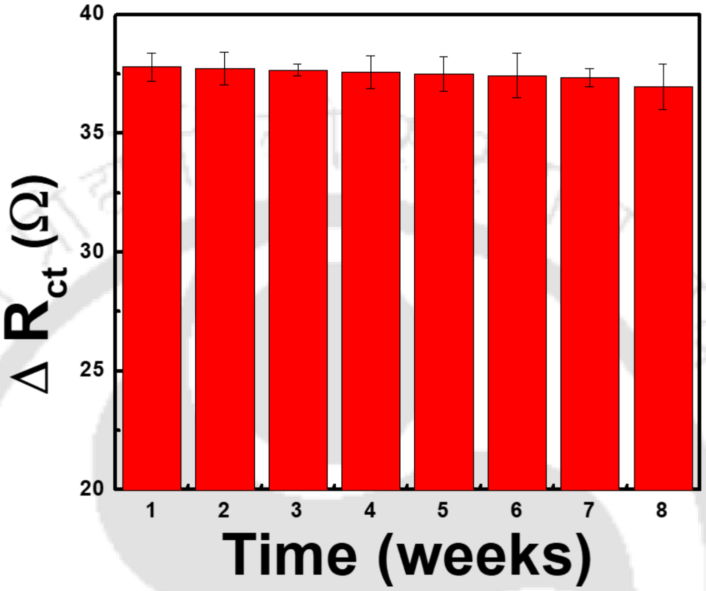

Figure 3.13: *Time dependent response of the fabricated SPCE/AuNPs/ Au-nano-dendroid /GO/Anti-ALP sensor probe.*

The reproducibility of the fabricated SPCE/AuNPs/Au-nano-dendroid/GO/anti-ALP biosensor was evaluated, which showed the RSD below than the < 2.3% even when the same fabrication process was followed, indicating the sensor fabrication is highly reproducible, and this variation is most likely due to the negligible deviation in the sensor fabrication steps and handling errors.

4. Conclusions:

We have developed a screen-printed based biosensor for the determination of ALP in clinical serum using the Au-nano-dendroid - GO based nanocomposites. The developed nanocomposite was characterized using various techniques including TEM, SAED, EDX, and XRD. Thereafter, SPCE/AuNPs/ Au-nano-dendroid/GO/Anti-ALP sensor was fabricated by following sequential deposition of the nanocomposite onto the SPCE chip. The fabricated SPCE/AuNPs/ Au-nano-dendroid /GO/Anti-ALP sensor probe is capable of delivering the ALP detection with wide range of concentration (100 - 1000 U/L) covering the ALP levels in various pathophysiological conditions (*viz.* bone disease, liver disease, carcinoid syndrome, *etc.*). The limit of detection was obtained to be 9.10 (±0.12) U/L. The biosensor showed high selectivity towards ALP even in presence of various coexisting molecules including, albumin, globulin, alanine, glucose, citric acid, uric acid and glutamic acid ($k_{sel} << 0.08$). The shelf life of the biosensor has also been evaluated, where the sensor probe was found to be stable up to 8 weeks. Apart from these, the fabricated biosensor has many attractive features such as its robustness, easy fabrication, and deliverable at the point of care use.

5. References:

Baranwal, A., Mahato, K., Srivastava, A., Maurya, P.K., Chandra, P., Phytofabricated metallic nanoparticles and their clinical applications, ***2016***. *RSC Advances* 6(107), 105996-106010.

Berezhetska, O., Liberelle, B., De Crescenzo, G., Cicoira, F., A simple approach for protein covalent grafting on conducting polymer films, ***2015***. *Journal of Materials Chemistry B* 3(25), 5087-5094.

Bodlaj, G., Hubmann, R., Saleh, K., Stojakovic, T., Biesenbach, G., Berg, J., Alkaline phosphatase predicts relapse in chronic hepatitis C patients with end-of-treatment response, ***2010***. *World journal of gastroenterology* 16(19), 2407-2410.

Buonaguro, F.M., Caposio, P., Tornesello, M.L., De Re, V., Franco, R., Cancer diagnostic and predictive biomarkers 2018, ***2019***. *BioMed research international* 2019.

Chandra, P., 2016. Nanobiosensors for personalized and onsite biomedical diagnosis. The Institution of Engineering and Technology.

Chandra, P., Tan, Y.N., Singh, S.P., 2017. Next generation point-of-care biomedical sensors technologies for cancer diagnosis. Springer.

Fu, L., Wu, K., Ji, J., Zhang, J., Guo, X., 2017. A highly sensitive disposable glucose biosensor based on platinum nanoflowers decorated screen printed carbon electrode. 2017 IEEE sensors, pp. 1-3.

Hallaway, B.J., O'Kane, D.J., 2000. Chemiluminescence assay of serum alkaline phosphatase and phosphoprotein phosphatases. Methods in Enzymology, pp. 391-401. Academic Press.

Jiang, H., Islam, M.S., Sazawa, K., Hata, N., Taguchi, S., Nakamura, S., Sugawara, K., Kuramitz, H., Development of an Electrochemical Bioassay Based on the Alkaline

Phosphatase Activity of Chlamydomonas reinhardtii to Assess the Toxicity of Heavy Metals, ***2016***. *Int. J. Electrochem. Sci* 11, 5090-5102.

Jimison, L.H., Hama, A., Strakosas, X., Armel, V., Khodagholy, D., Ismailova, E., Malliaras, G.G., Winther-Jensen, B., Owens, R.M., PEDOT:TOS with PEG: a biofunctional surface with improved electronic characteristics, ***2012***. *Journal of Materials Chemistry* 22(37), 19498-19505.

Keshaviah, A., Dellapasqua, S., Rotmensz, N., Lindtner, J., Crivellari, D., Collins, J., Molleoni, M., Thürlimann, B., Mendiola, C., Aebi, S., Price, K., Pagani, O., Simoncini, E., Castiglione Gertsch, M., Gelber, R., Coates, A., Goldhirsch, A., CA15-3 and alkaline phosphatase as predictors for breast cancer recurrence: a combined analysis of seven International Breast Cancer Study Group trials, ***2007***. *Annals of Oncology* 18(4), 701-708.

Kim, T.-I., Kim, H., Choi, Y., Kim, Y., A fluorescent turn-on probe for the detection of alkaline phosphatase activity in living cells, ***2011***. *Chemical Communications* 47(35), 9825-9827.

King, E., Delory, G., Acid and alkaline phosphatases in their relation to malignant disease, ***1948***. *Postgraduate medical journal* 24(272), 299.

Lee, J.Y., Ahn, J.K., Park, K.S., Park, H.G., An impedimetric determination of alkaline phosphatase activity based on the oxidation reaction mediated by Cu2+ bound to poly-thymine DNA, ***2018***. *RSC Advances* 8(20), 11241-11246.

Mahato, K., Chandra, P., Paper-based miniaturized immunosensor for naked eye ALP detection based on digital image colorimetry integrated with smartphone, ***2019***. *Biosensors and Bioelectronics* 128, 9-16.

Mahato, K., Nagpal, S., Shah, M.A., Srivastava, A., Maurya, P.K., Roy, S., Jaiswal, A., Singh, R., Chandra, P., Gold nanoparticle surface engineering strategies and their applications in biomedicine and diagnostics, ***2019***. *3 Biotech* 9(2), 57.

McComb, R.B., Bowers, G.N., Study of optimum buffer conditions for measuring alkaline phosphatase activity in human serum, ***1972***. *Clinical chemistry* 18(2), 97-104.

Ruan, C., Wang, W., Gu, B., Detection of Alkaline Phosphatase Using Surface-Enhanced Raman Spectroscopy, ***2006***. *Analytical Chemistry* 78(10), 3379-3384.

Takehana, K., Onomi, R., Hatate, K., Yamagishi, N., Determination of serum bone-specific alkaline phosphatase isoenzyme activity in captive Asian elephants (<i>Elephas maximus</i>) using an agarose gel electrophoresis method, ***2019***. *Journal of Veterinary Medical Science* advpub.

Valera, A.E., Nesbitt, N.T., Archibald, M.M., Naughton, M.J., Chiles, T.C., On-Chip Electrochemical Detection of Cholera Using a Polypyrrole-Functionalized Dendritic Gold Sensor, ***2019***. *ACS Sensors* 4(3), 654-659.

Wang, J.H., Wang, K., Bartling, B., Liu, C.-C., The detection of alkaline phosphatase using an electrochemical biosensor in a single-step approach, ***2009***. *Sensors (Basel)* 9(11), 8709-8721.

Wang, R., Liu, W.-D., Wang, A.-J., Xue, Y., Wu, L., Feng, J.-J., A new label-free electrochemical immunosensor based on dendritic core-shell AuPd@Au nanocrystals for highly sensitive detection of prostate specific antigen, ***2018***. *Biosensors and Bioelectronics* 99, 458-463.

Xi, C., Jin, C., ZHANG, H.-Y., Fu-Bing, W., Fang-Fang, W., Xing-Hu, J., Zhi-Ke, H., Colorimetric detection of alkaline phosphatase on microfluidic paper-based analysis devices, ***2016***. *Chinese Journal of Analytical Chemistry* 44(4), 591-596.

Chapter- IV

Development of miniaturized electrochemical nanobiosensor based on AuNPs-porous graphene-1,8-DAN for vitamin-C detection in fruit juice, human urine, and neurodegenerative diseased mice brain

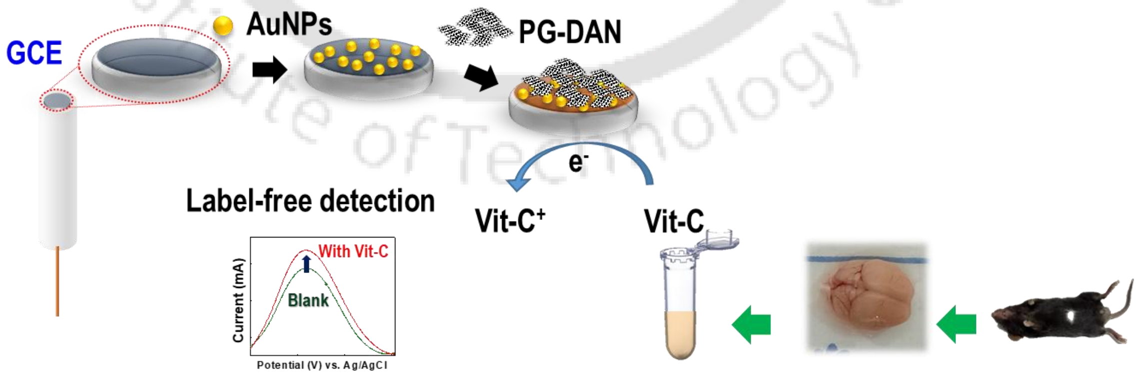

1. Introduction:

Here, we have studied the impact of porous nanomaterials based composite for engineering the sensor surface in electrochemical detections. For that, vitamin C (Vit-C) has been chosen as a model molecule, which is chemically known as ascorbic acid. Owing to its excellent antioxidant properties, it has found various physiological roles in living body (Wang et al.,2017). Its deficiency has been reported in many diseases including, scurvy and various neurodegenerative disorders such as cerebral ischemia, Alzheimer's, and Parkinson's disease (Kocot et al.,2017; Moretti et al.,2017), and is characterized as hypovitaminosis C, where the threshold serum level of Vit-C is 11µM or below. In its acute severity, the hypovitaminosis tends to the avitaminosis C as in the case of sudden infant death syndrome (SIDS) (Hattersley,1993; Prasad et al.,2008) due to no or trace level of Vit-C in biological fluid. Since SIDS occurs to neonates and infants, the blood serum based tests carry high risks of infection due to its invasive nature. Thus, to know the extent of such severity of Vit-C depletions, urine-based non-invasive tests would be one of the solutions, as Vit-C level in urine is reported to have the correlation with serum level of Vit-C (Teruuchi and Mochizuki,1959). In view of these, the ultrasensitive detection of Vit-C levels in various matrices may help clinicians to diagnose diseases associated with Vit-C levels. The classical Vit-C detections are majorly done by using titrimetric and fluorimetric methods. In the titrimetric process, Vit-C is titrated against dichloroindophenol (Evelyn et al.,1938) and potassium iodate (Deshmukh and Bapat,1955), which are also susceptible to other coexisting molecules. The fluorimetric methods are based on the oxidation of Vit-C followed by reaction of o-phenylenediamine producing fluorescent active quinoxaline derivatives are also susceptible to the accompanying fluorescence quenchers and enhancers (Tarrago-Trani et al.,2012). Therefore, these methods suffer from false positive signals due to the presence of interfering molecules in complex biological matrices including urine, serum *etc*. The advanced techniques for Vit-C detection in biological samples have also been reported using capillary zone electrophoresis (Tang and Wu,2005), liquid chromatography (Lima et al.,2016), flow injection coupled with spectrophotometric (Al-Shwaiyat et al.,2018), fluorescence (Kong et al.,2017), and chemiluminescence detectors (Xu et al.,2018). Apart from these, instrument assisted techniques *viz.* Fourier transform infrared (FTIR) (Oliveira-Folador et al.,2018; Yulia et al.,2014) and FT-Raman (Yang and Irudayaraj,2002) have also been reported for Vit-C detection, however, complexities in generated data due to their wavelength-dependent penetration depth can potentially lead to a falsified Vit-C detection (Fabian et al.,2005). Owing to the high precision and sensitivity, the commercial estimation of Vit-C has been done by ultra-performance liquid chromatography (UPLC) (Klimczak and Gliszczyńska-Świgło,2015) and high performance liquid chromatography (Mazurek and Jamroz,2015), that are highly advanced and extremely powerful systems. However, extreme sophistication, multistep nature, requirement of large sample volume, and inability of miniaturization limits their usage for understanding the close association of Vit-C in different physiological states. In order to address such limitations, various state-of-the-art methods have been reported following biosensor based methods (Chandra,2016), where electrochemical nanobiosensors have widely been studied for Vit-C detection based on its direct electron transfer behavior (Pisoschi et al.,2014). The main boundaries to these systems are the close redox potential of accompanying interfering molecules (Kamyabi and Shafiee,2012) and higher detection limits (Pisoschi et al.,2014). Importantly, the developed electrochemical nanobiosensors have never been applied to detect Vit-C in contrasting physiological states such as Vit-C level in healthy and diseased brain models, which are important to show its real clinical promise. Therefore, it would be interesting to develop a novel label-free biosensing strategy, which can offer a selective and sensitive detection of Vit-C in various real sample matrices. To do so, the possible ways includes are the introduction of novel nanocomposite materials that selectively catalyze Vit-C and / or segregate the oxidation peak potential effectively from other coexisting interfering molecules. Among all types of nanostructured materials, in recent years porous graphene based composites have greatly been studied for its application in waste water treatment (Tabish et al.,2018), adsorbent (Zhu et al.,2017), redox flow battery (Cao et al.,2017), and energy storage devices (Hooch Antink et al.,2018). Recently, the application of porous graphene has also reported for the detection of chemical (Yu et al.,2018) and biological (Yang et al.,2017) molecules, however, it has never been applied for Vit-C detection and for bio-molecular analysis in complex matrices such as mammalian / human tissues and cells. Therefore, porous graphene based nanocomposites could be an interesting and important material for nanobiosensor design and applications.

In the present work, we have hydrothermally synthesized a nanocomposite (PG-DAN) based on porous graphene and positively charge 1, 8-DAN for the detection of Vit-C (scheme 4.1A). The synthesized PG-DAN nanocomposite was characterized using scanning electron microscopy (SEM), field emission transmission electron microscopy (FETEM), and FTIR. A sensing probe was fabricated by coating the PG-DAN onto the AuNPs electro-deposited glassy carbon electrode (GCE) (scheme 4.1B), which was characterized by atomic force microscopy (AFM), cyclic voltammetry (CV), and electrochemical impedometric spectroscopy (EIS). Thereafter, the dose dependent detection of Vit-C was performed using the fabricated nanobiosensor probe to assess its analytical performance, *i.e.* linear dynamic range (LDR) and DL using differential pulse voltammetry (DPV). The practical applicability of the fabricated nanobiosensor was examined by testing Vit-C in human urine samples using spike and recovery method. The fabricated nanobiosensor was also applied for the comparative analysis of Vit-C levels in brain tissues of healthy and diseased mice models suffering from neurodegenerative disorders, which has also been validated using the high pressure liquid chromatography (HPLC) technique. Interference due to various components was studied and the long-term stability of designed nanobiosensor was evaluated.

2. Experimental:

2.1. Chemicals and instruments:

Potassium ferricyanide ($K_3Fe(CN)_6$), Potassium ferrocyanide ($K_4Fe(CN)_6.3H_2O$), sodium chloride (NaCl), Sodium phosphate dibasic (Na_2HPO_4), potassium chloride (KCl), Sodium phosphate monobasic (NaH_2PO_4), potassium permanganate ($KMnO_4$), and glucose ($C_6H_6O_6$) were purchased from Sisco Research Laboratory, India. Vitamin C ($C_6H_8O_6$), citric acid ($C_6H_8O_7$), uric acid ($C_5H_4N_4O_3$), urea (CH_4N_2O), Thiourea (CH_4N_2S), EDTA (Ethylenediaminetetraacetic acid ; $C_{10}H_{16}N_2O_8$), perchloric acid ($HClO_4$), dopamine hydrochloride ($C_8H_{11}NO_2{\cdot}HCl$), graphite flacks (C), 1,8-diaminonaphthalene ($C_{10}H_{10}N_2$), ammonium persulphate ($(NH_4)_2S_2O_8$), chloroauric acid ($HAuCL_4$), nafion ($C_7HF_{13}O_5S{\cdot}C_2F_4$), and acetaminophen ($C_8H_9NO_2$) were purchased from Sigma-Aldrich, USA. The acids solvents phosphoric acid (H_3PO_4), sulphuric acid (H_2SO_4), hydrochloric acid (HCl: 30%), hydrogen peroxide (H_2O_2), trifluoroacetic acid (CF_3COOH), ethanol (C_2H_5OH) and acetonitrile (C_2H_3N) were procured from Merck Millipore. All the chemicals used in experimentation were of AR/HPLC grade and were used without any purification steps. Double distilled water (DW) (Milli-Q; 18.5 MΩ) was used throughout the experiment. Phosphate buffered saline (PBS: 5mM, pH-7.0) was prepared using a previously reported method. (Kashish et al.,2017) The electrochemical characterization of the electrode was performed in 5 mM ferricyanide and ferrocyanide solution (Zobell's solution; 5mM, pH-7.0) prepared in PBS.

For the characterization of synthesized material, FTIR (Cary 630: Agilent, USA), and Field emission-transmission electron microscope (FETEM: Jeol-2100F: Jeol Ltd. Japan), scanning electron microscope (SEM: Sigma: Carl Zeiss Ltd, Germany) were used. The FTIR spectra were recorded in the range between 400 and 4000 cm^{-1} wavenumbers. The sensor probe surface was characterized by atomic force microscope (AFM: Innova SPM: Bruker, United States). All the electrochemical analyses have been performed using electrochemical workstation (Autolab: Metrohm, Netherland) with the conventional three cell electrode system, comprising glassy carbon electrode (GCE) as working, platinum electrode as counter and Ag/AgCl electrode (in saturated KCl) as reference electrode. The electrochemical impedance spectroscopy was performed using the frequency response analysis (FRA) module of electrochemical workstation, where the spectra were recorded at open circuit potential (V) *vs.* Ag/AgCl with the modulation aptitude of 10mV in the variable frequency range of 0.1 Hz to 100 KHz. The obtained spectra were analyzed using the circuit comprising of solution resistance connected in series and the resistance in charge transfer (R_{ct}) connected in parallel. For the mice acclimatization shelter IVC cages were used procured from Techniplast, Italy. The chromatographic analyses were performed using Dionex ultimate 3000 UHPLC system synchronized with Chromoleon console 7.2.8 version software.

2.2. Synthesis of PG-DAN:

Firstly, the GO was synthesized following modified Hummers method.(Zaaba et al.,2017) Briefly, 0.225 g of graphite flakes were treated with the 30 ml of the solution mixture prepared with concentrated H_2SO_4 and H_3PO_4 (9:1). Thereafter, $KMnO_4$ (1.32g) was added slowly and solution was allowed to stir for 6 hours. After that, H_2O_2 (30% *v/v*) was mixed and agitated for 10 minutes followed by the HCl (30%) treatment. In the next step, the product was extracted by centrifugation at 5000 rpm and dried overnight (scheme

4.1A (i-ii)). The synthesized GO was further used for the preparation of PG-DAN nanocomposite. To do this, the GO (22.5 mg), and the 1,8-DAN (11.25 mg) along with ammonium persulphate (0.02M) was suspended in 15 ml of water/acetonitrile mixture (2:1) and sonicated for 1 hour. Thereafter, the obtained suspension was transferred into the autoclave vessel and the mixture was heated hydrothermally at 180 ºC for 18 hours. The content was then extracted and dried overnight using freeze drier (scheme 4. 1A (iii-v)).

2.3. Sample preparation for high performance liquid chromatography:

For the HPLC analysis the mice brain samples (healthy /diseased) were prepared by following the standard protocol (Thrivikraman et al.,1974). For that, the brain tissue of dissected mice was extracted in the mobile phase extraction medium containing Perchloric acid (0.05 M), thiourea (0.002 M), and (0.001 M) disodium EDTA. Briefly, 10 µL of extraction medium was used for per milligram of brain tissue sample and it was kept in chilled ice for precipitate down the protein contents. Thereafter, the samples were centrifuged at 13000 rpm for 25 min at 4°C and supernatant was collected. For further dilution of standards and samples supernatant, the mobile phase (0.01% of trifluoroacetic acid) was used. The Vit-C was analyzed on syncronis C18 particle size 3µm, dimensions: 150 X 4.6 mm with gradient mode. The mobile phase composed of solvent A (0.01% of trifluoroacetic acid) and solvent B (100 % of methanol) filtered with 0.2µM filter. Further, the gradient was set as follows: T_{min}/% proportion of solvent (B): $_{o}$/5, $_{0\text{-}3}$/5, $_{5\text{-}8}$/95, $_{8\text{-}12}$/95, $_{12\text{-}13}$/5, $_{13\text{-}20}$/5. The flow rate of the mobile phase was set at 0.5 ml/min and the detection was carried out using a photodiode array detector at 244 nm. The total run time for the experimentation was 20 minutes and the retention time of ascorbic acid was found to be 5.2 min (Grotzkyj Giorgi et al.,2012).

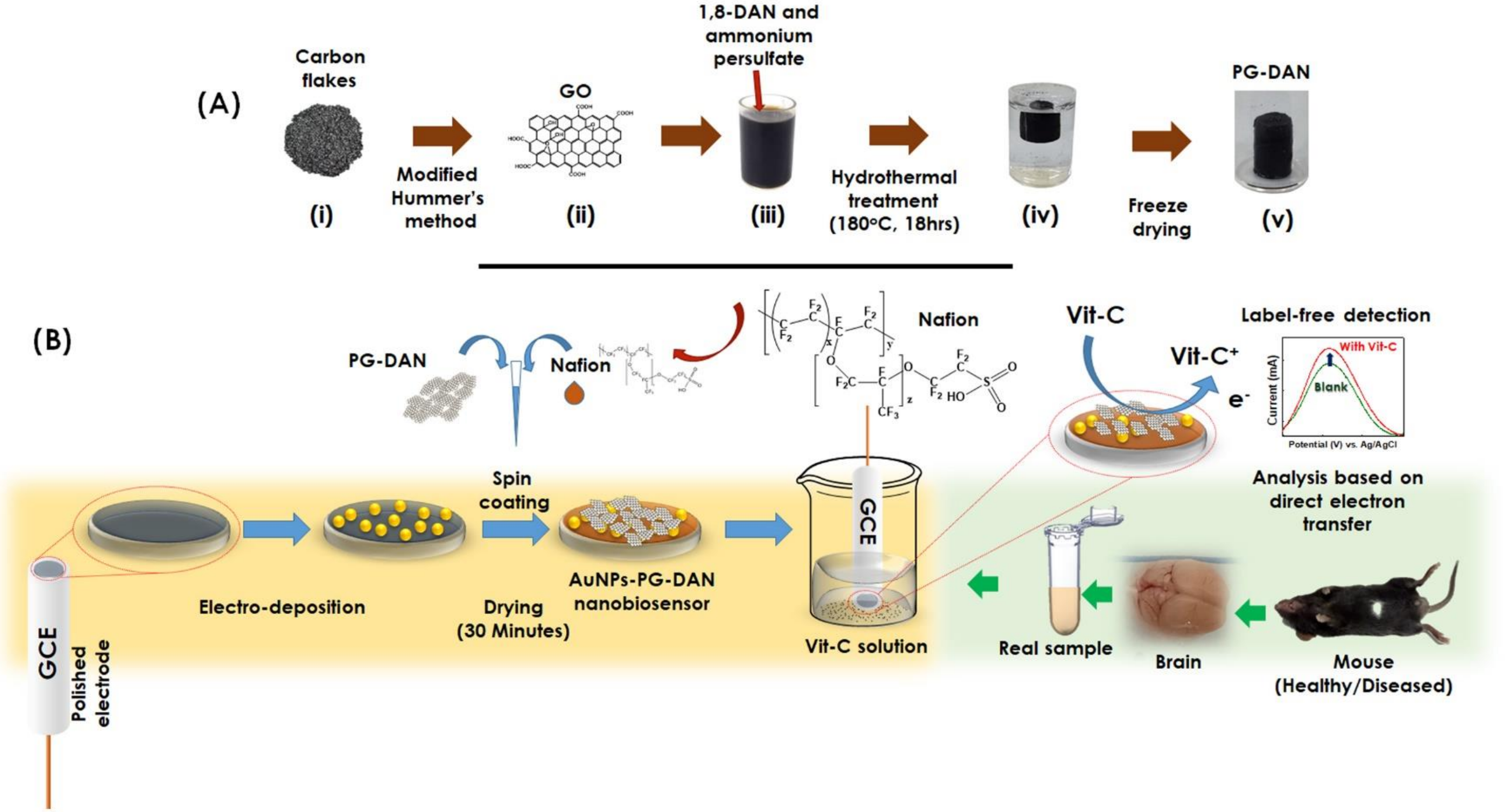

Scheme 4.1: *(A) Schematic representation of PG-DAN synthesis and (B) fabrication process of GCE/AuNPs/PG-DAN-Naf probe.*

2.4. Fabrication of GCE/AuNPs/PG-DAN-Naf nanobiosensor probe:

The detailed process of GCE/AuNPs/PG-DAN-Naf sensing probe fabrication is shown in scheme 4.1(B). At first, GCE electrode was polished with 0.05 µm alumna slurry on a microcloth pad and was rinsed with DW. After this, AuNPs were electrochemically deposited onto the GCE using a potential step method in an acidic solution (0.5 M H_2SO_4) containing 0.0025% $HAuClO_4$ by performing linear sweep voltammetry (LSV) from +1.5 to +0.4 (V) *vs.* Ag/AgCl. The provided conditions for AuNPs electrodeposition conditions are as follows: 60.0 s deposition time, − 0.6 V deposition potential, 0.1 V s^{-1} scan rate, and three times potential scanning. Thereafter, the GCE/AuNPs electrode was rinsed with DW and dried. In the next step, 10 mg/mL of PG-DAN was mixed with 0.1% nafion ultrasonically for 4 hrs and then the nanocomposite mixture was coated onto the GCE/AuNPs surface. After drying, the electrode was washed with PBS in order to remove the unbound materials from surface. Thereafter, electrode was dried and the final nanobiosensor probe was termed as GCE/AuNPs/PG-DAN-Naf.

2.5. Diseased and healthy mice brain sample preparation:

Mice (25-30 g) of 8-10 week old were procured from Palamur biosciences Telangana, India for real sample studies. The mice were housed in individually ventilated cages (IVC) with supplied corncob bedding of corncob granules (Sparcobb, Bangalore) and kept under controlled environment of humidity (65±10%) and temperature (25±2°C). The reversed 12/12 hrs light and dark cycle were maintained while housing animals for entire study period. Food as dry solid pellets (SAFE, France) along with filtered tap water access was provided *ad libitum* to animals throughout the study. The acclimatized mice were then randomly chosen and grouped (6 each) for control and diseased for further studies, where group 1 mice were taken as healthy and group 2 mice were diseased induced with the neurodegenerative disorder. Thereafter, the mice were sacrificed on 7th day with cervical dislocation and brain was removed out and dissected following a standard protocol (Spijker,2011). The excised homogenized brain was further used to prepare the sample for Vit-C analysis using GCE/AuNPs/PG-DAN-Naf nanobiosensor probe

3. Results and Discussions:

3.1. Characterization of the PG-DAN nanocomposite:

Scheme 4.1(A) shows overall development process of PG-DAN nanocomposite, where a black-colored nanocomposite cake was obtained as a final product (iv and v). Thereafter, we have systematically characterized this nanocomposite using SEM, TEM, and FTIR. Interestingly, in the SEM analysis of PG-DAN, a clear porous matrix was observed (Figure 4.1(A)), which was not observed when GO was analyzed separately (Figure 4.1(B)). The PG-DAN nanocomposite was also investigated using TEM where porous network like structures were observed (inset of figure 4.1(A)) that authenticates the porous nature of synthesized PG-DAN.

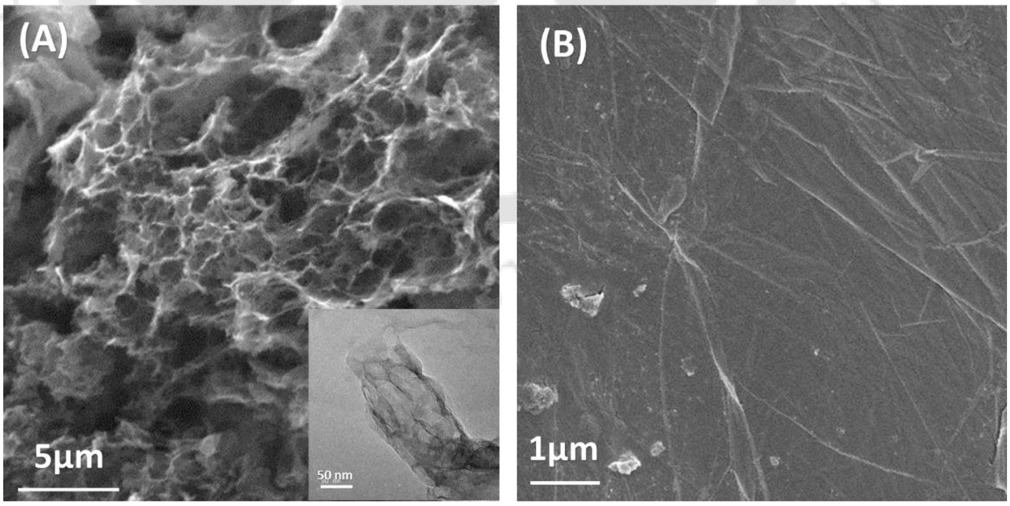

Figure 4.1: *FESEM micrograph of (A) PG-DAN (in inset, exfoliated TEM image) and (B) GO.*

We further extended the analysis to know the changes in functional groups and thus performed FTIR spectroscopy where we have recorded the spectra of precursor molecules (GO and 1,8-DAN) and PG-DAN nanocomposite separately, which was used to fabricate the sensing probe. The representative FTIR spectra for (i) GO (ii) 1,8-DAN monomer, and (iii) PG-DAN shown in figure 1(D). From the spectra of GO, peaks at 3290, 1707, 1548, 1390, 1201, and 1040 cm $^{-1}$ were observed due to hydroxyl (O-H) stretching, carboxyl (C=O) stretching, C=C stretching, C-OH, C-O-C, and C-O bending vibrations, respectively, indicating the successful synthesis of GO (Ossonon and Bélanger,2017).

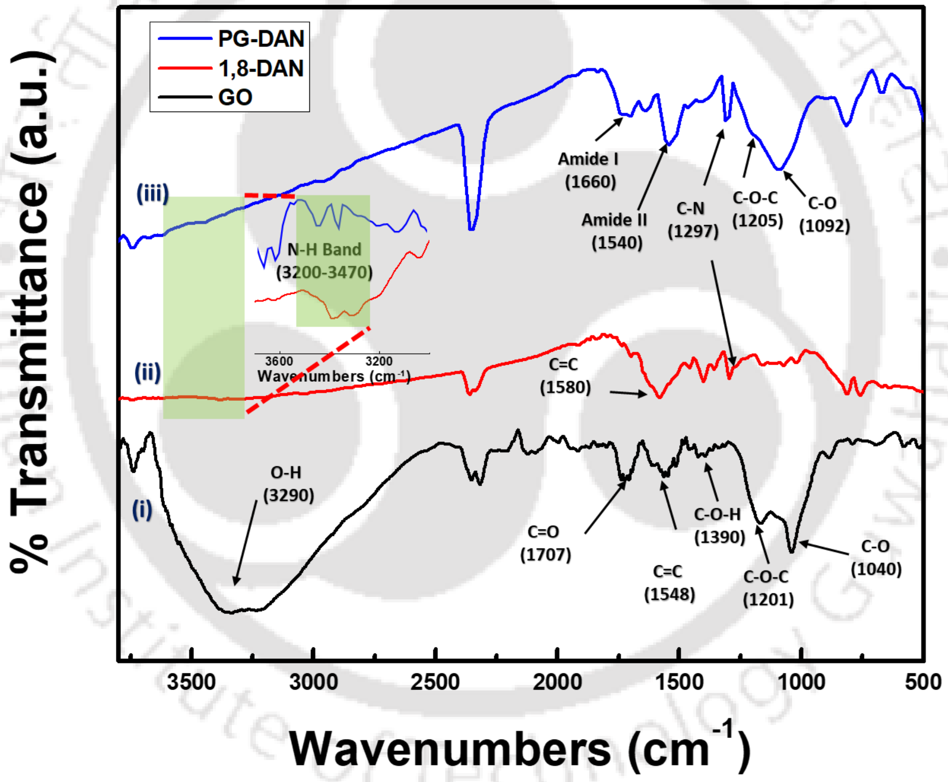

Figure 4.2: *FTIR spectra corresponding to (i) GO, (ii) 1,8-DAN, and (iii) PG-DAN.*

In the spectrum of 1,8-DAN, peaks at 1580, 1297, and 3360 cm^{-1} were observed due to characteristics peaks of aryl (C=C), (CN), and (NH) stretching vibrations, respectively. Thereafter, we have recorded the FTIR spectrum of PG-DAN, where no peak at 3290 cm^{-1} (OH stretch) was evident, indicating that GO has been reduced during the hydrothermal treatment process. While, peaks at 3360 cm^{-1} (NH) and 1297 cm^{-1} (CN) stretches were observed due to presence of 1,8-DAN in the composite. Importantly, the two new peaks at 1660 cm^{-1} (amide I) and 1540 cm^{-1} (amide II) were observed which were most likely due to the coupling of 1,8-DAN with GO forming amide linkage by replacing the existing carboxyl OH flanking groups.

3.2. Characterization of GCE/AuNPs/PG-DAN-Naf nanobiosensor probe:

Using the synthesized PG-DAN nanocomposite a nanobiosensor probe was fabricated as described in Scheme 4.1(B). The modified probe surfaces were characterized using AFM, where we recorded the surface topologies and *z-deflection* profiles (Figure 4.3) after every step of modification.

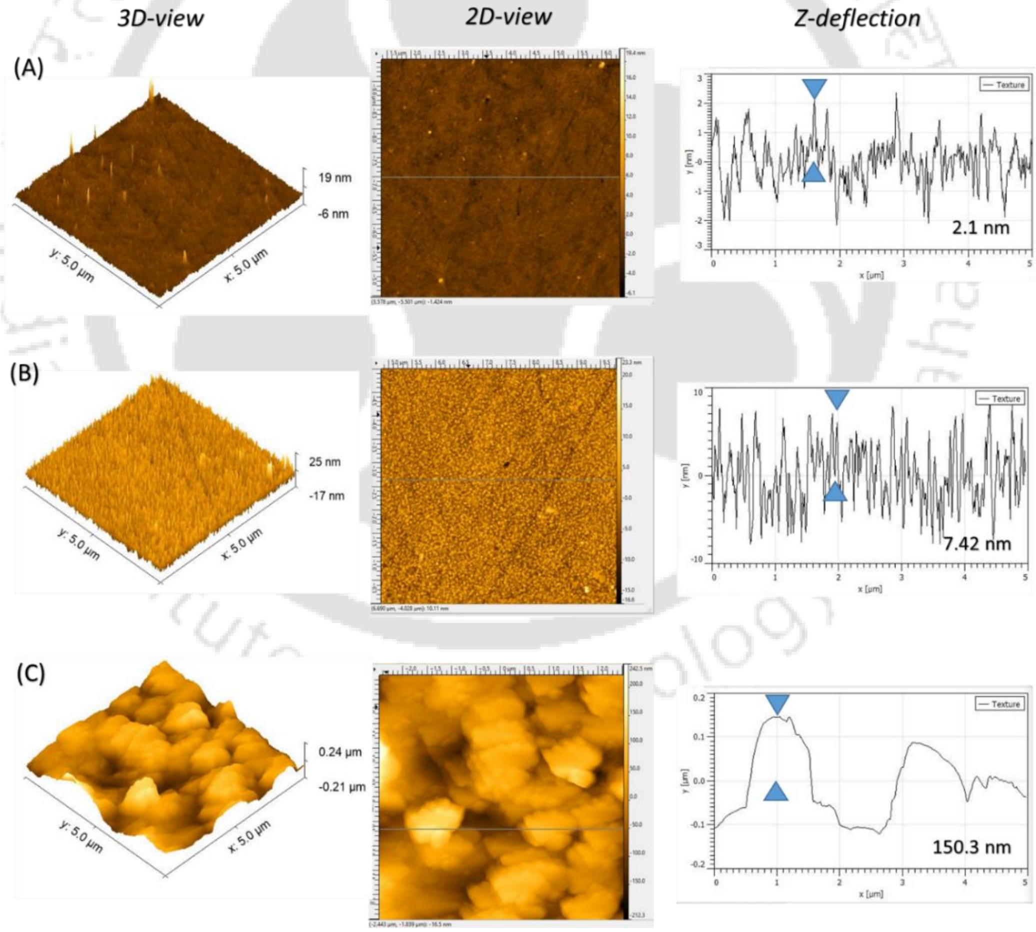

Figure 4.3: *The AFM micrographs (3D and 2D) and z-deflection profile of different probe surfaces (A) bare electrode, (B) AuNPs deposited electrode, and (C) PG-DAN-Naf coated surfaces.*

Firstly, the bare electrode surface was captured, where smooth morphology was observed with the z-deflection of 2.10 nm. After electro-deposition, change in the surface topology with clearly visible spherical nanostructures were observed due to the formation of AuNPs. The *z-deflection* in this case was increased and was found to be 7.42 nm. When PG-DAN-Naf was coated at the AuNPs deposited electrode surface, distinct morphological changes and a *z-deflection* of 150.30 nm were observed due to the presence of PG-DAN nanocomposite matrix. Thereafter, to assess the charge transfer properties of fabricated GCE/AuNPs/PG-DAN-Naf probe, we characterized the fabrication process using electrochemical methods. For that, the formation of AuNPs was characterized by LSV, where a clear reduction peak at 0.095 (V) vs. Ag/AgCl was observed which was due to the reduction of Au^{3+} to Au^0 on electrode surface, forming AuNPs (Figure not shown). Interestingly, the peak current at 0.095 V increased with three consecutive LSV sweeps, indicating the formation of highly conducting electrode surface. In the next step, modified electrode was characterized by recording CV in the potential window of -0.8 V to 0.8 V at a scan rate of 50 mV/s in 5mM Zobell's solution. Figure 4.4(A) shows the CV responses for bare GCE (black), GCE/AuNPs (red), GCE/PG-DAN-Naf (blue), and GCE/AuNPs/PG-DAN-Naf (green) surfaces. Representative voltammogram due to the redox process of $[Fe(CN)_6]^{3-/4-}$ was observed at bare GCE, while anodic (I_{pa}) and cathodic (I_{pc}) peak currents increased when GCE/AuNPs surface was examined. This was due to presence of deposited AuNPs on the GCE surface, which increases the conductivity and surface area of electrode. Further, bare GCE was modified with synthesized nanocomposite (PG-DAN-Naf) and CV was recorded to analyze the electrochemical compatibility of PG-DAN. Interestingly, we observed the increased I_{pa} and I_{pc} compare to the bare GCE and GCE/AuNPs surfaces, indicating that the nanocomposite is conducting and capable of giving amplified signal. It is interesting to note that, a new redox peak at -

0.03 / -0.21 V was observed for PG-DAN-Naf coated surface in CV, which was not present when bare GCE and GCE/AuNPs electrode was analyzed in the similar experimental conditions. This redox peak was most likely due to the electrochemical behavior of DAN present in sensing matrix (Jin et al.,1995). In final step, when we fabricated GCE/AuNPs/PG-DAN-Naf probe, maximum I_{pa} and I_{pc} were observed which was due to the synchronous effects of AuNPs and PG-DAN. Based on the results, GCE/AuNPs/PG-DAN-Naf sensing probe was applied for the analytical applications.

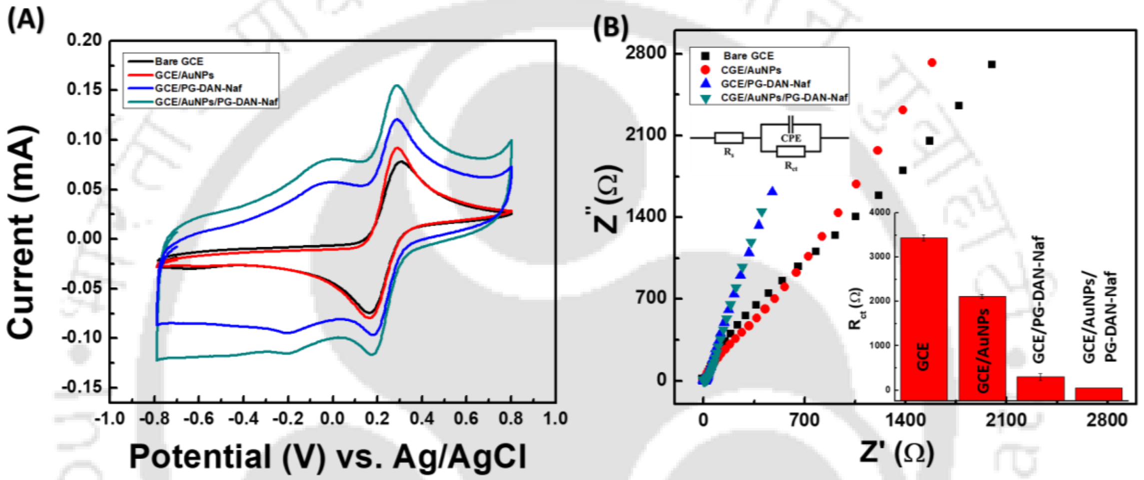

Figure 4.4: *(A) CV and (B) EIS responses at different surfaces of bare GCE(black), GCE/AuNPs(red), GCE/PG-DAN-Naf(blue), and GCE/AuNPs/PG-DAN-Naf (green) in PBS buffer containing potassium ferro/ferri cyanide (5mM; pH- 7.0; Scan rate: 50mV/S); histogram showing R_{ct} values in the different surfaces (in inset).*

The charge transfer through modified electrode is a complex phenomenon. In order to investigate the charge transfer behavior and stability of final sensing probe for electrochemical analysis, we have performed scan rate studies at bare GCE, GCE/AuNPs, GCE/PG-DAN-Naf, and GCE/AuNPs/PG-DAN-Naf. Here, CV responses were recorded at different scan rates (*i.e.*10-100 mV/s) in 5mM Zobell's solution. The peak currents in CV responses were obtained and plotted against the square root of scan rates for bare GCE,

GCE/AuNPs (figure not shown), GCE/PG-DAN-Naf (figure not shown), and GCE/AuNPs/PG-DAN-Naf (Figure 4.5). The I_{pa} and I_{pc} were found to be directly proportional to the square root of scan rates in all cases with the correlation coefficient between 0.997 and 0.999; indicating the stability and diffusion-controlled charge transfer processes at electrode surface.

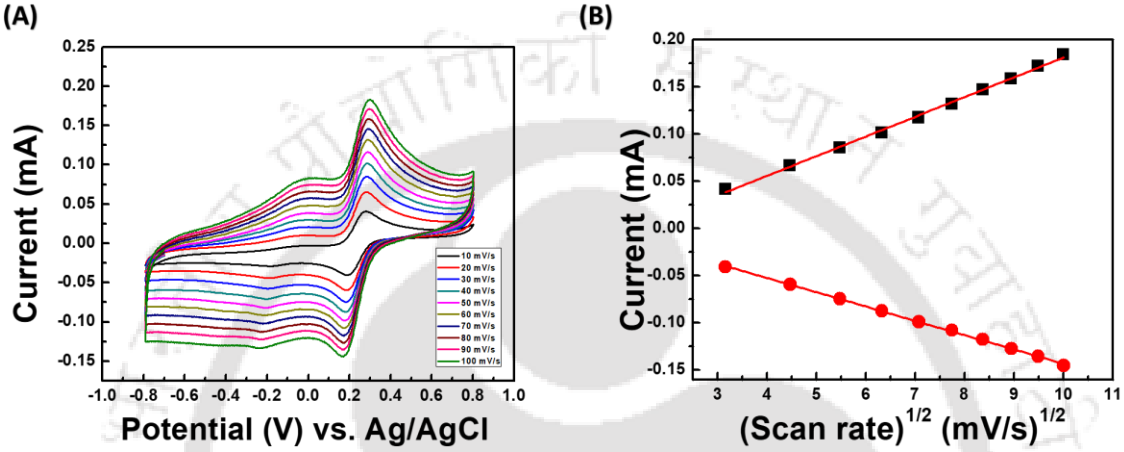

Figure 4.5: *(A) CV responses of GCE/AuNPs/PG-DAN-Naf sensor probe at different scan rates (10-100 mV/s) in PBS buffer containing potassium ferro/ferri cyanide (5mM; pH-7.0; Scan rate: 50mV/S), (B) Plot obtained using the Ipa and Ipc of scan rate dependent CV responses.*

To assess the importance of modified surface towards electrochemical sensing, we have calculated the diffusion coefficients (*D*) of bare GCE and each layer of the modified electrode using Randles - Sevcik's model (equation 4.1).

$$I_p = \left(2.69\times10^5\right) n^{3/2}\ ACD^{1/2}\ v^{1/2} \quad \text{………………….. Equation 4.1}$$

Where, I_p is the peak current (in ampere), n is the number of electron transferred in redox process (here n=1), A is the electrode surface area (in cm^2: here A = 0.01 cm^2), C is the concentration of electroactive species (in mole cm^{-3}), D is the diffusion coefficient (in $cm^2\ s^{-1}$), and v is the scan rate (in $V\ s^{-1}$).

The *D* values for bare GCE, GCE/AuNPs, GCE/PG-DAN-Naf, and GCE/AuNPs/PG-DAN-Naf modified surfaces were found to be 6.47 x 10^{-4}, 9.54 x 10^{-4}, 1.61 x 10^{-3}, and 2.66 x 10^{-3} cm^2s^{-1}, respectively, which clearly indicates the 4.12 fold higher transfer of charged species through the GCE/AuNPs/PG-DAN-Naf modified electrode surface than the bare GCE. The findings of Randles-Sevick's model clearly suggests that the developed sensing surface is highly conducting. The results obtained by CV were also validated using the EIS, where spectra in the Nyquist plot were recorded for bare GCE, GCE/AuNPs, GCE/PG-DAN-Naf, and GCE/AuNPs/PG-DAN-Naf (Figure 4.4(B)) surfaces to obtain the R_{ct}. The R_{ct} values obtained were 3441± 68.832 Ω, 2120 ± 42.41 Ω, 298.5 ± 17.97 Ω, and 50 ± 4.10 Ω for the bare GCE, GCE/AuNPs, GCE/PG-DAN-Naf, and GCE/AuNPs/PG-DAN-Naf surfaces, respectively. It is interesting to note that the lowest R_{ct} was obtained for GCE/AuNPs/PG-DAN-Naf surface compared to other tested surfaces. In this case, this was due to the fastest electron transfer kinetics at electrode/electrolyte interface. The results obtained in EIS also corroborates with the results of CV analysis. These results confirm that the developed GCE/AuNPs/PG-DAN-Naf probe is highly stable, conducting, and sensitive; hence, it is suitable for electrochemical analysis.

3.3. Analytical performance of GCE/AuNPs/PG-DAN-Naf nanobiosensor probe:

The GCE/AuNPs/PG-DAN-Naf nanobiosensor probe was further applied for detection of Vit-C. Here, the nanobiosensor was dipped in 5 mM PBS (Blank / no Vit-C) and LSV was recorded by sweeping the potentials between - 0.30 and 0.60 V. In this case, a peak at 0.07 V was observed, which was most likely due to the direct electron transfer of DAN present in the sensing matrix. Similar redox potentials for DAN has also been reported elsewhere (Abdelwahab et al.,2009; Jin et al.,1995). Thereafter, the GCE/AuNPs/PG-DAN-Naf electrode was dipped in a solution containing 10^{-3} M of Vit-C and LSV was recorded in the similar potential window. Interestingly, a sharp current response was observed at potential of 0.02 V for Vit-C. Comparable peak potential for Vit-C has also been reported at GCE/graphene nano-platelets electrode (Lim et al.,2014). In order to confirm and validate the peak observed at 0.02 V was merely due to the Vit-C interaction with nanobiosensor probe, we performed two separate control experiments. In first experiment, a concentration dependent study was performed, where we tested 10^{-9}, 10^{-6}, and 10^{-3} M of Vit-C. Figure 4.6 (A) shows the representative LSV curves, where current responses increased linearly with higher Vit-C concentrations, which was found to be significant to the current response when blank was analyzed ($p << 0.001$) Figure 4.6 (B). The linear regression equation for concentration dependent plot is expressed as follows: ΔI (mA) = 0.173 (±0.0032) + 0.0015 (± 0.000487) log Conc [Vit-C (M)] with the correlation coefficient of 0.975, indicating the ability of GCE/AuNPs/PG-DAN-Naf nanobiosensor probe for Vit-C detection correctly Figure 4.6 (C).

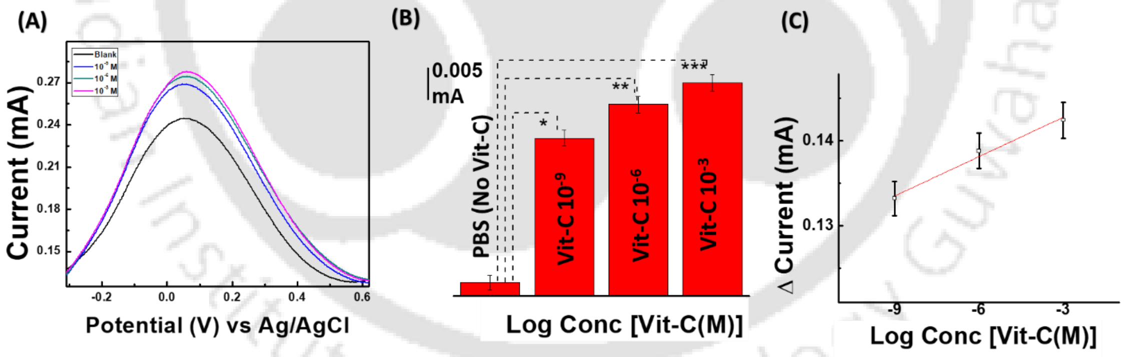

Figure 4.6: *(A) LSV responses of the GCE/AuNPs/ PG-DAN-Naf probe in PBS and different concentrations of Vit-C (10^{-9}, 10^{-6}, and 10^{-3}), (B) histogram showing comparative LSV response with and without Vit-C interaction to the sensor surface, and (C) dose dependent linear plot.*

In second experiment, a scan rate dependent study was performed at 10^{-3} M of Vit-C between 10 and 100 mV s^{-1}. Here, the oxidation peak current was found to be directly proportional to the square root of scan rates due to the diffusion control electrochemical process of Vit-C only. The results obtained from both the control experiments validate that the designed nanobiosensor probe is stable and is able to detect Vit-C accurately. After this, we further investigated the analytical performance of designed GCE/AuNPs/PG-DAN-Naf nanobiosensor by detecting various concentrations of Vit-C. Figure 4.7(A) shows the representative DPV curves, where the current response increases with the increase in Vit-C concentrations. Based on the DPV responses, a calibration plot was obtained which shows the LDR between 10^{-14} and 10^{-3} M of Vit-C (Figure 4.7 (B)).

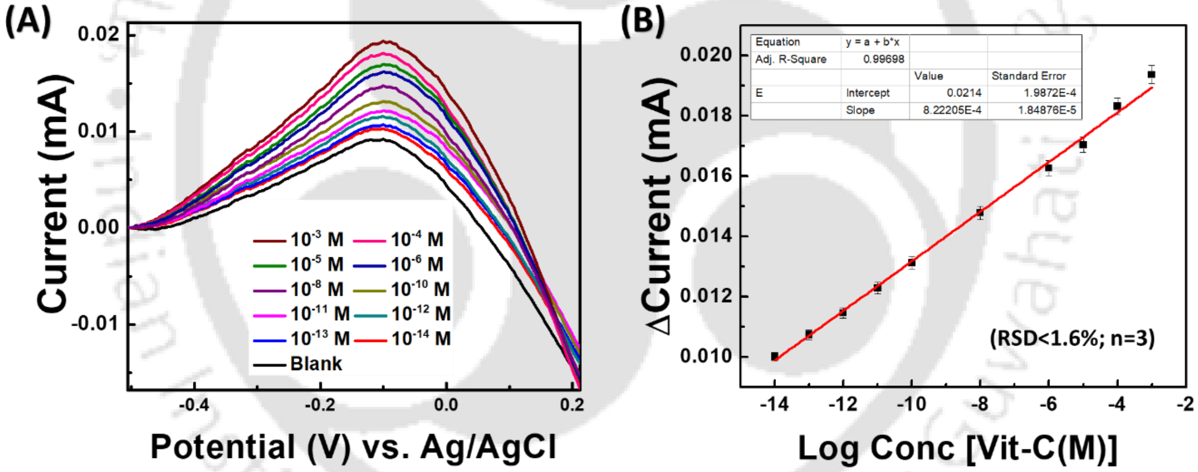

Figure 4.7: *(A) DPV responses of the GCE/AuNPs/PG-DAN-Naf probe with varying concentrations of AA (10^{-14} to10^{-3} M) and (B) shows the obtained calibration plot corresponding to the DPV signals.*

The linear regression equation of the calibration plot for Vit-C detection was expressed as follows: ΔI (mA)= 0.0214 (± 1.98 x 10^{-4}) + 8.22 x 10^{-4} (± 1.8 x 10^{-5}) log Conc [Vit-C (M)] with the correlation coefficient of 0.996. The DL of Vit-C was determined to be 4.4 (±0.02) x 10^{-17} M ((RSD< 4.2%, 95 % confidence level, n=3) using equation 4.2.

$$LOD=\frac{3SD_B}{Slope}=\frac{3SD_B}{\frac{dy}{dx}}=\frac{3SD_B}{\frac{dy}{d\ln x}\times\frac{d\ln x}{dx}}=\frac{3SD_B}{\frac{dy}{2.303(d\log x)}\times\frac{1}{x}} \quad \text{------------- Equation 4.2}$$

$$=\frac{3(2.303)SD_B x}{\frac{dy}{(d\log x)}}=\frac{3(2.303)SD_B x}{\text{slope of the semilog plot}}$$

Where, SD_B is standard deviation of blank; x is the limit of quantification or lowest concentration measured.

Importantly, in our case obtained DL is significantly lower as compared to the recently reported Vit-C nanobiosensors (Gopalakrishnan et al.,2018; Taleb et al.,2017). A comparison of analytical performance of the developed sensor with various recently reported Vit-C nanobiosensors is shown in table 4.1. It is important to note that our nanobiosensor probe possess facile fabrication steps and is devoid of any biomolecule even though it offers an unprecedented DL and a wide LDR. This clearly indicates the promise of developed nanobiosensor for robust and trace analysis of Vit-C in wide range of real sample matrices.

3.4. Interference study:

Another most critical parameter to analyze the biomedical values of developed nanobiosensors is selectivity (Mahato et al.,2018; Pallela et al.,2016). In order to study the interfering effects, GCE/AuNPs/PG-DAN-Naf probe was tested towards citric acid, uric acid, glucose, dopamine, urea, and acetaminophen, which coexists with Vit-C in various matrices. No signal was observed for citric acid, uric acid, acetaminophen, dopamine, and urea under the tested operational potential window. In the case of glucose, no signal was observed due to its inherent electrochemically inactive behavior and / or inability to be oxidized non-enzymatically at developed sensing surface.

Sl No.	Probe	LDR	DL	Real sample / Animal experiment		Detection time	References
1	Ag hierarchical nanostructures/GCE	0.17 µM - 1.80 mM	0.06 µM	NR	No	NR	(Zhang et al.,2018)
2	CdO Nanoparticles-SPCE	5 µM -150 µM	53.5 nM	Canned juice	No	NR	(Gopalakrishnan et al.,2018)
3	$NiFe_2O_4$/SPE	0.5 µM -100 µM	0.1 µM	Tablet	No	NR	(Jahani,2018)
4	ZnO nanoparticles/GCE	1 µM - 800 µM	0.312 µM	Urine Serum	No	NR	(Zhu and Xu,2017)
5	PCN-333 (Al) MOFs-KB/GCE	14.1 ± 0.2 - (5.5 ± 0.1) µM	4.6 (± 0.1) µM	NR	No	NR	(Wang et al.,2017)
6	MCNRs/GCE	10 µM -2770 µM	2.3 µM	Injection dose, soft drink and fresh lemon juice	No	NR	(Li et al.,2018)
7	TiO_2-AuNP-MWCNT-DHP/GCE	5.0 µM - 51 µM	1.2 µM	Pharmaceutical and fruit juice	No	NR	(Scremin et al.,2018)
8	ANF-C700/GCE	1 µM - 60 µM	117 nM	Urine samples	No	NR	(Taleb et al.,2017)
9	$Cu(OH)_2$NR/SPE	0.0125 mM -10 mM	NR	Tablets and urine samples	No	NR	(Raveendran et al.,2017)
10	**PG-DAN-Naf/AuNPs/GCE**	**10^{-14} M to 10^{-3} M**	**4.4×10^{-17} M**	**Urine sample**	**Mice brain**	**30 seconds**	**Present work**

Table 4.1: *Comparison table for the Vit-C determinations in recent literatures.*

The selectivity of GCE/AuNPs/PG-DAN-Naf probe was mathematically deduced by determining the selectivity coefficient k_{sel} using the equation 4.3.

$$k_{sel} = \frac{(Signal)_{interferent}}{(Signal)_{Vit-C}} \quad \text{--------------------------- Equation 4.3}$$

Where k_{sel} *is the coefficient of selectivity,* $(Signal)_{interferent}$ *is the signal strength shown by probe when treated with the interfering molecules, and* $(Signal)_{Vit-C}$ *is the signal strength corresponds to Vit-C.*

The calculated k_{sel} values for interfering molecules were extremely low ($k_{sel} << 1$), indicating that the fabricated nanobiosensor is highly selective towards Vit-C detection. We also performed T-test for Vit-C and calculated p-values against all interfering molecules, which were found to be << 0.001 (n = 3), indicating that the selectivity results are statistically significant. Figure 4.8 shows the histogram obtained from DPV responses of Vit-C and different interfering molecules at the nanobiosensor probe.

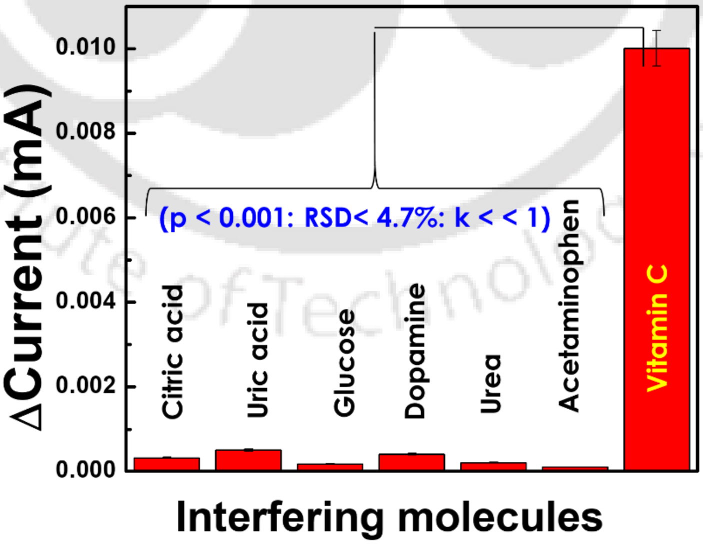

Figure 4.8: *Selectivity assay responses of GCE/AuNPs/PG-DAN-Naf sensor probe.*

3.5. Real sample analysis:

3.5.1. Vit-C detection in urine and fruit juice samples:

Firstly, both the real samples (urine and fruit juice) were equilibrated using the PBS in the ratio of 9:1 ratio (urine: buffer) and Vit-C of different concentrations were spiked followed by its detection using the nanobiosensor probe. It is worth mentioning that the urine samples were not subjected for any pretreatment step such as filtration or centrifugation before processing, however, the juice sample was kept for 15 minutes to settle down the fibrous parts. The results of these experiments were analyzed and % recoveries of Vit-C were calculated using equation 4.4.

$$\% \text{ Recovery} = \frac{([S]_{Vit-C} - [B]_{Vit-C})}{[SS]_{Vit-C}} \qquad \text{--------------------------- Equation 4.4}$$

Where, $[S]_{Vit-C}$ *and* $[B]_{Vit-C}$ *are the analytical responses of Vit-C in the spiked and blank urine samples, respectively; and* $[SS]_{Vit-C}$ *is the analytical response of* Vit-C *in the standard solutions.*

Figure 4.9 shows the signal response of Vit-C detected in urine samples where peak currents increased linearly with increase in the Vit-C concentrations from 10^{-14} to 10^{-3} M. The sensitivity of Vit-C detection was evaluated by comparing the Vit-C signals obtained from urine samples with blank buffer. Interestingly, the designed nanobiosensor is able to detect 88.56 to 99.50% of Vit-C from the urine samples. The analytical details for recovered Vit-C concentrations, RSD, and % recovery for all the tested concentrations are represented in table 4.2. Based on the dose dependent Vit-C detection in urine, a calibration plot was obtained which shows the linear regression equation as follows: ΔI (mA) = 0.01968 ($\pm$ 4.45 x 10^{-5}) + 7.49 x10^{-4} ($\pm 4.74\text{x}10^{-5}$) log Conc [Vit-C (M)] with the correlation coefficient of 0.965. The DL of 1.2 ($\pm$ 0.01) x 10^{-16} M (RSD<1.6%) was obtained in urine sample based on the standard deviation of three times consecutive analyses of the blank (95% confidence level; n=3), which indicates the fabricated nanobiosensors is powerful for real sample analysis and is highly reproducible.

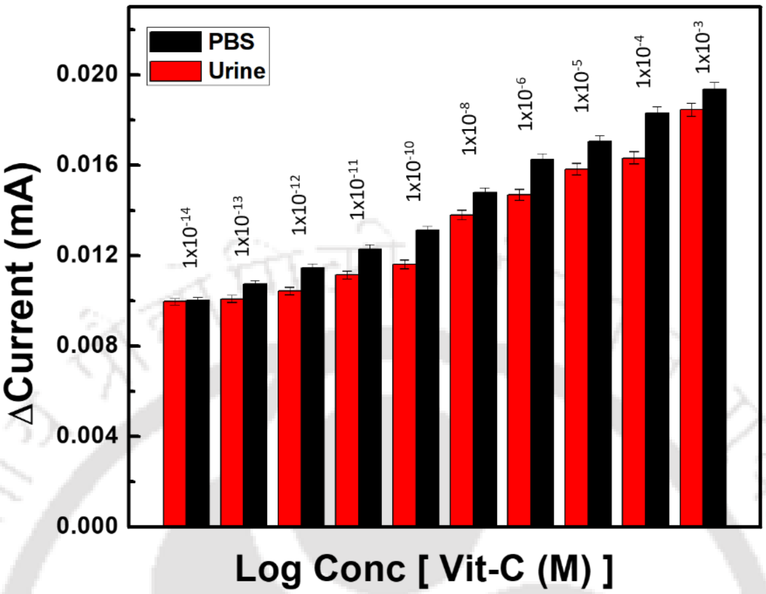

Figure 4.9: *Vit-C determination using fabricated GCE/AuNPs/PG-DAN-Naf sensor-probe in clinical urine sample.*

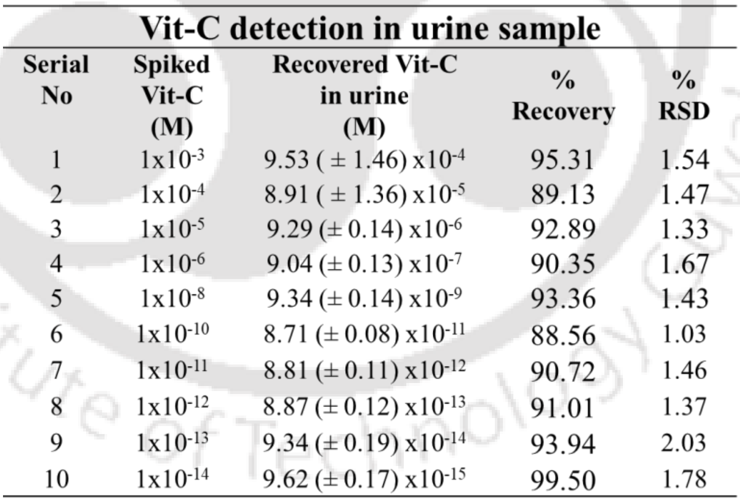

Vit-C detection in urine sample

Serial No	Spiked Vit-C (M)	Recovered Vit-C in urine (M)	% Recovery	% RSD
1	$1x10^{-3}$	$9.53\ (\pm 1.46)\ x10^{-4}$	95.31	1.54
2	$1x10^{-4}$	$8.91\ (\pm 1.36)\ x10^{-5}$	89.13	1.47
3	$1x10^{-5}$	$9.29\ (\pm 0.14)\ x10^{-6}$	92.89	1.33
4	$1x10^{-6}$	$9.04\ (\pm 0.13)\ x10^{-7}$	90.35	1.67
5	$1x10^{-8}$	$9.34\ (\pm 0.14)\ x10^{-9}$	93.36	1.43
6	$1x10^{-10}$	$8.71\ (\pm 0.08)\ x10^{-11}$	88.56	1.03
7	$1x10^{-11}$	$8.81\ (\pm 0.11)\ x10^{-12}$	90.72	1.46
8	$1x10^{-12}$	$8.87\ (\pm 0.12)\ x10^{-13}$	91.01	1.37
9	$1x10^{-13}$	$9.34\ (\pm 0.19)\ x10^{-14}$	93.94	2.03
10	$1x10^{-14}$	$9.62\ (\pm 0.17)\ x10^{-15}$	99.50	1.78

Table 4.2: *Details of dose dependent detection of Vit-C in clinical urine sample.*

A considerably higher DL (*i.e.* low sensitivity) in case of urine sample was most likely due to the negligible matrix effect of urine components. Similar to the urine sample, the sensor probe was tested Vit-C in fruit juice samples, where the amount of Vit-C recovered was found between 87.18 and 98.9 %. Figure 4.10 shows the histogram of peak currents obtained at different concentration of Vit-C spiked using the nanobiosensor. The details of recovered Vit-C concentrations, RSD, and % recovery at different concentrations are represented in Table 4.3.

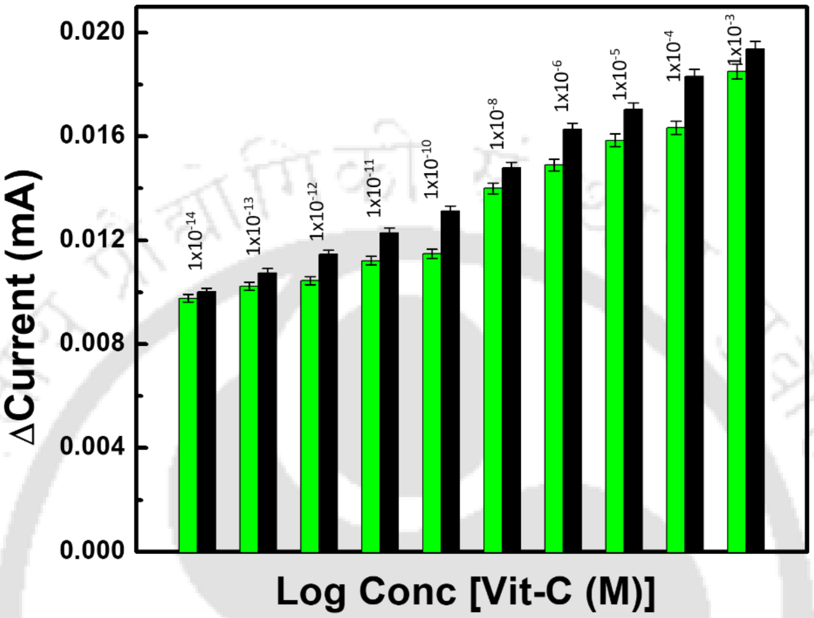

Figure 4.10: *Vit-C determination using fabricated GCE/AuNPs/PG-DAN-Naf sensor-probe in fruit juice samples.*

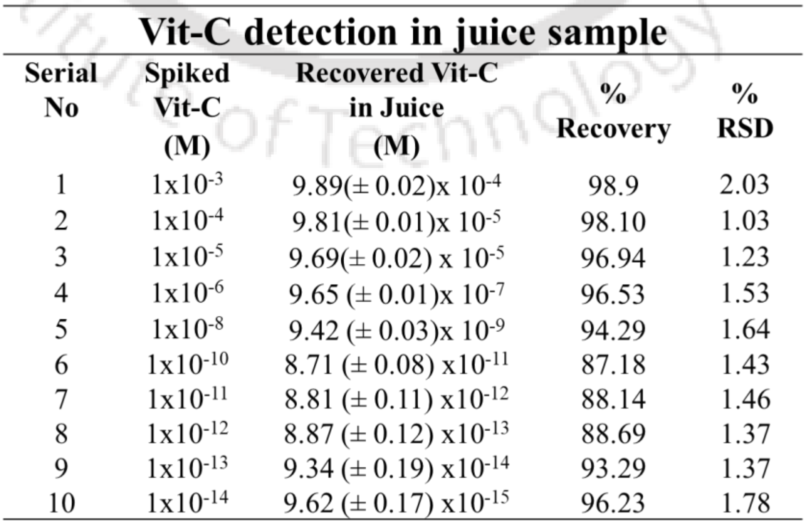

Vit-C detection in juice sample

Serial No	Spiked Vit-C (M)	Recovered Vit-C in Juice (M)	% Recovery	% RSD
1	$1x10^{-3}$	$9.89(\pm 0.02)x\ 10^{-4}$	98.9	2.03
2	$1x10^{-4}$	$9.81(\pm 0.01)x\ 10^{-5}$	98.10	1.03
3	$1x10^{-5}$	$9.69(\pm 0.02)\ x\ 10^{-5}$	96.94	1.23
4	$1x10^{-6}$	$9.65\ (\pm 0.01)x\ 10^{-7}$	96.53	1.53
5	$1x10^{-8}$	$9.42\ (\pm 0.03)x\ 10^{-9}$	94.29	1.64
6	$1x10^{-10}$	$8.71\ (\pm 0.08)\ x10^{-11}$	87.18	1.43
7	$1x10^{-11}$	$8.81\ (\pm 0.11)\ x10^{-12}$	88.14	1.46
8	$1x10^{-12}$	$8.87\ (\pm 0.12)\ x10^{-13}$	88.69	1.37
9	$1x10^{-13}$	$9.34\ (\pm 0.19)\ x10^{-14}$	93.29	1.37
10	$1x10^{-14}$	$9.62\ (\pm 0.17)\ x10^{-15}$	96.23	1.78

Table 4.3: *Details of dose dependent detection of Vit-C in fruit juice sample.*

3.5.2. Vit-C detection in brain of healthy and diseased mice:

Since it has been reported that the levels of Vit-C in brain is significantly different in healthy and neurodegenerative diseased cases (Covarrubias-Pinto et al.,2015; Quinn et al.,2003), we have attempted to detect the Vit-C in healthy and diseased mice (C57BL/6j strain) brain using GCE/AuNPs/PG-DAN-Naf nanobiosensor probe. For this purpose, the brain tissues were isolated from healthy and diseased mice followed by its homogenization. The detailed steps involved in sample preparation from mice are shown in scheme 4.2 (A-B). The isolated brain tissue samples were then equilibrated with PBS followed by Vit-C detection using the nanobiosensor probe. Vit-C was spiked in the brain tissue samples in the similar LDR as done in blank buffer (*i.e.* 10^{-14} to 10^{-3} M) and % recovery was evaluated using equation 4.4. Figure 4.11 shows the comparative Vit-C signal responses in blank buffer (black bars), brain tissues of healthy (red bars), and diseased mouse (blue bars). In both the test experiments, current response increases linearly with increase in Vit-C concentrations from 10^{-14} to 10^{-3} M. It was interesting to note that the % recovery in case of healthy mice were between 124.77 and 132.77% (RSD < 1.7 %, n = 5); while, % recovery in diseased mice brain samples were between 87.65 and 99.90% (RSD < 1.8 %, n = 5). Based on the dose dependent Vit-C detection in mice brain samples, calibration plots for both the cases were obtained, which show the linear regression equations as follows:

ΔI (mA) = 0.0267 (± 2.69 0x 10^{-4}) + 9.925 x 10^{-4} (±2.522 x 10^{-5}) log Conc [Vit-C (M)] and ΔI (mA) = 0.0192 (± 2.968 x 10^{-4}) + 7.050 x 10^{-4} (±1.855 x 10^{-5}) log Conc [Vit-C (M)] with the correlation coefficients of 0.989 and 0.960 for healthy (red bars) and diseased (blue bars) mice brain samples, respectively. The DL of 6.1(± 0.01) x 10^{-17} M (RSD<1.8%) and 2.1 (± 0.03) x 10^{-16} M (RSD < 2.1%) was obtained in the brain samples of healthy and diseased mice, respectively

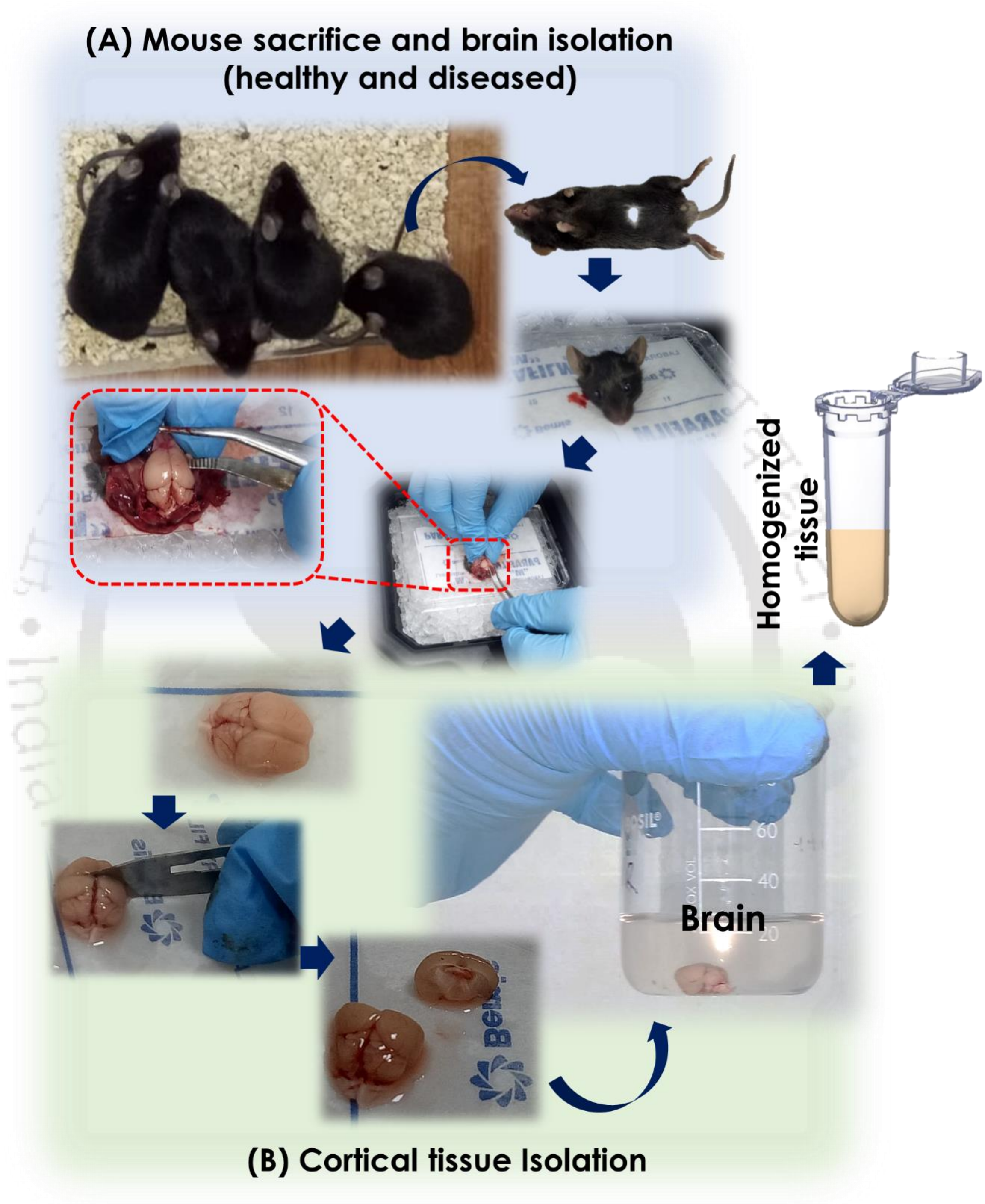

Scheme 4.2: *Schematic representation for the process for (A) brain tissue isolation from mice (strain:C57bl/6j), (B) dissection of cortical tissues for the sample preparation. (In collaboration with National Institute of Pharmaceutical Education and Research – Guwahati)*

based on the standard deviation of three times consecutive analyses of the blank (95% confidence level; n=3). This indicates the fabricated nanobiosensor is extremely powerful for trace Vit-C analysis in complex brain tissue samples. The analytical details of all the tested Vit-C concentrations, RSD, and % recovery in brain samples are shown in table 4.4.

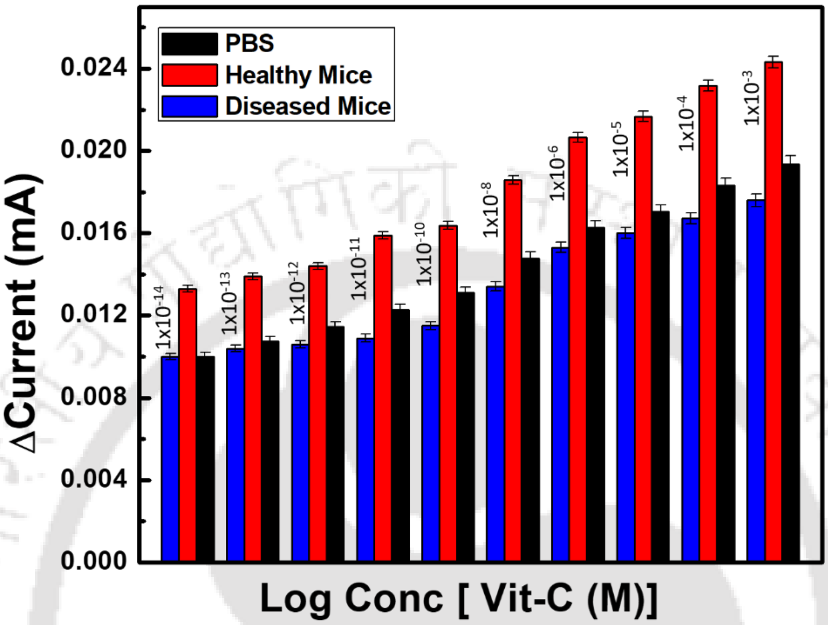

Figure 4.11: *Vit-C determination using fabricated GCE/AuNPs/PG-DAN-Naf sensor-probe in mice brain tissue samples.*

Vit-C detection in mice brain samples

Serial No	Spiked Vit-C (M)	Recovered Vit-C from healthy mice brain (M)	% Recovery	% RSD	Recovered Vit-C from diseased mice brain (M)	% Recovery	% RSD
1	$1x10^{-3}$	1.25 (± 0.0203) x 10^{-3}	125.52	1.37	0.90 (± 0.0147) x 10^{-3}	90.87	1.34
2	$1x10^{-4}$	1.26 (± 0.0204) x 10^{-4}	126.54	1.43	0.91 (± 0.0142) x 10^{-4}	91.31	1.42
3	$1x10^{-5}$	1.27 (± 0.0206) x 10^{-5}	127.23	1.23	0.93 (± 0.0152) x 10^{-5}	93.95	1.52
4	$1x10^{-6}$	1.26 (± 0.0205) x 10^{-6}	126.92	1.53	0.94 (± 0.0152) x 10^{-6}	94.09	1.47
5	$1x10^{-8}$	1.22 (± 0.0205) x 10^{-8}	125.77	1.64	0.90 (± 0.0147) x 10^{-8}	90.79	1.35
6	$1x10^{-10}$	1.22 (± 0.0185) x 10^{-10}	124.77	1.23	0.87 (± 0.0131) x 10^{-10}	87.65	1.34
7	$1x10^{-11}$	1.25 (± 0.0173) x 10^{-11}	129.37	1.53	0.88 (± 0.0173) x 10^{-11}	88.68	1.46
8	$1x10^{-12}$	1.22 (± 0.0234) x 10^{-12}	125.65	1.59	0.90 (± 0.0121) x 10^{-12}	92.49	1.74
9	$1x10^{-13}$	1.28 (± 0.0223) x 10^{-13}	129.42	1.02	0.96 (± 0.0154) x 10^{-13}	96.83	1.29
10	$1x10^{-14}$	1.27 (± 0.0261) x 10^{-14}	132.86	1.29	0.99 (± 0.0162) x 10^{-14}	99.90	1.07

Table 4.4: *Details of comparative dose dependent detection of Vit-C in healthy and diseased mice brain tissue sample.*

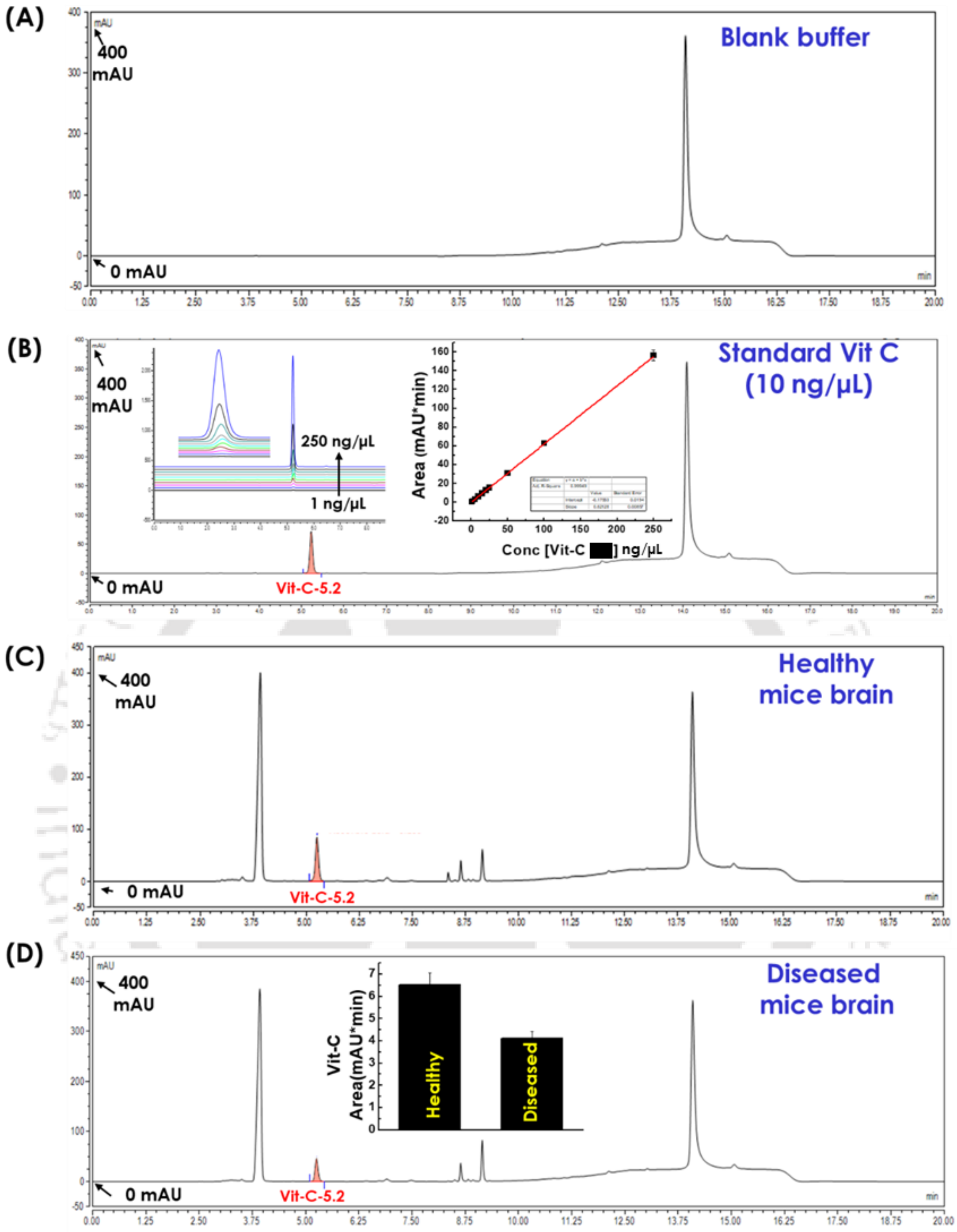

Figure 4.12: *The chromatograms for (A) Blank, (B) standard Vit-C (inset: dose dependent responses of the Vit-C in left and the obtained calibration plot in right), (C) Healthy mice brain, and (D) diseased mice brain for validation of contrasting level of of Vit-C level (inset the histogram showing he contrasting levels of Vit-C in healthy and diseased mice brain samples)*

It is worth mentioning that the significant difference in the Vit-C levels in healthy and diseased mice brain cells observed in our study ($p < 0.001$) was most likely due to the difference in residual Vit-C levels in the tested brain samples, which participated in respective signal generation. In order to validate the differential sensing of Vit-C by the developed nanobiosensor in the contrasting physiological states, complementary experiments were also performed using HPLC. All HPLC analysis was done using the same brain dialysate used in the electrochemical analysis to verify the results. For this purpose, firstly standard of Vit-C was injected in the column (figure 4.12 B), where a sharp peak was observed at 5.2 min due to the presence of Vit-C in the buffer solution, which was, however, not present when blank buffer (figure 4.12 A) was injected in the column. The peak at 5.2 min was merely due to the Vit-C, has also confirmed by its dose dependent analysis under similar experimental conditions (left inset of figure 4.12 B). Here, the signal increased with increase linearly with Vit-C concentrations between 1 ng/µL and 250 ng/µL, as shown in the calibration plot (right inset of figure 4.12 B), confirming that the peak at 5.2 min in merely due to Vit-C. After validating the standard Vit-C analysis in HPLC, we tested the Vit-C directly in healthy / diseased brain dialysate (figure 4.12 C-D). Interestingly, in this case significantly higher concentrations ($p < 0.01$) of Vit-C were observed in healthy mice brain samples compared to the diseased ones (inset figure 4.12 D). Similar observations of significantly higher Vit-C levels in healthy mice brain compared to diseased one are reported in the literature (Glasø et al.,2004; Quinn et al.,2003). The real sample results obtained in our study clearly shows the potential of developing nanobiosensor for Vit-C detection not only in body fluids, but also in mice brain tissues, suggesting its prospective clinical application. It is interesting to note that in all sets of real sample analysis, the % Vit-C recovery was over 87%, suggesting that the various real sample components (even unknown bio-chemicals) present in urine and mice brain do not foul or deteriorate the nanobiosensor surface.

3.6. Reproducibility and stability studies:

For the commercial viability of any nanobiosensor, the manufacturing reproducibility and stability is of major concern (Chandra et al.,2017; Mahato et al.,2017). In view of this, we have tested the fabricated GCE/AuNPs/PG-DAN-Naf probe for its reproducibility by detecting the current responses at five separately prepared nanobiosensors. The current responses in the tested probes were found to be negligibly altered when same fabrication steps were followed (RSD<4.1%), showing that the developed GCE/AuNPs/PG-DAN-Naf probe is highly reproducible. This small deviation was due to the minor variation in nanobiosensor fabrication and / or due to handling errors. The long-term stability has also been studied for the fabricated nanobiosensor at the concentration of 10^{-10} M Vit-C, where the nanobiosensor retained almost 95 ± 2 % of its original response up to six weeks (figure 4.13).

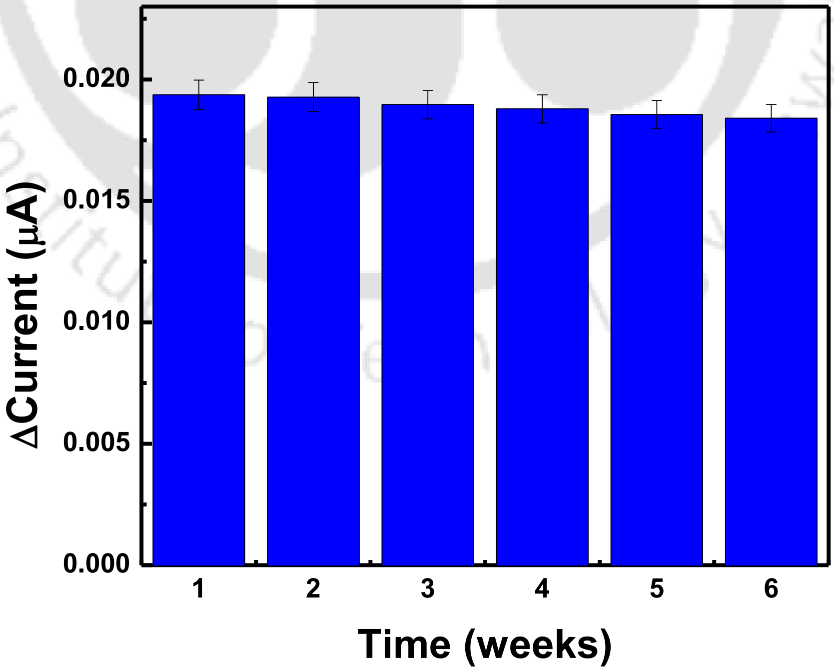

Figure 4.13: *Time dependent responses of the fabricated GCE/AuNPs/ PG-DAN-Naf sensor probe.*

Over this period, the current response decreased with time, suggesting that the developed GCE/AuNPs/PG-DAN-Naf nanobiosensor probe is stable up to six weeks.

4. Conclusions:

A facile, selective, stable, and highly sensitive nanobiosensor for Vit-C determination has been fabricated based on AuNPs and PG-DAN nanocomposite. The nanobiosensor was characterized by using SEM, TEM, FTIR, AFM, and electrochemical techniques. A wide LDR for Vit-C detection was obtained between $1x10^{-14}$ and $1x10^{-3}$ M with the DL of 4.4 (± 0.02) x 10^{-17} M (RSD < 4.2%) which was significantly lower compared to the most recent Vit-C nanobiosensor. The nanobiosensor was able to detect Vit-C in human urine, healthy and diseased mice brain samples with % recoveries between 87.65 % and 132.77 % at various concentrations. To the best of our knowledge, we have demonstrated for the first time an attomolar level Vit-C detection in healthy and diseased mice brain using an electrochemical nanobiosensor composed of AuNPs, porous graphene - DAN nanocomposite. The nanobiosensor was found to be highly selective against the various interfering molecules and was stable up to six weeks. The nanobiosensor system fabricated has many striking features such as; simplicity, rapidity, label-free and low-cost detection, hence it could be a method of choice for Vit-C detection in various samples. In future, the developed nnaobiosensor system can be translated towards a genuine miniaturized sensing device for various applications.

In this study, we have incorporated the porous - graphene- DAN based nanocomposite for the development of electrochemical sensing system and analyzed the analytical performance towards Vit-C, where we obtained the widest range and the least detection limit until date. However, the sensor probe was observed to be fouled on repeated usage in complex matrices due to the synergistic effect of the porous morphology of sensor surface and the presence of various bulky moieties in matrices. Thus, we have further extended the study to improvise the biosensing system by incorporating special type of nanocomposite containing nano-rattles (core-cage) and reduced graphene oxide (higher surface area). The detailed discussion is given in the next chapter.

5. Declaration:

The animal protocol and experimental methods were approved (NIPS/NIPER/18/025) by the Institutional Animal Ethics Committee (IAEC), North East Technical Education Society (NETES) Institute of Pharmaceutical Sciences (NIPS), Mirza, Kamrup, Assam, India.

6. References:

Abdelwahab, A.A., Lee, H.-M., Shim, Y.-B., Selective determination of dopamine with a cibacron blue/poly-1,5-diaminonaphthalene composite film, ***2009***. *Analytica Chimica Acta* 650(2), 247-253.

Al-Shwaiyat, M.k.E.A., Miekh, Y.V., Denisenko, T.A., Vishnikin, A.B., Andruch, V., Bazel, Y.R., Simultaneous determination of rutin and ascorbic acid in a sequential injection lab-at-valve system, ***2018***. *Journal of Pharmaceutical and Biomedical Analysis* 149, 179-184.

Cao, J., Zhu, Z., Xu, J., Tao, M., Chen, Z., Nitrogen-doped porous graphene as a highly efficient cathodic electrocatalyst for aqueous organic redox flow battery application, ***2017***. *Journal of Materials Chemistry A* 5(17), 7944-7951.

Chandra, P., 2016. Nanobiosensors for personalized and onsite biomedical diagnosis. The Institution of Engineering and Technology.

Chandra, P., Tan, Y.N., Singh, S.P., 2017. Next generation point-of-care biomedical sensors technologies for cancer diagnosis. Springer.

Covarrubias-Pinto, A., Acuña, A.I., Beltrán, F.A., Torres-Díaz, L., Castro, M.A., Old things new view: ascorbic acid protects the brain in neurodegenerative disorders, ***2015***. *International journal of molecular sciences* 16(12), 28194-28217.

Deshmukh, G.S., Bapat, M.G., Determination of ascorbic acid by potassium iodate, ***1955***. *Fresenius' Zeitschrift für analytische Chemie* 145(4), 254-256.

Evelyn, K.A., Malloy, H.T., Rosen, C., The determination of ascorbic acid in urine with the photoelectric colorimeter, ***1938***. *Journal of Biological Chemistry* 126, 645-654.

Fabian, H., Lasch, P., Naumann, D., Analysis of biofluids in aqueous environment based on mid-infrared spectroscopy, ***2005***. *Journal of biomedical optics* 10(3), 031103.

Glasø, M., Nordbø, G., Diep, L., Bøhmer, T., Reduced concentrations of several vitamins in normal weight patients with late-onset dementia of the Alzheimer type without vascular disease, ***2004***. *The journal of nutrition, health & aging* 8(5), 407-413.

Gopalakrishnan, A., Sha, R., Vishnu, N., Kumar, R., Badhulika, S., Disposable, efficient and highly selective electrochemical sensor based on Cadmium oxide nanoparticles decorated screen-printed carbon electrode for ascorbic acid determination in fruit juices, ***2018***. *Nano-Structures & Nano-Objects* 16, 96-103.

Grotzkyj Giorgi, M., Howland, K., Martin, C., Bonner, A.B., A Novel HPLC Method for the Concurrent Analysis and Quantitation of Seven Water-Soluble Vitamins in Biological Fluids (Plasma and Urine): A Validation Study and Application, ***2012***. *The Scientific World Journal* 2012, 1-8.

Hattersley, J.G., The Answer to Crib Death" Sudden Infant Death Syndrome"(SIDS), ***1993***. *Journal of Orthomolecular Medicine* 8(4), 229-245.

Hooch Antink, W., Choi, Y., Seong, K.-d., Kim, J.M., Piao, Y., Recent Progress in Porous Graphene and Reduced Graphene Oxide-Based Nanomaterials for Electrochemical Energy Storage Devices, ***2018***. *Advanced Materials Interfaces* 5(5), 1701212.

Jahani, S., Evaluation of the Usefulness of an Electrochemical Sensor in Detecting Ascorbic Acid using a Graphite Screen-printed Electrode Modified with NiFe2O4 Nanoparticles, ***2018***. *Anal. Bioanal. Electrochem.* 10(6), 739-750.

Jin, C.-S., Shim, Y.-B., Park, S.-M., Electropolymerization and spectroelectrochemical characterization of poly(1,5-diaminonaphthalene), ***1995***. *Synthetic Metals* 69(1), 561-562.

Kamyabi, M.A., Shafiee, M.A., Electrocatalytic oxidation of dopamine, ascorbic acid and uric acid at poly-2,6-diaminopyridine on the surface of carbon nanotubes/gc electrodes, ***2012***. *Journal of the Brazilian Chemical Society* 23, 593-601.

Kashish, Bansal, S., Jyoti, A., Mahato, K., Chandra, P., Prakash, R., Highly Sensitive in vitro Biosensor for Enterotoxigenic Escherichia coli Detection Based on ssDNA Anchored on PtNPs-Chitosan Nanocomposite, ***2017***. *Electroanalysis* 29(11), 2665-2671.

Klimczak, I., Gliszczyńska-Świgło, A., Comparison of UPLC and HPLC methods for determination of vitamin C, ***2015***. *Food Chemistry* 175, 100-105.

Kocot, J., Luchowska-Kocot, D., Kiełczykowska, M., Musik, I., Kurzepa, J., Does Vitamin C Influence Neurodegenerative Diseases and Psychiatric Disorders?, ***2017***. *Nutrients* 9(7), 659.

Kong, W., Wu, D., Li, G., Chen, X., Gong, P., Sun, Z., Chen, G., Xia, L., You, J., Wu, Y., A facile carbon dots based fluorescent probe for ultrasensitive detection of ascorbic acid in biological fluids via non-oxidation reduction strategy, ***2017***. *Talanta* 165, 677-684.

Li, X., Liu, J., Sun, M., Sha, T., Bo, X., Zhou, M., Amperometric sensing of ascorbic acid by using a glassy carbon electrode modified with mesoporous carbon nanorods, ***2018***. *Microchimica Acta* 185(10), 1-7.

Lim, C.S., Chua, C.K., Pumera, M., Detection of biomarkers with graphene nanoplatelets and nanoribbons, ***2014***. *Analyst* 139(5), 1072-1080.

Lima, D.R.S., Cossenza, M., Garcia, C.G., Portugal, C.C., Marques, F.F.d.C., Paes-de-Carvalho, R., Pereira Netto, A.D., Determination of ascorbic acid in the retina during chicken embryo development using high performance liquid chromatography and UV detection, ***2016***. *Analytical Methods* 8(27), 5441-5447.

Mahato, K., Maurya, P.K., Chandra, P., Fundamentals and commercial aspects of nanobiosensors in point-of-care clinical diagnostics, ***2018***. *3 Biotech* 8(3), 2-14.

Mahato, K., Srivastava, A., Chandra, P., Paper based diagnostics for personalized health care: Emerging technologies and commercial aspects, ***2017***. *Biosensors and Bioelectronics* 96, 246-259.

Mazurek, A., Jamroz, J., Precision of dehydroascorbic acid quantitation with the use of the subtraction method – Validation of HPLC–DAD method for determination of total vitamin C in food, ***2015***. *Food Chemistry* 173, 543-550.

Moretti, M., Fraga, D.B., Rodrigues, A.L.S., Preventive and therapeutic potential of ascorbic acid in neurodegenerative diseases, ***2017***. *CNS neuroscience & therapeutics* 23(12), 921-929.

Oliveira-Folador, G., Bicudo, M.d.O., de Andrade, E.F., Renard, C.M.-G.C., Bureau, S., de Castilhos, F., Quality traits prediction of the passion fruit pulp using NIR and MIR spectroscopy, ***2018***. *LWT* 95, 172-178.

Ossonon, B.D., Bélanger, D., Synthesis and characterization of sulfophenyl-functionalized reduced graphene oxide sheets, ***2017***. *RSC Advances* 7(44), 27224-27234.

Pallela, R., Chandra, P., Noh, H.-B., Shim, Y.-B., An amperometric nanobiosensor using a biocompatible conjugate for early detection of metastatic cancer cells in biological fluid, ***2016***. *Biosensors and Bioelectronics* 85, 883-890.

Pisoschi, A.M., Pop, A., Serban, A.I., Fafaneata, C., Electrochemical methods for ascorbic acid determination, ***2014***. *Electrochimica Acta* 121, 443-460.

Prasad, B.B., Tiwari, K., Singh, M., Sharma, P.S., Patel, A.K., Srivastava, S., Molecularly imprinted polymer-based solid-phase microextraction fiber coupled with molecularly imprinted polymer-based sensor for ultratrace analysis of ascorbic acid, ***2008***. *Journal of Chromatography A* 1198-1199, 59-66.

Quinn, J., Suh, J., Moore, M.M., Kaye, J., Frei, B., Antioxidants in Alzheimer's disease-vitamin C delivery to a demanding brain, ***2003***. *Journal of Alzheimer's Disease* 5(4), 309-313.

Raveendran, J., Krishnan, R.G., Nair, B.G., Satheesh Babu, T.G., Voltammetric determination of ascorbic acid by using a disposable screen printed electrode modified with Cu(OH)2 nanorods, ***2017***. *Microchimica Acta* 184(9), 3573-3579.

Scremin, J., Barbosa, E.C.M., Salamanca-Neto, C.A.R., Camargo, P.H.C., Sartori, E.R., Amperometric determination of ascorbic acid with a glassy carbon electrode modified with TiO2-gold nanoparticles integrated into carbon nanotubes, ***2018***. *Microchimica Acta* 185(5), 1-10.

Spijker, S., 2011. Dissection of Rodent Brain Regions. In: Li, K.W. (Ed.), Neuroproteomics, pp. 13-26. Humana Press, Totowa, NJ.

Tabish, T.A., Memon, F.A., Gomez, D.E., Horsell, D.W., Zhang, S., A facile synthesis of porous graphene for efficient water and wastewater treatment, ***2018***. *Scientific Reports* 8(1), 1817.

Taleb, M., Ivanov, R., Bereznev, S., Kazemi, S.H., Hussainova, I., Graphene-ceramic hybrid nanofibers for ultrasensitive electrochemical determination of ascorbic acid, ***2017***. *Microchimica Acta* 184(3), 897-905.

Tang, Y., Wu, M., A quick method for the simultaneous determination of ascorbic acid and sorbic acid in fruit juices by capillary zone electrophoresis, ***2005***. *Talanta* 65(3), 794-798.

Tarrago-Trani, M.T., Phillips, K.M., Cotty, M., Matrix-specific method validation for quantitative analysis of vitamin C in diverse foods, ***2012***. *Journal of Food Composition and Analysis* 26(1), 12-25.

Teruuchi, J., Mochizuki, H., Relationship between blood level and urinary excretion of vitamin C, ***1959***. *The Journal of vitaminology* 5(3), 223-228.

Thrivikraman, K.V., Refshauge, C., Adams, R.N., Liquid chromatographic analysis of nanogram quantities of ascorbate in brain tissue, ***1974***. *Life Sciences* 15(7), 1335-1342.

Wang, L., Gong, C., Shen, Y., Ye, W., Xu, M., Song, Y., A novel ratiometric electrochemical biosensor for sensitive detection of ascorbic acid, ***2017***. *Sensors and Actuators B: Chemical* 242, 625-631.

Xu, H., Cai, Q., Nie, Q., Qiao, Z., Liu, S., Li, Z., Ultrasensitive determination of ascorbic acid by using cobalt oxyhydroxide nanosheets to enhance the chemiluminescence of the luminol–H2O2 system, ***2018***. *RSC Advances* 8(42), 23720-23726.

Yang, H., Irudayaraj, J., Rapid determination of vitamin C by NIR, MIR and FT-Raman techniques, ***2002***. *Journal of Pharmacy and Pharmacology* 54(9), 1247-1255.

Yang, L., Xu, B., Ye, H., Zhao, F., Zeng, B., A novel quercetin electrochemical sensor based on molecularly imprinted poly(para-aminobenzoic acid) on 3D Pd nanoparticles-porous graphene-carbon nanotubes composite, ***2017***. *Sensors and Actuators B: Chemical* 251, 601-608.

Yu, L., Zhang, Q., Yang, B., Xu, Q., Xu, Q., Hu, X., Electrochemical sensor construction based on Nafion/calcium lignosulphonate functionalized porous graphene nanocomposite and its application for simultaneous detection of trace Pb2+ and Cd2+, ***2018***. *Sensors and Actuators B: Chemical* 259, 540-551.

Yulia, M., Suhandy, D., Ogawa, Y., Kondo, N., Investigation on the influence of temperature in l-ascorbic acid determination using FTIR-ATR terahertz spectroscopy: Calibration model with temperature compensation, ***2014***. *Engineering in Agriculture, Environment and Food* 7(4), 148-154.

Zaaba, N.I., Foo, K.L., Hashim, U., Tan, S.J., Liu, W.-W., Voon, C.H., Synthesis of Graphene Oxide using Modified Hummers Method: Solvent Influence, ***2017***. *Procedia Engineering* 184, 469-477.

Zhang, Y., Liu, P., Xie, S., Chen, M., Zhang, M., Cai, Z., Liang, R., Zhang, Y., Cheng, F., A novel electrochemical ascorbic acid sensor based on branch-trunk Ag hierarchical nanostructures, ***2018***. *Journal of Electroanalytical Chemistry* 818, 250-256.

Zhu, H., Xu, G., Electrochemical Determination of Ascorbic Acid Based on Hydrothermal Synthesized ZnO Nanoparticles, ***2017***. *International Journal of Electrochemical Science* 12, 3873 -3882

Zhu, Z.-Q., Dai, J.-F., Ma, C.-H., Sun, H.-X., Liang, W.-D., Li, A., Facile Preparation of Porous Graphene Oxide-Based Nanocomposite Xerogel for Selective Absorption, ***2017***. *ChemistrySelect* 2(27), 8493-8499.

Chapter- V

Novel electrochemical biosensor for serotonin detection based on gold nanorattles decorated reduced graphene oxide in biological fluids and *in vitro* model

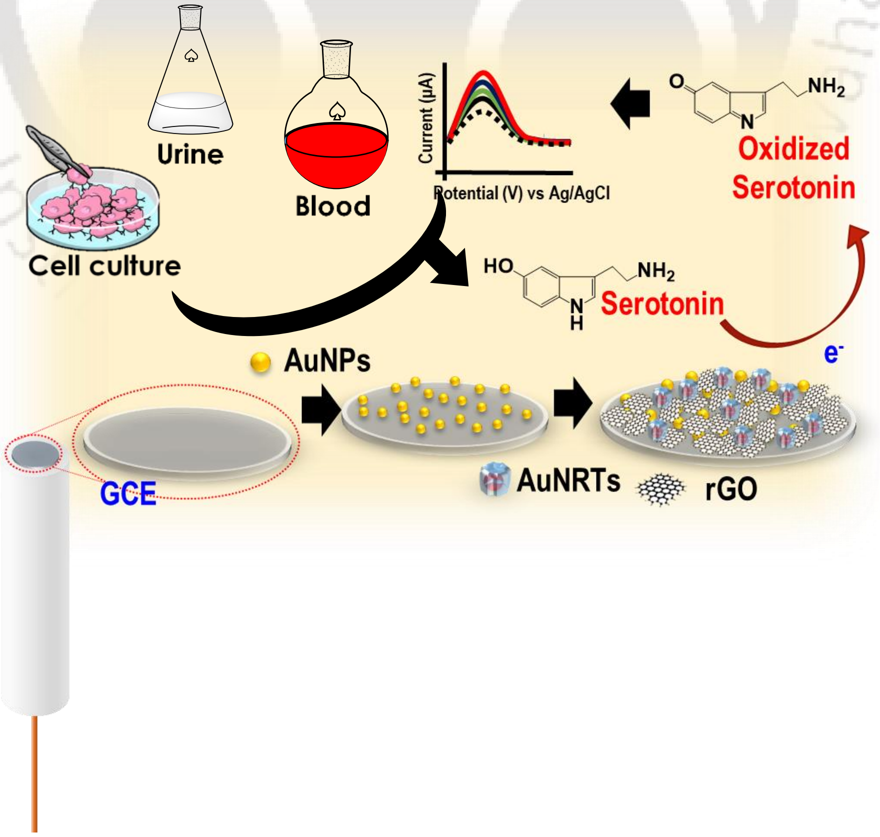

1. Introduction:

Biosensors are reported to develop the surface fouling in complex matrices such as blood, serum, and urine. Not only these, various other complex matrices of *in vitro, ex vivo*, and *in vivo* environments are also reported to exhibit the surface fouling due to the presence of bulky protein molecules, which eventually makes the biosensor less sensitive and non-reusable by blocking the interaction sites of the sensor probe for the interactions of target analytes. In view of this, we have developed a new type of material (nano-rattle) and decorated it with reduced graphene oxide for the clinically relevant detection of serotonin. Serotonin is one of the principal neurotransmitter (NTs), chemically known as 5-hydroxytryptamine and is regarded as molecule of contentment as it participates actively in controlling a number of behavioral as well as cognitive activities, such as sleep, anxiety, pain, hunger, learning, carnal activities *etc* (Godoy-Reyes et al.,2018). It is majorly produced by brain under physiological condition, where it functions in passing the information to various organs through central nervous system (Lacasse and Leo,2005). In addition, gastrointestinal tract has also been reported for secreting ST to control the intestinal movement (Camilleri,2009). The abnormal levels of ST have been related not only with various disorders *viz.* neurodegenerative diseases, autism, inflammatory syndromes, but also linked with a number of psychotic states such as depression, mood swing, attention-deficit hyperactivity disorder etc (Carver et al.,2009). The abnormally high serum level of ST is associated with various carcinoid tumors/syndromes, which commonly arises from gastrointestinal tract. Thus, ST determination in bio-fluids *viz.* serum and urine level have become one of the confirmatory tests for carcinoid tumors in clinics (Feldman,1986; Godoy-Reyes et al.,2018). The serum serotonin level in carcinoids have been reported > 400 ng/mL (*i.e.* 22.59 x 10^{-7} M) in case of tumorigenic growth, while further elevated level >1000 ng/mL (*i.e.* 56.74 x 10^{-7} M) was reported when tumors turn metastatic. This is much higher than the normal clinical serum level of ST, which is up to 300 ng/mL (*i.e.* 17.01 x 10^{-7} M) (Plapp,2019).

In clinical tests for the confirmation of such severity, ST has been determined in various bio-fluids urine and serum samples using the conventional methods, which are majorly based on fluorimeter (Andén and Magnusson,1967), capillary electrophoresis (Šolínová et al.,2018), high performance liquid chromatography (Patel et al.,2005), enzyme-based immunoassay (Maurer-Spurej et al.,2002), chemi-luminescence (Barnett et al.,1998), ELISA (Chauveau et al.,1991) and mass spectrometry (Yılmaz et al.,2019). These clinically accepted methods are extremely powerful and sensitive techniques, but involves a tedious process, sophisticated high-end instruments, longer time for determination, and are often required the sample pretreatment before testing, which not only restricts their utility for real time implications but also limits their usage in onsite point-of-care everyday determinations. In order to address these issues, a number of advanced strategies have also been employed; where electrochemical biosensor based systems have found great attention due to their comparable clinical performance *viz.* high sensitivity, ultrafast detection, and miniaturizability (Baranwal and Chandra,2018; Moon et al.,2018). Despite the advancement in the developed electrochemical ST determination, they suffer because of interfering signals due to the presence of inherently coexistent molecules and NTs *viz.* ascorbic acid, dopamine, epinephrine, norepinephrine *etc*. These interfering signals in such cases are contributed by their close reduction potentials (Wu et al.,2003), which not only make the systems insensitive but also non-selective. Therefore, in order to eliminate such limiting factors, the nanomaterial-empowered strategies were employed, where nanomaterials were introduced to achieve better-resolved determination of NTs by tuning the effective reduction potentials (Baranwal and Chandra,2018). In this context, a number of nanomaterials mediated determination techniques were employed by exploiting their intrinsic optoelectronic properties in nano-domain including a wide range of metallic and composites *viz.* metal oxides, polymers, and carbon based nanocomposites (Durairaj et al.,2018; Si and Song,2018). In recent advancements, caged-nanostructures, particularly nanocages and nanorattles have found a wide attention for various application including, adsorbent, drug delivery agent, nanoreactor *etc.* due to their extremely high surface area, porosity, and enhanced synergistic shape as well as size dependent properties of the constituting materials (Ahlawat et al.,2019; Priebe and Fromm,2015; Singh et al.,2018).

Since, ST biosensor relies on its electro-catalysis at probe surface, the electro-catalytic and conducting capability of constituent probe materials play a crucial role in the sensitive determination (Yang et al.,2015; Zestos,2018). In view of this, nanorattles-based conjugates could serve as a promising material for probe fabrication as these nanoconjugates not only provides larger surface area for electro-catalysis, but also capable of availing the selective channelization of redox active biogenic small molecules through its pores by restricting the bulky coexisting entities present in biological samples. These bulky groups often reported to foul the electrode surface and thereby decreases the sensitivity, when the biosensors are used in real matrices. Therefore, nanorattles based composites could be promising and important probe materials for ST biosensor design and application in various bio-based matrices.

In this study, we fabricated a biosensor using gold nanorattles (AuNRTs) based nano-composite for determining clinically relevant levels of ST in serum and urine samples. *In vitro* detection ability of the designed sensor probe was also examined by testing the ST in cellular environment. For that, firstly we have prepared AuNRTs using seed-mediated controlled synthesis methods followed by its doping with rGO sheets for the preparation of the nanocomposite. The prepared nanocomposite was then extensively characterized by

UV-Visible spectroscopy (UV-Vis), Transmission electron microscopy (TEM), selected area electron diffraction (SAED), and energy dispersive X-ray photoelectron spectroscopy (EDX). Thereafter, the sensing probe was fabricated by using AuNRTs-rGO nanocomposite coating on to the electrodeposited GCE/AuNPs surface. The probe fabrication was characterized by atomic force microscopy (AFM), cyclic voltammetry (CV) and electrochemical impedimetric spectroscopy (EIS). Further, the probe was used for the determination of ST in standard conditions, where the dose dependent study was performed and analytical performance (*viz.* LDR and DL) was obtained using differential pulse voltammetry (DPV). The practical implications of the probe were examined in serum, urine, and *in vitro* cell samples using spike and recovery method. The selectivity test for the fabricated probe towards ST was assessed and the shelf-life of developed biosensor was also evaluated.

2. Experimental:

2.1. Chemicals and instruments:

Chloroauric acid ($HAuCl_4$), silver nitrate ($AgNO_3$), hexadecyltrimethylammonium bromide (CTAB), sodium borohydride ($NaBH_4$), and L-ascorbic acid ($C_6H_8O_6$), citric acid ($C_6H_8O_7$), glucose ($C_6H_{12}O_6$), urea (CH_4N_2O), uric acid ($C_5H_4N_4O_3$), alanine ($C_3H_7NO_2$), serum albumin, glutamic acid, norepinephrine ($C_8H_{11}NO_3$), dopamine hydrochloride ($C_8H_{11}NO_2$: HCl), and epinephrine ($C_9H_{13}NO_3$), were procured from Sigma Aldrich, USA. Sodium phosphate dibasic (Na_2HPO_4), Sodium phosphate monobasic (NaH_2PO_4), Potassium ferrocyanide ($K_4Fe(CN)_6.3H_2O$), Potassium ferricyanide ($K_3Fe(CN)_6$), and sodium chloride (NaCl) were procured from Sisco-research laboratories India. Graphite flakes (C), potassium permanganate ($KMnO_4$), poly(allyl amine) hydrochloride (PAH), poly(vinylpyrrolidone) (PVP), and sulphuric acid (H_2SO_4) were procured from Merck Millipore, India.)

Phosphate buffered saline (PBS; 0.5 mM; pH- 7.0) and ruthenium hexamine (RuHex) solution (5mM; pH-7.0) was used throughout the experimentation. In electrochemical studies, the solutions of different concentration of analyte and interfering species were prepared using PBS. All solutions are prepared using deionized water (18.52 MΩ cm) (DW) which was obtained from Milli-Q system. For in vitro cell culture experiments, human embryonic kidney cell line was procured from NCCS, Pune (India). Dulbecco’s modified eagle’s medium (DMEM), penicillin/streptomycin antibiotic (Pen-Strep.), fetal bovine serum (FBS), trypsin-EDTA, Dulbecco’s phosphate buffer saline, disodium hydrogen phosphate, bovine serum albumin (BSA), and sodium dihydrogen phosphate for cell culture were obtained HIMEDIA, India.

Material characterization (FE-TEM imaging, SAED, EDX) was done using transmission electron microscopy (JEOL-JEM 2100, Japan). UV-Visible spectrophotometer (Agilent) was used for the preliminary confirmation of the cubic AuNRTs synthesis and composite material characterization of the electrochemical studies (cyclic voltammetry and electro-chemical impedance spectrometry) of the fabricated probe was performed by electrochemical workstation (Autolab, Metrohm, Netherland). For the electrochemical studies the conventional three cell electrode system, comprising glassy carbon electrode (GCE) as working, platinum electrode as counter and Ag/AgCl electrode (in saturated KCl) as reference electrode have been used. The frequency response analysis (FRA) module of electrochemical workstation has been used for the EIS measurement, where all spectra were recorded at the open circuit potential (V) *vs.* Ag/AgCl with the modulation aptitude of 10mV in the variable frequency range between 10 Hz to 1000 KHz. Thereafter, the resistance in charge transfer (Rct) was evaluated by analyzing the equivalent circuit of the spectra.

2.2. Synthesis of AuNRTs:

AuNRTs have been synthesized using seed mediated process involving the preparation of Au-octahedron seed preparation followed by the sequential coating of Ag and Au. The next step consists of the selective etching of the Ag to obtain AuNRTs. Briefly, in the first step core seed (Au-octahedron) were synthesized by reducing $HAuCl_4$ with ascorbic acid followed by the coating of silver shell on to the Au-octahedral structures (Khalavka et al.,2009; Singh et al.,2017). Here, the seed was prepared by mixing of $HAuCl_4$ (0.514 mL: 4.86 mM) in aqueous solution of CTAB (7.5 mL: 0.1 M), followed by the addition of deionized water (1.986 mL: 18.2 MΩ cm). Thereafter, the ice-cold $NaBH_4$ (0.6 mL: 10 mM) was injected into the 'seed solution' and it was allowed to stir. After that 120 microliters of seed solution was added to colorless 'growth solution', which was prepared by dissolving $HAuCl_4$ (82.3 μL: 4.86 mM), ascorbic acid (0.6 mL: 0.1 M) and CTAB (1.6 mL: 0.1 M) under magnetic stirrer. Further, the silver layer coating on it was achieved by the treatment of reducing solution of silver nitrate (0.5 mL: 10 mM) and ascorbic acid (2 mL: 0.1 M) to the synthesized Au-octahedrons followed by rigorous stir; and the solution was kept at 60 °C for 20 hrs. Then, the Ag-coated-Au-octahedrons were extracted sequentially using PAH (6 mg/mL in 6 mM NaCl) and PVP solutions (90 mM). In the final step, for synthesizing AuNRTs, $HAuCl_4$ was added dropwise to the Ag-coated-Au-octahedrons under moderate boiling conditions. The gradual appearance of dark blue color to the solution indicates the formation of AuNRTs. The solution was kept undisturbed for three hours in order to allow the settlement of AgCl salt comes out from the Ag-shell of precursor molecules during the galvanic conversion.

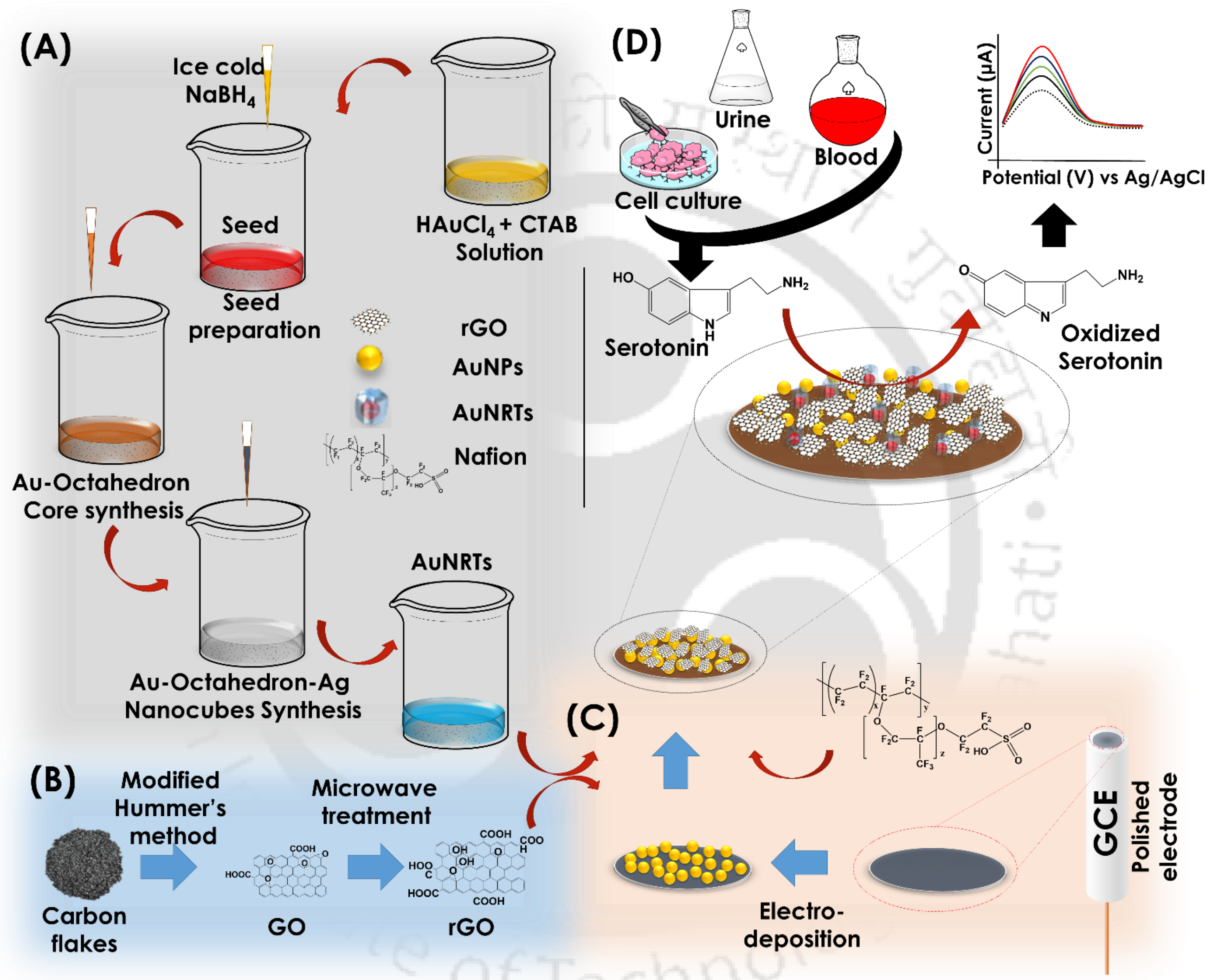

Scheme 5.1: *Schematic representation for the synthesis/deposition of AuNRTs (A), rGO (B), and AuNPs (C) on the GCE electrode surface. The probe development using AuNRTs-rGO-Naf nanocomposite and detection of ST (D).*

The schematic representation of AuNRTs synthesis has been shown in scheme 5.1(A). In order to obtain the concentrated purified solution, the AuNRTs solution was centrifuged at 5000 rpm for 1 hour and re-dispersed the pellet in deionized water.

2.3. AuNRTs-rGO-Naf nanocomposite preparation and fabrication of GCE/AuNPs/AuNRTs-rGO-Naf sensor probe:

The AuNRTs-rGO-Naf nanocomposite was prepared by doping AuNRTs in rGO containing Naf (0.1% in alcohol). For that, the AuNRTs were extracted in ethanol, where 1 ml of the previously synthesized aqueous solution was centrifuged at 8000 rpm for 10 minutes. Then, AuNRTs were re-suspended in 1 mL of ethanol. In the mean time, rGO solution was obtained by dissolving the rGO (10 mg/mL) in ethanol separately. Thereafter, these separately prepared solutions were mixed in the ratio of 1:5 (v/v) (optimized), which also contains 0.1% nafion. The solution was then sonicated for 4 hours in order to obtain AuNRTs-rGO-Naf nanocomposite solution. The sensor probe was developed using the obtained nanocomposite. In the first step, GCE electrode was polished with 0.05 µm alumina slurry on a microcloth pad and was rinsed with deionized water (DW). After this, AuNPs were electro-chemically deposited onto the GCE using a potential step method in an acidic solution (0.5 M H_2SO_4) containing 0.0025% $HAuCl_4$ by performing linear sweep voltammetry (LSV) between +1.5 and +0.4 (V) *vs.* Ag/AgCl. The provided conditions for AuNPs electrodeposition conditions are as follows: 60.0 s deposition time, − 0.6 V deposition potential, 0.1 V s^{-1} scan rate, and five times scanning of the potential. Thereafter, the GCE/AuNPs electrode was rinsed with DW and dried. In the next step, the AuNRTs-rGO-Naf nanocomposite solution (2 µL) was spin coated onto the GCE/AuNPs modified surface. The final probe was termed as GCE/AuNPs/AuNRTs-rGO-Naf. The detailed process of GCE/AuNPs/AuNRTs-rGO-Naf sensing probe fabrication is shown in scheme 5.1.

2.4. Mammalian cell culture and human serum sample preparation:

For the clinical implication of the fabricated GCE/AuNPs/AuNRTs-rGO-Naf sensor probe, human embryonic kidney cells and human blood serum were chosen for experiments in order to mimic the living complex biological systems. The human embryonic kidney cells (HEK cells) were cultured in DMEM medium in a T25 cell culture flask under aseptic conditions. The culture medium was supplemented with 100 units/mL of penicillin, 100 units/mL of streptomycin, and 10% heat-inactivated FBS. Then the culture flasks were incubated at 37˚C at 5% CO_2 and 95% humid condition. For the electrochemical studies, the cells were collected after trypsinization with gentle pipetting followed by centrifugation at 3000 rpm for 3 minutes under cold environment. Thereafter, the supernatant was discarded and the pellet containing the HEK cells was thoroughly washed by mild centrifugation with sterile buffer and suspended in PBS (pH 7.0). The number of cells in final analytical solutions was maintained at 1 x 10^6 cells / mL. For the human serum sample, the blood was collected from IIT Guwahati hospital, Assam, India, consented with the volunteers, which was further processed to obtain the serum using standard protocol. The obtained serum was then equilibrated with the PBS (pH=7.0) before using it for electrochemical studies.

3. Results and Discussions:

3.1. Characterization of the AuNRTs-rGO nanocomposite:

The AuNRTs-rGO nanocomposite has been systematically characterized using UV-Vis spectroscopy, FESEM, HRTEM, and SAED. In, UV-Vis spectrum (figure 5.1A (i); blue curve), a peak (λ_{max}) at 657 nm was observed in case of AuNRTs due to the SPR arising from the porous shell structure of AuNRTs (Singh et al.,2017). In addition, a shoulder at around 540 nm is contributed by the inner solid octahedron core present inside the cubic porous shell (Singh et al.,2017). The peak at 657 nm was reconfirmed by performing a dose dependent UV-Vis analysis, where spectrum was recorded with increasing concentration at 657 nm and hyperchromic peak shift was observed with increasing the concentration of AuNRTs (figure 5.1(B)). A dose dependent plot was obtained using the UV-Vis responses, which shows linear increment of peaks at λ_{max} (657 nm) indicating the peak λ_{max} is merely due to the AuNRTs (inset figure 5.1B). In the UV-Vis spectrum corresponding to rGO (figure 5.1 A (ii); red), an absorption peak near λ_{max} (260 nm) was observed due to the optical absorption of π-π* transition of aromatic C=C, C=O, and C–O bonds. Interestingly, in the UV-vis spectrum of nanocomposite comprising AuNRTs and rGO (figure 5.1A (iii); grey) two clear peaks near the 260 and 660 nm appeared, which were observed separately when these materials were tested individually. These results clearly indicate the formation of AuNRTs-rGO nanocomposite.

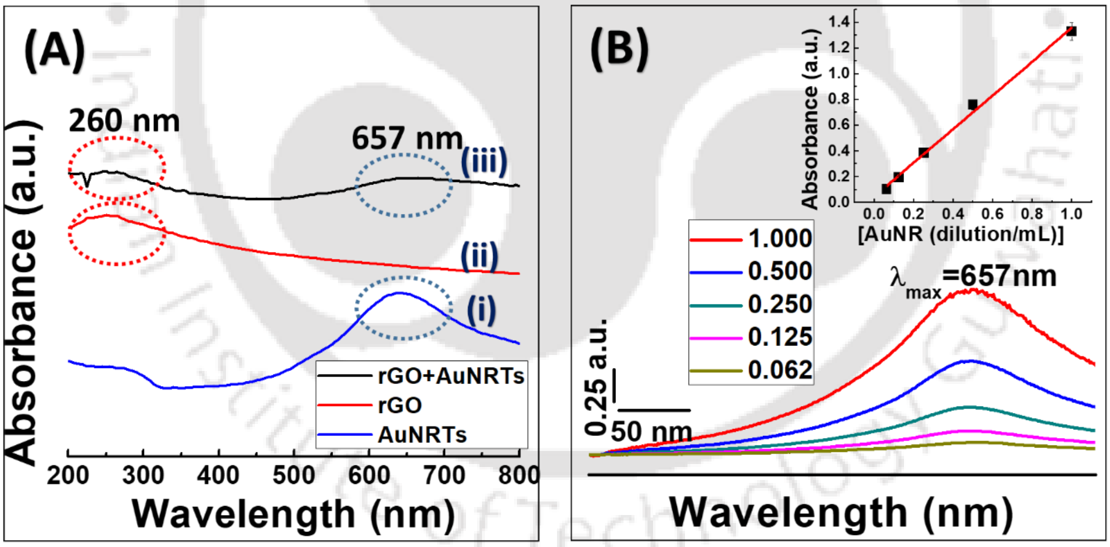

Figure 5.1: *(A) UV-Visible spectra of the (i) AuNRTs (ii) rGO, and (iii) AuNRTs – rGO nanocomposite. (B) Dose dependent responses of the AuNRTs (inset: calibration plot).*

Further, in order to validate the presence of AuNRTs with the rGO, we have characterized the AuNRT-rGO nanocomposite using the TEM. Figure 5.2 (A) shows the representative TEM micrograph of the synthesized nanocomposite, where it is evident that

AuNRTs (black squares) are present not only on the surface of rGO sheets, but also found entrapped within the multi-folded rGO layers, indicating the successful formation of the nanocomposite. The size distribution of the particles was obtained using set of the TEM micrographs and the average size of the particles were found to be 45.50 (± 1.25) nm (shown in figure 5.2(B)).

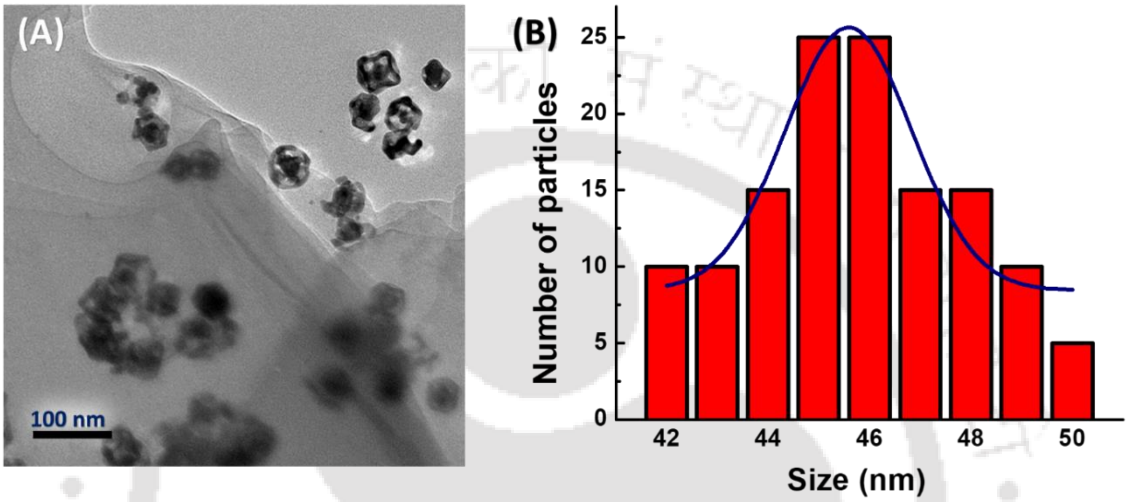

Figure 5.2: *(A) Representative TEM micrographs of AuNRTs - rGO nanocomposite, (B) Particle size distribution of AuNRTs.*

To study the crystal structures, we have further characterized the nanocomposite using HR-TEM and SAED. The representative HR-TEM micrograph and SAED pattern are shown in the figure 5.3(A) and 5.3(B), respectively. From the HR-TEM micrograph, it is evident that the synthesized AuNRTs are of crystalline in nature with the inter-planer distances *d* was obtained to be 0.22 nm, which is due to the presence of gold in AuNRTs. The SAED image shows the multiple concentric rings around central maxima indicating the polycrystalline nature of the nanocomposite, which is comprised of two highly crystalline components *viz.* AuNRTs and rGO. Further, to validate the elemental composition of the nanocomposites, we have complemented the characterization by using EDX and observed the elemental composition of C, O, and Au with the weight percentage of 85, 5, and 9 %, respectively (figure 5.3 (C)), indicating the nanocomposite have no other impurities.

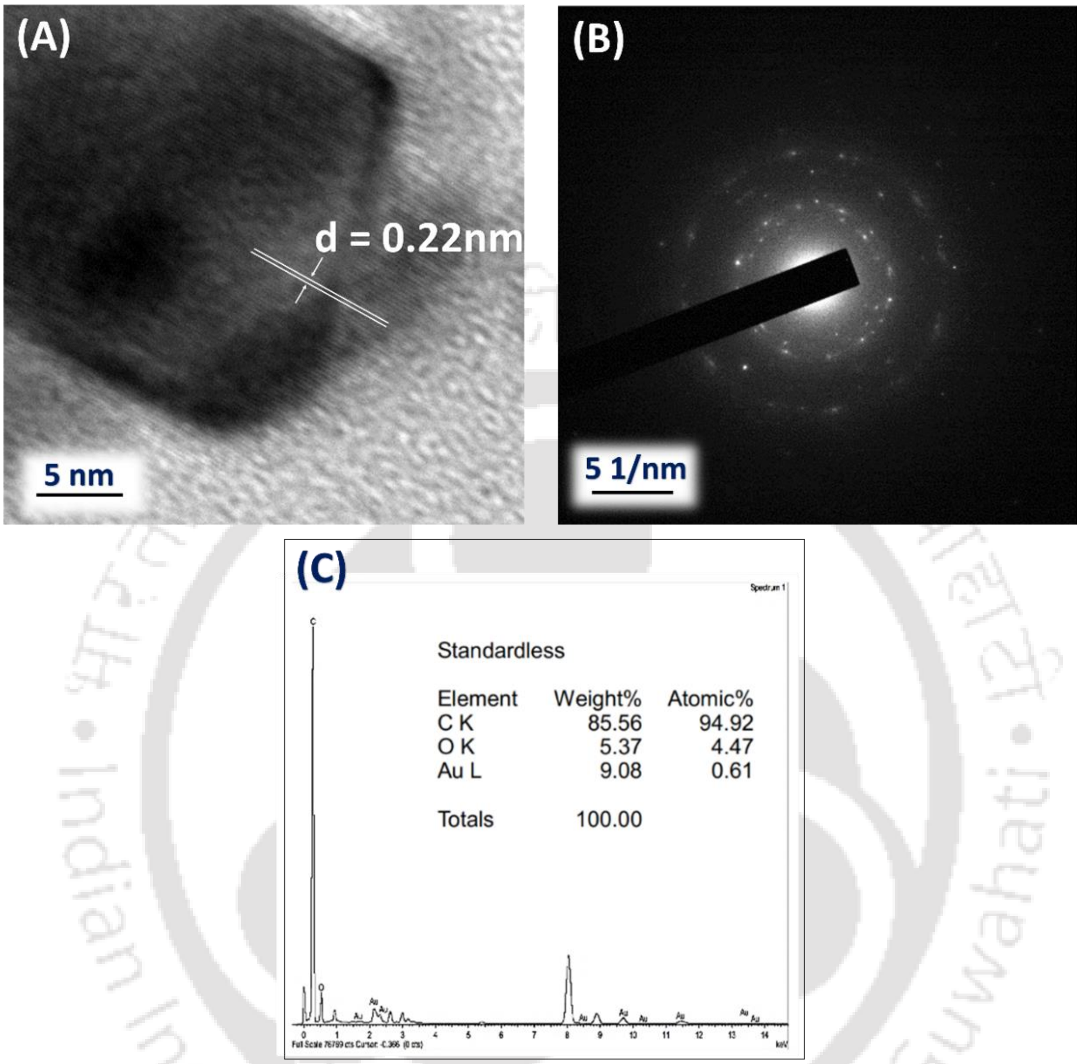

Standardless

Element	Weight%	Atomic%
C K	85.56	94.92
O K	5.37	4.47
Au L	9.08	0.61
Totals	100.00	

Figure 5.3: *(A) HR-TEM micrograph and d-fringe of the AuNRTs, (B) SAED pattern shown by AuNRTs-rGO nanocomposite, (C) EDX of the AuNRTs - rGO nanocomposite.*

3.2. Characterization of GCE/AuNPs/AuNRTs-rGO-Naf sensor probe:

Using the synthesized AuNRTs-rGO nanocomposite a sensor probe was fabricated as described in Scheme 5.1. In order to evaluate the electron transfer properties, the GCE/AuNPs/AuNRTs-rGO-Naf fabricated probe has been characterized extensively using the electrochemical methods. Firstly, the formation of AuNPs was characterized by

LSV, where a clear reduction peak at 0.095 (V) vs. Ag/AgCl was observed, which was due to the reduction of Au^{3+} to Au^0 on electrode surface, forming AuNPs (Figure not shown). Interestingly, the peak current at 0.094 V increased with three consecutive LSV sweeps, indicating the formation of highly conducting electrode surface due to the further deposition of AuNPs.

In the next step of characterization, the sensor probe was rinsed thoroughly with PBS, which is then dipped in to the electrochemical cell containing 5 mM RuHex solution (in PBS). Following this procedure to all modified surfaces, the linear sweep voltammograms were recorded at the scan rate of 50 mV/s and potential window of -0.75V to 0.4 V. Using, the voltammograms, the anodic peak current (I_{pa}) responses were obtained. Figure 5.4 shows the representative LSV responses of bare GCE (black), GCE/AuNPs (red), GCE/AuNRTs-Naf (blue), GCE/rGO-Naf (pink), GCE/AuNPs/AuNRTs-Naf (grey), and GCE/AuNPs/AuNRTs-rGO-Naf (yellow). The I_{pa} of RuHex redox couple at bare GCE is obtained, which increase after the AuNPs deposition due to the enhanced conductivity and surface area for electron transfer. The similar increment in the current has also been observed at the GCE/AuNRTs-Naf modified surface, indicating the conducting nature of the AuNRTs and its capability of assisting electrochemical signal. In the next surface, we have replaced AuNRTs with rGO and the response of the GCE/rGO-Naf surface was recorded in the similar experimental conditions. The subtle increment of the current in this case was also observed in the LSV responses, indicating the further enhancement of the conductivity of the modified surface. Intriguing by these interesting results, we have used the combination of the probe components and tested the responses. In the next step, GCE/AuNPs/AuNRTs-Naf has been fabricated and LSV was recorded using the modified electrode surface, the further increment in peak current than the previously tested modified surfaces was observed. In the final surface modification, AuNRTs decorated rGO has been employ to modify the electrode surface and LSV was performed using GCE/AuNPs/AuNRTs-rGO-Naf probe. It is interesting to note that, in this case maximum signal was observed due to the synergistic behavior of AuNRTs-rGO, which was present in the sensing matrix.

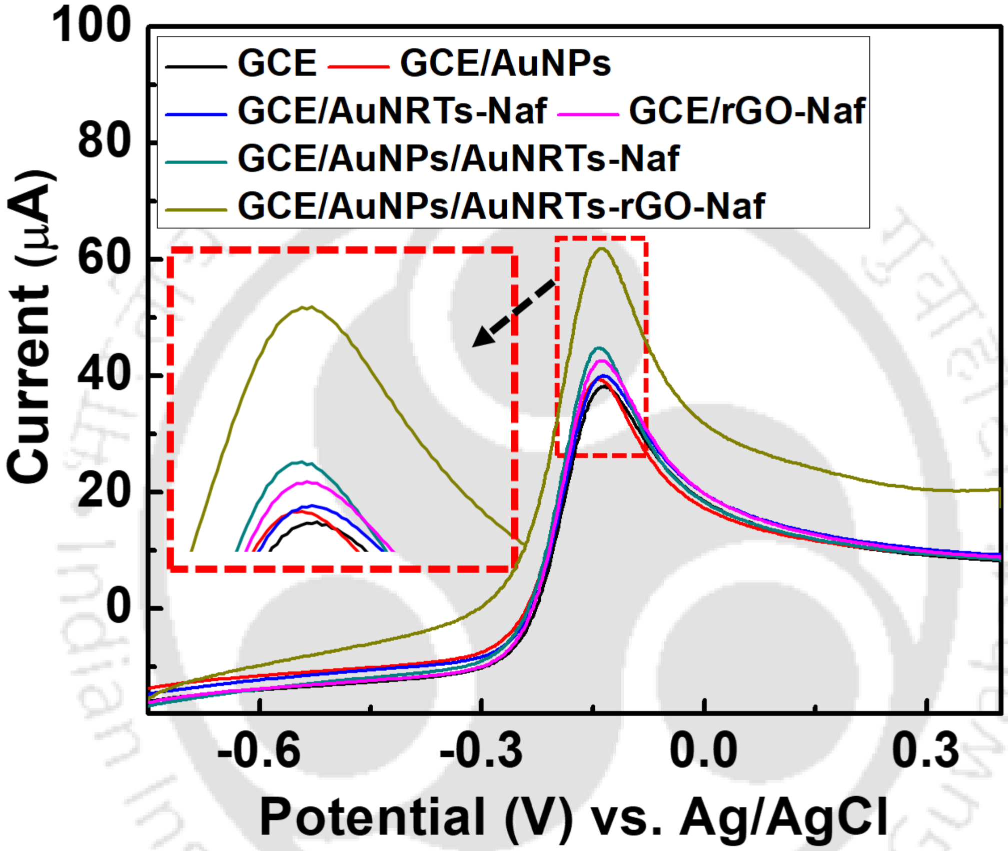

Figure 5.4: *LSV responses of the GCE, GCE/AuNPs, GCE/AuNRTs-Naf, GCE/rGO-Naf, GCE/AuNPs/AuNRTs-Naf, GCE/AuNPs/AuNRTs-rGO-Naf modified electrode surfaces.*

Therefore, for the further analyses we have used the GCE/AuNPs/AuNRTs-rGO-Naf as a sensor probe. In order to evaluate the importance of modified electrode surfaces towards electrochemical sensing, we have calculated the diffusion coefficients of bare GCE and for each layer of the modified electrode using Randles – Sevcik's model (equation 5.1).

$$I_p = \left(2.69\times10^5\right) n^{3/2} ACD^{1/2} v^{1/2} \quad \ldots\ldots\ldots\ldots\ldots\ldots\ldots. \text{ Equation 5.1}$$

Where I_p *is the peak current (in ampere), n is the number of electron transferred in redox process (here n=1), A is the electrode surface area (in* cm^2*: here A = 0.01* cm^2*), C is the concentration of electroactive species (in mole* cm^{-3}*), D is the diffusion coefficient (in* $cm^2\ s^{-1}$*), and v is the scan rate (in* $V\ s^{-1}$*).*

The diffusion coefficient (*D*) values for bare GCE, GCE/AuNPs, GCE/AuNRTs-Naf, GCE/rGO-Naf, GCE/AuNPs/AuNRTs-Naf, and GCE/AuNPs/AuNRTs-rGO-Naf modified surfaces were found to be 2.19 x 10^{-4}, 2.42 x 10^{-4}, 2.51 x 10^{-4}, 2.80 x 10^{-4}, 3.05 x 10^{-4}, and 5.40 x 10^{-3} cm^2s^{-1}, respectively. The findings of Randles - Sevcik model clearly indicates the ~ 2.5 fold higher transfer of charged species through the GCE/AuNPs/AuNRTs-rGO-Naf modified electrode surface than the bare GCE, thereby suggesting that the developed sensing surface is highly conducting. The results obtained by LSV were also validated using the EIS, where spectra in the Nyquist plot were recorded for bare GCE (black), GCE/AuNPs (red), GCE/AuNRTs-Naf, GCE/rGO-Naf (pink), GCE/AuNPs/AuNRTs-Naf (gray), and GCE/AuNPs/AuNRTs-rGO-Naf (yellow) (Figure 5.5 (A)) surfaces to obtain the R_{ct}. The R_{ct} values obtained were 1307.26 (± 45.75) Ω, 1257.12 (± 43.99) Ω, 1131.42 (±39.59) Ω, 1057.2 (± 37.00) Ω, 992.98 (± 34.75) Ω, and 174.72 (±10.11)Ω for the bare GCE, GCE/AuNPs, GCE/AuNRTs-Naf, GCE/rGO-Naf, GCE/AuNPs/AuNRTs-Naf, and GCE/AuNPs/AuNRTs-rGO-Naf surfaces, respectively (figure 5.5(B). It is interesting to note that the lowest R_{ct} was obtained for GCE/AuNPs/AuNRTs-rGO-Naf surface compared to other tested surfaces. This was due to the fastest electron transfer kinetics at electrode/electrolyte interface in this case. The result obtained in EIS also corroborates with the results of LSV analysis.

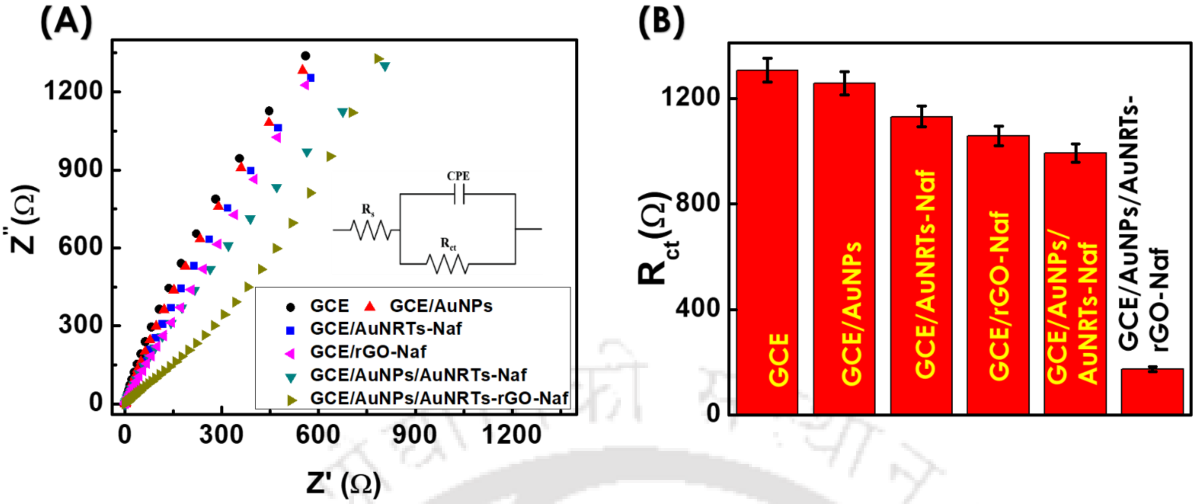

Figure 5.5: ***(A)*** *EIS responses of the GCE, GCE/AuNPs, GCE/AuNRTs-Naf, GCE/rGO-Naf, GCE/AuNPs/AuNRTs-Naf, GCE/AuNPs/AuNRTs-rGO-Naf modified electrode surfaces, (B) histogram showing the respective Rct values obtained from the EIS spectra.*

The charge transfer is a crucial parameter for the modified surfaces due to its complexity. In order to investigate the charge transfer behavior and stability of modified electrode surfaces for electrochemical analysis, we have performed scan rate studies at bare GCE, GCE/AuNPs, GCE/AuNRTs-Naf, GCE/rGO-Naf, GCE/AuNPs/AuNRTs-Naf, and GCE/AuNPs/AuNRTs-rGO-Naf (Figure 5.6). Here LSV responses were recorded at different scan rates (*i.e.*10-100 mV/s) in 5mM PBS containing RuHex solution and peak currents were plotted against the square root of scan rates. The I_{pa} was found to be directly proportional to the square root of scan rates in all cases with the correlation coefficient between 0.997 and 0.999; indicating the stability of sensor probe and diffusion-controlled charge transfer processes at modified electrode surfaces. These results confirm that the developed GCE/AuNPs/AuNRTs-rGO-Naf probe is highly stable, conducting, and sensitive; hence, it is suitable for electrochemical analysis.

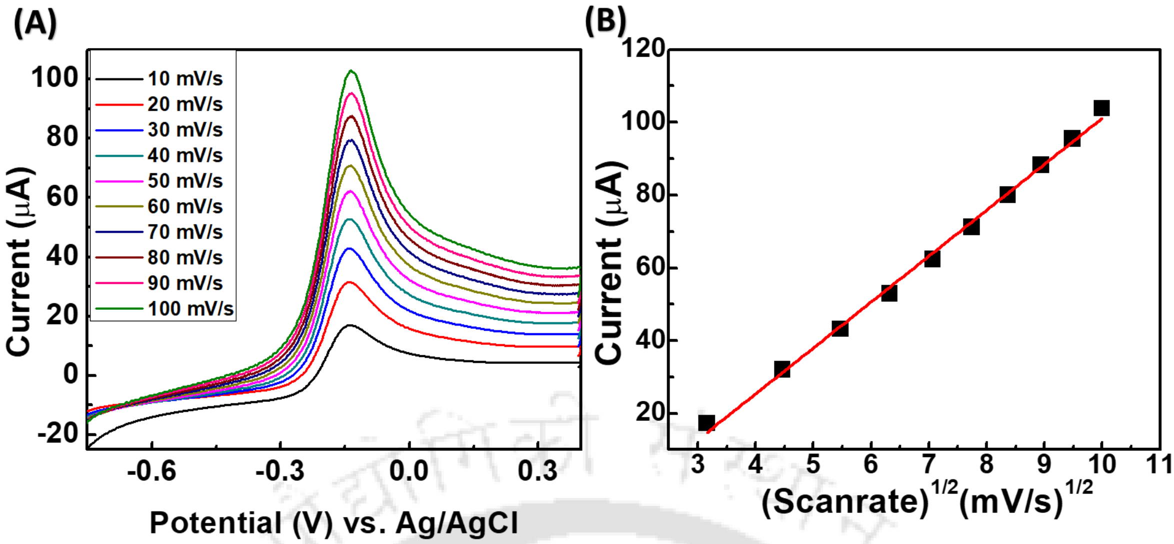

Figure 5.6: *(A) LSV responses of the GCE/AuNPs/AuNRTs-rGO-Naf modified surfaces at different scan rates (10-100 mV/s) and (B) scan rate dependent plot obtained from the LSV responses*

Thereafter, in order to confirm the macroscopic changes at the modified electrode surface, every deposition layers of final probe have been characterized using AFM by capturing the surface during the biosensor fabrication process and analyzed its surface roughness and *z-deflection*. Figure 5.7 shows the representative AFM micrographs and *z-deflection* pattern of the surfaces at different stages of fabrication. *i.e.* bare electrode (i), AuNPs deposited electrode (ii), and AuNRTs-rGO-Naf deposited electrode (iii). Firstly, the surface topology of bare electrode was captured where smooth morphology was observed. Using the micrograph, mean surface roughness, and *z-deflection* have been calculated, which were obtained to be 0.50 nm and 3 nm, respectively. Thereafter, AuNPs deposited surface was captured, where the generated micrograph shows a granular morphology with the mean surface roughness and *z-deflection* of the 4.81 nm and 11 nm, respectively; indicating the successful deposition of AuNPs onto the electrode surface. In the final step of fabrication, more dense film like morphology was observed with the mean surface roughness and *z-deflection* of 7.90 nm and 26 nm, respectively, indicating the stable coating of AuNRTs - rGO over the electrode surface.

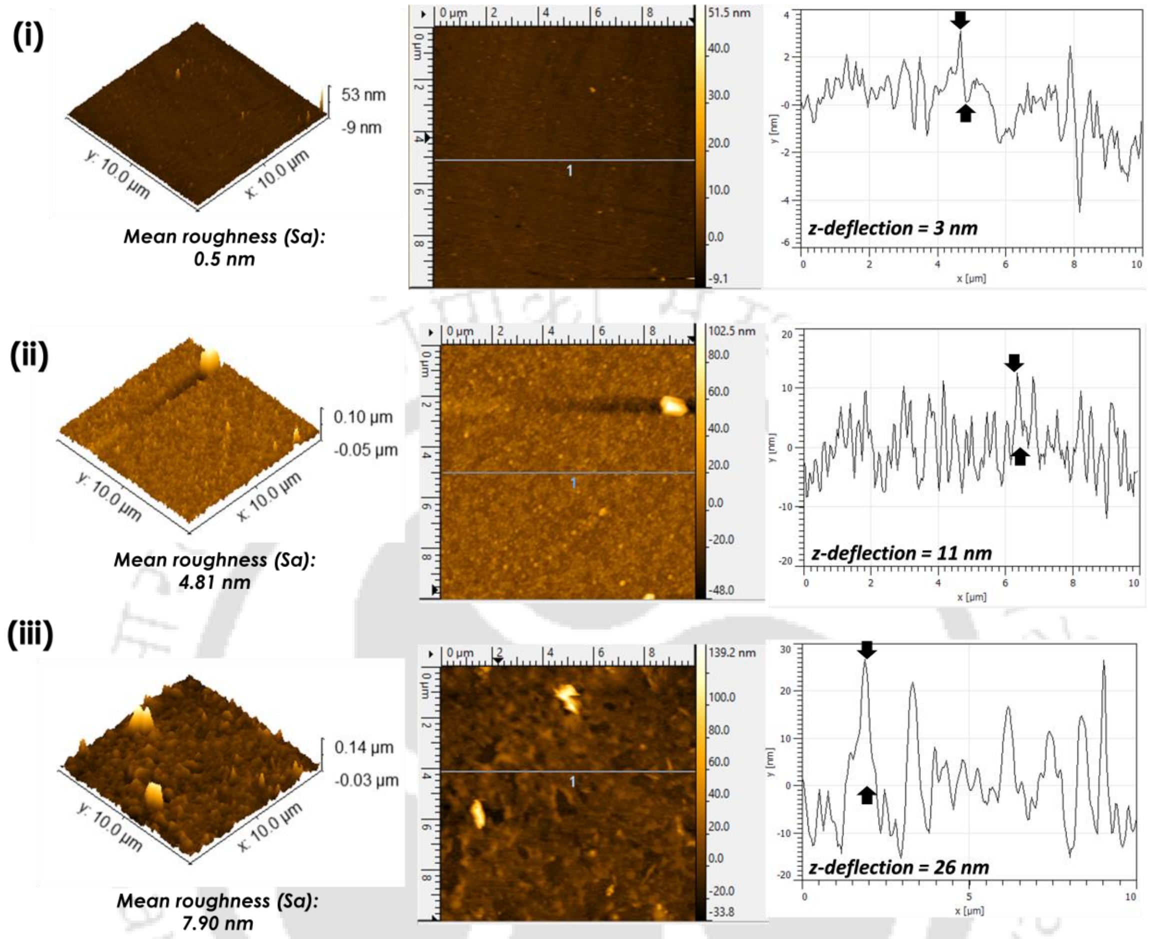

Figure 5.7: *AFM micrographs (2D and 3D) of the bare electrode surface (i), AuNPs deposited electrode surface (ii), and AuNRTs-rGO-Naf deposited surface (iii) with respective z-deflection profiles and mean surface roughness.*

3.3. Analytical performance of the GCE/AuNPs/AuNRT-rGO-Naf sensor probe:

After the successful characterization, the GCE/AuNPs/AuNRTs-rGO-Naf sensor probe was applied for the detection of ST. At first, we have tested the suitability of fabricated probe for ST detection. For that, bare GCE was dipped in 5 mM PBS (Blank / no ST) and LSV was recorded by sweeping the potentials between 0.25 and 0.60 V, where no peak was observed. In the subsequent step, the LSV response was recorded in 5 mM

PBS containing 10^{-3} M ST using bare GCE probe, where a broad peak at 0.39 V was observed, which is due to the presence of ST in electrolyte solution. Thereafter, the modified GCE/AuNPs/AuNRTs-rGO-Naf sensor probe was tested in same PBS solution containing 10^{-3} M ST and LSV was recorded in the similar potential window separately. Interestingly, a sharp amplified peak at a relatively lower potential 0.36 V was observed, which is due to the electro-catalytic activity of the modified electrode. The signal response of GCE/AuNPs/AuNRTs-rGO-Naf sensor surface was found with the two-fold increment than the bare GCE in presence at the same concentration of ST (*i.e.* 10^{-3}M), indicating the fabricated biosensor is capable of sensitive determination of ST (Figure 5.8 (A). In order to validate the peak observed at 0.37 V was merely due to the interaction of ST with sensor probe, we performed two separate control experiments. In first control experiment, a concentration dependent study was performed, where we tested $1x10^{-5}$, $3x10^{-5}$, $6x10^{-5}$, and $1x10^{-4}$M of ST. Figure 5.8 (B) shows the signal response, where current increased linearly with increasing ST concentrations. The representative dose dependent LSV responses are shown in inset of figure 5.8(B). The linear regression equation for concentration dependent plot is expressed as follows: $\Delta I\ (\mu A) = 14.87\ x10^{-6}\ (\pm\ 0.61x10^{-6}) + 2.18x10^{-6}\ (\pm 0.13x10^{-6})$ Log Conc. [ST (M)] with the correlation coefficient of 0.96, indicating the ability of GCE/AuNPs/AuNRT-rGO-Naf sensor probe for ST detection correctly. In second experiment, a scan rate dependent study was performed at 10^{-3} M of ST between 10 and 100 mV s^{-1} (Figure not shown). In this case, the oxidation peak current was found to be directly proportional to the square root of scan rates due to the diffusion controlled electrochemical process of ST only. The results obtained from both the control experiments validate that the designed sensor probe is stable and is able to detect ST accurately. Comparable peak potential for ST has also been reported at GCE/MWCNT-NiO electrode (Fayemi et al.,2017). After this, we further investigated the analytical performance of designed GCE/AuNPs/AuNRTs-rGO-Naf sensor by detecting various concentrations of ST, where differential pulse voltammetry (DPV) has been used for the further analysis as it offers sensitive determination (Bard et al.,1980).

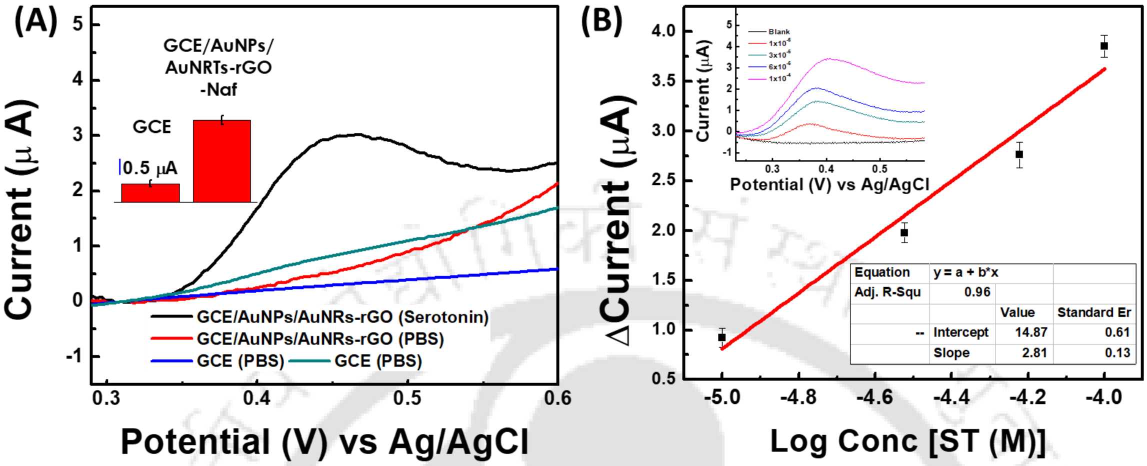

Figure 5.8: *(A) LSV responses of the GCE/AuNPs/AuNRTs-rGO-Naf in presence of blank and different concentrations of Serotonin (1x10*$^{-5}$*, 3x10*$^{-5}$*, 6x10*$^{-5}$*, 1x10*$^{-4}$*M). (B) Dose dependent LSV responses and corresponding calibration plot of serotonin at GCE/AuNPs/AuNRTs-rGO-Naf probe surface.*

Figure 5.9 (A) shows the representative DPV curves, where the current response increased linearly with the increase in the ST concentrations. Based on the DPV responses, a calibration plot was obtained, which shows the LDR between 3x10^{-6} and 1x10^{-3} M of ST (Figure 5.9 (B)). The linear regression equation of the calibration plot for ST detection was expressed as follows: ΔI (μA) = 3.80x10^{-6} (±0.38x10^{-6}) Log Conc. [ST (M)] + 20.41x10^{-6} (±1.66x10^{-6}) with the correlation coefficient of 0.95. The DL in this case was determined to be 3.87 (±0.02) x 10^{-7} M (RSD < 4.2%, 95 % confidence level, n=3) using equation 5.2.

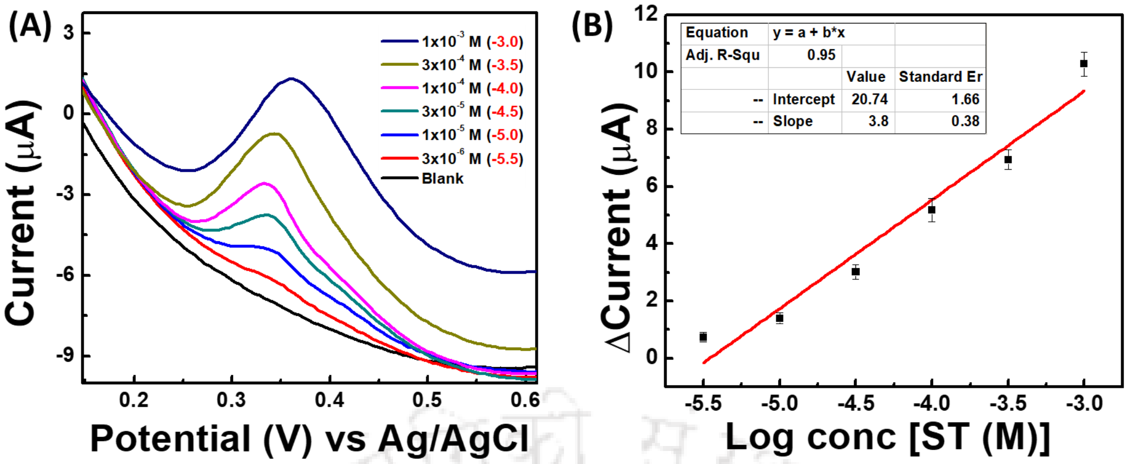

Figure 5.9: *(A) DPV responses of the serotonin in different concentrations, and (B) calibration plot obtained from the dose dependent DPV responses.*

$$LOD = \frac{3SD_B}{Slope} = \frac{3SD_B}{\frac{dy}{dx}} = \frac{3SD_B}{\frac{dy}{d\ln x}\times\frac{d\ln x}{dx}} = \frac{3SD_B}{\frac{dy}{2.303(d\log x)}\times\frac{1}{x}} \quad \text{-------- Equation 5.2}$$

$$= \frac{3(2.303)SD_B x}{\frac{dy}{(d\log x)}} = \frac{3(2.303)SD_B x}{\text{slope of the semilog plot}}$$

Where, SD$_B$ is standard deviation of blank; x is the limit of quantification or lowest concentration measured.

It is worth mentioning that the detection range in our case falls well in the clinical range related to various pathophysiological conditions including carcinoid syndromes/tumors (Feldman,1986; Plapp,2019) and pre-eclampsia (Vural et al.,1999).

3.4. Selectivity assay:

For the biomedical usage of any biosensor, it should have to be selective towards the target analyte. Therefore, to analyze the selectivity of developed biosensor, the interference assay is performed. (Mahato and Chandra,2018; Mahato et al.,2018; Pallela et al.,2016). Here, firstly the fabricated GCE/AuNPs/AuNRTs-rGO-Naf probe was tested towards ascorbic acid due to its coexistence in higher concentrations and close reduction potential (to ST) in the biological samples. Interestingly, in our case, no peak for ascorbic acid was observed. Not only this, citric acid, uric acid, glutamic acid have also been tested using the fabricated probe due to their coexistence with ST in various bio-fluids. In all the cases, no peak was observed, which were most likely due to the repulsion of these molecules from the negatively charged electrode surface. In addition to these, the interference effects of other coexisting molecules *viz.* glucose, urea alanine, and serum albumin present in bio-fluids have also been tested. In case of glucose, no peak was obtained due to its electrochemical inertness and inability of the probe to oxidize the glucose, whereas urea, alanine, and serum albumin were observed with no peaks in the operational window. In the biological matrices, other monoamine NTs *viz.* dopamine, epinephrine, and norepinephrine are profoundly reported in coexistence with ST; hence, the interference due to their presence is most likely event as they show close reduction potential to ST. Therefore, we have tested the GCE/AuNPs/AuNRTs-rGO-Naf fabricated probe for other NTs, where no current responses were observed at 0.36V, however, the peaks for these NTs were observed at 0.25 V. The results clearly indicates that these NTs do not interfere towards ST detection. The selectivity of GCE/AuNPs/AuNRTs-rGO-Naf probe was mathematically deduced by determining the selectivity coefficient $K_{selectivity}$ using equation 5.3.

$$K_{selectivity} = \frac{(Signal)_{interferent}}{(Signal)_{ST}} \qquad \text{------------------------- Equation 5.3}$$

Where $K_{selectivity}$ *is the coefficient of selectivity,* $(Signal)_{interferent}$ *is the signal strength shown by probe when treated with the interfering molecules, and* $(Signal)_{ST}$ *is the signal strength corresponds to ST.*

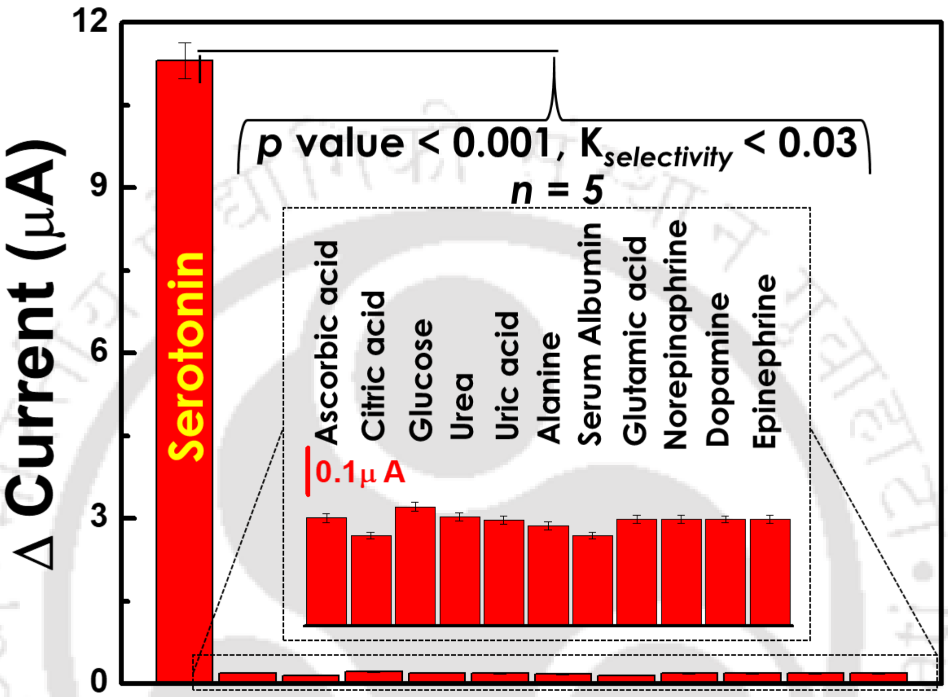

Figure 5.10: *Selectivity assay of GCE/AuNPs/AuNRTs-rGO-Naf sensor probe.*

The calculated $K_{selectivity}$ values for interfering molecules were found to be extremely low ($k_{selectivity} << 1$), indicating that the fabricated sensor is highly selective towards ST. We also performed T-test and calculated p-values against all interfering molecules, which were found to be << 0.001 (n = 3), indicating that the selectivity results are statistically significant. Figure 5.10 shows the histogram obtained from DPV responses of the interfering molecules and ST at the GCE/AuNPs/AuNRTs-rGO-Naf sensor probe.

3.5. Real sample analysis:

There are a number of pathophysiological conditions, where the variable levels of ST in urine, blood, and cellular systems were reported (Feldman,1986; Murugesan et al.,2018). Therefore, the detection ability of GCE/AuNPs/AuNRTs-rGO-Naf sensor probe was investigated in these matrices using spike and recovery method. Firstly, the urine samples have been tested, where urine samples were equilibrated with PBS and ST of different concentrations were spiked followed by its detection using the GCE/AuNPs/AuNRTs-rGO-Naf sensor probe. It is worth mentioning that the urine samples were not subjected to any pretreatment step such as filtration or centrifugation before processing. The results of these experiments were analyzed and % recoveries of ST were calculated using equation 5.4.

$$\% \text{ Recovery} = \frac{([S]_{ST} - [B]_{ST})}{[SS]_{ST}} \quad \text{--------------------------- Equation 5.4}$$

Where, $[S]_{ST}$ *and* $[B]_{ST}$ *are the analytical responses of* ST *in the spiked and blank urine samples, respectively; and* $[SS]_{ST}$ *is the analytical response of* ST *in the standard solutions.*

Figure 5.11 shows the signal response of ST detected in urine samples (red bars), where peak currents increased linearly with the increase in ST concentrations from 3×10^{-6} to 1×10^{-3} M. The sensitivity of ST detection was evaluated by comparing the DPV signals obtained from urine samples with blank buffer (black bars). Interestingly, the designed biosensor is able to detect 96.23% to 98.49% of ST from the human urine samples. The analytical details for recovered ST concentrations, RSD, and % recovery for all the tested concentrations are represented in table 5.1. Based on the dose dependent ST detection in urine, a calibration plot was obtained which shows the linear regression equation as follows: ΔI (μA) = 3.71(±0.33) x 10^{-6} log Conc [ST (M)] + 20.28 (±1.47) x10^{-6} M with the correlation coefficient of 0.959. The DL of 4.93 (±0.32) x10^{-7} M (RSD < 3.58 %) was obtained in human urine sample based on the standard deviation of three times consecutive analyses of the blank (95% confidence level; n=3), which indicates the fabricated biosensor is efficient to detect ST in human urine sample and is highly reproducible. Further, the fabricated probe was challenged for the determination of ST in relatively complex matrices. For this purpose, the fabricated probe was used for the determination of ST in clinical serum samples. Herein, human blood sample was obtained from nearby clinic and serum was extracted by following the standard protocol**.** Thereafter, the clinical serum was equilibrated with PBS and used for the determination of ST. Similar to the assessment in urine samples, here also, the different concertations (1x10^{-3} to 3x10^{-6}) of the ST were spiked and DPV responses were recorded (figure 5.11; blue bars). Based on the DPV responses, % recovery for ST were calculated against every spiked concentrations, which were found in between 84.62 and 90.69%, indicating the fabricated probe is capable of detecting even in the complex matrix like blood serum. Based on the dose dependent responses of GCE/AuNPs/AuNRTs-rGO-Naf probe in serum samples, a calibration plot was traced and the regression equation was obtained as follows: ΔI (μA) = 3.31(±0.34) x 10^{-6} log Conc [ST (M)] + 18.06 (±1.50) x10^{-6} M with the correlation coefficient of 0.947 and the DL of 8.73 (±0.35) x10^{-7} M (RSD < 4.92 %). After demonstrating the ability of the sensor probe to the successful ST detection in biological fluids, we enthusiastically extended our investigation towards *in vitro* detection of ST using the fabricated sensor probe. For this purpose, ST was spiked in the cellular environment in the range between 3x10^{-6} to 1x10^{-3} and analyzed the performance of fabricated sensor probe as performed in earlier cases. Figure 5.11 (gray bars) shows the dose dependent increment in ST signal when tested in *in vitro* settings. Similar to the above, here also we have obtained a calibration plot after plotting the peak currents of responses against

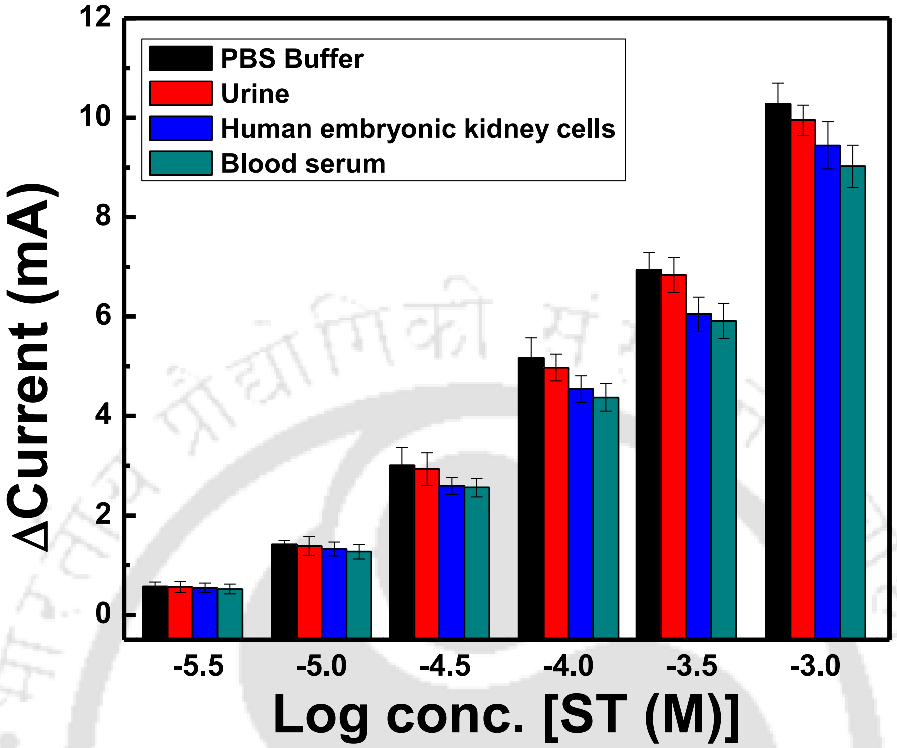

Figure 5.11: *Comparative concentration dependent determination of ST in PBS (black bars) urine (red bars), in vitro human embryonic kidney cells (blue bars) and blood serum (gray bars).*

concentration spiked. The regression equation was obtained as ΔI (μA) = 3.45 (±0.38) x 10^{-6} log Conc [ST (M)] + 18.79 (±1.66) x10^{-6} M with the correlation coefficient of 0.932. The DL in this case was found to be 7.37 (±0.27) x10^{-7} M (RSD < 4.92 %), indicating the biosensor is capable of detecting ST even in cellular environments. Thereafter, the % recovery was calculated and found in between 86.19 and 94.88%. The obtained recovered ST concentrations, % recovery, and RSD for serum and in vitro cellular samples were reported in the table 5. 1 (A-C).

(A) Urine

Spiked ST (M)	Recovered ST (M)	RSD	% Recovery
$3.00x10^{-06}$	$2.95(\pm0.19)x10^{-06}$	6.75	98.4
$1.00x10^{-05}$	$0.97(\pm0.06)x10^{-05}$	4.14	97.41
$3.00x10^{-05}$	$2.92(\pm0.17)x10^{-05}$	5.97	97.37
$1.00x10^{-04}$	$0.96(\pm0.05)x10^{-04}$	5.33	96.23
$3.00x10^{-04}$	$2.95(\pm0.14)x10^{-04}$	4.86	98.49
$1.00x10^{-03}$	$0.96(\pm0.03)x10^{-03}$	3.59	96.8

(B) Blood Serum

Spiked ST (M)	Recovered ST (M)	RSD	% Recovery
$3.00x10^{-06}$	$2.72(\pm0.19)x10^{-06}$	4.48	90.69
$1.00x10^{-05}$	$0.89(\pm0.06)x10^{-05}$	4.58	89.53
$3.00x10^{-05}$	$2.55(\pm0.17)x10^{-05}$	4.52	85.07
$1.00x10^{-04}$	$0.84(\pm0.05)x10^{-04}$	4.78	84.62
$3.00x10^{-04}$	$2.55(\pm0.14)x10^{-04}$	5.58	85.22
$1.00x10^{-03}$	$0.87(\pm0.03)x10^{-03}$	4.76	87.79

(C) Cell culture

Spiked ST (M)	Recovered ST (M)	RSD	% Recovery
$3.00x10^{-06}$	$2.84(\pm0.13)x10^{-06}$	4.73	94.88
$1.00x10^{-05}$	$0.93(\pm0.44)x10^{-05}$	4.69	93.23
$3.00x10^{-05}$	$2.58(\pm0.12)x10^{-05}$	4.78	86.19
$1.00x10^{-04}$	$0.87(\pm0.41)x10^{-04}$	4.50	87.82
$3.00x10^{-04}$	$2.61(\pm0.01)x10^{-04}$	4.68	87.15
$1.00x10^{-03}$	$0.91(\pm0.04)x10^{-03}$	4.65	91.86

Table 5.1: *Recovery table of ST from the real samples (A) urine, (B) blood serum, and (C) cell culture using the fabricated GCE/AuNPs/AuNRTs-rGO-Naf sensor probe*

It is interesting to note that the DL in all the real sample matrices was slightly higher compared to the standard buffer conditions, indicating the negligible matrix effect and excellent catalytic ability of GCE/AuNPs/AuNRTs-rGO-Naf sensor probe for the sensitive determination of ST even in unknown matrix components.

3.6. Reproducibility and stability studies:

Reproducibility and stability are the other parameters, which decide the commercialization of any such sensors (Chandra et al.,2017; Mahato et al.,2017). In order to test the fabricated GCE/AuNPs/AuNRTs-rGO-Naf sensor for its reproducibility, the current responses were recorded using the five separately prepared sensor probes. The current responses due to the GCE/AuNPs/AuNRTs-rGO-Naf probe were observed negligibly altered, when same fabrication procedure was followed (RSD < 3.9%), indicating the developed GCE/AuNPs/AuNRTs-rGO-Naf sensor probe is highly reproducible.

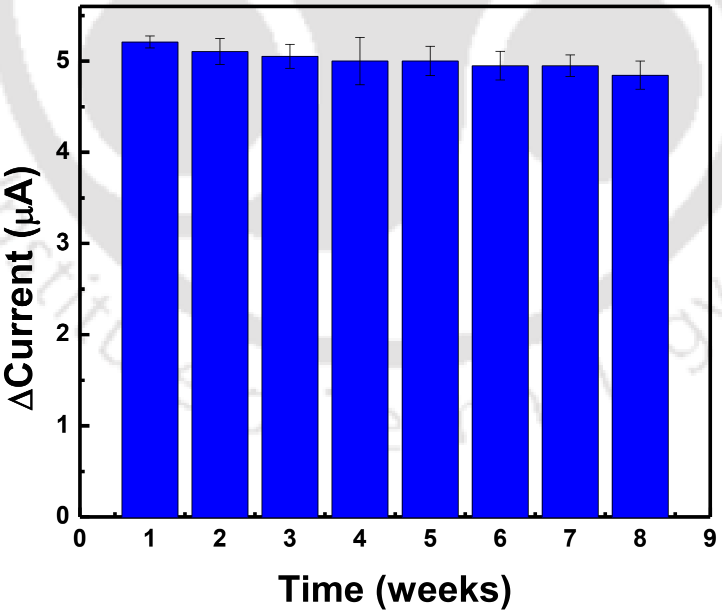

Figure 5.12: *Histogram obtained on shelf life study of the GCE/AuNPs/AuNRTs-rGO-Naf sensor probe tested using* 10^{-4} *M ST*

The small deviation was most likely due to the minor difference in sensor development and / or due to handling errors. The long-term stability has also been studied for the fabricated GCE/AuNPs/AuNRTs-rGO-Naf sensor probe, where the sensor was found to be stable until 8 weeks. Thereafter, the response decreases with time suggesting the developed GCE/AuNPs/AuNRTs-rGO-Naf sensing probe is stable up to 8 weeks.

4. Conclusions:

In this study, we have fabricated a novel facile robust biosensor based on the AuNRTs decorated -rGO nanocomposite for the determination of ST. After the successful characterization of the synthesized nanocomposite by UV-Vis, TEM, SAED, and EDX, it was employed to fabricate sensor probe and was characterized by AFM and electrochemical techniques. The biosensor shows excellent analytical performance with the wide DR of $3x10^{-6}$M $-1x10^{-3}$M and DL of 3.87 (±0.02) $x10^{-7}$ (RSD < 4.2%) M, which falls in concentrations for at various clinical conditions. The biosensor is capable of delivering highly selective and sensitive determination of ST in urine, blood serum samples, and *in vitro* (human embryonic kidney cells) models. The fabricated sensor shows excellent recoveries between 84.62 - 98.40% of ST in these samples, making it suitable for various clinical usages. To the best of our knowledge, we have demonstrated AuNRTs conjugated nanocomposite based electrochemical biosensor for ST determination for the first time. The biosensor shows high selectivity towards ST in comparison to the interfering molecules, and stable up to 8 weeks. The fabricated biosensor has many remarkable features including ease to handle, fast, label-free and inexpensive detection; thus, it could be a method of choice for ST determination in the biological and clinical samples. In the future, the developed biosensing system can be translated towards a genuine miniaturized sensing device for various applications.

5. References:

Ahlawat, M., Sarkar, A., Roy, S., Jaiswal, A., Gold Nanorattles with Intense Raman In Silica Nanoparticles (Nano-IRIS) as Multimodal System for Imaging and Therapy, ***2019***. *ChemNanoMat* 5(5), 625-633.

Andén, N.-E., Magnusson, T., An Improved Method for the Fluorimetric Determination of 5-Hydroxytryptamine in Tissues, ***1967***. *Acta Physiologica Scandinavica* 69(1-2), 87-94.

Baranwal, A., Chandra, P., Clinical implications and electrochemical biosensing of monoamine neurotransmitters in body fluids, in vitro, in vivo, and ex vivo models, ***2018***. *Biosensors and Bioelectronics* 121, 137-152.

Bard, A.J., Faulkner, L.R., Leddy, J., Zoski, C.G., 1980. Electrochemical methods: fundamentals and applications. wiley New York.

Barnett, N.W., Hindson, B.J., Lewis, S.W., Determination of 5-hydroxytryptamine (serotonin) and related indoles by flow injection analysis with acidic potassium permanganate chemiluminescence detection, ***1998***. *Analytica Chimica Acta* 362(2), 131-139.

Camilleri, M., Serotonin in the gastrointestinal tract, ***2009***. *Current opinion in endocrinology, diabetes, and obesity* 16(1), 53.

Carver, C.S., Johnson, S.L., Joormann, J., Two-Mode Models of Self-Regulation as a Tool for Conceptualizing Effects of the Serotonin System in Normal Behavior and Diverse Disorders, ***2009***. *Current Directions in Psychological Science* 18(4), 195-199.

Chandra, P., Tan, Y.N., Singh, S.P., 2017. Next generation point-of-care biomedical sensors technologies for cancer diagnosis. Springer.

Chauveau, J., Fert, V., Morel, A.M., Delaage, M.A., Rapid and specific enzyme immunoassay of serotonin, ***1991***. *Clinical Chemistry* 37(7), 1178-1184.

Durairaj, S., Sidhureddy, B., Cirone, J., Chen, A., Nanomaterials-Based Electrochemical Sensors for In Vitro and In Vivo Analyses of Neurotransmitters, ***2018***. *Applied Sciences* 8(9), 1-28.

Fayemi, O.E., Adekunle, A.S., Ebenso, E.E., Electrochemical determination of serotonin in urine samples based on metal oxide nanoparticles/MWCNT on modified glassy carbon electrode, ***2017***. *Sensing and Bio-Sensing Research* 13, 17-27.

Feldman, J.M., Urinary serotonin in the diagnosis of carcinoid tumors, ***1986***. *Clinical Chemistry* 32(5), 840-844.

Godoy-Reyes, T.M., Llopis-Lorente, A., Costero, A.M., Sancenón, F., Gaviña, P., Martínez-Máñez, R., Selective and sensitive colorimetric detection of the neurotransmitter serotonin based on the aggregation of bifunctionalised gold nanoparticles, ***2018***. *Sensors and Actuators B: Chemical* 258, 829-835.

Khalavka, Y., Becker, J., Sönnichsen, C., Synthesis of Rod-Shaped Gold Nanorattles with Improved Plasmon Sensitivity and Catalytic Activity, ***2009***. *Journal of the American Chemical Society* 131(5), 1871-1875.

Lacasse, J.R., Leo, J., Serotonin and depression: a disconnect between the advertisements and the scientific literature, ***2005***. *PLoS medicine* 2(12), e392.

Mahato, K., Chandra, P., Paper-based miniaturized immunosensor for naked eye ALP detection based on digital image colorimetry integrated with smartphone, ***2018***. *Biosensors and Bioelectronics*. 128, 9-16

Mahato, K., Maurya, P.K., Chandra, P., Fundamentals and commercial aspects of nanobiosensors in point-of-care clinical diagnostics, ***2018***. *3 Biotech* 8(3), 149.

Mahato, K., Srivastava, A., Chandra, P., Paper based diagnostics for personalized health care: Emerging technologies and commercial aspects, ***2017***. *Biosensors and Bioelectronics* 96, 246-259.

Maurer-Spurej, E., Dyker, K., Gahl, W.A., Devine, D.V., A novel immunocytochemical assay for the detection of serotonin in platelets, ***2002***. *British Journal of Haematology* 116(3), 604-611.

Moon, J.-M., Thapliyal, N., Hussain, K.K., Goyal, R.N., Shim, Y.-B., Conducting polymer-based electrochemical biosensors for neurotransmitters: A review, ***2018***. *Biosensors and Bioelectronics* 102, 540-552.

Murugesan, A., Rani, M.R.S., Hampson, J., Zonjy, B., Lacuey, N., Faingold, C.L., Friedman, D., Devinsky, O., Sainju, R.K., Schuele, S., Diehl, B., Nei, M., Harper, R.M., Bateman, L.M., Richerson, G., Lhatoo, S.D., Serum serotonin levels in patients with epileptic seizures, ***2018***. *Epilepsia* 59(6), e91-e97.

Pallela, R., Chandra, P., Noh, H.-B., Shim, Y.-B., An amperometric nanobiosensor using a biocompatible conjugate for early detection of metastatic cancer cells in biological fluid, ***2016***. *Biosensors and Bioelectronics* 85, 883-890.

Patel, B.A., Arundell, M., Parker, K.H., Yeoman, M.S., O'Hare, D., Simple and rapid determination of serotonin and catecholamines in biological tissue using high-performance liquid chromatography with electrochemical detection, ***2005***. *Journal of Chromatography B* 818(2), 269-276.

Plapp, F.V., 2019. Carcinoid Syndrome. ClinLabNavigator url:// http://www.clinlabnavigator.com/carcinoid-syndrome.html.

Priebe, M., Fromm, K.M., Nanorattles or Yolk–Shell Nanoparticles—What Are They, How Are They Made, and What Are They Good For?, ***2015***. *Chemistry–A European Journal* 21(10), 3854-3874.

Si, B., Song, E., Recent advances in the detection of neurotransmitters, ***2018***. *Chemosensors* 6(1), 1-24.

Singh, P., König, T.A.F., Jaiswal, A., NIR-Active Plasmonic Gold Nanocapsules Synthesized Using Thermally Induced Seed Twinning for Surface-Enhanced Raman Scattering Applications, ***2018***. *ACS Applied Materials & Interfaces* 10(45), 39380-39390.

Singh, P., Roy, S., Jaiswal, A., Cubic Gold Nanorattles with a Solid Octahedral Core and Porous Shell as Efficient Catalyst: Immobilization and Kinetic Analysis, ***2017***. *The Journal of Physical Chemistry C* 121(41), 22914-22925.

Šolínová, V., Žáková, L., Jiráček, J., Kašička, V., Pressure assisted partial filling affinity capillary electrophoresis employed for determination of binding constants of human insulin hexamer complexes with serotonin, dopamine, arginine, and phenol, ***2019***. *Analytica Chimica Acta*. 1052, 170-178.

Vural, P., Akgül, C., Canbaz, M., Yildirim, A., Urinary Serotonin and 5-Hydroxyindolacetic Acid Levels in Preeclampsia, ***1999***. *Turkish Journal of Medical Sciences* 29(2), 141-144.

Wu, K., Fei, J., Hu, S., Simultaneous determination of dopamine and serotonin on a glassy carbon electrode coated with a film of carbon nanotubes, ***2003***. *Analytical biochemistry* 318(1), 100-106.

Yang, C., Denno, M.E., Pyakurel, P., Venton, B.J., Recent trends in carbon nanomaterial-based electrochemical sensors for biomolecules: A review, ***2015***. *Analytica chimica acta* 887, 17-37.

Yılmaz, C., Taş, N.G., Kocadağlı, T., Gökmen, V., Determination of serotonin in nuts and nut containing products by liquid chromatography tandem mass spectrometry, ***2019***. *Food Chemistry* 272, 347-353.

Zestos, A.G., Carbon Nanoelectrodes for the Electrochemical Detection of Neurotransmitters, ***2018***. *International Journal of Electrochemistry* 2018, 1-19

Chapter VI

Summary and future works

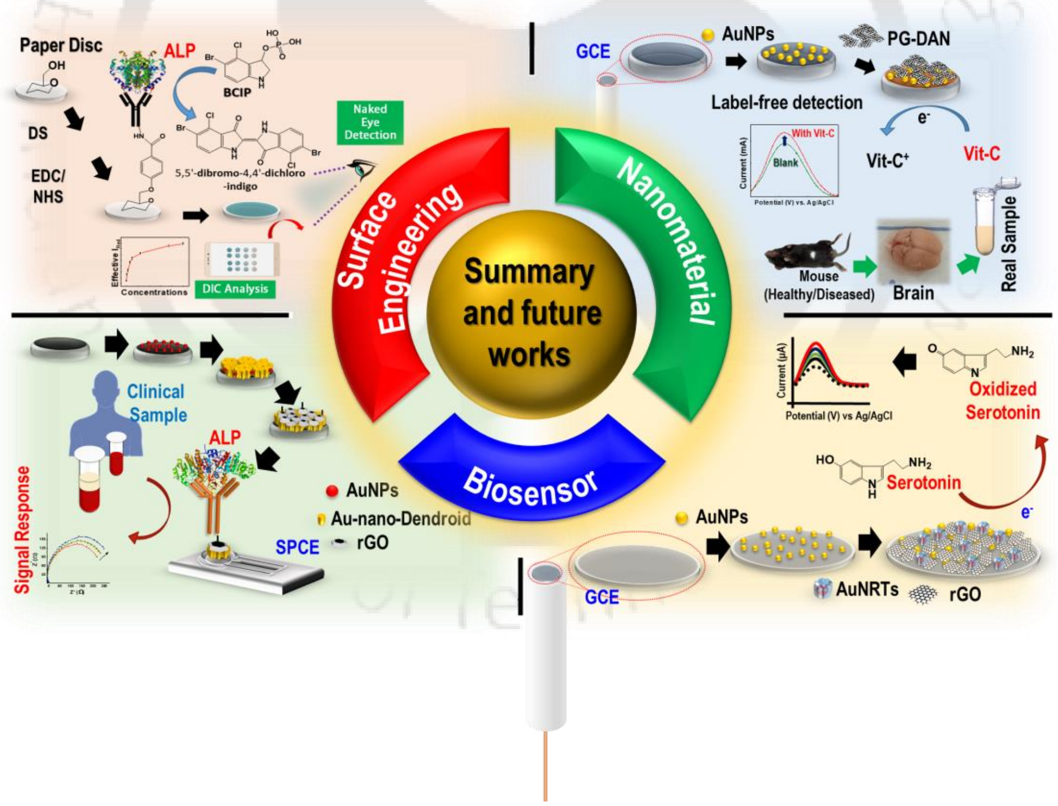

1. Summary

In this present work, we have studied the process of biosensor development by incorporating engineered surfaces and nanomaterials. In the first objective (chapter II), we have developed a biosensor by employing engineered paper surface to anchor the antibody for the selective determination of alkaline phosphatase. The biosensor showed the wide dynamic range from 10-1000 U/mL with the detection limit of 0.87 (±0.07) U/ml (RSD < 4.2%) U/mL, which falls in the alkaline phosphatase range of the raw milk. The biosensor exhibits high selectivity towards the alkaline phosphatase (k_{sel}<<1) and successfully recovered more 84% of the ALP, when spiked in pasteurized and raw milk. The biosensor is stable for four weeks. We have fabricated a point of use detection kit for the onsite determination of alkaline phosphatase in milk.

In the second objective (chapter III), we have employed nanomaterials on to the surface of sensor for obtaining the enhanced sensitivity. Here, Au-nano-dendroid-graphene oxide based metallic nanocomposite is used for the sensor fabrication. Here, we have developed a highly sensitive electrochemical biosensor for the determination of common biomarker for bone and liver health *i.e.* serum alkaline phosphatase, where the antibody of the serum alkaline phosphatase is immobilized covalently to the support matrix and sensor probe was characterized by using electrochemical techniques. Thereafter, the analytical performance of the sensor was rerecorded using electrochemical impedance spectroscopic technique. The sensor shows wide dynamic range of 100-1000 U/L with the detection limit of 9.32 (± 0.12) U/L (RSD < 3.4%). The stability of the sensor was found to be eight weeks. The sensor has shown remarkable sensitivity of the ALP determination in human serum sample where the level of 85.4 (± 0.31) U/L was obtained, which is comparable to the level obtained by clinically accepted method.

In the third objective (chapter IV), we have engineered the sensor surface by incorporating the porous nanomaterial to increase the area for the electron flow. Here, we have developed an ultrasensitive electrochemical nanobiosensor for vitamin-C detection based on porous graphene-1,8-diaminonepthelene nanocomposite coated on Au-nanoparticles deposited glassy carbon electrode surface. The nanobiosensor probe was fabricated using synthesized nanocomposite and characterized by physical and electrochemical techniques. The analytical performance of the developed nanobiosensor was studied using differential pulse voltammetric technique, which showed a wide dynamic range between $1x10^{-14}$ M and $1x10^{-3}$ M with the detection limit of 4.4 (± 0.02) x 10^{-17} M that is lowest compared to any Vitamin-C nanobiosensor reported in the literature till date. The practical applicability of fabricated nanobiosensor was examined by testing vitamin-C in human urine and fruit juice samples. Detection of vitamin-C was also performed directly in brain tissues of healthy as well as diseased mice models. The nanobiosensor was found to be highly selective (k_{sel}<<1) towards vitamin-C and stable up to six weeks.

In the fourth objective (chapter V), we developed a novel biosensor for the detection of serotonin using Au-nanorattles-reduced graphene oxide nanocomposite coated on to the Au-nanoparticle deposited glassy carbon electrode surface. The synthesized nanocomposite has been extensively characterized using the physical and electrochemical techniques and used for the sensor probe fabrication. The fabricated sensor probe surface was then characterized using electrochemical techniques and analytical performance were analyzed. The linear dynamic range was found to be of $1x10^{-3}$ M - $3x10^{-6}$M, respectively, which falls in the ranges of normal and clinical pathophysiological conditions such as carcinoid tumor and pre-eclampsia. The limit of detection was obtained to be of 3.87 (±0.02) $x10^{-7}$ (RSD < 4.2%) M. The fabricated biosensor shows high selectivity (k_{sel} << 1) towards the serotonin and capable of determining serotonin in different real matrices *viz.* urine, blood serum, and human embryonic kidney cell line. The shelf-life of sensor probe was then evaluated which was found to be stable for eight weeks.

2. Future works:

The future works that may be extended to:

- The future direction of this study may lead to the development of portable modules for onsite detection.
- The user interface of the DIC based determinations can be improvised for quicker onsite detection for milk quality checkups.
- For the extension of the electrochemical biosensor for ALP, a portable customized, cheaper device may be developed using microcontrollers / smartphone for the onsite determination of ALP.
- The work done in this study may be extended for the development of biosensors targeting various other molecules simply by tuning the existing antibody-antigen couple.
- The direct electro-chemical based multiplexed biosensors may be developed for the simultaneous determination of electrochemically active target analytes.

Annexures

Annexure 1

List of publications from thesis and associated works

1. **Kuldeep Mahato,** Pranjal Chandra*,'Paper-based Miniaturized Immunosensor for Naked Eye ALP Detection Based on Digital Image Colorimetry Integrated with Smartphone' Biosensors and Bioelectronics, 128 (2019), 9-16.
2. **Kuldeep Mahato,** Pranjal Chandra*,'A Disposable Biosensing Device For Naked-Eye Detection Of Milk Pasteurization Indicator' Science Trends (2019), DOI: 10.31988/SciTrends.47118.
3. **Kuldeep Mahato,** Pranjal Chandra*, 'A miniaturised paper-based kit for milk freshness analysis by the determination of alkaline phosphatase levels.' Asia Pacific Biotech News, 128 (2019).
4. **Kuldeep Mahato**, Sahil Nagpal, Mahero Ayesha Shah, Ananya Srivastava, Pawan Kumar Maurya, Shounak Roy, Amit Jaiswal, Renu Singh, Pranjal Chandra*, 'Gold Nanoparticles Surface Engineering Strategies and their Applications in Biomedicine and Diagnostics' 3 Biotech , 57 (2019), 1-19.
5. **Kuldeep Mahato**, Ashutosh Kumar, Pawan Kumar Maurya, and Pranjal Chandra*, 'Shifting Paradigm of Cancer Diagnoses in Clinically Relevant Samples Based on Miniaturized Electrochemical Nanobiosensors and Microfluidic Devices', Biosensors and Bioelectronics, 100 (2018), 411-28.
6. **Kuldeep Mahato**, Suveen Kumar, Ananya Srivastava, Pawan Kumar Maurya, Renu Singh, and Pranjal Chandra*, 'Electrochemical Immunosensors: Fundamentals and Applications in Clinical Diagnostics', in Handbook of Immunoassay Technologies (Elsevier, 2018), pp. 359-414.

7. **Kuldeep Mahato**, Pawan Kumar Maurya, and Pranjal Chandra*, 'Fundamentals and Commercial Aspects of Nanobiosensors in Point-of-Care Clinical Diagnostics', 3 Biotech, 8 (2018), 149.

8. **Kuldeep Mahato**, Ananya Srivastava, and Pranjal Chandra*, 'Paper Based Diagnostics for Personalized Health Care: Emerging Technologies and Commercial Aspects', Biosensors and Bioelectronics, 96 (2017), 246-59.

9. **Kuldeep Mahato**, Alisha Prasad, Pawan Kumar Maurya, and Pranjal Chandra*, 'Nanobiosensors: Next Generation Point-of-Care Biomedical Devices for Personalized Diagnosis', J Anal Bioanal Tech, 7 (2016), e125.

10. **Kuldeep Mahato**, Anupriya Baranwal, Ananya Srivastava, Pawan Kumar Maurya, and Pranjal Chandra*, 'Smart Materials for Biosensing Applications', in *Techno-Societal 2016, International Conference on Advanced Technologies for Societal Applications* (Springer, 2016), pp. 421-31.

11. Ira Bhatnagar, **Kuldeep Mahato**, Kranthi Kiran Reddy Ealla, Amit Asthana, and Pranjal Chandra*, 'Chitosan Stabilized Gold Nanoparticle Mediated Self-Assembled Glip Nanobiosensor for Diagnosis of Invasive Aspergillosis', International Journal of Biological Macromolecules, 110 (2018), 449-56.

12. Kashish, Surbhi Bansal, Anurag Jyoti, **Kuldeep Mahato**, Pranjal Chandra, and Rajiv Prakash*, 'Highly Sensitive in Vitro Biosensor for Enterotoxigenic Escherichia Coli Detection Based on Ssdna Anchored on Ptnps-Chitosan Nanocomposite', Electroanalysis, 29 (2017), 2665-71.

13. Alisha Prasad, **Kuldeep Mahato**, Pranjal Chandra*, Ananya Srivastava, Shrikrishna N Joshi, and Pawan Kumar Maurya, 'Bioinspired Composite Materials:

Applications in Diagnostics and Therapeutics', Journal of Molecular and Engineering Materials, 4 (2016), 1640004.

14. Alisha Prasad, **Kuldeep Mahato**, Pawan Kumar Maurya, and Pranjal Chandra*, 'Biomaterials for Biosensing Applications', J Anal Bioanal Tech, 7 (2016), e124.

15. Anupriya Baranwal, **Kuldeep Mahato**, Ananya Srivastava, Pawan Kumar Maurya, and Pranjal Chandra*, 'Phytofabricated Metallic Nanoparticles and Their Clinical Applications', RSC Advances, 6 (2016), 105996-6010.

16. Ashutosh Kumar, Buddhadev Purohit, **Kuldeep Mahato**, Pranjal Chandra, Advance engineered nanomaterials in point-of-care immunosensing for biomedical diagnostics. **(Accepted)**

17. Ashutosh Kumar; Sharmili Roy; Ananya Srivastava; Mastan Mukram Naikwade; Buddhadev Purohit; **Kuldeep Mahato**; VGM Naidu; Pranjal Chandra, Nanotherapeutics: A Novel and Powerful Approach in Modern Healthcare System ***(Accepted)**

18. **Kuldeep Mahato**, Uday Pratap Azad , Mohit Kwatra, Rajiv Prakash, Vegi Ganga Modi Naidu, Pranjal Chandra * Development of miniaturized electrochemical nanobiosensor based on AuNPs-porous graphene-1,8-DAN for vitamin-C detection in human urine and neurodegenerative diseased mice brain ***(communicated)**

19. **Kuldeep Mahato,** Buddhadev Purohit, Keshav Bhardwaj, Amit Jaiswal, Pranjal Chandra *, Novel electrochemical biosensor for serotonin detection based on gold nanorattles decorated reduced graphene oxide in biological fluids and in vitro model ***(communicated)**

20. **Kuldeep Mahato**, Budhhadev Purohit, Pranjal Chandra * Clinically comparable impedimetric determination of OMP based on electrochemically tuned Au-nanodorics-GO nanocomposite in human serum ***(Communicated)**

21. Ashutosh Kumar, Buddhadev Purohit, **Kuldeep Mahato**, Riddhipratim Mandal, Ananya Srivastava, Pranjal Chandra, Gold iron bimetallic nanoparticles impregnated reduced graphene oxide based label-free nanosensor for acetaminophen detection in unprocessed human urine. ***(Communicated)**

22. Budhhadev Purohit; **Kuldeep Mahato**; Ashutosh Kumar; Pranjal Chandra, Sputtering assisted enhanced peroxidase like activity of a repurposed dendritic nanochip for label-free hydrogen peroxide detection in blood sample ***(Communicated)**

23. Ashutosh Kumar, Sharmili Roy, Buddhadev Purohit, **Kuldeep Mahato**, Pranjal Chandra* Electrochemically nanotuned gold reduced graphene oxide nanocomposite for selective sensing of sinapic acid in unprocessed human urine. ***(Communicated)**

Annexure 2

Conferences presentations and workshop attended

1. **Kuldeep Mahato**, Ira Bhatnagar, Pranjal Chandra* Novel biosensor for invasive Aspergillosis at Research Conclave, Indian Institute of Technology, Guwahati on 16th March 2019
2. **Kuldeep Mahato**, Pranjal Chandra*, "A next-generation paper-based disposable diagnostic device for point-of-care determination of serum alkaline phosphatase" at Bioengineering 2018, National Institute of Technology Rourkela on 14th December 2018
3. Anupriya Baranwal, Adarsh Kumar Chiranjivi, **Kuldeep Mahato**, Vikash Kumar Dubey, Pranjal Chandra*. Understanding antileishmanial activity of silver nanoparticles synthesized using plant extract at PAPOTHECARY 2017, Guwahati University on 24th March 2017.
4. Buddhadev Purohit, **Kuldeep Mahato**, Ashutosh Kumar, Monalisha Ghosh Dastidar, Sharmili Roy, Pranjal Chandra *. Design of engineered dendritic nanochip for electrochemical characterisation of biologically important small molecules at Recent advancements in biochemical engineering and biotechnology (RABEB-2019), Indian Institute of Technology (BHU) Varanasi on 15-16th March 2019. Page number: 97-98.
5. Sharmili Roy, Monalisha Ghosh Dastidar, Buddhadev Purohit, Ashutosh Kumar, **Kuldeep Mahato**, Shrikrishnan N Joshi, Pranjal Chandra *. Design of chitosan-metal sheet based engineered nanocomposites matrix for bacterial preservation at Recent advancements in biochemical engineering and biotechnology (RABEB-

2019), Indian Institute of Technology (BHU) Varanasi on 15-16th March 2019. Page number: 93-94.

6. Ashutosh Kumar, **Kuldeep Mahato**, Buddhadev Purohit, Monalisha Ghosh Dastidar, Sharmili Roy, Vikash Kumar Dubey, Pranjal Chandra *. Designing potent metal nanoparticles against parasite causing human infectious disease at Recent Advancements in Biochemical Engineering and Biotechnology (RABEB-2019), Indian Institute of Technology (BHU) Varanasi on 15-16th March 2019. Page number: 90-91.

7. Monalisha Ghosh Dastidar, Ashutosh Kumar, **Kuldeep Mahato**, Buddhadev Purohit, Sharmili Roy, Lalit M Pandey, Pranjal Chandra*. Design of metallic nanoparticle-conducting monomer nanocomposites for their bioelectronic properties at Recent Advancements in Biochemical Engineering and Biotechnology (RABEB-2019), Indian Institute of Technology (BHU) Varanasi on 15-16th March 2019. Page number: 95-96.

8. Completed one day workshop on “Biomedical Device Technology” at IIT-Guwahati on 18th December 2017

9. Completed four days’ workshop on the “Antimicrobial resistance diagnostics challenge workshop organized by C-CAMP-Bangalore, India and University of Edinburgh, United Kingdom from 4th to 7th July 2017. *(Selected among twenty candidates across worldwide)*

10. Completed the three days workshop in “Advance microscopy and imaging techniques” organized by DSS Image-tech and Olympus Medical systems at IIT Guwahati on 18th -20th April 2017. *(Selected among twenty candidates worldwide)*

11. Completed three days workshop on " National workshop on MEMS/NEMS and theranostic devices at IIT Guwahati" 20th January 2016

Annexure 3
List of media coverages and highlights of ALP PAPER SENSOR

1. Vigyan Prasar (National science broadcaster under the Government of India):
   URL Link:
   http://vigyanprasar.gov.in/isw/paper-sensor-that-can-detect-freshness-of-milk.html

2. The Hindu:
   URL Link:
   https://www.thehindubusinessline.com/news/science/a-paper-sensor-that-can-detect-freshness-of-milk/article25880169.ece

3. Down to Earth:
   URL Link:
   https://www.downtoearth.org.in/news/food/a-paper-sensor-that-can-detect-freshness-of-milk-62643

4. The Biotech Times:
   URL Link:
   https://biotechtimes.org/2019/01/01/a-paper-sensor-that-can-detect-freshness-of-milk/?fbclid=IwAR34mTNWCIiInB-SrU6vRlvJ_E3wsdraCFgv3GiDHrdjzFsr76zzLgNI6Wo

5. Biovoice News:
   URL Link:
   https://www.biovoicenews.com/a-paper-sensor-that-can-detect-freshness-of-milk/

6. Biospectrum:
   URL Link:
   https://www.nuffoodsspectrum.in/inner_view_single_details.php?page=1&content_type=&vrtcl_panel_nm=&ele_id=NOR_5c2360034819c5.11488335

7. Science Trends (Renowned international science and technology publisher):
   URL Link:
   https://sciencetrends.com/a-disposable-biosensing-device-for-naked-eye-detection-of-milk-pasteurization-indicator/

8. Asia Pasic News Agency (Renowned international biotech publisher under “World scientific”):
   URL Link:
   https://www.asiabiotech.com.sg/23/2303/23030016x.html

9. Tech2.org:
   URL Link:
   https://tech2.org/india/a-paper-sensor-that-can-detect-the-freshness-of-milk/

10. 36kr Media, China:
    URL Link:

https://www.36kr.com/p/5170266

11. Tw Yahoo News:
    URL Link:
    https://tw.news.yahoo.com/%E6%BD%AE%E7%A7%91%E6%8A%80-%E7%A0%94%E7%A9%B6%E4%BA%BA%E5%93%A1%E7%A0%94%E7%99%BC%E4%B8%80%E6%AC%A1%E6%80%A7%E7%94%9F%E7%89%A9%E5%82%B3%E6%84%9F%E8%A3%9D%E7%BD%AE%EF%BC%8C%E5%8F%AF%E7%94%A8%E6%96%BC-013550261.html

12. Nature:
    URL Link:
    https://www.natureasia.com/en/nindia/article/10.1038/nindia.2019.4?fbclid=IwAR1JROWQDeoReU_bmHZCkdACCTDX74IQKDCEtf17C6AgN7_tM_JLBPIL7ak

13. Techno Health Hub:
    URL Link:
    http://www.technohealthhub.com/paper-biosensor-detects-freshness-of-milk-with-94-percent-accuracy-iit-guwahati/

14. Food Marketing & Technology India Magazine:
    URL Link:
    http://fmtmagazine.in/news/paper-sensor-can-detect-freshness-milk/

15. Food Safety and Standards Authority of India (FSSAI) Publication:
    URL Link:
    https://www.linkedin.com/company/fssai/

16. The Logical Indian's:
    URL Link:
    https://thelogicalindian.com/video/awareness/simple-paper-kit-to-test-freshness-of-milk/
    https://www.youtube.com/watch?v=DmTl0ocDPfk

17. UPSC Current Affairs News of January 2' 2019:
    URL Link:
    https://www.upsciasexams.com/current-affair-pdf-download/231

18. Insights IAS Current Affairs :
    URL Link:
    http://www.insightsonindia.com/2019/01/03/a-paper-sensor-that-can-detect-freshness-of-milk/

19. Current Affairs GkToday:
    URL Link:
    https://currentaffairs.gktoday.in/paper-sensor-detect-freshness-milk-01201964043.html

20. India Science Journal:
    URL Link:
    http://www.indiansciencejournal.in/health-2/iit-scientists-develop-paper-sensor-that-can-detect-freshness-of-milk-532552

21. India News Today:
    URL Link:
    http://www.indianews-today.com/news/a-paper-sensor-that-can-detect-freshness-of-milk

22. News LYF:
    URL Link:
    https://www.newslyf.com/single/A-paper-sensor-that-can-detect-freshness-of-milk-BusinessLine

23. Latest GK GS:
    URL Link:
    http://www.latestgkgs.com/current-affairs-6697-a

24. Eenadu HAI BUJJI Ramoji Group :
    URL Link:
    http://www.eehibu.com/whatsnew/3572/A-paper-sensor-to-detect-milk--

25. FOOD SAFETY LATEST:
    URL Link:
    http://foodsafetylatest.blogspot.com/2019/01/a-paper-sensor-that-can-detect.html

26. Clean Future:
    URL Link:
    http://www.cleanfuture.co.in/2019/01/04/a-paper-sensor-that-can-detect-freshness-of-milk/

27. Biotechnika:
    URL Link:
    https://www.biotecnika.org/2019/01/simple-paper-based-test-to-detect-milk-freshness-by-iit-g-researchers/

28. Engineering Insider:
    URL Link:
    https://engineeringinsider.org/now-you-can-find-milk-quality-and-freshness-technology-given-by-iit-guwati/

29. The Silicon Review India:
    URL Link:
    http://thesiliconreview.in/science-and-technology/new-milk-quality-testing-device

30. Research Stash:
    URL Link:

https://www.researchstash.com/2019/01/03/a-paper-sensor-that-can-detect-freshness-of-milk/

31. True News Recorder:
URL Link:
https://truenewsrecorder.xyz/2019/a-paper-kit-that-can-detect-freshness-of-milk-with-smartphone/

32. Transparency Market Research Blog.com USA:
URL Link:
https://tmrblog.com/researchers-develop-paper-sensors-to-detect-freshness-of-milk/

33. Rjasthan Partika 6th January 2019:
URL Link:
http://epaper.patrika.com/1968814/Rajasthan-Patrika-Jaipur/Rajasthan-Patrika-Jaipur#page/10/2

34. Infomagic kerala 5th January 2019:
URL Link:
https://translate.google.com/translate?hl=en&sl=ml&u=https://www.infomagic.com/news/kerala-tech-news/iit-guwahati-develops-paper-sensor-to-detect-freshness-of-milk/5/42994&prev=search

35. Food Industry Reports:
URL Link:
http://food.industry-report.net/2019/01/08/iit-guwahati-invents-paper-kit-to-test-freshness-of-milk/

36. Times alert :
URL Link:
https://timesalert.com/detect-the-freshness-of-milk/30795/

37. Kerala classified:
URL Link:
https://www.infomagic.com/news/kerala-tech-news/iit-guwahati-develops-paper-sensor-to-detect-freshness-of-milk/5/42994

38. Neucrad Health India :
URL Link:
http://neucradhealth.in/paper-sensor-attached-with-mobile-app-can-detect-freshness-of-milk-now/

39. Kerala News:
URL Link:
https://malayalam.gizbot.com/news/a-paper-sensor-that-can-detect-freshness-milk/articlecontent-pf66684-013537.html

40. Blog Daddy News:
URL Link:

https://www.blogdady.com/a-paper-sensor-that-may-discover-freshness-of-milk/

41. Pesproppt Wordpress:
URL Link:
https://pesproppt.wordpress.com/2019/01/02/45990/

42. TODAY NEWS TAMIL:
URL Link:
https://www.youtube.com/watch?v=sWmDZHgts-4

43. The India Saga:
URL Link:
http://theindiasaga.com/social-sector/iit-guwahati-scientists-invented-paper-based-biosensor-for-confirmation-of-milk-pasteurization

44. IIT Delhi Library News:
URL Link:
http://library.iitd.ac.in/news/News%20Clips,%20January%2026-February%201,%202019.pdf

45. Rajya Sabha TV : Science Monitor:
URL Link:
https://www.youtube.com/watch?v=I073G3uCShY&t=770s

46. Rajya Sabha TV: Gyan Vigyan:
URL Link:
https://www.youtube.com/watch?v=bL7v0EbU2bg

47. NEWS Highlights, India’s Latest News, Embassy of India in Jakartha Malaysia:
URL Link:
https://www.indianembassyjakarta.gov.in/users/assets/pdf/bulletin/Final_English_Version%20_of_E_Bulletin_31_December_6_Januari_2019.pdf

48. I-Next Focus, Dainik Jagaran:
URL Link:
http://inextepaper.jagran.com/2034253/Gorakhpur-Hindi-ePaper,-Gorakhpur-Hindi-Newspaper-InextLive/20-02-19#page/5/2

49. Health eHelp :
URL Link:
http://healthehelp.in/right-from-the-mobile-app-go-to-the-correctness-of-the-milk/

50. Jāṇasuddi (Kannada):
URL Link:
https://www.youtube.com/watch?v=Lq_OGx2hbQc&feature=youtu.be

51. Flibboard:
URL Link:

https://flipboard.com/@flip_india/india-science-%28top-stories%29-e84nafi9z/a-paper-sensor-that-can-detect-freshness-of-milk/a-dRnMsSQxTwq30lzQY4mbsA%3Aa%3A106586776-4d1b8e954a%2Fgov.in

52. TODAY NEWS TAMIL:
URL Link:
https://www.youtube.com/watch?v=sWmDZHgts-4

53. BUSINESS WIRE, DUBLIN (UK):
URL Link:
https://www.businesswire.com/news/home/20190130005286/en/2019-Innovations-Optical-Sensors-MEMS-Piezoelectric-Sensors

54. Research and Markets:
URL Link:
https://www.researchandmarkets.com/research/brrc73/2019_innovations?w=4

55. AP NEWS; DUBLIN--(BUSINESS WIRE):
URL Link:
https://www.apnews.com/8fa716d6395e4156bbf1dcb78c0a7edf

56. Frost and Sullivan:
URL Link:
https://store.frost.com/innovations-in-optical-sensors-mems-piezoelectric-sensors-terahertz-imaging-sensors-mems-gas-sensors-smartphone-optical-sensors-gmr-magnetometers-food-monitoring-sensors-and-radar-sensors.html#section1

57. Agriculture Science and Technology Decision Making Information Platform (Taiwan): URL Link:
http://agritech-foresight.atri.org.tw/article/contents/1695

58. Cowsmopolitan Dairy Magazine (Funded by Government of Canada):
URL Link:
https://www.cowsmo.com/news/paper-sensor-created-to-ensure-freshness-of-milk/

59. Latest GKGS Current affairs:
URL Link:
http://www.latestgkgs.com/current-affairs-6697-a

60. Current affairs:
URL Link:
https://www.affairscloud.com/current-affairs-january-4-2019/

61. GK Today:
URL Link:
https://currentaffairs.gktoday.in/paper-sensor-detect-freshness-milk-01201964043.html

62. KaaShiv InfoTech, Chennai:

URL Link:
https://www.kaashivinfotech.com/current-affairs-january-06-2019/

63. Civils Daily:
URL Link:
https://www.civilsdaily.com/news/a-paper-sensor-that-can-detect-freshness-of-milk/
64. A Shankar IAS Academy:
URL Link:
https://www.tnpscthervupettagam.com/paper-sensor-to-detect-freshness-of-milk/

65. Insight IAS :
URL Link:
https://www.insightsonindia.com/2019/01/03/a-paper-sensor-that-can-detect-freshness-of-milk/
66. VINSONI IAS ACADEMY:
URL Link:
http://www.vinsonias.com/DynImg/540dba7f-0868-4e64-8d45-65ffad32ab69.pdf

67. SANSAR LOCHAN:
URL Link:
https://www.sansarlochan.in/sansar-daily-current-affairs-03-january-2019/

68. Bsc4 Success:
URL Link:
https://bsc4success.com/ga-03-04-jan-2019/

69. Gradeup UPSC:
URL Link:
https://gradeup.co/upsc-current-affairs-04012019-i

70. Vajiram and Ravi Current Affairs:
URL Link:
https://www.vajiramandravi.com/pdf_upload/current_affairs/jan_2019/Index%20Page%20(January%20%202019).pdf

71. SP Lessons:
URL Link:
https://www.splessons.com/lesson/current-affairs-4-january-2019/

72. Manabadi.co.in: Current Affairs:
URL Link:
http://www.manabadi.co.in/articles/Latest-current-affairs/Current-affairs-Description.aspx?id=6861

73. BlueGK Ocean of Knowledge:
URL Link:
https://bluegk.com/insights-daily-current-affairs-pib-03-january-2019/

74. Bankers Daily:

URL Link:
http://bankersdaily.in/daily-current-affairs-january-4-2019/

75. Exam 360 :
URL Link:
https://exam360.wordpress.com/2019/01/06/current-affairs-this-week-06-01-2019/

76. KG IAS Academy:
URL Link:
https://www.kgmechias.com/2019/01/06/current-affairs5-january-2019/

77. Embibe Current Affairs:
URL Link:
https://www.embibe.com/exams/current-affairs-january/

A paper sensor that can detect freshness of milk

Home › Biotech News › Simple Paper Based Test To Detect Milk Freshness By IIT-G Researchers

Biotech News January 4, 2019

Simple Paper Based Test To Detect Milk Freshness By IIT-G Researchers

Trending : This simple paper biosensor detects freshness of milk with 94 percent accur

Home › Health › This simple paper biosensor detects freshness of milk with 94 percent accuracy: IIT Guwahati

This simple paper biosensor detects freshness of milk with 94 percent accuracy: IIT Guwahati

January 2, 2019 Sekhar. M Health No Comment

Home > HEALTH > IIT scientists develop paper sensor that can detect freshness of milk

IIT scientists develop paper sensor that can detect freshness of milk

A paper sensor that can detect freshness of milk

Kollegala Sharma | Updated on January 01, 2019

A paper sensor that can detect freshness of milk

IIT Guwahati scientists develop a new detection kit that could make testing freshness of milk easy and fast

Home » Clean Facts » A Paper Sensor That Can Detect Freshness Of Milk

IN CLEAN FACTS, GUEST ARTICLE, HEALTH, INNOVATIONS, NEWS, TECHNOLOGY

GUEST ARTICLE JANUARY 4, 2019 0 SHARE

A Paper Sensor That Can Detect Freshness Of Milk

Home › Agriculture › DairyTech › A paper sensor that can detect freshness of milk

Agriculture DairyTech News Bytes Top News

A paper sensor that can detect freshness of milk

Figure A-1: *Media highlights of ALP paper sensor*

A paper sensor that can detect freshness of milk

written by BioTech Times Desk | January 1, 2019

Volume 23, Number 03, March 2019

Driven by curiosity — Exclusive interview with Nobel laureate Ada Yonath: Her journey in science wasn't always crystal clear

2019 Innovations in Optical Sensors, MEMS Piezoelectric Sensors, Terahertz Imaging Sensors, MEMS Gas Sensors, Smartphone Optical Sensors, GMR Magnetometers, Food Monitoring Sensors, and Radar Sensors - ResearchAndMarkets.com

January 30, 2019 04:46 AM Eastern Standard Time

DUBLIN--(BUSINESS WIRE)--The "Innovations in Optical Sensors, MEMS Piezoelectric Sensors, Terahertz Imaging Sensors, MEMS Gas Sensors, Smartphone Optical Sensors, GMR Magnetometers, Food Monitoring Sensors, and Radar Sensors" report has been added to **ResearchAndMarkets.com's** offering.

"Innovations in Optical Sensors, MEMS Piezoelectric Sensors, Terahertz Imaging Sensors, MEMS Gas Sensors, Smartphone Optical Sensors, GMR Magnetometers, Food Monitoring Sensors, and Radar Sensors"

Tweet this

This issue of Sensor TechVision Opportunity Engine profiles advancements in miniature optical sensors, MEMS piezoelectric pressure sensors, terahertz imaging sensors, MEMS gas sensors, compact integrated color/ambient light/proximity sensors, giant magneto resistance sensors, low pressure sensors, automotive image sensors, sensors for healthcare, sensors for determining milk freshness, eddy current sensors for bearing surface monitoring, and automotive radar sensors.

A Disposable Biosensing Device For Naked-Eye Detection Of Milk Pasteurization Indicator

Figure A-2: *Media highlights of ALP paper sensor*

BIOGRAPHY

Kuldeep Mahato is currently a research scholar at the Laboratory of Bio-Physio sensors and Nano-bioengineering, Department of Biosciences and Bioengineering, Indian Institute of Technology Guwahati, INDIA. He hails from Ranchi, Jharkhand. He holds a degree of Bachelors of Technology (B.Tech.) in biotechnology from National Institute of Technology Durgapur, West Bengal. He has qualified in GATE 2013 and GATE 2015 with the percentile 96+ percentiles. After graduating, he worked as junior research fellow at the Council of Scientific and Industrial Research-Central Mechanical Engineering Research Institute, Durgapur until 2015. Thereafter, he joined Indian Institute of Technology Guwahati for his doctoral studies under the supervision of Dr. Pranjal Chandra, Professor (Assist.) and Ramanujan Fellow. His research work is centered at the development of biosensors based on engineered surfaces and nanomaterials. He has published / communicated more than 23 high impact journals, which included Biosensors and Bioelectronics, Journal of Biological Macromolecules, Electroanalysis, 3 Biotech etc. He has filed one patent from his doctoral thesis work. He is also an invited reviewer of a prestigious scientific journal of material science and energy technology, Elsevier.